UNIVERSIDADE
BEIRA INTERIOR

Impacto dos Processos Mecânicos do *Converting* nas Propriedades do Papel *Tissue*

Impact of Mechanical Converting Processes on Tissue Paper Properties

Joana Magalhães Gonçalves Costa Vieira

Tese para obtenção do Grau de Doutor em
Ciência e Engenharia dos Materiais Fibrosos
(3º ciclo de estudos)

Orientador: Prof.ª Doutora Ana Paula Nunes de Almeida Alves da Costa
Coorientador: Prof. Doutor Paulo Torrão Fiadeiro

Júri
Professor Doutor Paulo Jorge da Silva Almeida
Professor Doutor Mohamed Naceur Belgacem
Professor Doutor Paulo Jorge Tavares Ferreira
Professor Doutor Rogério Manuel Santos Simões
Professora Doutora Maria Emília da Costa Cabral Amaral
Professora Doutora Ana Paula Nunes de Almeida Alves da Costa
Doutora Paula Cristina de Oliveira Rodrigues Pinto

março de 2023

Folha em branco

Declaração de Integridade

Eu, Joana Magalhães Gonçalves Costa Vieira, que abaixo assino, estudante com o número de inscrição D2546 no 3º ciclo de estudos do curso de Ciência e Engenharia dos Materiais Fibrosos da Faculdade de Engenharia, declaro ter desenvolvido o presente trabalho e elaborado o presente texto em total consonância com o **Código de Integridades da Universidade da Beira Interior**.

Mais concretamente afirmo não ter incorrido em qualquer das variedades de Fraude Académica, e que aqui declaro conhecer, que em particular atendi à exigida referenciação de frases, extratos, imagens e outras formas de trabalho intelectual, e assumindo assim na íntegra as responsabilidades da autoria.

Universidade da Beira Interior, Covilhã, 02 de março de 2023

Assinado por: **JOANA MAGALHÃES GONÇALVES COSTA VIEIRA**
Num. de Identificação: 11681129
Data: 2023.03.02 15:42:57+00'00'

CARTÃO DE CIDADÃO

Folha em branco

“All sorts of things can happen when you’re open to new ideas and playing around with things.”

Stephanie Kwolek,
Chemist who invented Kevlar and
winner of the Lavoisier Medal for technical achievements.

Folha em branco

This thesis was carried out under the Project inpactus – innovative products and technologies from eucalyptus, Project N.º 21874 funded by Portugal 2020 through European Regional Development Fund (ERDF) in the frame of COMPETE 2020 nº246/AXIS II/2017.

Cofinanciado por:

COMPETE 2020
PROGRAMA OPERACIONAL COMPETITIVIDADE E INTERNACIONALIZAÇÃO

PORTUGAL 2020

UNIÃO EUROPEIA
Fundo Europeu
de Desenvolvimento Regional

Folha em branco

Acknowledgements

Words cannot express my gratitude to my supervisors Dr. Ana Paula Costa and Dr. Paulo Fiadeiro for their invaluable patience, guidance and expertise knowledge shared with me. I also could not have undertaken this journey without the funding under the Project InPaCTus – Innovative products and technologies from eucalyptus, Project N. º 21874 funded by Portugal 2020 through European Regional Development Fund (ERDF) in the frame of COMPETE 2020 nº246/AXIS II/2017 and the constructive criticism and feedback of the project pivot Dr. Ana Margarida Carta. Additionally, this endeavor would not have been possible without the generous support from Universidade da Beira Interior, the Navigator Company and Raiz for the availability of facilities and raw materials. Thanks, should also go to my research unit Fiber Materials and Environmental Technologies (FibEnTech-UBI) under the vice coordination of Dr. Rogério Simões, on the extent of the project reference UIDB/00195/2020, and the research unit Center for Mechanical and Aerospace Science and Technologies (C-MAST-UBI), on the extent of the project reference UIDB/00151/2020, both funded by the Fundação para a Ciência e a Tecnologia, IP/MCTES through national funds (PIDDAC).

I am also grateful to my friend Dr. Marcelo Leite Ribeiro from University of São Paulo for all the support and expertise in the finite element method analysis, to Dr. António Mendes for all the support and expertise in the optical system and to the technician Nuno Santos from FabLab of UBI for all the support in digital design and 3D printing of the embossing plates. I would like to extend my sincere thanks to Dr. Maria Emília Amaral and Dr. Joana Curto for the extra financial support with my research grant and to my classmates, university department professors, project co-workers, InPaCTus project manager Msc. Cristina Gil and laboratory technicians who motivate, advice, brainstorm and made suggestions in my study. Special thanks to the company PCE Iberica S.L. Instrumentacíon for the donation of the Durometer PCE-DDA equipment that was used in this work to determine the apparent hardness of the rubber rollers and plates.

Lastly, I would be remiss in not mentioning my husband André for his technical-scientific support, for his support for our daughters when he was away and for all the motivation, encouragement, and inspiration in the right moments. I'd like to recognize all the entertainment and emotional support from my daughters Sara e Raquel, parents, brothers and other family members and friends who kept my spirits and motivation high during this process. I would also like to thank my cats Shadow and Kyra and my dog Nikky for all the affection and dedication and for always being there waiting for me.

Folha em branco

Resumo

O papel *tissue* está verdadeiramente enraizado no cotidiano da sociedade moderna devido à grande variedade de produtos que possibilitam diferentes aplicações. Para este tipo de indústria, é um enorme desafio produzir os melhores produtos para fidelizar o consumidor final. O papel *tissue* é um papel caracterizado principalmente pela sua baixa gramagem e resistência à tração, e pela sua elevada suavidade, absorção de líquidos e alongamento. Consoante o segmento de produto a ser produzido, tem de se ter em conta qual/quais destas características são essenciais, por exemplo, no papel higiénico o foco é a suavidade e absorção, já nos rolos de cozinha é a absorção e a resistência à tração em húmido, nos guardanapos a suavidade, a absorção e a resistência à tração em húmido e nos lenços faciais a suavidade. Essas propriedades devem ser adaptadas para atender aos requisitos do consumidor final, que variam muito para os diferentes países do mundo. O processo de produção do papel *tissue* usa a celulose virgem como principal matéria-prima e envolve duas etapas: a formação da própria folha de papel *tissue* (papel base *tissue*) e sua transformação em diferentes tipos de produtos acabados. Este trabalho aborda essencialmente esta segunda etapa, onde ocorre a transformação do papel base *tissue* em produtos acabados e o seu impacto nas propriedades dos produtos produzidos. Durante o processo de transformação da folha base de papel *tissue*, também chamado de processo de conversão (*converting*), as propriedades adquiridas na etapa anterior são alteradas, pois a folha é sujeita a sucessivas operações que a vão deformar de forma permanente. A máquina de conversão é caracterizada por diversas operações, sendo as principais: bobinagem/desenrolamento, *embossing*/laminação, perfuração, corte, embalagem e paletização. O processo de conversão manifesta ser muito complexo e com um enorme impacto nas propriedades do papel *tissue* acabado. O *embossing* é a operação chave do processo de transformação do papel *tissue*, pois é aquela que mais afeta as propriedades finais do produto acabado. Esta operação consiste na marcação de um padrão na folha base de papel *tissue* por aplicação de pressão, com o propósito de produzir papéis esteticamente mais apelativos ao consumidor final e/ou ser um meio de identificação de uma marca. Para além de afetar visualmente o papel, também afeta as propriedades finais dos produtos acabados, adicionando uma terceira dimensão *z* com uma matriz de compressão, aumentando sua capacidade de absorção de líquidos e seu volume, mas, por outro lado, reduzindo a sua suavidade e resistência à tração.

Sendo a *embossing* a operação mais impactante da transformação do papel base *tissue* e tendo em conta o sistema de *embossing* industrial, foi desenvolvido um sistema que permitisse o estudo à escala laboratorial do impacto desta operação nas propriedades físico-mecânicas do papel *tissue*, em função dos diferentes parâmetros de operação da máquina de *converting*, como o acabamento dos pontos e/ou traço que compõem o padrão de *embossing*, dureza da borracha de *embossing*, pressão, temperatura e humidade, tanto em folhas laboratoriais (isotrópicas) como em folhas base de papel *tissue* industrial (anisotrópicas e crepadas). Como este *set-up* laboratorial permite controlar todos os parâmetros de operação individualmente, foi possível otimizar o processo de *embossing* a nível laboratorial e foi feita a sua validação pelo método dos elementos finitos. Assim, para cada novo padrão exclusivo que a indústria de papel *tissue* pretenda implementar, poderá testá-lo laboratorialmente antes de fazer o seu *scale-up*.

Com o sistema de *embossing* laboratorial primeiramente iniciou-se um estudo para se perceber como a pressão afeta as principais propriedades do papel *tissue*. Foram usadas folhas de papel base *tissue* industrial e foi alcançada uma pressão ótima de 2.8 bar para este sistema de *embossing* laboratorial. Conseguiram-se distinguir dois efeitos que ocorrem na folha de papel base *tissue* durante a operação de *embossing* com a pressão, a densificação da folha e a deformação permanente da folha com a marcação do padrão de relevo. O efeito da pressão ao densificar a folha de papel confere-lhe um ganho de resistência mecânica, mas sem diferenças em termos de absorção de líquidos. Os dois padrões de *embossing* (deco e micro) apresentaram comportamentos diferentes com o efeito da pressão, mas ambos evidenciaram perdas tanto nas propriedades mecânicas como na suavidade. Estas perdas foram menos acentuadas para a pressão 2.8 bar, uma vez que a densificação é máxima para esta pressão. Por outro lado, o método dos elementos finitos (FEM) não conseguiu mostrar como a pressão afeta a resistência do papel.

Outro parâmetro de operação que também tem impacto nas propriedades finais dos produtos *tissue* é a da dureza da borracha utilizada no contra-rolo ao rolo de aço de *embossing* com padrão gravado. Foram estudadas três configurações diferentes de empilhamento de placas de borracha com durezas diferentes em folhas de papel base *tissue* industrial. Este estudo permitiu concluir que para se obter uma maior suavidade, a melhor solução foi onde se usaram duas placas de borracha com durezas diferentes, e a placa de borracha com maior dureza estava em contacto com a folha de papel de *tissue*. Este resultado corrobora a futura tendência industrial em que é apontado o uso de rolos de borracha na operação de *embossing* com uma camada interna de baixa

dureza e uma camada externa de alta dureza. O método de elementos finitos para além de validar os resultados obtidos, mostrou-se uma ferramenta confiável para testar virtualmente outras configurações, como, por exemplo, três ou mais placas de borracha com durezas diferentes.

O impacto da geometria do acabamento das linhas e pontos dos padrões a serem gravados nas propriedades finais do papel *tissue* foi outro parâmetro de operação objeto de estudo. Este trabalho foi desenvolvido recorrendo a folhas de papel base *tissue* industrial e concluiu-se que embora os padrões com geometria de acabamento reto apresentassem individualmente maior valor de suavidade, quando montado o protótipo de produto acabado com 2 folhas (deco + micro), a maior suavidade foi obtida para a geometria de acabamento redondo. Foi confirmado que o valor de suavidade diminui com o aumento do *bulk*, sendo mais acentuado para o padrão de *embossing* micro. Não se encontraram diferenças relevantes na cinética de espalhamento da gota de líquido ao longo do tempo, donde se pode inferir que a geometria de acabamento das linhas e pontos dos padrões de *embossing* não afeta esta propriedade neste tipo de produtos. O método de elementos finitos também neste caso, permitiu entender melhor o efeito da geometria de acabamento do padrão na folha de papel *tissue*, e os resultados da simulação estão de acordo com os resultados experimentais, mostrando a mesma tendência onde os padrões com geometria redonda marcaram mais a folha de papel *tissue* do que os padrões com formas retas.

O sistema de *embossing* laboratorial, também foi usado de modo a investigar o efeito desta operação de *converting*, em folhas base *tissue* industriais e em folhas laboratoriais. Para avaliar a influência dos padrões de *embossing*, a composição das fibras e o processo de crepagem, foram utilizados como amostras folhas de papel base *tissue* industrial, folhas laboratoriais produzidas a partir de uma suspensão fibrosa obtida da desintegração da folha industrial (mantendo a mesma composição fibrosa) e folhas laboratoriais produzidas a partir de uma pasta *kraft* industrial de eucalipto branqueada nunca seca. A folhas laboratoriais foram produzidas com uma gramagem de 17 g/m^2 (gramagem similar à da folha de papel base *tissue* industrial) e não prensadas. Os resultados indicaram que o processo de *embossing* produziu estruturas mais volumosas e mais porosas, à custa de perdas nas propriedades mecânicas e de suavidade, mais acentuadas para o padrão micro do que para o padrão deco. O efeito da composição fibrosa mostrou que um aumento na resistência mecânica impactou negativamente na suavidade das folhas laboratoriais. As folhas laboratoriais de composição 100% eucalipto apresentaram maior suavidade do que as folhas laboratoriais cuja composição é uma mistura de fibra curta e longa. Verificou-se que a

crepagem existente na folha de papel base *tissue* industrial, confere-lhe uma alta capacidade de alongamento que é praticamente inexistente nas folhas de papel laboratorial. Além disso, devido a esta operação, as amostras de papel industriais apresentam uma porosidade aparente maior do que as amostras de papel laboratorial. A análise pelo método de elementos finitos (FEM) permitiu validar os resultados experimentais, comprovando que o padrão micro possui um valor de campo de tensão maior e, consequentemente, uma resistência mecânica menor.

Para além do uso do sistema de *embossing* laboratorial e de modo a aprofundar o impacto da *embossing* nas propriedades de produtos acabados *tissue*, foram efetuados outros estudos a partir de produtos acabados industrialmente e comercializados. A capacidade de absorção sendo também uma propriedade fundamental dos papéis *tissue*, foi um dos estudos desenvolvidos. Neste trabalho, foram comparadas as capacidades de absorção de quatro papéis base *tissue* industriais diferentes, bem como os respetivos papéis higiénicos industriais de 2 folhas a que deram origem. Concluiu-se que a operação de *embossing* aumentou notoriamente a espessura e consequentemente, o *bulk* do papel higiénico. Além disso, verificou-se também que entre as várias amostras de papel higiénico não houve variação percetível no tempo de absorção de água, pois as amostras apresentaram morfologia e porosidade semelhantes. No entanto, verificou-se que onde *bulk* aumentou mais (cerca de 150%), resultou num aumento da capacidade de absorção de água (cerca de 60%).

Outro estudo importante para aprofundar a operação de *embossing* foi o impacto da sequência de empilhamento de um papel higiénico com número de folhas ímpar (neste caso 5 folhas). As duas configurações possíveis, 1 e 2 (padrão deco:micro de 3:2 e 2:3 folhas, respetivamente) foram objeto de estudo. Os produtos produzidos industrialmente com as duas configurações, tiveram origem nas mesmas bobines mãe de papel base *tissue*. Globalmente, verificou-se que a sequência de empilhamento das folhas influenciou as propriedades do papel higiénico acabado. Para as configurações 1 e 2, após o processo de *embossing*, foram registados aumentos de *bulk* de 46% e 40%, respetivamente, e aumentos de capacidade de absorção de água de 2% e 17%, respetivamente. Em relação às propriedades mecânicas, ambas as configurações apresentaram maior impacto negativo causado pelo padrão de *embossing* deco. Para fins comerciais e para atender às preferências do consumidor final, o papel higiénico com a configuração 1 apresentou-se mais adequado para preferências de resistência mecânica e o papel higiénico com a configuração 2 foi o que se apresentou mais adequado para preferências de capacidade de absorção. Em relação à suavidade, a sequência de empilhamento também afetou os resultados, onde a configuração 2 se

revelou o produto mais macio e agradável ao toque, com um valor global de *handfeel* de 75.3 HF, e o produto produzido com a configuração 1 apresentou-se mais áspero e menos agradável ao toque, com um valor global de *handfeel* de 68.0 HF.

Outra operação que ocorre na máquina de *converting* e que também tem impacto tanto nas propriedades deste tipo de produtos, como na operabilidade da própria máquina, é a operação de perfuração ou picotagem. Foi também desenvolvido um sistema que permitisse o estudo à escala laboratorial do impacto desta operação na eficiência de perfuração dos produtos acabados. Este sistema de perfuração aplica-se a todos produtos de papel *tissue*, tais como papel de cozinha ou papel higiénico, que necessitem de ser particionados de acordo com as necessidades do consumidor final. As perfurações facilitam esse particionamento, promovendo a separação das folhas ou serviços, pela linha de perfuração sem os rasgar. Porém, o papel perfurado tem de ser suficientemente forte para se manter unido sob uma certa tensão, mas por outro lado tem de ser fraco o suficiente para que a folha ou serviço possa ser destacado do rolo de modo fácil, sem rasgar, com pouco esforço e ao longo da linha perfurada horizontal reta ou padronizada. Este equilíbrio é dado pela eficiência de perfuração. Quanto maior a eficiência de perfuração, mais fácil será a separação do serviço. Neste contexto, o sistema de perfuração laboratorial desenvolvido, permite testar novos tipos de perfuração à escala laboratorial, permitindo transpor os resultados à escala industrial, e avaliar problemas associados com a perfuração dos produtos, bem como testar novos padrões de perfuração.

Como a satisfação do consumidor pode depender do desempenho da perfuração, foi utilizado o sistema de perfuração laboratorial para perfurar diferentes papéis higiénicos comerciais (em marcas e número de folhas) para avaliar sua eficiência de perfuração. Com este estudo verificou-se uma estabilização da eficiência de perfuração a partir de uma distância de corte de 6 mm e um acréscimo de 15% na distância de corte para a lâmina de laboratório para corresponder à eficiência de perfuração industrial. Foi também utilizado o método de elementos finitos (FEM) para simular a curva de progressão da eficiência de perfuração em função da distância de corte. Desta análise confirmou-se o comportamento da evolução da eficiência de perfuração com o aumento da distância de corte e a sua estabilização a partir da distância de corte de 6 mm.

Outro estudo com interesse para compreender o impacto da perfuração, foi a avaliação da perfuração de produtos higiénicos comerciais. Neste trabalho, foram estudados os comportamentos mecânicos de 15 papéis comerciais de diferentes produtores europeus, com composições e número de folhas igualmente diferentes. Uma análise qualitativa da

qualidade dos cortes, juntamente com uma análise quantitativa das dimensões dos mesmos cortes foi realizada através de um sistema ótico. Uma análise usando o método de elementos finitos foi efetuada onde se conseguiu examinar o comportamento da concentração de tensões no furo da perfuração e a influência da distância de corte. Os resultados mostraram que uma distância de corte igual ou inferior a 2.0 mm não deve ser utilizada nestes tipos de papéis, e a eficiência de perfuração aumentou com o aumento da distância de corte, independente do número de folhas que compõem o papel higiénico. O fator de concentração de tensões também foi determinado e chegou-se a um valor limite de 0.11. Papéis higiénicos para rasgarem na linha de perfuração, conforme desejado, precisam de ter um fator de concentração de tensões acima deste valor limite.

Resumindo, é na máquina de *converting* onde se acrescenta valor aos produtos de papel *tissue*, e por isso estas máquinas estão em constante evolução. No início da transformação do papel *tissue*, o papel era rebobinado à mão num mandril e quando apareceu a primeira máquina semiautomática eram enrolados apenas alguns LOGs por minuto. Atualmente, o design do produto tem um papel muito importante, pois para além da aparente sofisticação é também a chave para a otimização das suas propriedades. Por isso, cada vez mais se usa o *embossing* e a impressão neste tipo de produtos, e os padrões de design estão em constante mudança e otimização. Devido às exigências de mercado, é imperativo para o produtor a adaptabilidade deste tipo máquina e a sua rápida atualização, pois responder aos requisitos do consumidor final é a sua principal motivação. O facto de a automação das máquinas de *converting* ir até ao fim da linha (paletização), permite ao produtor controlar melhor a qualidade e o preço do produto que apresenta ao consumidor, que, em última análise, tem maior probabilidade de sucesso o produtor que tiver os produtos certos e que reflitam as necessidades e desejos dos clientes. A vantagem vai se encontrar nos produtores que utilizam a tecnologia mais recente, pois com a desaceleração da economia, os produtos vão ter de ser redesenhados de modo a encontrar um preço mais baixo, o que significa fazer um esforço adicional para produzir os produtos ao menor custo assim como baixar o custo de transporte pelos canais de distribuição. Este trabalho permite assim auxiliar o produtor a otimizar os parâmetros de operação ao longo da máquina de *converting*, apontando algumas modificações, como substituir o rolo de borracha de dureza única por um de dureza variável, ou encontrar a pressão ótima da máquina em que a resistência mecânica é maximizada, e que ao serem implementadas vão melhorar a qualidade do produto produzido, agregando-lhe valor.

O digital *twining* dos vários processos de *converting*, aqui apresentado pelo método de elementos finitos, demostrou ser uma ferramenta de modelação fiável para testar alterações que se queiram introduzir no processo, virtualmente e com custos reduzidos. Este procedimento é uma tendência num futuro próximo, porque permite a otimização em ambiente digital, sem necessitar de proceder a diversas tentativas erro para determinar os parâmetros ótimos dos processos.

Devido à elevada concorrência e sigilo entre os diferentes produtores e fornecedores de papel *tissue*, existem poucas pesquisas e publicações relacionadas com a produção e seu impacto nas propriedades finais destes tipos de produtos de papel *tissue*. Esta tese, mostra alguns avanços que se fez e que se tem feito nesta área de pesquisa, pois a maioria dos estudos aqui referenciados são muito recentes o que indica uma ligeira abertura da indústria em criar parcerias para aprofundar estes impactos mecânicos nas propriedades dos produtos acabados.

Palavras-chave

Absorção; Comportamento Mecânico; *Converting*; *Embossing*; Método Elementos Finitos; Papel *Tissue*; Perfuração; Propriedades; Suavidade.

Folha em branco

Abstract

Tissue paper is truly rooted in the daily life of modern society due to the wide variety of products that make different applications possible. For this type of industry, it is a huge challenge to produce the best products to retain the final consumer. Tissue paper is a paper characterized mainly by its low grammage and tensile strength, and by its high softness, liquid absorption, and elasticity. Depending on the product segment to be produced, it is necessary to consider which of these characteristics are essential, for example, in toilet paper the focus is on softness and absorbency, in kitchen rolls it is on absorbency and wet strength, softness on napkins, absorption and wet strength and softness on facial tissues. These properties must be adapted to meet end consumer requirements, which vary greatly for the different countries in the world. The tissue paper production process uses virgin cellulose as the main raw material and involves two steps: the formation of the tissue paper sheet itself (tissue base paper) and its transformation into different types of finished products. This work essentially addresses this second stage, where the transformation of tissue base paper into finished products takes place and its impact on the properties of the products produced. During the tissue paper base sheet transformation process, also called the conversion process, the properties acquired in the previous step are altered, as the sheet is subjected to successive operations that will permanently deform it. The converting machine is characterized by several operations, the main ones being winding/unwinding, embossing/laminating, perforating, cutting, packaging, and palletizing. The converting process proves to be very complex and has a huge impact on the properties of the finished tissue paper. Embossing is the key operation in the tissue paper transformation process, as it is the one that most affects the final properties of the finished product. This operation consists in marking a pattern on the tissue paper base sheet by applying pressure, with the purpose of producing papers that are more appealing to the final consumer and/or being a mean to recognize a brand. In addition to visually affecting the paper, it also affects the final properties of the finished products, adding a more pronounced third Z dimension with a compression matrix, increasing its liquid absorption capacity and volume, but, on the other hand, reducing its softness and tensile strength.

Since embossing is the most impacting operation in the transformation of tissue paper and taking into account the industrial embossing process, a system was developed that would allow the study on a laboratory scale of the impact of this operation on the

physical-mechanical properties of tissue paper, depending on the different operating parameters of the converting machine, such as the finishing of the dots and/or lines of the embossing pattern, hardness of the embossing rubber, pressure, temperature and humidity, both on laboratory sheets (isotropic handsheets) and on industrial base tissue paper (anisotropic and creped sheets). As this laboratory set-up makes it possible to control all the operating parameters individually, it was possible to optimize the embossing process at a laboratory level and its validation was carried out using the finite element method. Thus, for each new unique standard that the tissue paper industry intends to implement, they can test it in the laboratory before making the scale-up.

Using the laboratory embossing system, we started by studying how pressure affects the main properties of tissue paper. Industrial base tissue paper sheets were used and an optimum pressure of 2.8 bar was achieved for this system. It was possible to distinguish two effects that occur in the tissue paper sheet during the embossing operation with pressure, the densification of the sheet and the permanent deformation of the sheet with the mark of the pattern. The effect of pressure when densifying the paper sheet gives it a gain in mechanical strength, but without differences in terms of liquid absorption. The two embossing patterns (deco and micro) showed different behaviors with the effect of pressure, but both showed losses in both mechanical properties and softness. These losses were less pronounced for the pressure 2.8 bar since the densification is maximum for this pressure. On the other hand, the finite element method failed to show how pressure affects paper strength.

Another operating parameter that also impacts the final properties of tissue products is the influence of the hardness of the rubber used in the counter-roller to the embossed steel roll with an engraved pattern. Three different configurations of stacking rubber plates with different hardness on sheets of industrial tissue paper were studied. This study allowed us to conclude that to obtain greater softness, the best solution was where two rubber plates with different hardness were used, and the rubber plate with greater hardness was in contact with the tissue paper sheet. This result corroborates the future industrial trend in which the use of rubber rollers in the embossing operation with an inner layer of low hardness and an outer layer of high hardness is pointed out. The finite element method, in addition to validating the results obtained, proved to be a reliable tool to virtually test other configurations, such as, for example, three or more rubber plates with different hardness.

The impact of the geometry of the finishing of the lines and dots of the patterns to be embossed, on the final properties of the tissue paper was another operating parameter object of study. This work was carried out using industrial base tissue paper sheets and it was concluded that although the patterns with straight finish geometry individually presented a higher softness value, when the prototype of a finished product with 2 plies (deco + micro) was assembled, the greater softness was obtained for the round finish geometry. It was confirmed that the softness value decreases with increasing bulk, being more pronounced for the micro embossing pattern. No relevant differences were found in the kinetics of liquid droplet scattering over time, from which it can be inferred that the finish geometry of the lines and dots of the embossing patterns does not affect this property in this type of products. The finite element method also in this case, allowed a better understanding of the effect of the pattern finishing geometry on the tissue paper sheet, and the simulation results matches with the experimental results, showing the same trend where the patterns with round geometry marked more tissue paper sheet than patterns with straight finishing.

The laboratory embossing system was also used to investigate the effect of this converting operation on industrial base tissue paper sheets and handsheets. To evaluate the influence of the embossing patterns, the fiber composition and the creping process, industrial base tissue paper sheets, handsheets produced from a fibrous suspension obtained from the disintegration of the industrial sheet were used as samples (keeping the same fibrous composition) and handsheets produced from a never-dry bleached eucalyptus industrial kraft pulp. The handsheets were produced with a grammage of 17 g/m^2 (grammage similar to the industrial base tissue paper) and not pressed. The results indicated that the embossing process produced more bulky and porous structures, at the expense of losses in mechanical and softness properties, which were more pronounced for the micro pattern than for the deco pattern. The effect of fibrous composition showed that an increase in mechanical properties negatively impacted the softness of handsheets. Handsheets composed of 100% eucalyptus showed greater softness than handsheets whose composition is a mixture of short and long fiber. It was found that the crepe existing in the sheet of industrial base tissue paper, gives it a high elongation capacity that is practically non-existent in the handsheets. Furthermore, due to this operation, industrial paper samples have a higher apparent porosity than handsheets samples. The analysis by the finite element method allowed the validation of the experimental results, proving that the micro pattern has a higher stress field value and, consequently, a lower mechanical strength.

In addition to the use of the laboratory embossing system and to deepen the impact of embossing on the properties of finished tissue products, other studies were carried out on industrially and commercialized finished products. The absorption capacity, also being a fundamental property of tissue papers, was one of the studies developed. In this work, the absorption capacities of four different industrial base tissue papers were compared, as well as the respective 2-ply industrial toilet papers that they originated. It was concluded that the embossing operation increased the thickness and, consequently, the bulk of the toilet paper. Furthermore, it was also found that among the various samples of toilet paper there was no perceptible variation in the water absorption time, as the samples presented similar morphology and porosity. However, it was found that where bulk increased the most (about 150%), it resulted in an increase in water absorption capacity (about 60%).

Another important study to deepen the embossing operation was the impact of the sequence of stacking a toilet paper with an odd number of plies (in this case 5 plies). The two possible configurations, 1 and 2 (deco:micro pattern of 3:2 and 2:3 plies, respectively) were the object of study. The industrially produced products with both configurations were originated from the same base tissue mother-reels. Overall, the sheet stacking sequence was found to influence the properties of the finished toilet paper. For configurations 1 and 2, after the embossing process, bulk increases of 46% and 40%, respectively, and water absorption capacity increases of 2% and 17%, respectively, were recorded. Regarding the mechanical properties, both configurations had a greater negative impact caused by the deco embossing pattern. For commercial purposes and to meet the preferences of the final consumer, toilet paper with configuration 1 was more suitable for mechanical strength preferences and toilet paper with configuration 2 was the most suitable for preferences of absorbency. Regarding softness, the stacking sequence also affected the results, where configuration 2 proved to be the smoothest and most pleasant to the touch product, with an overall handfeel value of 75.3 HF, and the product produced with configuration 1 presented rougher and less pleasant to the touch, with an overall handfeel value of 68.0 HF.

Another operation that takes place in the converting machine and which also impacts both the properties of this type of product and the operability of the machine itself is the perforating operation. A system was then developed that would allow a laboratory-scale study of the impact of this operation on the perforation efficiency of the finished products. This perforation system applies to all tissue paper products, such as kitchen paper or toilet paper, that need to be portioned according to the needs of the end consumer. The perforations facilitate this portioning, promoting the separation of

sheets or services, by the perforation line without tearing them. However, the perforated paper must be strong enough to hold together under a certain tension, but on the other hand it should be weak enough that the sheet or service can be detached from the roll easily, without tearing, with little effort along the straight or patterned horizontal perforated line. This balance is given by the perforation efficiency. The higher the perforation efficiency, the easier the service separation will be. In this context, the developed laboratory perforating system allows testing new types of cuts distances on a laboratory scale, allowing the results to be transposed to an industrial scale, and allows to evaluate problems associated with the perforation of products, as well as testing new cutting patterns.

As customer satisfaction can depend on the perforation performance, the laboratory perforation system was used to perforate different commercial toilet papers (in brands and number of plies) to evaluate their perforation efficiency. With this study, it was verified a stabilization of the perforation efficiency from a cut distance of 6 mm and a 15% increase in the cut distance for the laboratory blade to correspond to the industrial perforation efficiency. The finite element method was also used to simulate the progression curve of perforation efficiency as a function of cut distance. This analysis confirmed the behavior of the evolution of the perforation efficiency with the increase of the cut distance and its stabilization from the cut distance of 6 mm.

Another study with interest to understand the impact of perforation was its evaluation in commercial toilet products. In this work, the mechanical behavior of 15 commercial toilet papers from different European producers, with equally different compositions and number of plies, was studied. A qualitative analysis of the quality of the cuts, together with a quantitative analysis of the dimensions of the same cuts, was performed through an optical system. An analysis using the finite element method was carried out where it was possible to examine the behavior of the stress concentration in the cut hole and the influence of the cut distance. The results showed that a cut distance equal to or less than 2.0 mm should not be used in these types of papers, and the perforation efficiency increased with the increasing of the cut distance, regardless of the number of plies that make up the toilet paper. The stress concentration factor was also determined and a limit value of 0.11 was reached. Toilet papers to tear at the perforation line, as desired, need to have a stress concentration factor above this limit value.

Resuming, it is in the converting machine where value is added to tissue paper products, which is why these machines are constantly evolving. At the beginning of the tissue paper transformation, the paper was rewound by hand on a mandrel and when

the first semi-automatic machine appeared, only a few LOGs were wound per minute. Currently, product design plays a very important role, as in addition to its apparent sophistication, it is also the key to optimizing its properties. Therefore, more and more products are embossed and printed, and design patterns are constantly changing and optimizing. Due to market demands, the adaptability of this type of machine and its rapid updating is imperative for the producer, as meeting the requirements of the final consumer is his main motivation. The fact that the automation of the converting machines goes all the way to the end of the line (palletization), allows the producer to better control the quality and price of the product he presents to the consumer, who, in the last analysis, has a greater probability of success for the producer who have the right products that reflect the needs and wants of customers. The advantage will be found in producers who use the latest technology, because with the slowdown in the economy, products will have to be redesigned to find a lower price, which means making an additional effort to produce the products at the lowest cost possible as well as lowering the cost of transportation through distribution channels. This work thus helps the producer to optimize the operating parameters along the converting machine, pointing out some modifications, such as replacing the single hardness rubber roller with one of variable hardness, or finding the optimal pressure of the machine in which the resistance mechanics is maximized, and that when implemented will improve the quality of the product produced, adding value.

The digital twining of the various converting processes, presented here by the finite element method, proved to be a reliable modeling tool to test changes that are intended to be introduced in the process, virtually and with reduced costs. This procedure is a trend in the near future, because it allows optimization in a digital environment, without having to make several attempts and errors to determine the optimal parameters of the processes.

Due to the high competition and secrecy between different tissue paper producers and suppliers, there is little research and publications related to the production and its impact on the final properties of these types of tissue paper products. This thesis shows some advances that have been made in this area of research, since most of the studies referenced here are very recent, which indicates a slight opening of the industry to create partnerships to deepen these mechanical impacts on the properties of finished products.

Keywords

Absorption, Converting, Embossing, Finite Element Method, Mechanical Behavior, Perforation, Properties, Softness, Tissue Paper.

Folha em branco

Index

Chapter 1 – Thesis Framework 1

1. Objectives 1
2. Thesis organisation 2

Chapter 2 – State of Art 3

1. Article I - Converting Operations Impact on Tissue Paper Product Properties – A Review 4

Chapter 3 – Embossing Study 25

1. National Patent I Draft – Laboratorial Embossing System (Sistema Laboratorial de *Embossing*) 29
2. Article II – Embossing Pressure Effect on Mechanical and Softness Properties of Industrial Base Tissue Papers with Finite Element Method Validation 48
3. Article III – FEM Analysis Validation of Rubber Hardness Impact on Mechanical and Softness Properties of Embossed Industrial Base Tissue Papers 63
4. Article IV – Embossing Lines and Dots Geometry Effect on the Key Tissue Paper Properties with Finite Element Method Analysis 85
5. Article V – Mechanical and softness characterization of “deco” and “micro” embossed tissue papers using finite element model (FEM) validation 103
6. Article VI – Impact of embossing on liquid absorption of toilet tissue papers 121
7. Article VII – Impact of 5-Ply Toilet Paper Configuration on Its Mechanical and Absorption Properties 132

Chapter 4 – Perforation Study 144

1. National Patent II Draft – Laboratorial Perforation System (Sistema Laboratorial de Perfuração) 146
2. Article VIII – Toilet Paper Perforation Efficiency 159
3. Article IX – Mechanical Behavior of Toilet Paper Perforation 171

Chapter 5 – Conclusions 187

1. Main Achievements 187
   - 1.1 Development of embossing system 187
   - 1.2 Impact of the embossing process on tissue paper products 187
   - 1.3 Development of perforation system 189
   - 1.4 Perforation efficiency evaluation 190
2. Contribution of the Study 190
3. Directions of Future Research 191

Appendix 192
Appendix A – Additional Studies 193
A1. Article X – Experimental dataset supporting the physical and mechanical characterization of industrial base tissue papers 195
A2. Article XI – Characterization of absorbency properties on tissue paper materials with and without “deco” and “micro” embossing patterns 203
A3. Article XII – Influence of Tissue Paper Converting Conditions on Finished Product Softness 218
Appendix B – Conference Presentations 231
B1. Abstract I – Embossing Pressure Effect on Mechanical and Softness Properties of Industrial Base Tissue Papers with Finite Element Method Validation 232
B2. Abstract II – Embossing Influence on the 3D Structure and Key Properties of Tissue Paper 237

Folha em branco

Lista de Figuras

Chapter 1
Figure 1 – Flow diagram of the thesis 2

Folha em branco

Acronym List

3D	Three Dimensional
AD	Anno Domini
CCD	Charged-Coupled Device
CD	Cross Direction
CED	Cupriethylenediamine
C-MAST	Center for Mechanical and Aerospace Science and Technologies
DCT	Dry Crepe Technology
DPv	Polymerization Degree
ERDF	European Regional Development Fund
EU	European Union
FCT	Fundação para a Ciência e Tecnologia
FEM	Finite Element Method
FibEnTech	Fiber Materials and Environmental Technologies
HCL	Hydrochloric Acid
HF	Handfeel
IPE	Isotropic Plasticity Equivalent
ISO	International Standard Organization
JP	Japan
MD	Machine Direction
NaCl	Sodium Chloride
$NaHCO_3$	Sodium Hydrogencarbonate
NEST	Point-to-Valley
PTP	Point-to-Point
QA I	TSA algorithm for base tissue paper
RAIZ	Forest and Paper Research Institute
SEM	Scanning Electron Microscope
TAD	Through Air Drying
TP II	TSA algorithm for tissue products
TSA	Tissue Softness Analyser
UBI	Universidade da Beira Interior
USA	United States of America
VUMAT	User explicit subroutine to define mechanical constitutive behavior of a material
WRV	Water Retention Value
^{o}SR	Schöpper Riegler Degree

Folha em branco

Chapter 1 – Thesis Framework

1. Objectives

The main objective of this study is to investigate the impact of converting operations, namely embossing and perforation, on the final properties of tissue paper products. By understanding how the key properties of tissue products behave with the operating conditions, it is possible to optimize and improve the quality of the produced products. In order to achieve this main objective, this study was subdivided into 4 different tasks:

1. Develop a laboratory embossing system that would allow evaluating the impact of each of its operating conditions, namely, pressure, rubber hardness and finishing geometry of the lines and dots of the embossing patterns, on the key properties of the finished products;
2. Evaluate the behavior of the properties of finished products, both industrially and laboratory processed;
3. Develop a laboratory perforation system that would allow evaluating the impact of each of the cut distance on the perforation efficiency of the finished products;
4. Evaluate the mechanical behavior of the perforation efficiency of finished products, both industrially and laboratory processed.

2. Thesis organisation

This thesis is composed by 5 chapters, being Chapter 1 the one that presents the objectives and structure of the document. Chapter 2 highlights the research topic, through an extensive literature review and which is presented by an invited peer-reviewed review article (submitted) by the scientific journal BioResources. Chapter 3 addresses the first two tasks of the main objective, namely the study of the impact of embossing and its operating conditions on the properties of finished tissue products. This chapter is composed by a patent (in preparation) referring to the laboratory embossing system developed and 6 peer-reviewed scientific articles, of which the first 3 refers to the individual evaluation of the embossing operating conditions (pressure, rubber hardness and finishing geometry of the lines and dots of the embossing pattern, respectively), the fourth compares the properties in handsheets and industrial base tissue paper sheets, the fifth presents the impact of the embossing on the absorption capacity and finally the sixth is related to the impact of the embossing with the stacking sequence in the embossing patterns in a finished product with an odd number of plies (case study 5 plies). Chapter 4 focuses on the other two tasks of the main objective, namely the study of the impact of cut distance on the perforation efficiency of finished tissue products. This chapter is composed also by a patent (in preparation) alluding to the developed laboratory perforation system and 2

peer-reviewed scientific articles, where the first article makes a comparison between laboratory and industrial perforation and the second article evaluates the perforation efficiency of commercial tissue products. Chapter 5 sets out the main conclusions reached with the carried-out work, what contributions these studies can make to the industry and points out directions for future investigations in this area of study. In summary, the main body of this thesis comprises a total of 2 patents and 9 articles. Figure 1 presents the flow diagram of the structure of this thesis.

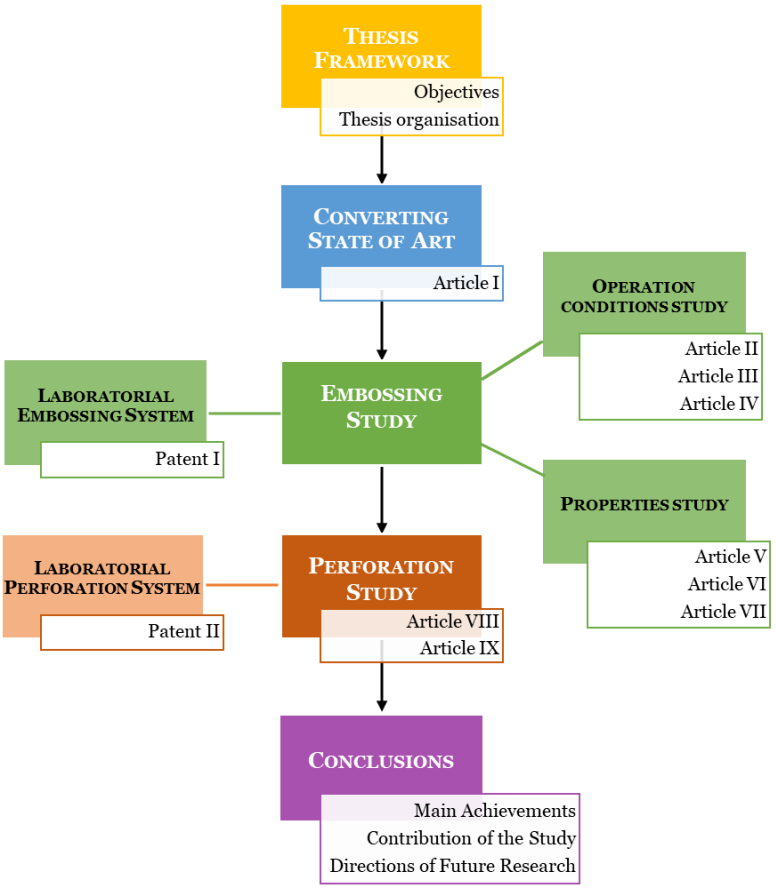

Figure 1 – Flow diagram of the thesis

In addition, three other auxiliary studies to this work were developed and published and are presented in Appendix A. Some results of this work were presented at two renowned international conferences, whose abstracts can be found in Appendix B.

Chapter 2 – State of Art

1. Article I - Converting Operations Impact on Tissue Paper Product Properties – A Review

Vieira, J.C., Fiadeiro, P.T., Costa, A.P.
BioResources, 2022 (submitted 16/09/2022)

A review of literature provided in Article I identifies the different mechanical causes that affects the final tissue paper product properties in the converting machine. This extensive review of literature also identifies the different components of the converting machine and what happens and how those affect the paper in each one. Additionally, it delivers an overview of the research and development that has been made related to this area of study. From this review, a detailed understanding of the converting machine is achieved and pointed out that the embossing and perforation sections are the ones that affects more the tissue paper properties. On the other hand, due to the lack of publications it was challenging to carry out this work, but it was also a motivation to carry on this investigation.

The overall contribution in Article I of Joana Costa Vieira was 90% to the concept development, analysis, drafting and revising the final submission; Paulo Torrão Fiadeiro and Ana Paula Costa contributed in reviewing, editing, and providing important technical inputs by 5%, respectively.

Converting Operations Impact on Tissue Paper Product Properties – A Review

Joana C. Vieira*, Paulo T. Fiadeiro, and Ana P. Costa

Tissue paper is deep-rooted in the daily life of modern society due to its different types of products that allows various applications. The challenge of reaching the best products for the final consumer is noteworthy. Tissue paper is a low grammage paper that is mainly characterized by its softness, tensile strength, liquid absorption, and elasticity. These characteristics are essential when producing products for domestic use such as toilet paper, kitchen rolls, hand towels, napkins, and facial tissues. The tissue paper production process has virgin cellulose as its main raw material and involves two stages: the formation of the tissue paper sheet itself and its transformation into different types of finished products. During the tissue paper sheet transformation process, also called the converting process, the properties acquired in the previous stage change, as the paper is subjected to different operations that will permanently deform it. Converting is characterized by several operations, the main ones are unwinding, winding, embossing, laminating, perforation, cutting, packaging, and palletizing. Embossing consists of marking a pattern on the paper sheet by applying pressure, with the intent to produce papers that are more aesthetically pleasing to the final consumer and/or a mean to identifying a particular brand. Embossing, in addition to visually affecting the paper, also affects its final properties, increasing the liquid absorption capacity and its bulk, but on the other hand, reduces its softness and tensile strength. The gluing of the layers sheets is called lamination and occurs simultaneously with the embossing operation. After the embossing and lamination operations are completed, the sheet passes through two blades in the transverse direction where it is perforated and sent to the winder. In the winder, the sheet is rolled into a cardboard tube, forming the LOG. The LOG's are directed to the cutter where the smallest rolls are obtained with the desired dimensions. These rolls are then packaged and palletized to be sent to the distributor. The converting process proves to be very complex and has a huge impact on the finished tissue paper properties. In this review, the authors intend to explore into the different steps of converting and how they impact the different properties of finished tissue paper products.

Keywords: Converting operations; Embossing; Finishing; Paper properties; Perforation; Tissue paper; Winding

Contact information: Fiber Materials and Environmental Technologies (FibEnTech-UBI), Universidade da Beira Interior, R. Marquês D'Ávila e Bolama, 6201-001 Covilhã, Portugal.
**Corresponding author: joana.costa.vieira@ubi.pt*

INTRODUCTION

The tissue paper market has been expanding worldwide, explained by the increase in the consumption of hygiene products because of the increase in quality-of-life standards. The main tissue paper products that can be find on the market include paper towels, napkins, facial tissues, and toilet paper, and they play an important role in modern life. These tissue paper products contribute to improving hygiene, comfort, and convenience in our society, helping to reduce the spread of disease. Figure 1 presents the graph of evolution and forecast of consumption for domestic and sanitary tissue paper products, based on the data published by Lamberg et al. (2012), in the ten global regions considered.

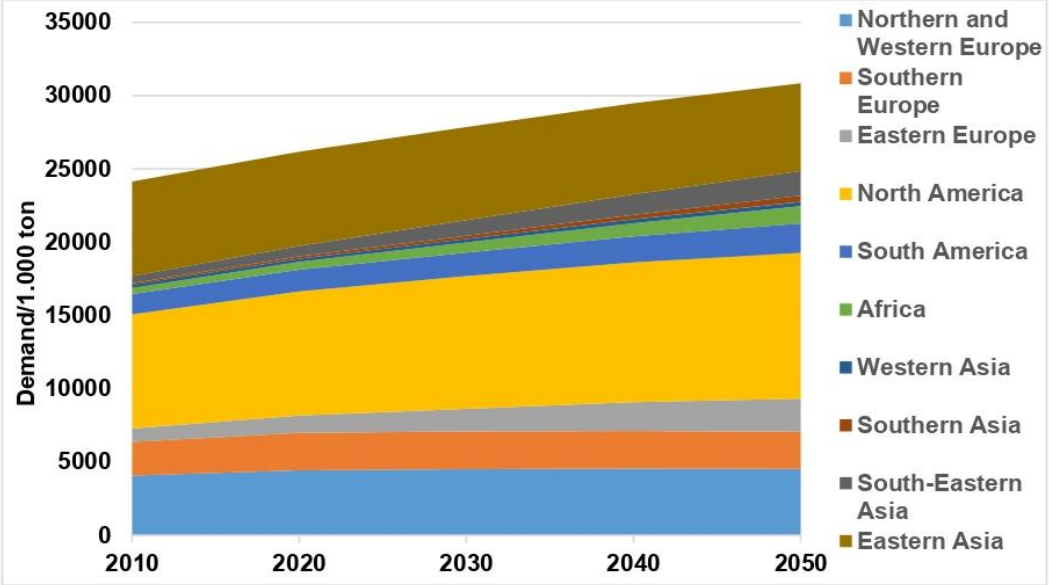

Fig. 1. Evolution and forecast of consumption for domestic and sanitary tissue paper products in world regions between 2010 and 2050.

From the analysis of Fig. 1, it is relevant to point out that the consumption of tissue paper products in developed countries is more or less stable, while for developing countries, there is room for greater growth in this type of products. Figure 2 shows the growth rates pie chart of the main types of domestic and sanitary tissue paper products, based on the data published by Lamberg et al. (2012), in the global regions considered.

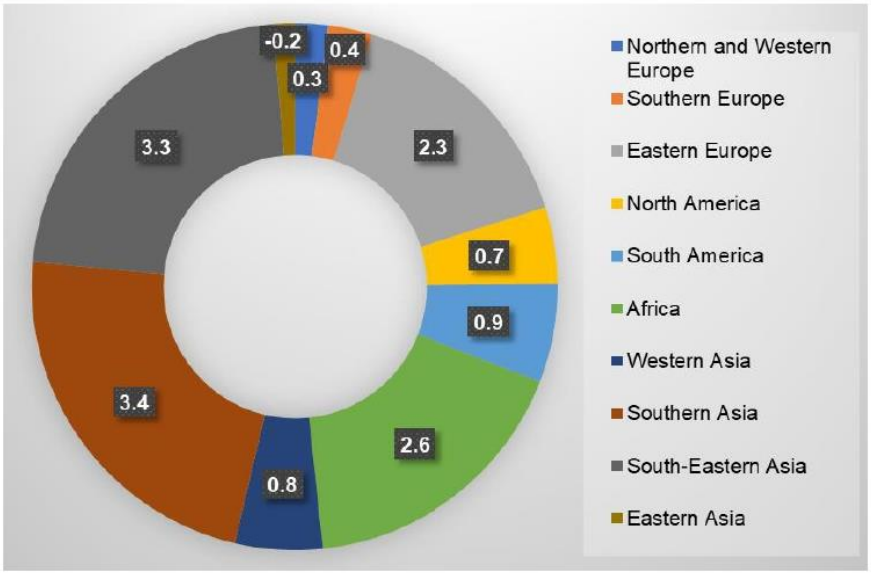

Fig. 2. Growth rates of major types of household and sanitary tissue paper products in world regions.

Figure 2 confirms the growth trend in consumption of this type of products, apart from Eastern Asia, where there is an inverse trend. The growth in demand for these products has led to an increase in the number of producers to satisfy the market and make it more competitive. For companies to achieve a competitive advantage, they are constantly looking for continuous improvement, optimization of production processes and reduction of operating costs, in order to increase product quality levels and satisfy customer requirements. An important factor in the tissue paper market segment is customer satisfaction, who look for softness as a main property in certain products or absorbency in others, depending on their final purpose. Thus, the properties of tissue paper must be in accordance with consumer requirements (see Fig. 3). Tissue paper can then be defined as a cellulosic-based product composed of virgin and/or recycled fibers, produced with a low grammage, high flexibility, high bulk, creped and depending on its application (toilet paper, paper towels, napkins), embossed (Galli 2022; Vieira et al. 2020). Commercially, tissue paper products can be classified according to the purpose of use both at home (referred to as "consumer" or At Home – AtH products) and/or in public places (referred to as HORECA products - HOtel REstaurants and Coffee, or Away From Home – AFH) (Galli 2022).

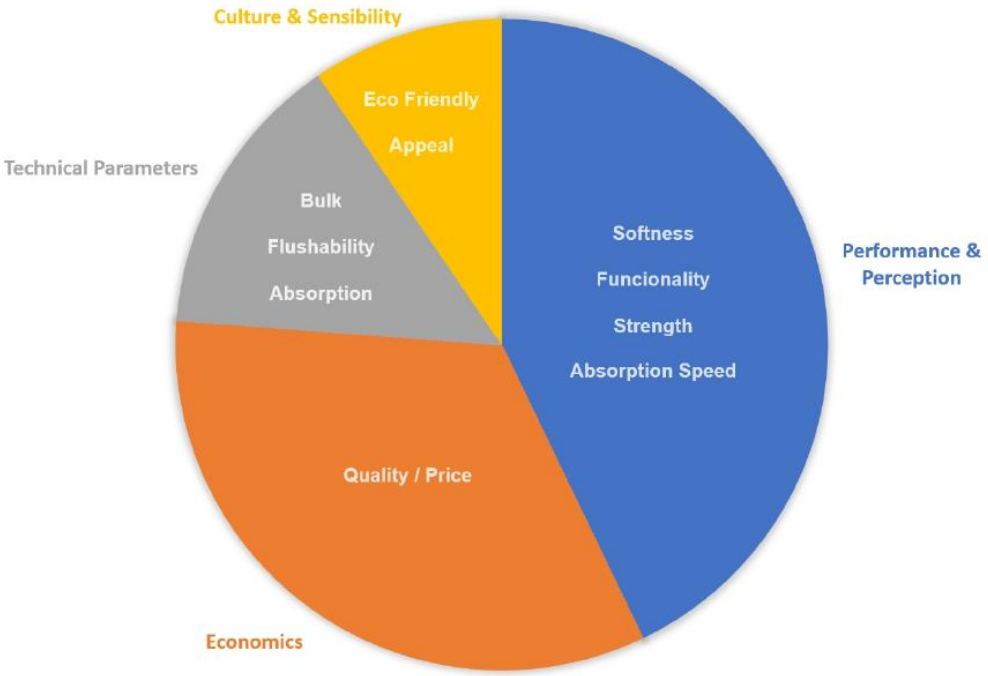

Fig. 3. Factors that affect tissue paper product consumer requirements.

It is through tissue paper conversion technology that, based on the requirements determined by the consumer, it is possible to produce finished paper products with the desired special properties and of high quality (Kimari 2000; Spina and Cavalcante 2018). The tissue paper converting process is characterized by several operations, being the main ones: unwinding, winding, printing, laminating, perforating, cutting, packaging, and palletizing (Cigolini and Rossi 2004; Kimari 2000). Products can be divided into two

groups: rewound products such as kitchen rolls and toilet paper as they are unrolled and rolled up in the conversion process and folded products such as napkins and handkerchiefs. The sequence of the converting operations for the rewound products can be seen in Fig. 4 and for the folded products in Fig. 5.

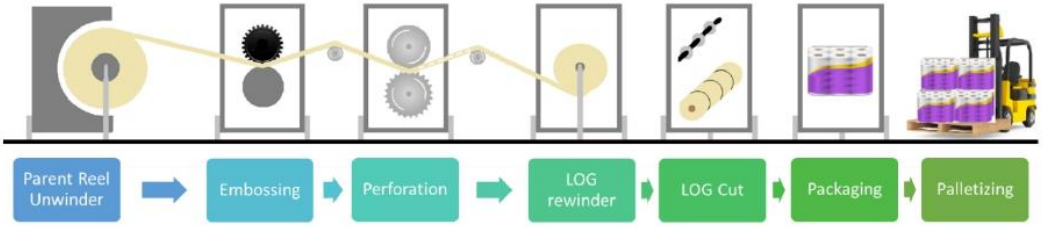

Fig. 4. Processes involved in converting the paper reel to the finished rewound products.

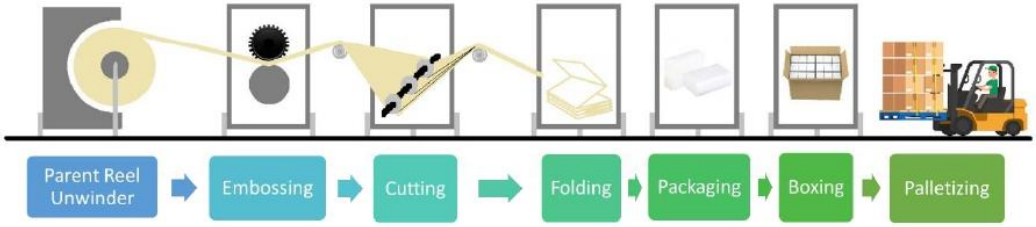

Fig. 5. Processes involved in converting the paper reel to the finished folded products.

Paper converting technology needs to deal with all these requirements to give paper products special properties. One of the most important aspects to face during paper converting is the control of the production process, due to its nature as a continuous process. In fact, modern paper machines cannot operate efficiently without strict quality control of products and processes. One way to perform the quality control by analyzing process problems and automatically recommend effective corrections is the implementation of a program and the corresponding procedures for the monitoring of paper converting operations, including the laminating of paper sheets. The paper properties are monitored by a set of actuator arrays, which act perpendicularly to the direction of movement of the paper sheet passing through the machine. Controller feedback is tailored to provide performance, ensuring robust uncertainty modeling. Basically, it is important to use both offline and online analyzes to define the characteristic product and process properties to guarantee the high quality of the final product (Spina and Cavalcante 2018). In order to better understand the converting process and how it impacts on the properties of the final product, a detail analysis of each the involved operations separately are addressed in the following sections.

Unwinder

In the tissue paper industries, winders and rewinders are key components in the first stage of the complex converting process. Winding, unwinding, and then rewinding on a spool are, in fact, operations that require a precise execution to obtain a final product that,

once wound, maintains the characteristics and quality resulting from the production process. This is due to the delicate nature of the material itself and the need to preserve the creping and density obtained in the production process to maintain the softness and bulk that distinguish it (D'Olivo 2021; Pejic 2016). The unwinders are responsible for unwinding the Parent Reel that leaves the tissue paper machine to obtain finished reels with smaller dimensions, the Mother Reels, if necessary. The reels used in tissue paper converting are generally very heavy. It is possible to use coils with a length of two to five meters and a diameter of up to about three meters, with weights that can reach 5 tons (Paolinelli et al. 2022). The tissue paper converting machine may need up to four unwinders, as the final product is made up of several sheets. If the number of sheets of the finished product exceeds the number of unwinders, in rewinders outside the converting machine, a Mother Reel with multiple sheets will be created. For example, in a converting machine with two unwinders, to produce a finished product of 3 sheets, you will have to feed the machine with a Mother Reel of 2 sheets and another with 1 sheet (Paolinelli et al. 2022). For tissue paper reels, the unwinding itself takes place by means of motorized belts, called peripheral unwinding. Each material has certain properties and characteristics that will affect the correct winding and/or unwinding process. An incorrect or inaccurate rewinding/unwinding process can cause permanent damage to the tissue paper sheet, where excessive elongation of the wound material implies substantial loss of desired characteristics such as crepe and bulk (A.Celli Group 2022; D'Olivo 2021).

Sheet tension control during the unwind/rewind operation is very complex and subject to many variables. However, it is important to obtain proper control of the spool tension to avoid defects and compromise the properties of the sheet of paper. In addition, high-quality, automated tension control of the sheet is dependent on the traction provided by the machine's idler rollers. It is important to find out the reasons behind the production problems in this section of the converting machine. That said and knowing that winding defects occur less than 5% of the time, Table 1 presents the most common problems and the respective solutions that may occur (Williams 2019).

Table 1. Problems and respective solutions that may occur in the unwinding/rewinding operation (Williams 2019).

Troubleshooting	Illustration	Problem	Solution
Offset Core		Abrupt shift in location along the edge of the roll.	The web should be wound uniformly, but faster at the start of the roll.
Concave or Convex Rolls	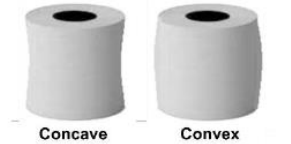	Caused by progressive roll edge misalignment. Only noticed after the roll has started to be unwound.	Controlling the hardness of the wind, reducing web tension, or reducing cross-deckle caliper variation.
Crushed Core		The core has been mishandled or was incorrectly inserted into the shaft.	Paper core restorer (only restore the ends of the roll).

Poor Start	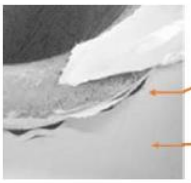	Appearance between the web near the core *vs* Appearance of the remaining roll.	The web needs to be tightened before attaching to the core. Must use good quality cores and properly stored or start with proper tension, nip and/or torque.
Edge Curl		Revealing curled or shaggy paper edge.	Slitters should be adjusted to a proper depth or reducing sheet tension.
Baggy or Slack Ends	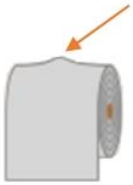	Web width is not uniform, loose, and tight zones will occur across the entire width of the sheet. This lamination defect can cause difficulties in subsequent operations.	They are a result of non-uniform web thickness and cross-deck gauge variation needs to be kept to a minimum. Wind as smoothly as possible and adjust the clamp accordingly.
Machine Tension Burst		Defects are related to fiber separation. In the case of cross-machine the defect is not visible at the edge of the roll, whereas full machine-direction it is.	The roll needs to be wound softer. Partial breakdown of tension in the machine direction can be caused by non-uniform variation of the transverse clamp, needs to be minimized.
Dished Rolls		Rolls that are wound with a forward edge misalignment.	Cores hardness does not increase during winding, and have a good, hard start at the core.
Trim Wound in Rolls		When winder trim is not collected properly into the trim removal system, it will follow the web into the winding roll.	The air velocity at the system inlet must be greater than the winding velocity, or make sure that the displacements are not greater than the width of cut.
Starred rolls		Rolls have a star pattern at the ends of the rolls it is due to the shifting of the layers of web, usually beginning at or near the core and continuing outward toward the outer wraps.	Start wind tight then steadily soften roll hardness as diameter increases. Also, make sure the cross-caliper variation is at a minimum.

In the case of an automatic unwinder in which the spool is unwind through a combination of a peripheral and a central unwinder, when the finished spool is lifted by motorized counterpoints of the central unwinder and placed on top of the unwinding station, to be later removed. Thus, by means of a shuttle it is possible to insert a new spool into the unwind station. The central unwinder is double and has two pairs of tailstocks, thus allowing the first pair of tailstocks to be in the upper position when a spool is running low, while the second pair of tailstocks is available to engage the new spool inserted by the shuttle. In combination with the peripheral unwinder, it then allows the start of the unwinding of the sheet (Paolinelli et al. 2022). The tissue paper sheet is then routed to the embossing section for both types of products and lamination in the case of rewound products.

Embossing / Lamination

Embossing processed tissue paper products is a sensitive process due to the presence of different factors such as flexibility, weight, softness, and attractive design of the paper (DeMaio and Patterson 2008; Pejic 2016). Therefore, several aspects of processing need to be addressed with control methodologies. Product quality also depends on various physical parameters such as temperature, humidity, and pressure. The influence of geometrical and material parameters on the mechanical response of fibers used in papermaking is also critical (DeMaio and Patterson 2008; Kimari 2000). Embossing is an example of compressive formation on paper in the converting process. These can be stamped to increase the properties of the finished product, such as: liquid absorption capacity, and softness. This process can produce papers with aesthetically pleasing designs, occasionally for the purpose of product identification distinguishing them from other competitors. Embossing takes place by layers, on top of one or several layers of a multi-layer paper, deco recording, and on the bottom, a micro-engraving of one or several layers of a multi-layer paper. The resulting product with more than one layer, has properties that cannot be obtained in a paper with a single constituent layer (Digby 2012).

Embossing patterns for tissue papers serve to improve several properties such as porosity, hygroscopicity, thickness/bulk, flexibility, and absorbency. Embossing creates a graphic element allowing drawings to be raised or depressed on paper. A metallic cylinder (embossing roll) with a relief image engraved on its surface is pressed against the sheet(s) of paper (see Fig. 6).

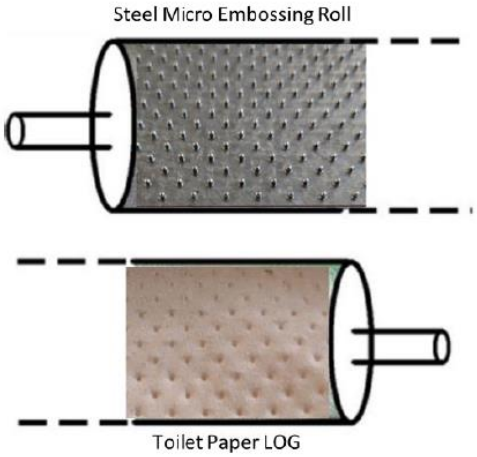

Fig. 6. Example of a steel embossing roll and its toilet paper LOG.

Currently, several types of embossers are used, and the pressure, rubber hardness, temperature and humidity of the paper can be varied to obtain different products (Biagiotti 2017; DeMaio and Patterson 2008).

During tissue paper production, the greatest bulk loss usually occurs in the pressing stage. Therefore, in the transformation process, the most common method that is used to increase bulk is dry embossing, but depending on the pressure used in this step, the bulk created can be short-lived, and can also be lost when tissue paper is wetted again (Janda 2017). Each tissue paper fibrous composition has a predetermined limit to the embossing pressure, beyond which the strength properties of the sheet are destroyed and consequently impair the runnability of the converting machine, and/or the quality requirements of the finished product. Thus, the tissue paper sheet loses engraving marks if embossing takes place in its elastic zone. On the other hand, if the embossing is produced close to the breaking point of the sheet (excessive pressure applied), the paper becomes fragile, which can cause failures in the converting process (Assis et al. 2018; Giannini 2019). As embossing is a mechanical compression process in the tissue paper converting, the pressure used is an operating condition that is essential to control to produce quality toilet paper (Spina and Cavalcante 2018). From the work developed by Vieira et al. (2022a), it was shown that the mechanical properties suffer a negative impact with the embossing operation. In addition, the micro embossing pattern was shown to have a greater impact on thickness, increase in volume and loss of mechanical properties. From another study developed by Vieira et al. (2022b), the authors concluded that there is an optimal pressure for the embossing process, in which the mechanical strength properties are maximized (through the densification of the tissue paper sheet) without impacting too much on the softness and absorption value of liquids. This optimum pressure is the limit beyond which the structural degradation of the tissue paper sheet takes place. This study is in line with the previously mentioned in which the micro pattern is the one who most affects the structure of the sheet of paper. On the other hand, from the samples under study, it was possible to perceive that the greater or lesser loss of mechanical properties or softness depends on their fibrous composition.

With the evolution of the embossing and lamination process, different solutions emerged until nowadays, and the most common is the use of an engraved steel roller

working against a roller with a rubber cover that can vary from 45 to 98 Sh-A. The evolution was an increasing of the hardness of the rubber covering, until presently where appear new studies in which the change of the conventional rubber covering is encouraged to the introduction of a double layer covering: an inner layer with low hardness and an outer layer with high hardness (in contact with the tissue paper sheet), with the aim of making the outer layer (surface of the rubber roll) more flexible (Biagiotti 2017). Each type of rubber has its own characteristics and depending on these they can be chosen as they are better for temperature resistance, and/or chemical resistance, and/or abrasion resistance and/or long service life. The rubber of the roll undergoes different stresses with the embossing process. If the rubber hardness value were determined during the embossing process, it would be altered due to the stresses caused both in terms of pressure and temperature. Thus, the performance of the rubber roll will influence the engraving of the embossing pattern and, consequently, the properties of the tissue paper and directly on the final product (Huff and Bell 2005). As demonstrated in the study developed by Vieira et al. (2022c), the highest softness value was found for the double layer solution, with an inner layer of 48 Sh-A (upper layer) and an outer layer in contact with the paper sheet of 60 Sh-A (bottom layer). The results of this work also point out to an increase in softness with increasing rubber hardness for the replication of conventional coverage. The loss of mechanical strength and greater bulk, on the other hand, became more accentuated for the micro pattern and for lower rubber hardness.

The dimensions and the finishing geometry of the embossing elements (lines or points) are a limitation of this process. For example, patterns with thin embossing elements cannot be engraved too deeply as they are prone to tearing the tissue paper sheet. On the other hand, in order to obtain a high-quality embossing pattern engraving, the tissue paper's ability to stretch and adapt to the relief is equally important, which is also a physical limitation. Currently, there are no standardized finishing geometries and/or designs that objectively define the impact they will have on the final properties of the tissue papers/products (Pál et al. 2020). Khan (2021) showed that the mechanical properties of the embossed product were affected both by the density of dots (number of dots/cm^2) of the embossing pattern, as well as by the height of the dots and the angle that the dot makes with the base. Khan (2021) concluded that there is a greater loss of mechanical properties for a higher density of dots, and a greater height of the dots which consequently lead to a greater deformation of the tissue paper sheet. On the other hand, a dot with a higher base angle (cylindrical dot geometry – 90° angle with the base) leads to a lower loss of mechanical properties due to less deformation of the tissue paper sheet. In addition to the work developed by Khan (2021), another study was carried out in this area by Vieira et al. (2022d). In this study the authors showed that the finishing geometry of the line and dots (straight or round) of the embossing pattern has an impact on the mechanical properties and softness of the products. The finishing of the straight embossing elements showed a higher softness value when evaluated individually. When mounting the 2-ply prototype of the deco and micro patterns, with the same finishing, the greatest softness was obtained for the prototype with the round finishing geometry. As the micro pattern is the one that most impacts the structure of the paper, obtaining greater bulk, it is with this pattern that the lowest values of softness and mechanical strength are obtained. On the other hand, within both relief patterns (deco and micro), the straight finishing geometry is the one with the greatest loss of mechanical strength. With this work, in terms of finishing geometry of the embossing elements of the two patterns, the round finishing also stands out, as it doubles the bulk value when compared to tissue paper before embossing.

A tissue paper sheet laminating process presupposes that at least in an engraving NIP of one of the patterns, at least two tissue paper sheets are combined and engraved. So, another factor that can influence the properties of tissue products in this section of converting is the stacking sequence of sheets in a finished multilayer product with an odd number of sheets. In the study developed by Vieira et al. (2020a), two different stacking sequences of a 5-ply toilet paper were analyzed (see Fig. 7), and their impact on their final properties. of the final consumer.

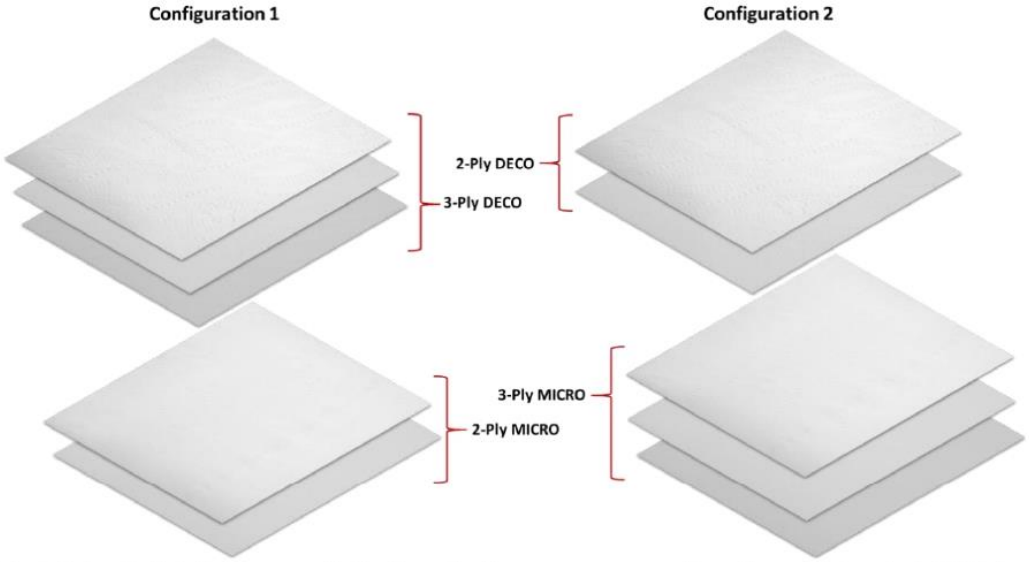

Fig. 7. The 5-ply toilet paper with the two stacking sequence configurations (Vieira et al. 2020a).

Configuration 1 is composed of 3 sheets with deco embossing and 2 sheets with micro embossing, and configuration 2 is composed in reverse. It was found that in configuration 1 the bulk and water absorption capacity increased by 46% and 2%, respectively. While for configuration 2, bulk and water absorption capacity increased by 40% and 17%, respectively. The mechanical properties decreased considerably due to the embossing process. However, configuration 1 showed to be the one with the lowest losses. Regarding softness, the stacking sequence also affected the results, where configuration 2 proved to be the softest and most pleasant to the touch product, with an overall handfeel value of 75.3 HF, and the product produced with configuration 1 presented rougher and less pleasant to the touch, with an overall handfeel value of 68.0 HF (Mendes et al. 2020). Thus, it can be concluded that the number of sheets that enter each embosser in the stacking sequence influences the final properties of the paper and can be adapted to the requirements.

Liquid absorption is a very important property for many tissue products, its main purpose being to clean/absorb liquids. Liquid absorption is generally divided into absorption capacity and absorption rate. The absorbency reflects the maximum amount of water that the paper can absorb, and is expressed in g water/g fiber, while the absorption rate measures how quickly the product absorbs this amount of water (Kullander 2012). In European and International trade, both water absorption time and water absorption capacity represent important parameters in the field of tissue paper product comparison (Tutuş et al. 2016). In the work developed by Vieira et al. (2020b), it was shown that the embossing

operation significantly increases the thickness and bulk of tissue paper. On the other hand, the embossing operation has no impact on the water absorption time when comparing papers with and without any embossing pattern. Regarding the water absorption capacity, the embossing operation proved to have a great impact. It was found that the greater the increase in bulk achieved with the embossing operation, the greater is the water absorption capacity. Currently, the embossing operation is a common step in the tissue paper converting because it creates empty spaces between the sheets of paper and the absorption capacity of the paper increases. Thus, the absorption performance of a multilayer paper is far superior to that of a single-layer (Zhipeng et al. 2022).

The finite element simulation (FEM) was also used by the authors Khan (2021) and Vieira et al. (2022a,b,c,d) whose results validated and corroborated the results obtained experimentally. This tool proved to be useful, as it can allow simulating other studies with different parameters variations, providing approximate results to the real ones.

Within this section, tissue paper decoration also takes place. This decoration can be done by colored glue or by printing. Any of these techniques are coupled to the converting machine as an additional process to embossing/laminating and the result is shown in Fig. 8 (Galli 2022; Star Label 2018).

a) Flexographic Printing b) Color Glue lamination

Fig. 8. Decorated tissue products: a) tissue napkin printing with aqueous flexographic ink, and b) tissue kitchen towel lamination with blue color glue

The most used printing process is flexography, which allows printing at high speed, being suitable for this type of products. In addition, it allows cost-effective, high-quality printing of mass-produced products (Star Label 2018). Ink is transferred to tissue paper from the Anilox roll and through cells etched onto the printing plate (Johnson 2008). To print a porous paper such as tissue paper, it will be necessary to spend more ink, as it penetrates the structure of the paper instead of staying on the surface. Consequently, it will affect negatively absorption, softness, and mechanical properties (Theohari et al. 2014). In lamination with the glue decoration technique, this is replaced by a colored glue that will glue the sheets that make up the final product by the joining dots/lines (Galli 2022). This methodology has a lower impact on the properties of tissue papers than the printing technique. The greater or lesser impact of these decoration techniques on the tissue paper properties are related to the greater or lesser decorated area, for example, a larger decorated area implies a greater impact on the final properties.

Perforation

Perforation in tissue paper products is used for the purpose of facilitating the portioning of paper sheets. The main products in which this process is used are toilet paper, kitchen towels, and facial tissues (Baggot et al. 2006; Ogg and Habel 1992; Pejic 2016; Schulz and Gracyalny 1998).

In the converting machine, perforation takes place at high speed. A roll with several diagonally arranged blades, which will be pressed against the tissue paper sheet, cutting it at the points of contact (Perini et al. 2021). Then, it is created the called perforation line, in which there are bonding areas, uncut areas that prevent the sheet from separating prematurely, and holes with a predetermined cut distance. The distance between two perforation lines determines the length of the "sheet" to be detached by the end consumer (Baggot et al. 2006; Chih 2018; Ogg and Habel 1992). Figures 9 and 10 schematically present these concepts.

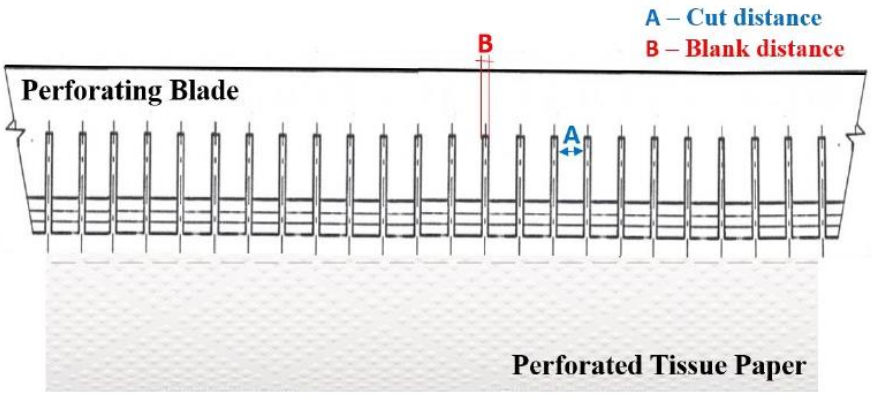

Fig. 9. Perforation scheme with identification of the cut and the connection areas (Vieira et al. 2021).

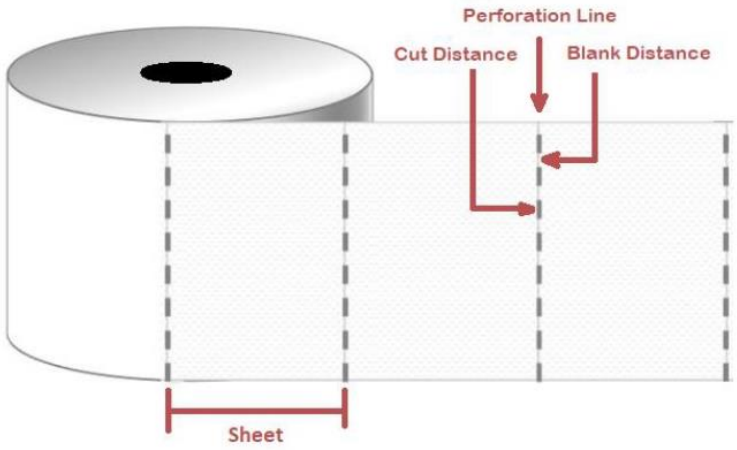

Fig. 10. Schematic of a roll with identification of the perforation lines (Vieira et al. 2022e).

product) (Brown 1991; Guarini et al. 2022; Kimari 2000; Pejic 2016). Both types of saws are always placed perpendicular to the LOG (Brown 1991; Guarini et al. 2022).

This section of the converting machine includes at least one sharpening unit placed on the opposite side of the cut where an abrasive is in contact with the cutting blade. The sharpening units come into operation as soon as the sensors detect the wear of the saw. Periodically the blades must be replaced as the wear and sharpening of the blade progressively decreases both the diameter of the blade and its cutting capacity (Guarini et al. 2022).

The most common problems that can be found due to LOG cutting blades are crushed core caused by increased axial eccentricity and blade distortion due to cutting speed limitation, ragged edges caused by an unadjusted blade life and consequently stoppages for successive blade changes, bias cut caused by poor blade orientation in relation to the LOG (Ahuja et al. 2009), and dirty rolls of dust caused by the maintenance of LOG's saws (Pejic 2016).

In the case of cutting tissue paper for folding, the saws are presented as those of continuous movement for the LOG's, in which they are arranged side by side separated by the distance defined for the dimension of the finished product, as schematically represented in Fig. 4.

Folding

Folding is a typical converting operation for hand towels, facial tissues, napkins, and folded toilet paper. There are two types of converting machines that produce folded tissue paper products: those that fold the paper sheets with vacuum, and those that fold the paper sheets through a folding head composed by a pair of rotating steel cylinders with folding clamps, called the inter-folders. To produce premium products, it is necessary to guarantee a good bending quality as well as a good alignment of the sheets (Yasui 2017).

Regarding the folding itself, there are several types. The most common types of folds are represented in Fig. 11.

Fig. 11. Schematic representation of the main types of tissue paper folds.

The most traditional form of folding is the C-fold. This type of folding is used in low quality products, but it creates an additional difficulty in its usage making the end consumer to take several sheets at the same time, which is more than essential. Then, there is the V-fold, also known as the Zig Zag fold, which is also used in low quality products. With this style of folding, the user can already have a greater control over its use, as it dispenses one sheet at a time. The V-fold type of folding is commonly used in facial tissue products. The most used fold for premium products is the Z-fold. This type of fold provides

controlled use by the user, one sheet at a time being dispensed. The sheets feature a clean cut and open automatically. Finally, the quarter fold (or ¼ Fold) which is the main fold used in napkins. This type of fold does not require a dispenser for its use (Galli 2022; Pearroc Ltd 2022).

Regarding the product marketing, the type of folding can also be used as a way for the producer and the consumer to distinguish the quality of the product and perceive its respective final properties.

Packaging / Boxing

Generally, in converting machines, the packaging section is closed, and production is carried out at high speed, so it is important to have means of detecting the problems that occur in the packaging sequence to solve them as quickly as possible, to guarantee improved quality of the products (Rempel 2022). It is very rare that the packaging process damages the integrity of rolls/stacks of tissue paper, affecting their properties, but sometimes deformation can occur during bagging (Pejic 2016).

Generally, rolled products are stacked with the core vertically, while folded products (without core) are placed inside cardboard boxes. This is due to the fact that during the storage of the pallets, they are often superimposed, so the lower pallet needs resistance to support the upper pallet, thus jeopardizing the integrity of the products. Thus, in the case of products with a core, the resistance is given by the core itself, in the case of products without a core, the resistance is given by the cardboard box in which the products are packed (Galli 2022).

Rewound Products

The tissue paper rolls then arrive at the packaging section. Due to the high number of packaging configurations used for roll tissue products (from single roll packages to multi-packs up to 90 rolls), it is challenging for converting machines to comply with these configuration changes smoothly. On the other hand, it is equally challenging for this type of machine to be adaptable to the material used for packaging, as it is increasingly necessary to consider the sustainability of the materials used (Alberti 2020).

In this section, the rolls are grouped according to the amount predetermined by the machine operator, and then wrapped in a paper sheet for packaging (which can be closed with glue) or in a plastic, which is usually done with polyethylene or bioriented polypropylene (whose packaging is closed using hot air) (Brown 1991; Pejic 2016). Depending on the model of the converting machine, the rolls can be packed in several layers. Each set of rolls that form a layer is lifted and placed on the bottom layer, and so on, until achieve the number of layers predetermined. Then, they are all packed together or bagged (Michelini 2022). Next, these packages can be placed directly stacked on pallets or first in cardboard boxes, and then on pallets to be stored in the finished product warehouse (Brown 1991; Pejic 2016).

Folded Products

After the embossing, cutting and folding process, the stacks of folded paper are sent to the packaging section. These tissue paper stacks, depending on their final application, can undergo various types of packaging. For example, the napkins are packed in a plastic film in predetermined amounts, and then the napkin packs are packed in a cardboard box. Hand towels, on the other hand, are wrapped in a paper or plastic film and then stacked

inside a cardboard box. The packs of facial tissues, with about 8-10 tissues per pack, are packed in a plastic film, which will be perforated, and a self-adhesive label will be glued (creating the opening and closing of the pack), then a predefined group of these packs is placed in a bag and later in a cardboard box for later dispatch (Michelini 2022).

Palletizing

Now that the products are packed, they go to the palletizing section. The main problem that can exist in this section is the fact that the suction cups/robot arms can deform the packages, damaging the product contained therein. In addition to the bad appearance caused in the packaging, this results in a problem for the palletization itself, as deformed packaging takes up more space, reducing the efficiency of packaging stacking. It can also increase the amount of plastic wrap used to close the pallet (Reynolds 2015).

On the other hand, there are deformations that can be purposeful. In Brazil, most of the population goes to the supermarket by public transport or on foot, traveling long distances, and therefore transporting toilet paper is challenging. Also, the apartments are very small, and the toilet paper took up a lot of space. Thus, by packing a set of rolls and then compressing them with the packaging film, this significantly reduces their size, solving the population problem. This packaging method of reducing the size of roll packaging by compression was called *Just One Hug* (Kim and Mauborgne 2021). With the reduction in packaging, the efficiency of palletization was also improved, as a greater number of rolls per pallet could be transported, as shown in Figure 12.

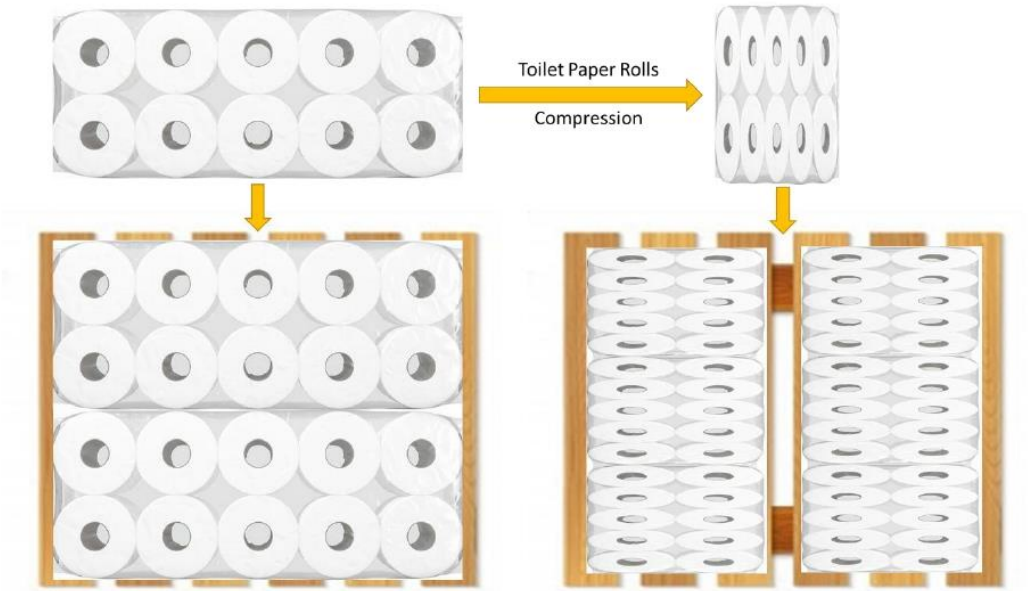

Fig. 12. Schematic representation of rolls packages palletization with and without compression.

In Brazil, cargo is transported mainly by road, and thus, being able to transport more rolls per pallet, caused a decrease in transport costs. With the *Just One Hug* packaging method, there was a drop of around 15% in transport costs and 19% in the amount of packaging material used, reducing the price for the consumer, in addition to satisfying the

packaging dimensions reduction requirements, without reducing the amount of product. As this compression impacts the properties of the finished product, such as bulk and softness, this packaging method was combined with products composed by recycled fibers (lower quality products) (Kim and Mauborgne 2021).

FINAL CONSIDERATIONS

It is in the converting machine where value is added to tissue paper products, which is why these machines are constantly evolving. At the beginning of the tissue paper transformation, the paper was rewound by hand on a mandrel, and when the first semi-automatic machine appeared, it was wound at a few LOG's per minute. Currently, product design plays a very important role, as in addition to its apparent sophistication, it is the key to optimizing its properties. Therefore, more and more products are engraved and printed, and design patterns are constantly changing and optimizing. These machines have become very sophisticated and uninterrupted, being able to be computer controlled and quickly programmed to produce the desired product. The fact that the automation of the converting machines goes all the way to the end of the line (palletization), allows the producer to have a better control of the quality and price of the product he presents to the consumer, who, in the final analysis, has an improved chance of success for the producer who have the right products that reflects the needs and desires of customers. The advantage will be found in producers who use the latest technology, because with the slowdown in the economy, products will have to be redesigned to find a lower price, which means making an additional effort to produce the products at the lowest possible price cost as well as lowering the cost of transportation through distribution channels. Thus, the digital twining of the several converting processes is a modeling tool, because it allows optimization in a digital environment, without having to make several attempts and errors to determine the optimal parameters of the processes (Spirent 2020).

Due to the high competition and secrecy between different tissue paper producers and suppliers, there are few studies and publications related to the production, and its impact on the final properties of these types of tissue paper products, as already observed by other authors (Assis et al. 2018). This review article shows that some progress has been made and that most of the findings referenced here are very recent, which indicates a slight opening of the industry in creating partnerships to deepen these mechanical impacts on the properties of the finished products.

FUTURE DIRECTIONS

1. Within the converting operations, the embossing is the one that have a major impact on the quality of tissue products. For that reason, in a near future, it deserves a special attention in new and innovative research and development methodologies to follow-up the digital transition and fulfill the exigent consumer requirements.

2. The natural evolution of the embossing process tends to go in the direction of change the conventional rubber covering by the introduction of a double layer covering with an inner layer with low hardness and an outer layer with high hardness rubbers.

3. The final quality of the tissue products is mostly related with the patterns and the corresponding finishing geometries of the embossing. It is a challenge to be able to integrate the design of the embossing patterns, the respective type of finish geometry, and the density of the marked area in an automatic procedure that allows to predict the final properties and quality of the final tissue product.

4. Due to market demands, the adaptability of converting machines and their rapid updating is imperative for the producer, because responding to consumer requirements is their main motivation.

5. The digital twining of the several converting processes is an emerging simulation tool that will be a trend in a near future because it will permit an optimization in a digital environment transition.

REFERENCES CITED

A.Celli Group. (2022). "How to maintain the softness and bulkiness of tissue during rewinding", *Papnews*, Italy (Accessed Jun. 23, 2022). https://www.papnews.com/insight/how-to-maintain-the-softness-and-bulkiness-of-tissue-during-rewinding-thanks-to-a-celli-solutions/

Ahuja, R., Graham, D., and Isaacs, T. (2009). "Surface Engineered Log Saws for Enhanced Tissue Conversion Productivity & Quality", International Knife and Saw, Florence, South Carolina, USA, 10. https://www.uctcoatings.com/wp-content/uploads/downloads/2010/06/Tissue-2009-Paper-Final.pdf

Alberti, G. (2020). "Primary packaging: challenges — and solutions — for tissue converters" (Accessed Jun. 23, 2022). https://blog.koerber-tissue.com/primary-packaging-challenges-and-solutions-for-tissue-converters

Assis, T., Reisinger, L., Pal, L., Pawlak, J., Jameel, H., and Gonzalez, R. (2018). "Understand the Effect of Machine Technology and Cellulosic Fibers on Tissue Properties - A Review", *BioResources*, 13(2), 4593–4629. DOI: 10.15376/biores.13.2.DeAssis

Baggot, J., Gropp, R. F., and Wojcik, S. (2006). "System and Method for Severing or Perforating a Web", Patent Nº US 2006/0014616, Greenville, USA.

Biagiotti, M. (2017). "Tissue Embossing Developments | The Tissue Story" (Accessed Jan. 8, 2019). https://www.tissuestory.com/2017/11/21/tissue-embossing-developments/

Brown, S. R. (1991). "Overview of tissue finishing and converting" *Tappi Journal*, Tissue Converting, 91–94. https://imisrise.tappi.org/TAPPI/Products/91/OCT/91OCT091.aspx

Chih, C.-K. (2018). "Perforation Design & Calculation of Toilet Paper Rewinder," *China Pulp and Paper*, 37(9), 38–42. DOI: 10.11980/j.issn.0254-508X.2018.09.007

Cigolini, R., and Rossi, T. (2004). "Improving productivity of automated tissue converting lines: an empirical model and a case study," *Production Planning & Control*, 15(5), 550–563. DOI: 10.1080/09537280412331280921

DeMaio, A., and Patterson, T. (2008). "Similarities in Bonding Influence between Pre-failure Tensile Creep and Stress–strain Behavior of Paper," *Mechanics of Materials*, 40(3), 133–149. DOI: 10.1016/j.mechmat.2007.06.007

Digby, P. (2012). "pd-Tissues - Trees to Paper" (Accessed Feb. 13, 2019). http://pd-tissues.co.uk/trees-to-paper.aspx

D'Olivo, I. (2021). "Problems in Tissue rewinding: how to solve them with our A.Celli E-WIND® T100 Rewinder" (Accessed Apr. 20, 2022). https://www.acelli.it/en/blog/problems-tissue-rewinding-e-wind-t100-rewinder

Galli, E. (2022). "Module 4 - Tissue paper production process and properties," Tecnicelpa Course - Introduction to the paper production process, 6-8 July, University of Beira Interior, Covilhã, Portugal.

Giannini, D. (2019). "Resistance: part IV," *Körber LinkedIn* (Accessed Sep. 8, 2021). https://www.linkedin.com/pulse/resistance-part-iv-dario-giannini/>

Guarini, C., Betti, G., Catalini, A., and Giurlani, G. (2022). "Cutting Machine for Paper Material LOGs with a Sharpening Unit", Patent Nº US 20220176579, USA.

Huff, S., and Bell, J. (2005). "How Do You Know You^{TM}ve Got the Right Cover for Your", AIMCAL Fall Technical Conference 2005 and 19th International Vacuum Web Coating Conference 2005, Myrtle Beach, South Carolina, USA, 8. ISBN 978-1-62276-074-9

ISO 12625-1 (2019). "Tissue Paper and Tissue Products - Part 1: Vocabulary". International Organization for Standardization, Geneva, Switzerland.

Janda, B. (2017). "Sheet Structure Process Effect on Tissue Properties", *TAPPI TISSUE 360º* (Accessed Dec. 13, 2018). https://tissue360.tappi.org/2017/12/28/sheet-structure-process-effect-on-tissue-properties/

Johnson, J. (2008). "Aspects of flexographic print quality and relationship to some printing parameters," Faculty of Technology and Science, Chemical Engineering, Karlstads universitet, Karlstad. https://www.diva-portal.org/smash/get/diva2:5784/FULLTEXT01.pdf

Khan, A. A. (2021). "Development of model to simulate embossing of tissue paper - Effect of embossing on mechanical performance of tissue," Thesis for Master of Science (M.Sc.) in Engineering Mechanics, KTH Royal Institute of Technology, Stockholm, Sweden. https://www.diva-portal.org/smash/get/diva2:1590118/FULLTEXT01.pdf

Kim, C., and Mauborgne, R. (2021). "How a Consumer-Goods Giant Made its Toilet Paper Stand Apart," *Blue Ocean Strategy* (Accessed Jun. 28, 2022). https://www.blueoceanstrategy.com/blog/how-a-consumer-goods-giant-made-its-toilet-paper-stand-apart/

Kimari, O. (2000). *Papermaking science and technology: 18 - Paper and Board Grades by Hannu Paulapuro*, (J. Gullichsen, H. Paulapuro, Suomen Paperi-Insinöörien Yhdistys, and Technical Association of the Pulp and Paper Industry, eds.), Fapet Oy, Helsinki, Finland. ISBN 978-952-5216-18-9

Kullander, J. (2012). "Evaluation of furnishes for tissue manufacturing," Faculty of Technology and Science, Chemical Engineering, Karlstads universitet, Karlstad. http://www.diva-portal.org/smash/get/diva2:545882/fulltext01.pdf

Lamberg, J. A., Ojala, J., Peltoniemi, M., and Särkkä, T. (Eds.). (2012). *The Evolution of Global Paper Industry 1800–2050*, World Forests, Springer Netherlands, Dordrecht. DOI: 10.1007/978-94-007-5431-7

Mendes, A. de O., Vieira, J. C., Carta, A. M., Galli, E., Simões, R., and Fiadeiro, P. T. (2020). "Influence of Tissue Paper Converting Conditions on Finished Product Softness," *BioResources*, 15(3), 7178–7190. DOI: 10.15376/biores.15.3.7178-7190

Michelini Tissue Consulting. (2022). "Tissue Converting" (Accessed Jun. 21, 2022). https://www.tissueasy.com/_tissue-converting.php

Mukai, T., and Shimizu, Y. (2003). "Toilet paper roll with perforated line", Patent Nº JP2003061861A, Japan.

Ogg, R. G., and Habel, M. A. (1992). "Perforator blade for paper products and products made therefrom", Patent Nº US 5114771, Cincinnati, USA.

Pál, M., Banjanin, B., Dedijer, S., Vladić, G., and Bošnjaković, G. (2020). "Preliminary analysis of image processing-based evaluation of embossing quality," in: *Proceedings - The Tenth International Symposium GRID 2020*, University of Novi Sad, Faculty of technical sciences, Department of graphic engineering and design, 269–279. DOI: 10.24867/GRID-2020-p29

Paolinelli, A., Boschi, L., and Ricci, M. (2022). "Unwinder for reels and unwinding method", Patent Nº US 11254534, USA.

Pearroc Ltd. (2022). "Types of Hand Towel Folds" (Accessed Jun. 21, 2022). https://www.pearroc.com/paper/hand-towels-z-fold-interfold-cfold/products/types-of-hand-towel-folds

Pejic, D. (2016). "Identifying and reducing converting paper waste - A case study at SCA's paper mill in Lilla Edet.," Master's Thesis, Chalmers University of Technology, Gothenburg, Sweden. https://odr.chalmers.se/bitstream/20.500.12380/245804/1/245804.pdf

Perini, F., Giurlani, G., and Pelaia, F. (2021). "Rewinder for the production of paper logs", Patent Nº US 20190337748, USA.

Rempel, M. (2022). "Effectively solving tissue production, converting and packaging problems using event capturing camera systems," *Papnews*, Italy (Accessed Jun. 23, 2022). https://www.papnews.com/insight/effectively-solving-tissue-production-converting-packaging-problems-using-event-capturing-camera-systems/

Reynolds, P. (2015). "Reliability comes to palletizing," *Packaging World*, Chicago, IL, USA (Accessed Jun. 28, 2022). https://www.packworld.com/machinery/secondary-end-of-line/article/13367395/reliability-comes-to-palletizing

Schulz, G., and Gracyalny, D. (1998). "Method and Apparatus for Pinch Perforating Multiply Web Material", Patent Nº 5755654, Wiscosin, USA.

Spina, R., and Cavalcante, B. (2018). "Characterizing Materials and Processes Used on Paper Tissue Converting Lines," *Materials Today Communications*, 17, 427–437. DOI: 10.1016/j.mtcomm.2018.10.006

Spirent. (2020). "Simplifying 5G with the Network Digital Twin - White Paper" (Accessed Jul. 7, 2022). https://assets.ctfassets.net/wcxs9ap8i19s/3BEsXS0UL7Y97v8GxtMINJ/3a3331afaf5a20711a7750b5b520bdf7/WP-Simplifying-5G_with-the-Network-Digital-Twin.pdf

Star Label. (2018). "Flexography 101: The Basics of the Flexographic Printing Process," *Star Label Products* (Accessed Sep. 6, 2022). https://www.starlabel.com/blog/flexography/

Theohari, S., Fraggedakis, E., Tsimis, D., Tsigonias, M., and Mandis, D. (2014). "Effect of paper properties on print quality by flexographic method", 46th Annual International Conference on Graphic Arts and Media Technology, Management and Education, Athens.

Tutuş, A., Çiçekler, M., and Çali, A. (2016). "Tissue Papers in Turkey and Some Physical and Optical Properties," *SDÜ Fen Bilimleri Enstitüsü Dergisi*, 20(1). DOI: 10.19113/sdufbed.98003

Vieira, J. C., Mendes, A. de O., Carta, A. M., Fiadeiro, P. T., and Costa, A. P. (2020a). "Impact of 5-Ply Toilet Paper Configuration on Its Mechanical and Absorption Properties," *BioResources*, 15(4), 7475–7486. DOI: 10.15376/biores.15.4.7475-7486

Vieira, J. C., Mendes, A. de O., Carta, A. M., Galli, E., Fiadeiro, P. T., and Costa, A. P. (2020b). "Impact of Embossing on Liquid Absorption of Toilet Tissue Papers," *BioResources*, 15(2), 3888–3898. DOI: 10.15376/biores.15.2.3888-3898

Vieira, J. C., Mendes, A. de O., Ribeiro, M. L., Vieira, A. C., Carta, A. M., Fiadeiro, P. T., and Costa, A. P. (2022a). "Embossing Pressure Effect on Mechanical and Softness Properties of Industrial Base Tissue Papers with Finite Element Method Validation," *Materials*, 15(12), 4324. DOI: 10.3390/ma15124324

Vieira, J. C., Mendes, A. de O., Ribeiro, M. L., Vieira, A. C., Carta, A. M., Fiadeiro, P. T., and Costa, A. P. (2022b). "FEM Analysis Validation of Rubber Hardness Impact on Mechanical and Softness Properties of Embossed Industrial Base Tissue Papers," *Polymers*, 14(12), 2485. DOI: 10.3390/polym14122485

Vieira, J. C., Mendes, A. de O., Ribeiro, M. L., Vieira, A. C., Carta, A. M., Fiadeiro, P. T., and Costa, A. P. (2022c). "Embossing Lines and Dots Geometry Effect on the Key Tissue Paper Properties with Finite Element Method Analysis," *Polymers*, 14(17), 3448. DOI: 10.3390/polym14173448

Vieira, J. C., Morais, F., de Oliveira Mendes, A., Ribeiro, M. L., Carta, A. M., Curto, J., Amaral, M. E., Fiadeiro, P. T., and Costa, A. P. (2022d). "Mechanical and softness characterization of 'deco' and 'micro' embossed tissue papers using finite element model (FEM) validation," *Cellulose*. DOI: 10.1007/s10570-022-04618-2

Vieira, J. C., Vieira, A. C., Mendes, A. de O., Carta, A. M., Fiadeiro, P. T., and Costa, A. P. (2021). "Mechanical Behavior of Toilet Paper Perforation," *BioResources*, 16(3), 4846–4861. DOI: 10.15376/biores.16.3.4846-4861

Vieira, J. C., Vieira, A. C., Mendes, A. de O., Carta, A. M., Fiadeiro, P. T., and Costa, A. P. (2022e). "Toilet Paper Perforation Efficiency," *BioResources*, 17(1), 492–503. DOI: 10.15376/biores.17.1.492-503

Williams, B. (2019). "Roll Winding Defects - A Brief Troubleshooting Guide," *Montalvo Corporation* (Apr. 20, 2022). https://www.montalvo.com/article-library/roll-winding-defects-troubleshooting-guide/

Yasui, S. (2017). "Manufacturing method for tissue-paper product", Patent Nº Patent Number: WO2017168877 A1, Ehime, Japan.

Zhipeng, Z., Kuibin, D., Chenxi, L., Xingye, A., Haibing, C., Bin, L., and Hongbin, L. (2022). "Factors Affecting the Absorption Performance of Tissue Paper," *China Pulp and Paper*, 41(6), 89–94. DOI: 10.11980/j.issn.0254-508X.2022.06.014

Article submitted: September 16, 2022

Folha em branco

Chapter 3 – Embossing Study

1. National Patent I Draft – Laboratorial Embossing System (Sistema Laboratorial de *Embossing*)

Vieira, J.C., Vieira, A.C., Mendes, A.O., Carta, A.M., Fiadeiro, P.T., Costa, A.P. (in preparation)

A detailed description of the embossing system developed is provided in the draft of the national Patent I. Each component that composes this laboratory system is identified and its main advantages and disadvantages are also pointed out. Additionally, it delivers the main results that validate the use of the laboratory embossing system developed. The developed laboratory embossing system presented by Patent I draft, proved to be a useful tool for small scale studies, with a lower cost before moving on to pilot scale studies.

The overall contribution in the development of Patent I of Joana Costa Vieira was 70% to the concept development, analysis, drafting and revising the final submission; André Costa Vieira contributed 10% in the concept development, drafting and revising the final submission; António de Oliveira Mendes, Ana Margarida Carta, Paulo Torrão Fiadeiro and Ana Paula Costa contributed in reviewing, editing, and providing important technical inputs by 5%, respectively.

2. Article II – Embossing Pressure Effect on Mechanical and Softness Properties of Industrial Base Tissue Papers with Finite Element Method Validation

Vieira, J.C., Mendes, A.O., Ribeiro, M.L., Vieira, A.C., Carta, A.M., Fiadeiro, P.T., Costa, A.P.
Materials, 2022, 15(12), 4324
https://doi.org/10.3390/ma15124324

With Article II, it was intended to understand how the embossing operation acted on the tissue paper sheet and to achieve an optimal pressure for the developed system. This study made it possible to verify that two effects occurred with the embossing pressure, the densification of the sheet and the marking of the embossing pattern, and that both effects acted in opposite directions, balancing the results of the final properties. The developed laboratory embossing system, proved to be a useful tool for this study, allowing pressure variation and keeping the remaining operating conditions constant and controlled. On the other hand, both the optical system and the FEM simulation proved to be very useful auxiliary tools for a better understanding of the effects that occurred in this study.

The overall contribution in Article II of Joana Costa Vieira was 70% to the concept development, analysis, drafting and revising the final submission; António de Oliveira Mendes contributed 7% with the optical system data, drafting and revising the final submission; Marcelo Leite Ribeiro contributed 7% with the FEM analysis, drafting and revising the final submission; André Costa Vieira, Ana Margarida Carta, Paulo Torrão Fiadeiro and Ana Paula Costa contributed in reviewing, editing, and providing important technical inputs by 4%, respectively.

3. Article III – FEM Analysis Validation of Rubber Hardness Impact on Mechanical and Softness Properties of Embossed Industrial Base Tissue Papers

Vieira, J.C., Mendes, A.O., Ribeiro, M.L., Vieira, A.C., Carta, A.M., Fiadeiro, P.T., Costa, A.P.
Polymers, 2022, 14(12), 2485
https://doi.org/10.3390/polym14122485

Was intended with Article III, to understand how the rubber hardness as one of the components embossing operation acted on the tissue paper sheet, to achieve an optimal rubber hardness for the developed system. This study made it possible to verify that the use of variable rubber hardness in the embossing operation would improve the key softness property of tissue products. The developed laboratory embossing system, proved to be a useful tool for this study, allowing rubber hardness variation and keeping the remaining operating conditions constant and controlled. On the other hand, both the optical system and the FEM simulation proved to be very useful auxiliary tools for a better understanding of the effects that occurred in this study.

The overall contribution in Article III of Joana Costa Vieira was 70% to the concept development, analysis, drafting and revising the final submission; António de Oliveira Mendes contributed 7% with the optical system data, drafting and revising the final submission; Marcelo Leite Ribeiro contributed 7% with the FEM analysis, drafting and revising the final submission; André Costa Vieira, Ana Margarida Carta, Paulo Torrão Fiadeiro and Ana Paula Costa contributed in reviewing, editing, and providing important technical inputs by 4%, respectively.

4. Article IV – Embossing Lines and Dots Geometry Effect on the Key Tissue Paper Properties with Finite Element Method Analysis

Vieira, J.C., Mendes, A.O., Ribeiro, M.L., Vieira, A.C., Carta, A.M., Fiadeiro, P.T., Costa, A.P.
Polymers 2022, 14(17), 3448
https://doi.org/10.3390/polym14173448

To understand better how the finishing geometry of lines and dots of the engraved steel patterns acted on the tissue paper sheet and its final properties, the Article IV was designed. This study made it possible to verify that the finishing geometry of lines and dots have a great impact in the embossing operation and the round finishing should be the choice that will improve the key softness property of tissue products. The developed laboratory embossing system, proved to be a useful tool for this study, allowing changing the finishing geometry of the patterns and keeping the remaining operating conditions constant and controlled. On the other hand, both the optical system and the FEM simulation proved to be very useful auxiliary tools for a better understanding of the effects that occurred in this study.

The overall contribution in Article IV of Joana Costa Vieira was 70% to the concept development, analysis, drafting and revising the final submission; António de Oliveira Mendes contributed 7% with the optical system data, drafting and revising the final submission; Marcelo Leite Ribeiro contributed 7% with the FEM analysis, drafting and revising the final submission; André Costa Vieira, Ana Margarida Carta, Paulo Torrão Fiadeiro and Ana Paula Costa contributed in reviewing, editing, and providing important technical inputs by 4%, respectively.

5. Article V – Mechanical and softness characterization of “deco” and “micro” embossed tissue papers using finite element model (FEM) validation

Vieira, J.C., Morais, F., de Oliveira Mendes, A., Ribeiro, M.L., Carta, A.M., Curto, J.M.R., Amaral, M.E., Fiadeiro, P.T., Costa, A.P.
Cellulose, 2022, 29(10), pp. 5895–5912
https://doi.org/10.1007/s10570-022-04618-2

The Article V was created to understand better how the embossing operation acted on different types of tissue paper sheets (industrial and handsheets) on its final properties. This study made it possible to verify that the crepe present in industrial sheets gives it elasticity and flexibility, the presence of long fiber gives the paper mechanical strength, and its absence improves the softness properties. The developed laboratory embossing system, proved to be a useful tool for this study, allowing changing the type of tissue paper used (industrial and handsheets) and keeping the remaining operating conditions constant and controlled. On the other hand, both the optical system and the FEM simulation proved to be very useful auxiliary tools for a better understanding of the effects that occurred in this study.

The overall contribution in Article V of Joana Costa Vieira was 50% to the concept development, analysis, drafting and revising the final submission; Flávia Morais contributed 21% analysis, drafting and revising the final submission; António de Oliveira Mendes contributed 7% with the optical system data, drafting and revising the final submission; Marcelo Leite Ribeiro contributed 7% with the FEM analysis, drafting and revising the final submission; Ana

Margarida Carta, Joana Curto, Mª Emília Amaral, Paulo Torrão Fiadeiro and Ana Paula Costa contributed in reviewing, editing, and providing important technical inputs by 3%, respectively.

6. Article VI – Impact of embossing on liquid absorption of toilet tissue papers

Vieira, J.C., de Oliveira Mendes, A., Carta, A.M., Galli, E., Fiadeiro, P.T., Costa, A.P.
BioResources, 2020, 15(2), pp. 3888–3898
https://doi.org/10.15376/biores.15.2.3888-3898

In order to a deepen the study of the impact of the embossing operation on the absorption of tissue products, Article VI allowed it from commercial finished products and the respective industrial base tissue paper from which they were produced. This study made it possible to verify that bulk and porosity are the structural properties that most affect absorption capacity.

The overall contribution in Article VI of Joana Costa Vieira was 70% to the concept development, analysis, drafting and revising the final submission; António de Oliveira Mendes contributed 10% with the optical system data, drafting and revising the final submission; Ana Margarida Carta, Enrico Galli, Paulo Torrão Fiadeiro and Ana Paula Costa contributed in reviewing, editing, and providing important technical inputs by 5%, respectively.

7. Article VII – Impact of 5-Ply Toilet Paper Configuration on Its Mechanical and Absorption Properties

Vieira, J.C., Mendes, A.D.O., Carta, A.M., Fiadeiro, P.T., Costa, A.P.
BioResources, 2020, 15(4), pp. 7475–7486
https://doi.org/10.15376/biores.15.4.7475-7486

Another important study related to the embossing operation is presented in Article VII and reports the impact on the final properties of the stacking sequence in a tissue finished product with an odd number of plies. This study made it possible to verify that in a 5-ply toilet paper, having 2 or 3 sheets in the deco embossing and the rest in the micro embossing, had a different impact on the final properties of the product, so it is another factor to consider when producing these types of products.

The overall contribution in Article VII of Joana Costa Vieira was 75% to the concept development, analysis, drafting and revising the final submission; António de Oliveira Mendes contributed 10% with the optical system data, drafting and revising the final submission; Ana Margarida Carta, Paulo Torrão Fiadeiro and Ana Paula Costa contributed in reviewing, editing, and providing important technical inputs by 5%, respectively.

DESCRIÇÃO

"SISTEMA DE GOFRAGEM LABORATORIAL PARA PRODUTOS PAPELEIROS"

A gofragem é a operação principal do processo de transformação de produtos papeleiros, assim como a que mais afeta as propriedades finais do produto acabado. A presente invenção diz respeito a um sistema de gofragem laboratorial para produtos papeleiros que compreende uma prensa (1) que compreende um prato plano superior (2), um prato plano inferior (3), ambos posicionados paralelamente entre si, entre os quais é colocado um conjunto de gofragem (10), e em que os pratos planos se movem, simultaneamente, ou um em relação ao outro, verticalmente, através de meios de acionamento de movimento, e de forma a exercer pressão sobre o conjunto de gofragem. O conjunto de gofragem compreende pelo menos uma placa superior de elastómero (11,12), pelo menos uma folha intermédia de um produto papeleiro (13) e uma placa inferior com uma face com um padrão de gofragem gravado (14) e em que esta face fica virada para a folha do produto papeleiro (13).

A invenção diz ainda respeito a um processo de gofragem de produtos papeleiros através do sistema descrito.

Esta invenção permite o estudo à escala laboratorial do impacto de um determinado padrão de gofragem nas propriedades físico-mecânicas de materiais papeleiros.

DESCRIÇÃO

"SISTEMA DE GOFRAGEM LABORATORIAL PARA PRODUTOS PAPELEIROS"

Área da Invenção

A presente invenção diz respeito a um sistema de gofragem laboratorial para produtos papeleiros, mais particularmente um sistema que compreende uma prensa de dois pratos que compreende um conjunto de gofragem de pelo menos uma placa superior de elastómero e uma placa inferior com uma face com um padrão de gofragem gravado.

Estado da arte

Desde que se iniciou a transformação do produto papeleiro (converting), tal como o produto tissue, a gofragem era já uma importante operação do *converting*, sendo um processo em que o único objetivo era aumentar o volume da folha de papel. Existiam apenas, um ou dois padrões de gravação disponíveis, não havendo grande diferenciação para o consumidor final. Com o avanço tecnológico na produção de papel *tissue*, ao longo dos anos, a operação de gofragem passou a ter como sua principal função a estética, passando o aumento de volume para segundo plano. Assim, o número e o tipo de padrões de gofragem aumentaram significativamente e os fabricantes de papel *tissue* passaram a desenvolver padrões personalizados e exclusivos. No entanto, é necessário ter presente que os padrões escolhidos pelo produtor podem influenciar negativamente as propriedades mecânicas do papel *tissue*, fazendo com que o papel, mesmo que esteticamente mais interessante, perca suavidade, capacidade de absorção e resistência. Para papéis *tissue* de qualidade superior pretende-se gofrados que desenvolvam as propriedades chave *tissue*, sem as prejudicar de forma severa, sendo necessário um compromisso entre a estética do padrão de gofragem e as propriedades/qualidade do papel final [1,2].

Existem no mercado máquinas de *converting* piloto automáticas, de produção contínua alimentadas por rolo de papel *tissue* base industrial com um modo de operação semelhante a máquinas industriais, e que operam a uma escala e velocidade menor. Estas usam geralmente rolos de gofragem gravados a laser e rolos de borracha com uma dureza pré-

1

determinada. Adicionalmente, são operadas com condições padrão industriais, tornando-se mais difícil e dispendioso a alteração de determinados parâmetros de operação com este sistema. Este tipo de máquina apresenta vantagens quando se trata de um produto acabado com uma quantidade de amostra relevante. Por outro lado, torna-se desvantajoso quando apenas se pretendem realizar testes isolados ou preliminares, para análise das propriedades papeleiras para um determinado padrão de gofragem [3,4]. Para além das máquinas pilotos, existe também um sistema laboratorial que permite gravar o padrão de gofragem numa placa em cartão com resina depositada e uma calandra com dois rolos de borracha cuja rotação dos mesmos é manual. Depois o padrão escolhido é transposto para uma máquina piloto com gravação a laser do rolo de gofragem, como anteriormente apresentado. Os sistemas piloto acarretam um custo elevado para testar um novo padrão associado à gravação de um rolo de aço gofrador e à utilização de papel *tissue* em bobine, cuja dimensão tem de estar adaptada a esse tipo de máquina.

Referências

[1] Bredahl, G., Reichling, B., Schnikoreit, W. (2003). "Embossing Device" USA, Patent N°: US 2003/0110961 A1.

[2] Hilbig, K., Liplijn, M., Reinheimer, H. (2005). "Method of making a thick and smooth embossed tissue" USA, Patent N°: US 2005/0230069 A1.

[3] Nakamura, M., Endo, Y. (2007). "Tissue paper product and method of embossing tissue paper" WO, Patent N°: WO2008069085A1.

[4] Wilhelm, L. (2005). "Embossing roll and Embossed substract" WO, Patent N°: WO2005065928A1.

Sumário da Invenção

A presente invenção diz respeito a um sistema de gofragem laboratorial para produtos papeleiros que compreende uma prensa (1) que compreende um prato plano superior (2), um prato plano inferior (3), ambos posicionados paralelamente

entre si, entre os quais é colocado um conjunto de gofragem (10), e em que os pratos planos se movem, simultaneamente, ou um em relação ao outro, verticalmente, através de meios de acionamento de movimento, e de forma a exercer pressão sobre o conjunto de gofragem.

Numa forma preferencial da invenção, o conjunto de gofragem compreende pelo menos uma placa superior de elastómero (11,12), pelo menos uma folha intermédia de um produto papeleiro (13) e uma placa inferior com uma face com um padrão de gofragem gravado (14) e em que esta face fica virada para a folha do produto papeleiro (13).

Numa forma preferencial da invenção, os pratos planos (2,3) compreendem resistências elétricas embutidas (4,5).

Numa forma preferencial da invenção, os pratos planos (2,3) compreendem meios de circulação de um fluído aquecido a temperaturas superiores à temperatura ambiente, medido através de um controlador de temperatura (6).

Numa forma preferencial da invenção, os meios de acionamento de movimento são selecionados do grupo que consiste em cilindros hidráulicos, cilindros pneumáticos, alavancas mecânicas e parafusos acoplados a um redutor.

Numa forma preferencial da invenção, o sistema compreende ainda meios de controlo de pressão (7) de prensagem dos meios de acionamento de movimento, meios de controlo de temperatura (6) dos pratos planos, meios de controlo de tempo de prensagem (8) e meios de controlo de humidade ambiente (9).

Numa forma preferencial da invenção, os meios de controlo são selecionados do grupo que consiste em meios analógicos e digitais.

Numa forma preferencial da invenção, os meios de controlo são pré-programáveis.

Numa forma preferencial da invenção, os meios de controlo da humidade ambiente são selecionados do grupo que consiste em câmara ambiental e exsicador com atmosfera saturada.

Numa forma preferencial da invenção, o padrão de gofragem gravado da placa inferior (14) do conjunto de gofragem (10)

apresenta um relevo tridimensional que compreende pontos e/ou traços.

Numa forma preferencial da invenção, o produto papeleiro apresenta uma gramagem de até 100 g/m^2.

A presente invenção diz ainda respeito a um processo de gofragem laboratorial de um produto papeleiro através do sistema descrito, que compreende os seguintes passos:

a) produção de um padrão de gofragem com um relevo tridimensional de traços e/ou linhas na placa inferior (14) do conjunto de gofragem (10);
b) colocação do conjunto de gofragem (10) entre os pratos planos (2,3) da prensa (1);
c) acionamento dos meios de movimento de forma a que os pratos planos (2,3) exerçam pressão sobre o conjunto de gofragem (10) durante um período de tempo e a uma pressão pré-determinados;
d) libertação do produto papeleiro gofrado (13) pelo afastamento dos pratos planos da prensa (2,3).

Numa forma preferencial da invenção, o padrão de gofragem é produzido por meios selecionados do grupo que consiste em processos de maquinagem que consiste em fresagem, corte a laser, eletroerosão e manufatura aditiva.

Numa forma preferencial da invenção, o processo compreende ainda antes do passo c) um passo adicional de aquecimento dos pratos planos da prensa até uma temperatura pré-determinada.

Breve Descrição das Figuras

A Figura 1 descreve o sistema laboratorial de gofragem para produtos papeleiros da presente invenção, onde é visível a prensa (1), o prato plano superior (2), o prato plano inferior (3), com resistências elétricas embutidas (4,5), um meio de controlo de temperatura (6), um meio de controlo de pressão (7), um meio de controlo do tempo de prensagem (8) e um meio de controlo de humidade ambiente (9).

A Figura 2 representa o conjunto de gofragem (10), que compreende placas superiores de elastómero (11,12), um produto papeleiro (13) e uma placa inferior com uma face com um padrão de gofragem gravado (14).

A Figura 3 representa duas possíveis geometrias de acabamento das linhas e pontos dos padrões de gofragem.

A Figura 4 representa as imagens de papéis *tissue* gofrados com dois empilhamentos de borracha de dureza (Sh-A) diferentes.

A Figura 5 representa imagens de papéis *tissue* gofrados com duas geometrias de acabamento (reta (15) e arredondada (16)).

A Figura 6 representa o *bulk* de papéis *tissue* gofrados com dois empilhamentos de borracha de dureza (Sh-A) diferentes.

A Figura 7 representa o *bulk* de papéis *tissue* gofrados com duas geometrias de acabamento (reto e redondo).

Descrição da invenção

A presente invenção tem como principais vantagens apresentar-se como um sistema versátil à escala laboratorial, pois permite utilizar vários tipos de elastómero de diferentes durezas, permite testar todo o tipo de padrão pretendido nas placas gravadas e avaliar as suas propriedades papeleiras; permite a sua utilização em diferentes tipos de papéis, cartão, cartolinas, papéis revestidos e não revestidos, tanto industriais como laboratoriais, nomeadamente o papel *tissue*; os resultados obtidos não dependem do operador do equipamento; e permite controlar os parâmetros do processo tanto isoladamente como em conjunto.

Assim, tendo em conta o sistema de gofragem industrial, esta invenção permite o estudo à escala laboratorial do impacto de um determinado padrão de gofragem nas propriedades físico-mecânicas do papel *tissue*, em função dos diversos parâmetros de operação da máquina de *converting*, como o acabamento dos pontos e/ou traços que compõem o padrão de gofragem, dureza da borracha de gofragem, pressão, temperatura e humidade, tanto em folhas laboratoriais como em folhas base de papel *tissue* industrial. Esta invenção permite controlar todos os

parâmetros de operação e assim otimizar o processo de gofragem a nível laboratorial e a sua validação, para cada novo padrão exclusivo que a indústria de materiais papeleiros pretenda implementar, antes do seu *scale-up*.

A presente invenção diz assim respeito a um sistema de gofragem laboratorial que compreende uma prensa (1), que pode ser acionada hidráulica ou pneumaticamente por cilindros, ou mecanicamente por meio de uma alavanca ou de um parafuso acoplado a um redutor, que permita variar a pressão de forma calibrada. A prensa (1) compreende um prato plano superior (2) e um prato plano inferior (3), paralelos entre si, e em que a pressão é exercida, havendo a possibilidade que ambos se movam ou apenas um, estando o outro fixo. No exemplo representado pode ver-se uma prensa hidráulica (1), onde a pressão do prato superior móvel (2) sobre o prato inferior fixo (3) é aplicada através de um cilindro hidráulico com controlo de pressão dos cilindros através de um manómetro (7).

O tempo entre o fecho e a abertura, no exemplo descrito, é controlado através de um controlador pré-programável (8) que aciona a válvula para a abertura, depois de um determinado tempo pré-definido após o fecho acionado por um botão.

Os pratos da prensa (2,3), no exemplo descrito têm a temperatura controlada através de um controlador pré-programável (6) capaz de automaticamente ligar e desligar as resistências elétricas embutidas nos dois pratos (4,5), quando o sensor termostático atinge o limite inferior (para ligar) ou o limite superior (para desligar). O controlo de temperatura pode ainda ser obtido por meio de circulação de um fluído aquecido, uma vez que a temperatura no processo de gofragem no máximo deverá ser inferior à temperatura máxima admissível do papel, que é cerca de 220°C.

Entre os pratos da prensa (2,3), encontra-se e sendo colocados antes do processo de acionamento, um conjunto de gofragem (10). Este conjunto (10) que compreende uma ou mais placas superiores de um elastómero (11,12), uma ou um número de folhas de um produto papeleiro (13); e uma placa inferior com um padrão de gofragem gravado (14). Esta placa com o padrão de gofragem (14) numa das faces em relevo tridimensional pode ser produzida por fresagem, corte a

laser, eletroerosão, manufatura aditiva, permitindo um acabamento de precisão elevada. Esta face gravada (14) deverá, no conjunto de gofragem (10), ficar virada para o produto papeleiro (13), enquanto a face lisa fica em contato com o prato da prensa (3).

Este sistema que compõe o conjunto de gofragem (10) permite variar as placas de elastómero (11,12), permitindo assim variar a rigidez final do conjunto, o que influencia a qualidade do produto acabado. Por outro lado, a placa gravada com o padrão de gofragem (14) pode ter diferentes acabamentos da terminação do pico/traço. Na Figura 3, estão representados dois tipos de acabamento da terminação do pico: reta (15) e arredondada (16). Este acabamento variável também influencia a qualidade do produto final.

Nas Figuras 4 e 5 estão apresentadas imagens de papéis *tissue* gofrados com a invenção apresentada, onde são visíveis as diferenças provocadas pelas variações nas condições de operação deste sistema. Na Figura 4 pode-se observar as diferenças nas marcas de gofrado, para dois diferentes padrões (DECO e MICRO), em função da dureza das placas de borracha usadas no processo (configuração de duas placas com durezas 45 e 70 Sh-A empilhadas com diferente ordem). Na Figura 5 pode-se observar as diferenças nas marcas de gofrado, para dois diferentes padrões (DECO e MICRO), em função da geometria de acabamento das placas gofradoras de aço (reto (15) ou redondo (16)). Os gráficos apresentados nas Figuras 6 e 7 evidenciam respetivamente, a profundidade das marcas observadas nas Figuras 4 e 5.

Finalmente, a este sistema também pode acoplar-se uma câmara ambiental ou um exsicador com atmosfera saturada, para permitir o estudo da influência da humidade na operação de gofragem e nas propriedades do produto acabado.

No âmbito da presente invenção, um elastómero diz respeito a um qualquer material de borracha composto de polímeros capazes de recuperar sua forma original após serem esticados em grandes extensões. No âmbito da presente invenção podem ser usados elastómeros como, mas não limitados a Neoprene, SBR (borracha de estireno butadieno). Pode ser usada mais do que uma placa de elastómero com a mesma ou com durezas (escala de dureza em Sh-A) diferentes.

O sistema descrito é usado num processo de gofragem laboratorial de um produto papeleiro que consiste num primeiro passo de produção de um padrão de gofragem com um relevo tridimensional de traços e/ou linhas na placa inferior (14) do conjunto de gofragem (10). De seguida, ocorre a colocação do conjunto de gofragem (10) entre os pratos planos (2,3) da prensa (1).

Os meios de movimento são acionados de forma a que os pratos planos (2,3) exerçam pressão sobre o conjunto de gofragem (10) durante um período de tempo e a uma pressão pré-determinados.

O ocorre, por fim, a libertação do produto papeleiro gofrado (13) pelo afastamento dos pratos planos da prensa (2,3).

Existe ainda a possibilidade de aquecimento dos pratos planos da prensa até uma temperatura pré-determinada.

8

Reivindicações

1. Um sistema de gofragem laboratorial para produtos papeleiros caracterizado por compreender uma prensa (1) que compreende um prato plano superior (2), um prato plano inferior (3), ambos posicionados paralelamente entre si, entre os quais é colocado um conjunto de gofragem (10), e em que os pratos planos se movem, simultaneamente, ou um em relação ao outro, verticalmente, através de meios de acionamento de movimento, e de forma a exercer pressão sobre o conjunto de gofragem.

2. Sistema de acordo com a reivindicação anterior, caracterizado por o conjunto de gofragem compreender pelo menos uma placa superior de elastómero (11,12), pelo menos uma folha intermédia de um produto papeleiro (13) e uma placa inferior com uma face com um padrão de gofragem gravado (14) e em que esta face fica virada para a folha do produto papeleiro (13).

3. Sistema de acordo com qualquer uma das reivindicações anteriores, caracterizado por os pratos planos (2,3) compreenderem resistências elétricas embutidas (4,5).

4. Sistema de acordo com qualquer uma das reivindicações anteriores, caracterizado por os pratos planos (2,3) compreenderem meios de circulação de um fluído aquecido a temperaturas superiores à temperatura ambiente, medido através de um controlador de temperatura (6).

5. Sistema de acordo com qualquer uma das reivindicações anteriores, caracterizado por os meios de acionamento de movimento serem selecionados do grupo que consiste em cilindros hidráulicos, cilindros pneumáticos, alavancas mecânicas e parafusos acoplados a um redutor.

6. Sistema de acordo com qualquer uma das reivindicações anteriores caracterizado por compreender ainda meios de controlo de pressão (7) de prensagem dos meios de acionamento de movimento, meios de controlo de temperatura (6) dos pratos planos, meios de controlo de tempo de prensagem (8) e meios de controlo de humidade ambiente (9).

7. Sistema de acordo com qualquer uma das reivindicações anteriores caracterizado por os meios de controlo serem selecionados do grupo que consiste em meios analógicos e digitais.

8. Sistema de acordo com qualquer uma das reivindicações anteriores caracterizado por os meios de controlo serem pré-programáveis.

9. Sistema de acordo com qualquer uma das reivindicações anteriores caracterizado por os meios de controlo da humidade ambiente serem selecionados do grupo que consiste em câmara ambiental e exsicador com atmosfera saturada.

10. Sistema de acordo com qualquer uma das reivindicações anteriores, caracterizado por o padrão de gofragem gravado da placa inferior (14) do conjunto de gofragem (10) apresentar um relevo tridimensional que compreende pontos e/ou traços.

11. Sistema de acordo com qualquer uma das reivindicações anteriores, caracterizado por o relevo tridimensional que compreende pontos e/ou traços, possuir um acabamento do tipo reto (15), arredondado (16), piramidal ou cónico.

12. Sistema de acordo com qualquer uma das reivindicações anteriores, caracterizado por os elastómeros das placas superiores serem selecionados do grupo que consiste em Neoprene, Borracha de estireno butadieno.

13. Sistema de acordo com qualquer uma das reivindicações anteriores, caracterizado por o produto papeleiro apresentar uma gramagem de até 100 g/m^2.

14. Processo de gofragem laboratorial de um produto papeleiro através do sistema reivindicado nas reivindicações anteriores, caracterizado por compreender os seguintes passos:
    e) produção de um padrão de gofragem com um relevo tridimensional de traços e/ou linhas na placa inferior (14) do conjunto de gofragem (10);
    f) colocação do conjunto de gofragem (10) entre os pratos planos (2,3) da prensa (1);
    g) acionamento dos meios de movimento de forma a que os pratos planos (2,3) exerçam pressão sobre o conjunto de gofragem (10) durante um período de tempo e a uma pressão pré-determinados;
    h) libertação do produto papeleiro gofrado (13) pelo afastamento dos pratos planos da prensa (2,3).

15. Processo de acordo com a reivindicação anterior, caracterizado por a placa com o padrão de gofragem ser produzido por meios selecionados do grupo de processos de maquinagem que consiste em fresagem, corte a laser, eletroerosão e manufatura aditiva.

16. Processo de acordo com as reivindicações 11 e 12, caracterizado por compreender ainda, antes do passo c) um passo adicional de aquecimento dos pratos planos da prensa até uma temperatura pré-determinada.

Figura 1

1/7

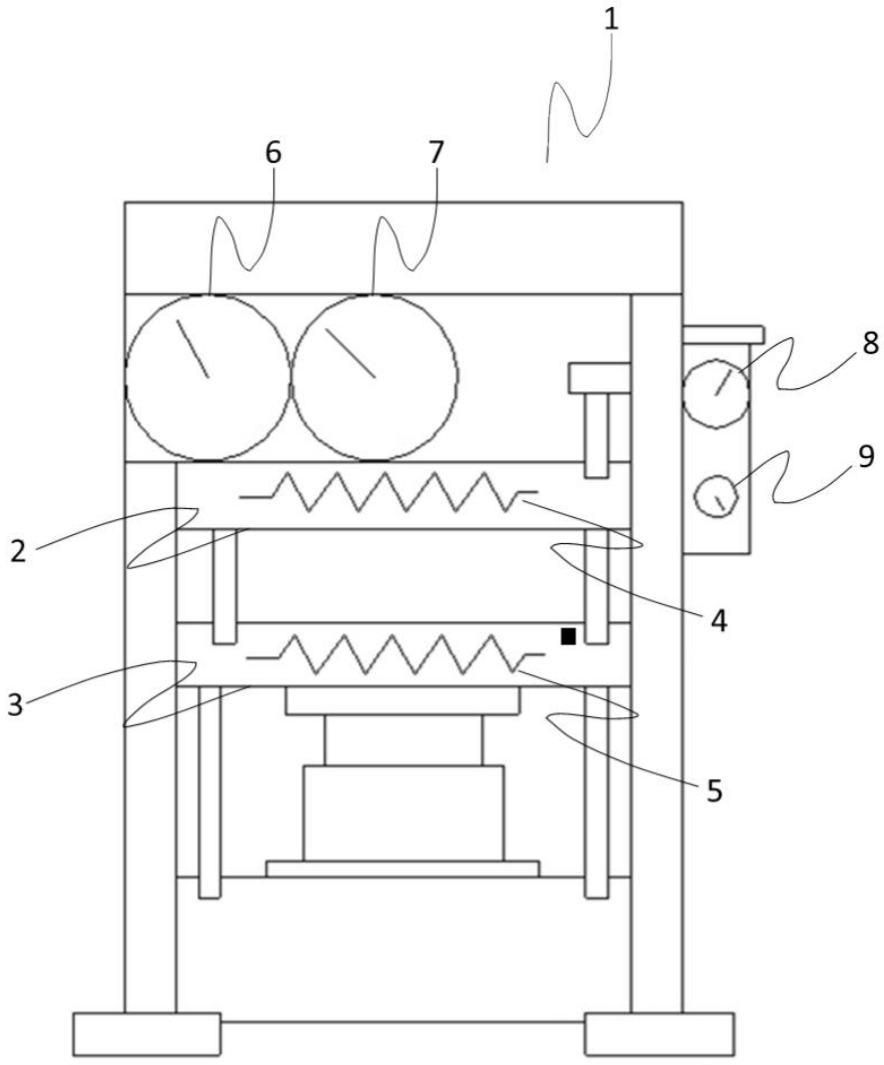

Figura 2

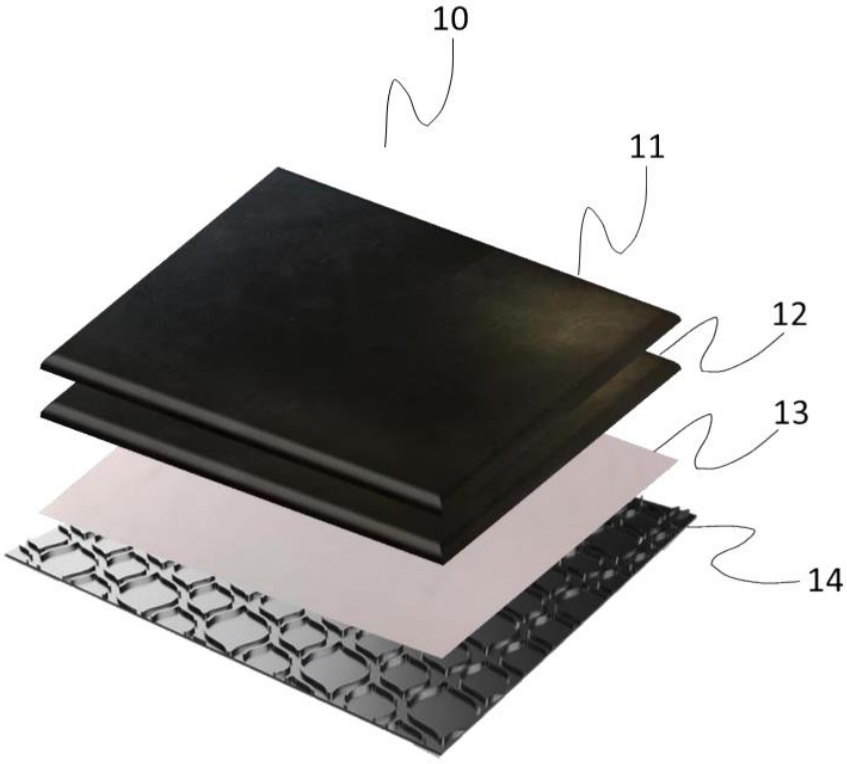

Figura 3

3/7

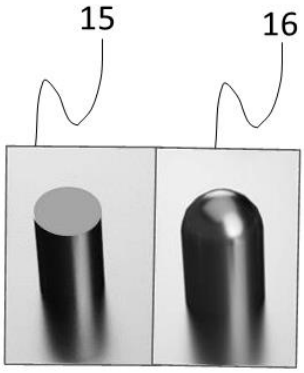

Figura 4

4/7

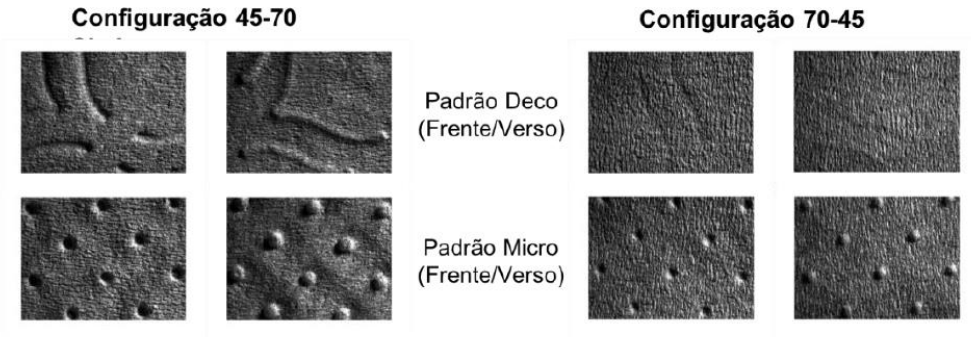
Configuração 45-70
Configuração 70-45
Padrão Deco
(Frente/Verso)
Padrão Micro
(Frente/Verso)

Figura 5

5/7

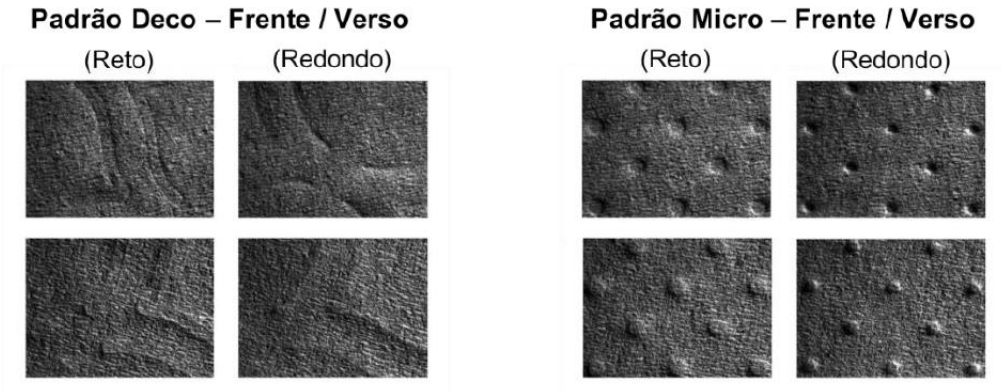
Padrão Deco – Frente / Verso
(Reto)
(Redondo)
Padrão Micro – Frente / Verso
(Reto)
(Redondo)

Figura 6

6/7

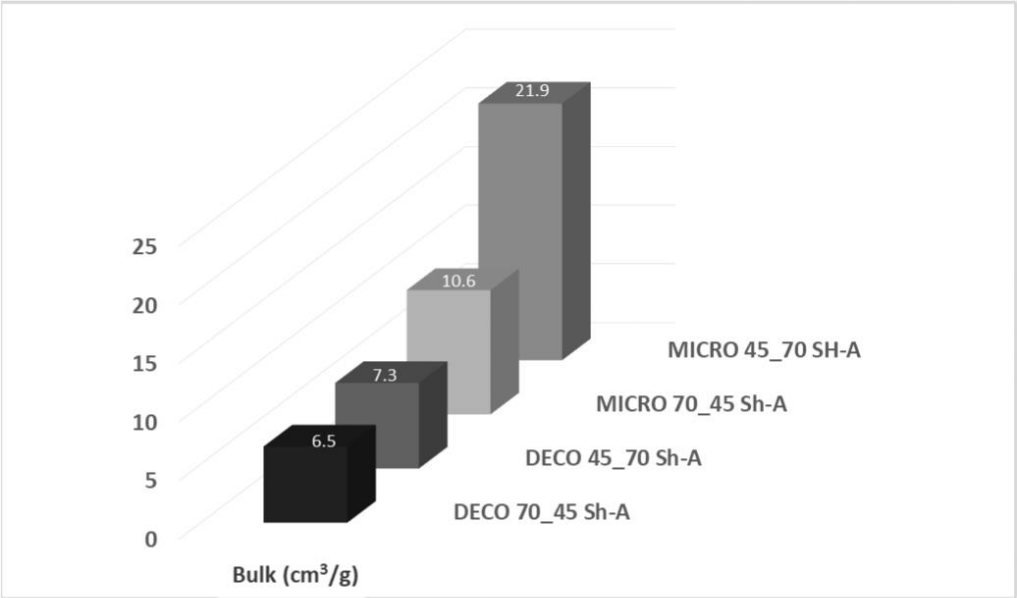
21.9
10.6
7.3
6.5
25
20
15
10
5
0
MICRO 45_70 SH-A
MICRO 70_45 Sh-A
DECO 45_70 Sh-A
DECO 70_45 Sh-A
Bulk (cm³/g)

Figura 7

7/7

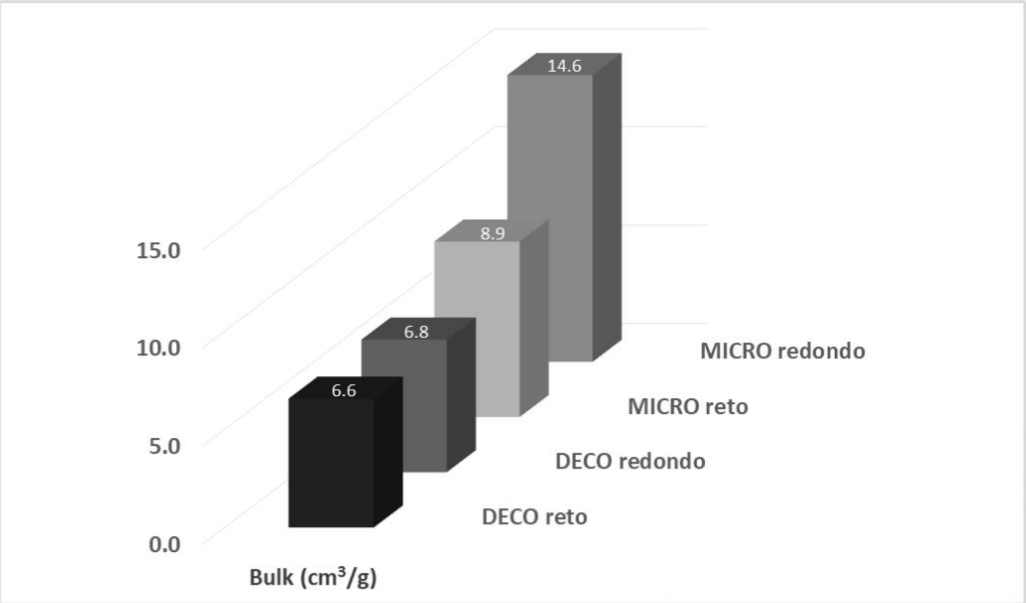
14.6
8.9
6.8
6.6
15.0
10.0
5.0
0.0
MICRO redondo
MICRO reto
DECO redondo
DECO reto
Bulk (cm³/g)

materials

MDPI

Article

Embossing Pressure Effect on Mechanical and Softness Properties of Industrial Base Tissue Papers with Finite Element Method Validation

Joana Costa Vieira [1,*], António de O. Mendes [1], Marcelo Leite Ribeiro [1,2], André Costa Vieira [3], Ana Margarida Carta [4], Paulo Torrão Fiadeiro [1] and Ana Paula Costa [1]

[1] Fiber Materials and Environmental Technologies Research Unit (FibEnTech-UBI), University da Beira Interior, Rua Marquês d'Ávila e Bolama, 6201-001 Covilhã, Portugal; ant.mendes@ubi.pt (A.d.O.M.); malribei@usp.br (M.L.R.); fiadeiro@ubi.pt (P.T.F.); anacosta@ubi.pt (A.P.C.)
[2] Aeronautical Engineering Department, São Carlos School of Engineering, University of São Paulo, São Carlos 05508-060, SP, Brazil
[3] Center for Mechanical and Aerospace Science and Technologies (C-MAST-UBI), University da Beira Interior, R. Marquês D'Ávila e Bolama, 6201-001 Covilhã, Portugal; andre.costa.vieira@ubi.pt
[4] Forest and Paper Research Institute (RAIZ), R. José Estevão, Eixo, 3800-783 Aveiro, Portugal; ana.carta@thenavigatorcompany.com
* Correspondence: joana.costa.vieira@ubi.pt

Abstract: Embossing is a converting process in which the surface of a tissue paper sheet is changed under high pressure, allowing different functions. In this work, the authors intend to study how the embossing pressure affects the main properties of tissue paper, using a laboratory embossing system. An optimum pressure was achieved at 2.8 bar to this embossing laboratory set-up. The effect of pressure when densifying the paper sheet gives it a gain in mechanical strength but no differences in terms of liquid absorbency. The two embossing patterns present different behaviors but both evidence losses in mechanical and softness properties. On the other hand, the finite element method (FEM) does not show clear evidence of how the pressure affects the paper strength. For the deco die, it is possible to observe that the amount of yielding is slightly higher for lower pressure (2.4 bar), but this plasticity state parameter is very similar for 2.8 bar and 3.2 bar. For the micro die, FEM simulations of the manufacturing pressure do not show a considerable impact on the amount of plasticity state of the material; only for 3.2 bar, it shows a change in the pattern of the plasticity state of the paper during the embossing processes. In the end, to achieve a final product with excellent quality, it is important to make a compromise between the various properties.

Keywords: embossing prototype; eucalyptus-based fibrous materials; FEM simulation; mechanical properties; pressure; softness; tissue paper

Citation: Vieira, J.C.; Mendes, A.d.O.; Ribeiro, M.L.; Vieira, A.C.; Carta, A.M.; Fiadeiro, P.T.; Costa, A.P. Embossing Pressure Effect on Mechanical and Softness Properties of Industrial Base Tissue Papers with Finite Element Method Validation. *Materials* **2022**, *15*, 4324. https://doi.org/10.3390/ma15124324

Academic Editors: Geoffrey R. Mitchell and Nuno Alves

Received: 20 April 2022
Accepted: 16 June 2022
Published: 18 June 2022

1. Introduction

Tissue paper production in the last 10 years has increased mainly in Western Europe, having matched the production in North America, which until then was the leading producer of this kind of paper [1]. Nowadays, the importance of tissue paper should be highlighted.

Tissue paper can be defined as a cellulosic-based product (composed with virgin or recycled fibers) manufactured with low grammage, creped, and depending on the application, embossed (toilet paper, paper towels, and napkins). The most important properties of these papers are good flexibility, high surface smoothness, high bulk, and high capacity for liquid absorption. Tissue paper is creped, which causes a decrease in tensile strength in machine direction (MD) while increasing the sheet thickness, volume, and fiber-free ends. The creping process increases the elongation capacity in MD, resulting in a decrease in the Young modulus [2].

A roll of toilet paper is obtained at the end of the converting-line machine where one or more tissue paper mother reels are placed on cylindrical shafts. Different individual operations constitute the converting line, which includes the unwind, embossing, rewinder, perforation, LOG saws, and packaging [3].

Embossing is a forming process in which the surface of a substrate is changed under the influence of high embossing pressure. Embossing creates an image raised above the line of the paper surface and gives it a third dimension, the z-direction [4]. As a result, this process gives to the tissue sheet a certain texture. The embossing operation permits us different purposes. This process can be used to produce a flexibility effect, to exhibit an aesthetic pattern, or to promote bonding between several overlapping sheets of paper [5]. Embossing is the most prevalent process of all in the converting line, and it allows changing the paper's intrinsic properties [6]. Embossers can perform this in a few ways. Embossing rollers can be steel–steel or rubber–steel. Steel rolls have engraved patterns, and when the embossed sheets are laminated (glued) they maintain a constant match [3,5].

Tissue paper experts have long recognized that the physical–mechanical properties of these products, such as grammage, thickness, strength, softness, and liquid absorption, are very important. Research and development has focused on improving each of these parameters without affecting the others simultaneously [7]. Balancing the different properties in paper converting is the main challenge to this industry. The embossing process contributes positively to bulk, liquid absorption, and softness (related to volume), and negatively to strength and surface softness. The lamination process, on the other hand, contributes positively to bulk (in some cases), absorption and smoothness (related to volume), and negatively to surface smoothness. The lotionizing process contributes to good softness at the cost of liquid absorption. Thus, for each process in the converting line, the impaired properties are available to be exchanged for others according to the requirements of the final product [6].

Grammage is one of the main properties of tissue paper. This is apparently a simple measurement but a very important one and gives us an initial indirect estimate of the amount of fiber present in the sample. Another equally important property is thickness, which indicates how bulky the base tissue paper is, or final product is. In the converting process, there is a potential loss of volume that can be compensated by the embossing process or by the development of a pattern that can compensate for this loss [8,9]. In fact, it is in the converting process that tissue paper thickness experiences the greatest changes, mainly caused by the embossing operation. So, the thickness of the final product is affected by the embossing pattern, embossing depth, nip pressure, lamination, and adhesiveness of the interlayer bonding. The embossing process is incorporated into the converting line to partially compensate for the loss of thickness in the converting process (web tensions used to control paper from unwinding to the rewinder and narrow nips along the machine) [9,10]. This is a critical point and the main reason why it is important to know and understand the thickness behavior during the entire conversion process. The embossing pattern, the handling of the final toilet paper, and the packaging strongly determine the final characteristics of this product, seen and felt by the final consumer [9,10].

Conventional tissue paper focuses on reducing the pressing step where the greatest loss of paper sheet volume occurs. Dry embossing is the most common method to increase bulk, but the volume created can be short-lived. A tight winding process produces a flatter sheet. More relevantly, the embossing pattern definition and volume are lost once the dry tissue paper is wetted again [2].

A paper with high strength or with a suitable elongation allows it to be processed at high speeds and/or create a high bulk after embossing. In opposition, it becomes more difficult to process the paper in the converting line (such as loss of sheet control, reduced speed, and/or lower embossing pressure) if its mechanical performance is not adequate [9,11].

As tissue paper has very low grammage, it therefore is more sensitive to variations in strength. In tissue paper, the main source of strength is the bonds between the cellulose

fibers that compose it. Consequently, the strength of tissue paper is directly proportional to the number of fibers and their surface area. The type of cellulose fiber used is one of the most important factors when it comes to the strength of tissue paper. Generally, fiber blends are used to optimize the strength of the tissue paper sheet. Long fibers (softwood) contribute to the strength itself, while short fibers (hardwood) contribute to softness. Therefore, density has a direct influence on strength, as the greater the number of fibers in a given area, the greater the number of connections to be created [9,12].

Another critical factor regarding the tensile strength of tissue paper is its anisotropy. The strength of the sheet in MD gives us information about the tension that the sheet will be able to resist during the entire process without breaking. Specifically, in the embossing operation, the tensile strength and elongation in both directions determines the runnability of the sheet in the paper machine, where higher values allow greater prominence in the z-direction. All paper has a limit for embossing, where higher values generally result in greater volume, to the point where embossing will destroy the sheet strength properties and values fall below the minimum required to meet the machine's production specifications, the conversion requirements, and/or the quality requirements of the finished product. As a result, in the embossing operation, it is essential to have the proper elongation and strength value to create the desired volume for a certain product. If the embossing takes place in the elastic zone of the paper sheet (minimum embossing), after embossing, it recovers and returns to its original form, losing the volume that the embossing process had just created. On the other hand, if embossing occurs near the breaking point (over embossing), the paper will be destroyed due to excessive pressure applied. In addition, the consequent loss in tensile strength may cause the failure of the paper sheet in the winding process [9,13].

Quantifying softness is a topic of many articles and controversies, both academically and industrially. However, all agree on the inverse and relatively linear relationship of the tensile strength of tissue paper with both mechanical and human panel softness [2,14]. Softness is also dependent on the embossing technology and patterns used to engrave the base tissue paper [15].

The quality of the final product, in addition to controlling its properties, also depends on the different physical operating parameters of the converting machine, such as temperature, humidity, and pressure. Embossing is a type of mechanical compression operation in the tissue paper manufacturing process, where pressure is a key parameter to produce a quality toilet paper [16]. From the previous work of Vieira et al. [17], the embossing operation was shown to have a negative impact on mechanical properties, being more pronounced for the micro embossing pattern. Additionally, this pattern also has a higher impact on the thickness and bulk increase. This article investigates the impact on the key properties of toilet paper of one of the main operational parameters in embossing: pressure. Using a laboratory embossing system, two different toilet base tissue papers were embossed at different pressures and after that tested for thickness, mechanical strength, and TSA smoothness. FEM analysis was also used to provide a better understanding of how the embossing patterns (deco and micro) affect the mechanical properties.

2. Materials and Methods

2.1. Materials

To perform this work, industrial toilet base tissue paper (only creped) from two different Portuguese factories was used. Both papers are composed of a mixture of bleached hardwood (*Eucalyptus globulus*) and softwood (*pinus*) kraft pulps, with hardwood being present in greater quantities. These two papers were selected because they have a very similar grammage and because the respective paper machines operate differently. The industrial base tissue paper designated by A was produced on a machine with a double headbox and steel creping blade, and the industrial base tissue paper designated by B was produced on a machine with a single headbox and ceramic creping blade. After the densification operation, these papers have the index d followed by the corresponding pressure value in their nomenclature, e.g., $A_{d\,2.8}$, and after the embossing operation it is the

index me (micro embossing) and de (deco embossing), also followed by the corresponding pressure value, e.g., $A_{me\ 2.8}$.

2.2. Methods

This work started by determining the grammage of the two industrial base tissue paper samples, which were measured using the paper tissue standard ISO 12625-6:2005 [18]. Then, the Fiber Tester from Lorentzen & Wettre was used to perform the morphological characterization analysis. Before executing the test, the samples were properly disintegrated, and the equipment calibrated according to the producer's specifications. This test allows us to evaluate tissue paper samples in terms of length weighted in length of fibers (mm), width (µm), fines in length (%), and coarseness (mg/100 m).

Analyzing the embossing operation itself, the occurrence of two phenomena can be verified: the compression of the paper sheet and the engraving of the pattern. As can be seen in Figure 1, the thickness of the sheet itself decreases with increasing pressure, causing its densification. On the other hand, the overall thickness of the sheet due to embossing pattern engraving increases with increasing pressure.

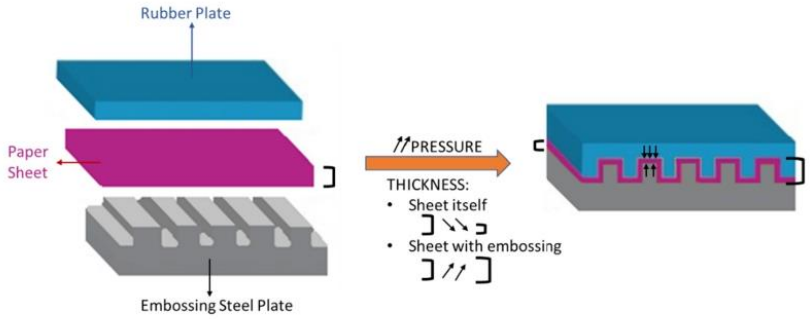

Figure 1. Scheme of the embossing process with pressure action effects.

Thus, the work continued to study these two effects. First, we proceeded to understand the densification effect of the sheet by compressing both base tissue paper samples with a flat steel plate and a rubber plate with a hardness of 60.3 ± 1.21 shore A (10 measurements along the rubber plate with a durometer PCE-DDA equipment), and the pressure was varied for values from 2.0 to 3.6 bar in 0.4 bar increments. In this procedure, the study of the liquid interaction with the different densified paper structures to evaluate spreading dynamics was also considered through an optical system [19], which has been used in previous studies [20–23]. The system works by ejecting droplets of approximately 0.5 µL of dyed water toward the surface of the densified paper samples and, simultaneously, a set of images of the droplets' interaction was registered during a period of 3.0 s.

Secondly, from the results obtained for densification, deco and micro embossing were carried out, also for both samples, using the same operating conditions but with steel plates with the embossing patterns, as shown in Figure 2. In this case, the pressure applied was 2.4, 2.8 and 3.2 bar. All sheets obtained by both methodologies were tested in terms of thickness/bulk, their mechanical tensile strength in the machine direction (MD), and in the transverse direction (CD). Tensile tests were conducted in a Thwing-Albert® VantageNX Universal testing machine according to the tissue standard ISO 12625-4:2005 [24], and thickness and bulk were measured using a FRANK-TPI® Micrometer according to the tissue standard ISO 12625-3:2014 [25]. In addition to these tests the apparent porosity (theoretical porosity) was determined by calculation using Equation (1):

$$P\ (\%) = 100 \times [1 - (\rho_{sample}/\rho_{cellulose})] \quad (1)$$

where $\rho_{cellulose}$ is the cellulose density (assumed 1.6 g/cm^3) and ρ_{sample} is the sample apparent density (in g/cm^3), which is the inverse of the bulk (cm^3/g) and calculated by the ratio between the grammage (g/m^2) and the thickness (μm) of the sheet [26].

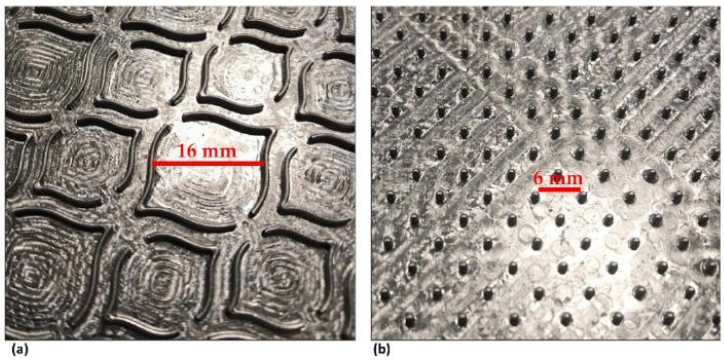

Figure 2. Photographs of steel embossing plates: (**a**) deco embossing, and (**b**) micro embossing.

Both samples that were produced with an embossing pattern and the two initial base tissue papers were subjected to softness tests by the Tissue Softness Analyzer (TSA) from EMTEC®. The TP II algorithm and the QA I algorithm were used for the computation of the handfeel (HF), respectively. All the tested samples were prepared to meet the machine requirements.

2.3. Finite Element Method (FEM)

An FEM was proposed to improve the understanding of pressure on the paper manufacturing process. Two different die patterns were used for simulations (deco and micro), and their effects on the paper stress field and plasticity were analyzed regarding three different manufacturing pressures (2.4, 2.8 and 3.2 bar). As ABAQUS™ does not have anisotropic plasticity, to model the paper plasticity an orthotropic elastic–plastic material model [27] was implemented as a user material subroutine for explicit simulations (VUMAT), linked to the commercial finite element software ABAQUS™, to model paper plasticity. This material model allows considering paper anisotropic behavior, since paper response is highly dependent of fiber orientation [27]. The model assumes the decomposition of the strain tensor into elastic strain tensor plus plastic strain tensor (Equation (2)), and the volume is conserved.

$$\varepsilon_{ij} = \varepsilon^e_{ij} + \varepsilon^p_{ij} \tag{2}$$

where ε_{ij} is the total strain, ε^e_{ij} is the elastic strain, and ε^p_{ij} is the plastic strain.

The model uses the concept of an isotropic plasticity equivalent [28], which is a fictitious material that relates the orthotropic stress state to the isotropic stress state. The relation between the actual Cauchy stress tensor and the isotropic plasticity equivalent (IPE) deviatoric tensor is given in Equation (3).

$$s_{ij} = L_{ijkl}\sigma_{kl} \tag{3}$$

where s_{ij} is the deviatoric IPE stress tensor, σ_{kl} is the Cauchy stress, and L_{ijkl} is the fourth-order transformation tensor shown in Equation (4) for plane stress:

$$L = \begin{bmatrix} 2A & C-A-B & 0 \\ C-A-B & 2B & 0 \\ B-C-A & A-B-C & 0 \\ 0 & 0 & 3D \end{bmatrix} \tag{4}$$

where the parameters A, B, C, and D are obtained from the experiments using the following equations (Equations (5)–(12)) [27]:

$$A = \sqrt{1 - 12x^2} \tag{5}$$

$$B = 3(y - x) \tag{6}$$

$$C = 3(y + x) \tag{7}$$

$$D = \frac{K_{12}^{n/(n+1)}}{\sqrt{3}} \tag{8}$$

$$x = \sqrt{\frac{\alpha^2}{24(3\alpha^2 + \beta^2 - 4\beta + 4)}\left(\beta + 1 - \sqrt{6\beta - 3\alpha^2 - 3}\right)} \tag{9}$$

$$y = \frac{\alpha}{4x} - A \tag{10}$$

$$\alpha = K_{33}^{2n/(n+1)} - K_{22}^{2n/(n+1)} \tag{11}$$

$$\beta = K_{33}^{2n/(n+1)} + K_{22}^{2n/(n+1)} \tag{12}$$

The parameters K_{ii} and n (in Equations (8), (11) and (12)) relate to the fit curve of the experimental data applying the Ramberg–Osgood methodology. For the MD direction tensile test, the Equation (13) is used:

$$\varepsilon_{11} = \frac{\sigma_{11}}{E_{11}} + \left(\frac{\sigma_{11}}{E_0}\right)^n \tag{13}$$

For the CD direction, the Equation (14) is used:

$$\varepsilon_{kk} = \frac{\sigma_{kk}}{E_{kk}} + \left(\frac{K_{kk}E_{kk}}{E_0}\right)^n, \quad k = 2, 3 \tag{14}$$

Note that for Equation (14) the repeated indices do not mean the usual summation rule used in the indicial notation. Finally, the parameter K_{12} is obtained using Equation (15).

$$\gamma_{12} = \frac{\sigma_{12}}{G_{12}} + \left(\frac{K_{12}\sigma_{12}}{E_0}\right)^n \tag{15}$$

The Hooke's law for plane stress small-strain linear elastic orthotropic material is defined by Equation (16):

$$\sigma = C\varepsilon^e \tag{16}$$

where σ is the Cauchy stress tensor, C is the plane stress linear elastic orthotropic constitutive law, and ε^e is the small-strain elastic tensor.

As plane stress was adopted for these simulations, the effect of the paper densification comes from the experimental tensile test for each configuration of die model and paper. The implementation of this model is similar to the well-known J_2 flow theory for isotropic materials using the backward-Euler algorithm. As mentioned before, this material model was implemented as a user material subroutine for explicit simulations linked to the commercial finite element software ABAQUS™ version 6.14 (Waltham, MA, USA).

The explicit solver was used to overcome convergence issues that are usual when using the implicit solver. On the other hand, the stable time increment is very small, resulting in long time simulations. The simulations were performed using a workstation with two intel Xeon E5-2630 8 cores (16 cores total with 32 threads) with 256 Gb RAM. The FEM dimensions and boundary conditions are presented in Figure 3. The die patterns' dimensions are representative of the actual die dimensions to result in a reasonable computational cost and to keep the precision capability. The base dimension is the same, but it is thick enough to

allow the deformation without severe interference in the die and paper kinematics. The paper follows the same dimensions of the die and basis.

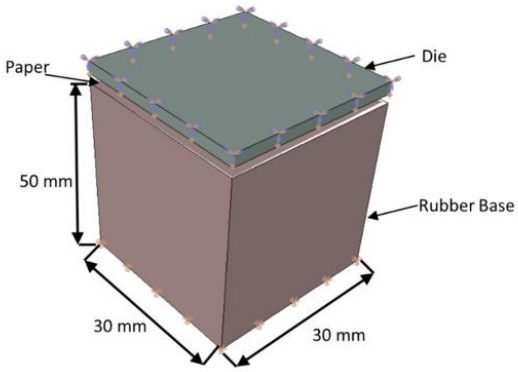

Figure 3. Model dimensions and boundary conditions.

All the displacement degrees of freedom are restricted in the bottom of the soft base. A prescribed displacement is applied on the top of the die. The other degrees of freedom are restricted. For the interactions between the parts, the model considers hard contact for normal behavior, and the tangential behavior is modeled with a penalty of 0.3 for the friction coefficient. The model has 473,694 elements for the simulation of micro die and 476,153 elements for the deco die. For both patterns, the paper was simulated using a 4-node reduced integration membrane element (M3D4R). The structured mesh has a total of 250,000 elements. For micro die, the 4-node reduced integration element (S4R) was used. The total number of elements is 7694 elements. The same element is used for the deco die, but for this die, 10,314 elements were used. Finally, the rubber base was modeled using 8-node tridimensional elements (C3D8). A total of 216,000 elements were used. This model uses 3 different types of material constitutive models: linear elastic for steel die ($E = 200$ GPa, $\mu = 0.33$) and a hyperelastic isotropic material model for the rubber basis (C10 = 0.18 MPa and D1 = 0.0), and the paper was modeled using an orthotropic elastic–plastic user material model (E11 = 13.89 MPa, E22 = E33 = 4.23 MPa, $\mu = 0.33$, and G12 = 2.1 MPa).

The tensile test in machine direction (MD) and cross direction (CD) were used to obtain the basic mechanical properties and the plastic parameters necessary for the IPE model (Equations (4)–(15)) used for these simulations. Then, the data points were used for the plastic parameter calculation, and a linear interpolation between those points were used to obtain the stress for a given plastic strain. It is important to mention that this procedure was applied for each combination of the paper densification and die model.

3. Results

As intended, the grammage values obtained are very similar. For sample A, a grammage of 16.9 ± 0.01 g/m^2 was obtained, and for sample B one of 16.7 ± 0.05 g/m^2. Figure 4 presents the morphological characterization for the two samples, A and B.

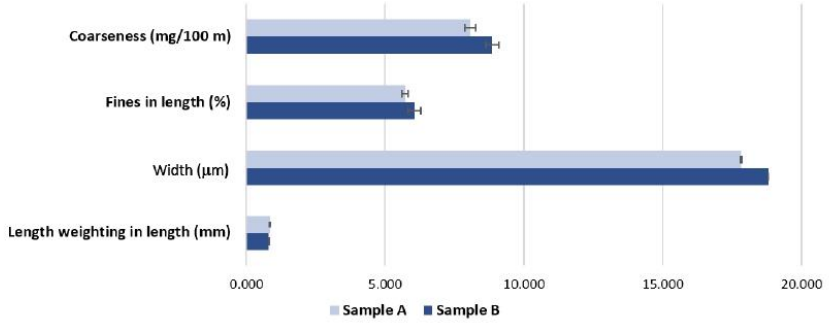

Figure 4. Morphological characterization of the two base tissue paper samples.

To assess the impact of embossing pressure on tissue paper properties, we started by isolating the effect of pressure without the embossing patterns and how it impacted the properties and then, under the same conditions, what its impact is with the deco and micro embossing patterns.

3.1. Sheet Densification

Figure 5 shows the behavior of apparent density and mechanical strength of the two samples for different pressures and without embossing patterns.

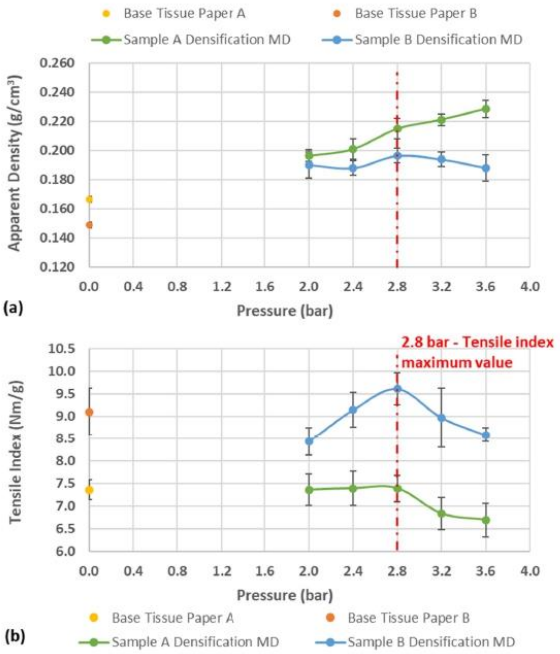

Figure 5. Results obtained for: (**a**) apparent density and (**b**) tensile index with the pressure increase in the base tissue paper densification of the samples A and B.

Figure 6 allows the observation of the SEM images of samples A and B, at two magnifications (×100 and ×300) at peak pressures before and after it. The measurements in yellow correspond to the crepe wave height (µm) without any mechanical compression, which has a different interpretation than the thickness of tissue paper measured by the ISO standard.

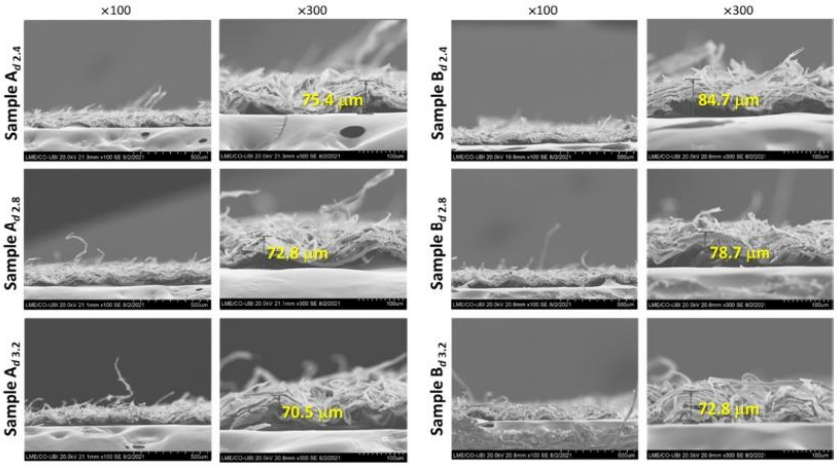

Figure 6. SEM images of samples A and B at two magnifications (×100 and ×300), at pressures of 2.4, 2.8, and 3.2 bar. The measurements presented in yellow corresponds to the height of the crepe wave.

The water dynamic spreading area evolutions measured on the non-compressed base tissue papers and those compressed at the optimal pressure of 2.8 bar are presented in Figures 7 and 8, respectively, for the samples A and B.

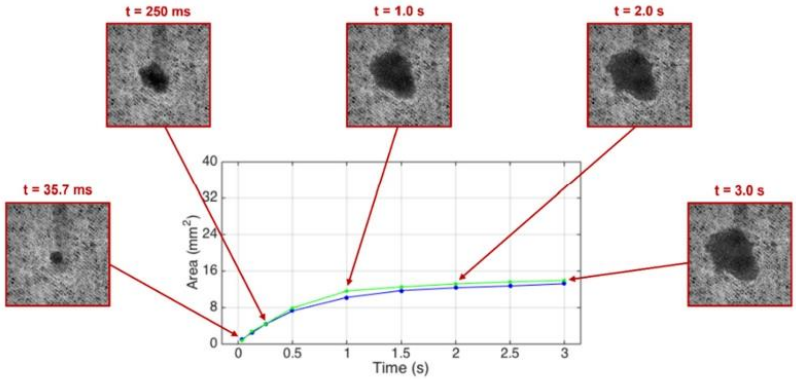

Figure 7. Water spreading area as a function of time for the non-compressed (blue line) and compressed (green line) base tissue paper sample A. The insets show the spreading area in different instants of time.

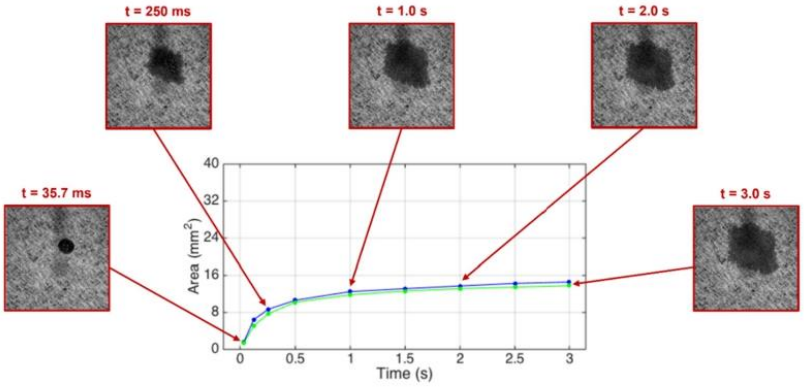

Figure 8. Water spreading area as a function of time for the non-compressed (blue line) and compressed (green line) base tissue paper sample B. The insets show the spreading area in different instants of time.

3.2. Sheet Embossing

The A and B sample results obtained for thickness, bulk, and apparent porosity for peak pressures, before and after, with deco and micro embossing, are presented in Tables 1 and 2, respectively.

Table 1. Thickness, bulk, and apparent porosity results for the base tissue paper samples A and B at different pressures with deco embossing.

Pressure (Bar)	Sample A_{de}				Sample B_{de}			
	Thickness (mm)		Bulk (cm^3/g)	Apparent Porosity (%)	Thickness (mm)		Bulk (cm^3/g)	Apparent Porosity (%)
	$\bar{x}$	$\pm\sigma$			$\bar{x}$	$\pm\sigma$		
0	0.102	0.001	6.01	89.2	0.112	0.002	6.71	90.3
2.4	0.100	0.001	5.89	89.0	0.117	0.002	7.00	90.7
2.8	0.101	0.002	5.99	89.2	0.111	0.001	6.62	90.2
3.2	0.102	0.001	6.01	89.2	0.110	0.002	6.60	90.2

Table 2. Thickness, bulk, and apparent porosity results for the base tissue paper samples A and B at different pressures with micro embossing.

Pressure (Bar)	Sample A_{me}				Sample B_{me}			
	Thickness (mm)		Bulk (cm^3/g)	Apparent Porosity (%)	Thickness (mm)		Bulk (cm^3/g)	Apparent Porosity (%)
	$\bar{x}$	$\pm\sigma$			$\bar{x}$	$\pm\sigma$		
0	0.102	0.001	6.01	89.2	0.112	0.002	6.71	90.3
2.4	0.152	0.013	8.98	92.8	0.209	0.019	12.49	94.8
2.8	0.203	0.014	12.01	94.6	0.258	0.021	15.44	95.8
3.2	0.252	0.010	14.88	95.6	0.270	0.018	16.14	96.0

The mechanical strength behavior with the pressure for the two embossing patterns in samples A and B are represented in Figure 9.

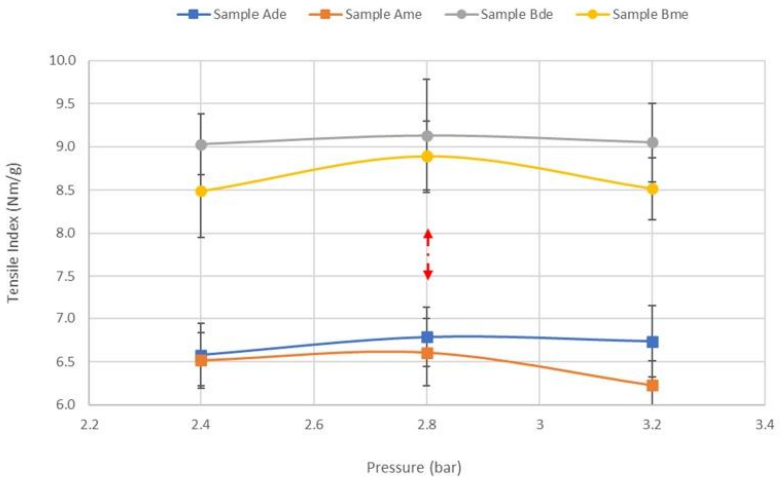

Figure 9. Results obtained for tensile index with the pressure increase in the samples A and B with deco and micro embossing.

Finally, Figure 10 shows the behavior of the important softness property with embossing pressure for the two patterns alone and combined in a final two-ply product.

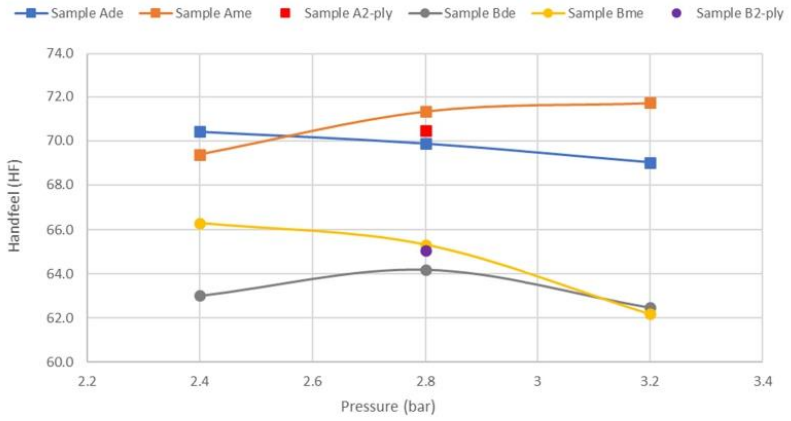

Figure 10. Results obtained for handfeel (HF) with the pressure increase in the samples A and B with deco and micro embossing.

3.3. Finite Element Method (FEM)

The material model implemented as a VUMAT allows observing the plasticity state (SDV9) for each embossing pattern and manufacturing pressure and corroborates the experiments results for sample A. The influence of pressure in the manufacturing process impacts in the plasticity of the paper. For the deco die, the differences on yielding are presented in Figure 11.

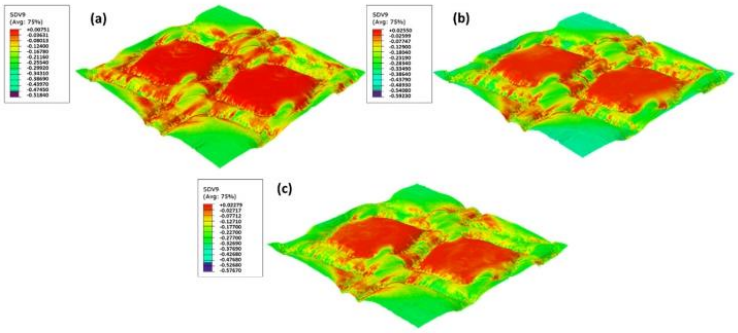

Figure 11. The yield function for deco die for different pressures: (**a**) 2.4 bar, (**b**) 2.8 bar, and (**c**) 3.2 bar.

For the microdie, the differences in yielding are presented in Figure 12.

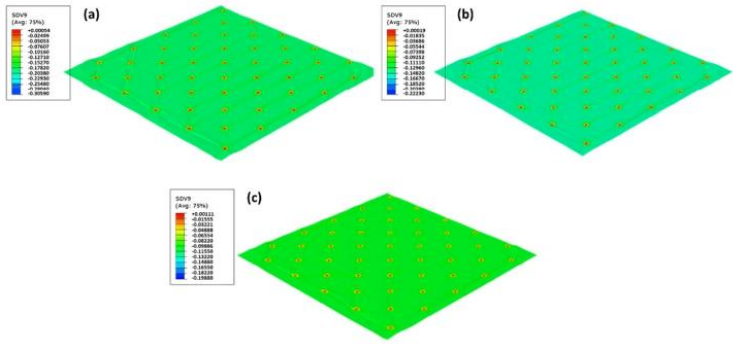

Figure 12. The yield function for micro die for different pressures: (**a**) 2.4 bar, (**b**) 2.8 bar, and (**c**) 3.2 bar.

4. Discussion

Analyzing Figure 4, for the length weighed in the length of the fibers, the values obtained are similar, but on the other hand, the coarseness and fiber width values are higher in sample B. These higher values indicate the existence of recycled fiber or broken process fiber in the fibrous composition of sample B. This information helps to evaluate the results of the remaining properties.

4.1. Sheet Densification

Examining Figure 5b, what immediately stands out is the peak at 2.8 bar pressure, where the maximum tensile index is obtained. Both samples show the same peak at the same pressure. On the other hand, looking at Figure 5a, there is an increase in apparent density when compared with the initial value, but above 2.8 bar the samples behave differently. This can be explained by the fact that sample B is not entirely composed of virgin fiber and therefore, from a pressure of 2.8 bar, the structure of the sheet itself is degraded by breaking the fiber bonds and opening the fibrous structure when the pressure is released, which means an increase in thickness.

Looking at the images in Figure 6, it is clear that in both cases, with increasing pressure, crepe waves decreased their height. In the case of sample B, the visible destruction of the crepe wave should be noted, with a redistribution of the fibers occupying the empty spaces

of the crepe waves. These images corroborate the results discussed above, in which sample B has a more fragile fibrous sheet structure.

From this first part of the work, we can already see that there is an optimal pressure for the embossing process, where the effect of pressure when densifying the paper sheet can be advantageous, as the gain in mechanical strength can counterbalance the losses with the embossing operation.

The blue and green lines in the Figures 7 and 8 show a very similar spreading dynamic evolution in time and within the same range, so there are no relevant differences between the non-compressed and compressed paper samples. However, it can be seen that the spreading evolution in the initial instants ($t < 1.0$ s) is faster for the base tissue paper B when compared with the base tissue paper A. It can be stated that this pressure (2.8 bar) does not affect the spreading of the liquids, but its structure densification is responsible for their different behaviors in the initial instants.

4.2. Sheet Embossing

Comparing Tables 1 and 2, the structural properties of the paper sheet are more affected by the micro embossing pattern than by the deco, as expected. It should be noted that the structural property most affected is thickness, where for the micro embossing pattern an increase of 147% was obtained, while for the deco embossing pattern it remained practically constant with increasing pressure. Because the remaining structural properties are directly related to thickness, they did not undergo major changes for the deco embossing pattern, but for the micro embossing pattern the changes were in accordance with those obtained for thickness. These findings were verified in both samples, A and B.

It can be seen from Figure 9 that the peak at 2.8 bar pressure also occurs in all cases. Just as the micro embossing pattern is what highly affects the structural properties, it is also what impacts the most in the mechanical properties. Comparing the industrial toilet base tissue paper with and without embossing, for the micro embossing pattern, we obtained a loss of about 10% and 2% for sample A and B, respectively. Regarding the embossing deco pattern, as expected, this loss is smaller, obtaining about 8% and 0% for samples A and B, respectively. These results are in line with what was previously discussed, proving that the densification of the sheet was advantageous, so that the loss of mechanical properties by the embossing operation was minimized for the pressure of 2.8 bar.

Looking at Figure 10, the first statement that we can make is that the HF value for a two-ply final product with the two patterns will be between the HF values obtained for each pattern separately. Furthermore, the embossing deco pattern, in both cases, has lower HF values than the micropattern. Contrary to what happens with mechanical strength, it is not at 2.8 bar that the highest HF values are obtained. It is only for the case of the embossing deco pattern of sample B that the highest HF value is obtained for the pressure of 2.8 bar. Comparing the HF of industrial toilet base tissue paper with and without embossing, for the micro embossing pattern, we obtained a loss of about 9% and 12% for sample A and B, respectively. Regarding the embossing deco pattern, as expected, this loss is slightly higher, obtaining about 11% and 13% for samples A and B, respectively. It is necessary to make a compromise between the different properties in order to obtain the best possible result for the final product. Thus, there would be no effective gain in softness if the embossing process was operated at a pressure greater than 2.8 bar and the integrity of the fibrous structure of the paper sheet compromised.

4.3. Finite Element Method (FEM)

Despite the small differences for each pressure, it is possible to observe that the amount of yielding is slightly higher for the lower pressure (2.4 bar), but this plastic state parameter is very similar for 2.8 bar and 3.2 bar. Thus, the lower pressure model is more prone to fail since it has a higher area of greater yielding. For this simulation, the manufacturing pressure does not considerably influence the plasticity state. Only for 3.2 bar is a change in the pattern of the paper during the embossing processes shown. However, these differences

are very small, and the finite element results do not allow to predict the differences in the strength of the paper.

5. Conclusions

This work allowed us to conclude that there is an optimal pressure for the embossing process, in which the mechanical strength is maximized without losing much of the softness value. With this laboratory embossing set-up, the optimum pressure achieved is 2.8 bar. The effect of pressure when densifying the paper sheet gives it a gain in mechanical strength but no differences in terms of liquid absorbency.

The authors can also conclude from this work that the two embossing patterns present different behaviors. The micro embossing pattern is the one that most affects the structure of the paper sheet, both in terms of structural properties and in terms of mechanical strength. On the contrary, the softness is more affected by the embossing deco pattern.

The work conducted with this laboratory embossing set-up came to corroborate the loss of mechanical properties and softness with the embossing process, regardless of the embossing pattern. Sample A was most affected in terms of mechanical properties, while sample B lost more in terms of softness, despite the use of any of the embossing patterns. Thus, the greater or lesser loss of mechanical or softness properties is dependent on the fibrous composition of each sample. In the end, it is essential to make a compromise between the diverse properties in order to achieve a final product with excellent quality.

Finally, the FEM allowed, for the deco embossing pattern, to understand the effect of pressure on the strength of the paper. On the other hand, for the micro embossing pattern, the FEM does not show clear evidence of how the manufacturing pressure affects the paper strength.

Author Contributions: J.C.V.: Data acquisition and curation, investigation, writing—original draft, and writing—review and editing. A.d.O.M.: Image data acquisition and curation, writing—original draft, and writing—review and editing. M.L.R.: FEM analysis, writing—original draft, simulation supervision, and writing—review and editing. A.C.V.: FEM analysis, writing—original draft, simulation supervision, and writing—review and editing. A.M.C.: project pivot and writing—review and editing. P.T.F.: supervision and writing—review and editing. A.P.C.: project supervisor and writing—review and editing. All authors have read and agreed to the published version of the manuscript.

Funding: The authors gratefully acknowledge the funding of this work that was carried out under the Project InPaCTus—Innovative Products and Technologies from Eucalyptus, Project Nº 21874 funded by Portugal 2020 through the European Regional Development Fund (ERDF) in the frame of COMPETE 2020 nº 246/AXIS II/2017. The authors are also very grateful for the support given by research unit Fiber Materials and Environmental Technologies (FibEnTech-UBI), on the extent of the project reference UIDB/00195/2020, and by the Center for Mechanical and Aerospace Science and Technologies (C-MAST-UBI), on the extent of the project reference UIDB/00151/2020, both funded by the Fundação para a Ciência e a Tecnologia, IP/MCTES through national funds (PIDDAC).

Institutional Review Board Statement: Not applicable.

Informed Consent Statement: Not applicable.

Data Availability Statement: Not applicable.

Acknowledgments: The authors would like to also thank the company PCE Iberica S.L. Instrumentacíon for the donation of the Durometer PCE-DDA equipment that was used in this work to determine the apparent hardness of the rubber plates. Finally, the authors acknowledge the materials, access to equipment and installations, and all the general support given by The Navigator Company, RAIZ, and the Optical Center, Department of Physics, Department of Textile Science and Technology, and Department of Chemistry of the Universidade da Beira Interior.

Conflicts of Interest: The authors declare no conflict of interest.

References

1. Berg, P.; Lingqvist, O. Pulp, Paper, and Packaging in the next Decade: Transformational Change. *McKinsey Co. Pap. For. Prod. Pract.* **2019**, 11.
2. Janda, B. Sheet Structure Process Effect on Tissue Properties. Available online: https://tissue360.tappi.org/2017/12/28/sheet-structure-process-effect-on-tissue-properties/ (accessed on 13 December 2018).
3. Brown, S.R. Overview of Tissue Finishing and Converting. *Tappi J.* **1991**, *74*, 91–94.
4. Delić, G.; Vladić, G.; Pál, M.; Banjanin, B.; Dedijer, S. Performance Evaluation of Paper Embossing Tools Produced by Fused Deposition Modelling Additive Manufacturing Technology. *J. Graph. Eng. Des.* **2017**, *8*, 47–54. [CrossRef]
5. Bredahl, G.; Reichling, B.; Schnikoreit, W. Embossing Device. United States Patent Application U.S. 2003/0,110,961 A1, 2003. p. 14.
6. Ingalls, C. *Adding Quality through Finishing Processes*; Paperloop: Miami, FL, USA, 2002.
7. Hilbig, K.; Liplijn, M.; Reinheimer, H. Method of Making a Thick and Smooth Embossed Tissue. United States Patent Application U.S. 2005/0,230,069 A1, 20 October 2005. p. 9.
8. Giannini, D. What Measurements Are Necessary to Understand the Impact of Converting on the Nowadays Tissue Market? Available online: https://www.linkedin.com/pulse/what-measurements-necessary-understand-impact-tissue-market-giannini/ (accessed on 8 September 2021).
9. Assis, T.; Reisinger, L.; Pal, L.; Pawlak, J.; Jameel, H.; Gonzalez, R. Understand the Effect of Machine Technology and Cellulosic Fibers on Tissue Properties—A Review. *BioResources* **2018**, *13*, 4593–4629. [CrossRef]
10. Giannini, D. Paper Thickness/Caliper: Part I. Available online: https://www.linkedin.com/pulse/paper-thicknesscaliper-part-i-dario-giannini/ (accessed on 8 September 2021).
11. Giannini, D. Resistance (Tensile Strength): Part I. Available online: https://www.linkedin.com/pulse/resistance-tensile-strength-part-i-dario-giannini/ (accessed on 8 September 2021).
12. Giannini, D. Resistance Measurement in Tissue Paper Industry (Part II). Available online: https://www.linkedin.com/pulse/resistance-measurement-tissue-paper-industry-part-ii-dario-giannini/ (accessed on 8 September 2021).
13. Giannini, D. Resistance: Part IV. Available online: https://www.linkedin.com/pulse/resistance-part-iv-dario-giannini/ (accessed on 8 September 2021).
14. Khan, A.A. Development of Model to Simulate Embossing of Tissue Paper—Effect of Embossing on Mechanical Performance of Tissue. Master's Thesis, KTH Royal Institute of Technology, Stockholm, Sweden, 2021.
15. Pawlak, J.J.; Frazier, R.; Vera, R.E.; Wang, Y.; Gonzalez, R. Review: The Softness of Hygiene Tissue. *BioRes* **2022**, *17*, 3509–3550. [CrossRef]
16. Spina, R.; Cavalcante, B. Characterizing Materials and Processes Used on Paper Tissue Converting Lines. *Mater. Today Commun.* **2018**, *17*, 427–437. [CrossRef]
17. Vieira, J.C.; Morais, F.; de Oliveira Mendes, A.; Ribeiro, M.L.; Carta, A.M.; Curto, J.; Amaral, M.E.; Fiadeiro, P.T.; Costa, A.P. Mechanical and Softness Characterization of "Deco" and "Micro" Embossed Tissue Papers Using Finite Element Model (FEM) Validation. *Cellulose* **2022**, *29*, 5895–5912. [CrossRef]
18. *ISO 12625-6:2005*; Tissue Paper and Tissue Products—Part 6: Determination of Grammage 2005. ISO: Geneva, Switzerland, 2015.
19. de Oliveira Mendes, A.; Fiadeiro, P.T.; Ramos, A.M.M.; de Sousa, S.C.L. Development of an Optical System for Analysis of the Ink–Paper Interaction. *Mach. Vis. Appl.* **2013**, *24*, 1733–1750. [CrossRef]
20. Fiadeiro, P.T.; de Mendes, A.; Ramos, A.M.; de Sousa, S.C. *Study of the Ink-Paper Interaction by Image Analysis: Surface and Bulk Inspection*; Martins, M.F.P.C., Ed.; Proc. SPIE 8785; SPIE: Porto, Portugal, 2013; p. 8785BV. [CrossRef]
21. Sousa, S.C.L.; de Mendes, A.O.; Fiadeiro, P.T.; Ramos, A.M.M. Dynamic Interactions of Pigment-Based Inks on Chemically Modified Papers and Their Influence on Inkjet Print Quality. *Ind. Eng. Chem. Res.* **2014**, *53*, 4660–4668. [CrossRef]
22. Curto, J.M.R.; Mendes, A.O.; Conceição, E.L.T.; Portugal, A.T.G.; Fiadeiro, P.T.; Ramos, A.M.M.; Simões, R.M.S.; Santos, M.J. Development of an Innovative 3D Simulator for Structured Polymeric Fibrous Materials and Liquid Droplets. In *Mechanical and Materials Engineering of Modern Structure and Component Design*; Öchsner, A., Altenbach, H., Eds.; Advanced Structured Materials; Springer International Publishing: Cham, Switzerland, 2015; Volume 70, pp. 301–321. ISBN 978-3-319-19442-4.
23. Morais, F.P.; Vieira, J.C.; Mendes, A.O.; Carta, A.M.; Costa, A.P.; Fiadeiro, P.T.; Curto, J.M.R.; Amaral, M.E. Characterization of Absorbency Properties on Tissue Paper Materials with and without "Deco" and "Micro" Embossing Patterns. *Cellulose* **2021**, *29*, 541–555. [CrossRef]
24. *ISO 12625-4:2005*; Tissue Paper and Tissue Products—Part 4: Determination of Tensile Strength, Stretch at Break and Tensile Energy Absorption 2005. ISO: Geneva, Switzerland, 2005.
25. *ISO 12625-3:2014*; Tissue Paper and Tissue Products—Part 3: Determination of Thickness, Bulking Thickness and Apparent Bulk Density and Bulk 2014. ISO: Geneva, Switzerland, 2014.
26. Vieira, J.C.; de Mendes, A.O.; Carta, A.M.; Galli, E.; Fiadeiro, P.T.; Costa, A.P. Impact of Embossing on Liquid Absorption of Toilet Tissue Papers. *BioResources* **2020**, *15*, 3888–3898. [CrossRef]
27. Mäkelä, P.; Östlund, S. Orthotropic Elastic–Plastic Material Model for Paper Materials. *Int. J. Solids Struct.* **2003**, *40*, 5599–5620. [CrossRef]
28. Karafillis, A.P.; Boyce, M.C. A General Anisotropic Yield Criterion Using Bounds and a Transformation Weighting Tensor. *J. Mech. Phys. Solids* **1993**, *41*, 1859–1886. [CrossRef]

polymers

MDPI

Article

FEM Analysis Validation of Rubber Hardness Impact on Mechanical and Softness Properties of Embossed Industrial Base Tissue Papers

Joana Costa Vieira [1,*], António de O. Mendes [1], Marcelo Leite Ribeiro [1,2], André Costa Vieira [3], Ana Margarida Carta [4], Paulo Torrão Fiadeiro [1] and Ana Paula Costa [1]

[1] Fiber Materials and Environmental Technologies Research Unit (FibEnTech-UBI), University da Beira Interior, R. Marquês D'Ávila e Bolama, 6201-001 Covilhã, Portugal; ant.mendes@ubi.pt (A.d.O.M.); malribei@usp.br (M.L.R.); fiadeiro@ubi.pt (P.T.F.); anacosta@ubi.pt (A.P.C.)
[2] Aeronautical Engineering Department, São Carlos School of Engineering, University of São Paulo, São Carlos 05508-060, SP, Brazil
[3] Center for Mechanical and Aerospace Science and Technologies (C-MAST-UBI), University da Beira Interior, R. Marquês D'Ávila e Bolama, 6201-001 Covilhã, Portugal; andre.costa.vieira@ubi.pt
[4] Forest and Paper Research Institute (RAIZ), R. José Estevão, Eixo, 3800-783 Aveiro, Portugal; ana.carta@thenavigatorcompany.com
* Correspondence: joana.costa.vieira@ubi.pt

Abstract: The embossing operation is one of the processes of tissue paper converting The embossing parameters influence the final properties of tissue products, such as mechanical, softness, and bulk. In this study, the influence of the rubber hardness used against the embossing steel rolls with a pattern created by intaglio engraving was studied. Three different configurations of rubber plates stacking, each plate with different hardness, were studied. After embossing, mechanical properties, softness, and bulk were evaluated to analyze the effect of rubbers hardness on these properties. Furthermore, a Finite Element Model of the embossing operation was used that considered the same rubber plates stacking configurations used in experiments, and it was able to replicate the experimental results. This work led us to conclude that the configuration where two rubber plates with different hardness, where the rubber plate with higher hardness is in contact with the tissue paper sheet, has shown to be the best solution to obtain higher softness. These findings support the use of embossing operations rubber rolls with a low hardness internal layer and a high hardness external layer in industry. Thus, finite element models were also shown to be reliable tools to virtually test other configurations, such as, for example, three or more rubber plates with different hardness. Since embossing is one of the tissue paper transformation operations with the greatest impact on the key properties of the final product, this study allows the producer to optimize them by varying the hardness of the rubber roll, as well as its configuration.

Keywords: embossing prototype; FEM simulation; mechanical properties; optical visual inspection; rubber hardness; softness characterization; tissue paper

Citation: Vieira, J.C.; Mendes, A.d.O.; Ribeiro, M.L.; Vieira, A.C.; Carta, A.M.; Fiadeiro, P.T.; Costa, A.P. FEM Analysis Validation of Rubber Hardness Impact on Mechanical and Softness Properties of Embossed Industrial Base Tissue Papers. *Polymers* **2022**, *14*, 2485. https://doi.org/10.3390/polym14122485

Academic Editor: Emin Bayraktar

Received: 31 May 2022
Accepted: 16 June 2022
Published: 18 June 2022

1. Introduction

The embossing process comprises the step of passing the base tissue paper sheet through a nip formed by two rolls. A first steel roll, where the pattern is engraved, and a second steel roll with a rubber cover [1,2]. This operation is very important for tissue paper conversion, since causes an increase in volume, absorption capacity, and visual appeal, which are fundamental characteristics for the final consumer.

Tissue paper producers have, over the years, based the embossing and lamination process on two different types: nested (or point-to-valley) and point-to-point (PTP). The latter was first developed by Procter & Gamble in the 1960s, where great care is needed with the synchronization of the rollers to ensure correct point-to-point alignment [3]. Nystrand in

1970, instead, designed a method in which a point is aligned with a valley, where, although the rollers have yet to be synchronized to maintain the point-to-valley, this synchronization does not have to be perfect, because the alignment between a point and a valley allows a higher margin of error [3].

Over the years, many different solutions have emerged for the embossing and lamination process, in the end using one rubber cover steel roll. Today, this solution is the standard design for all converting machines. The hardness of the rubber cover has been increased to a value of 70 Sh-A. The current trend is to change the conventional rubber cover and introduce a double layer cover: a soft inner layer (with low hardness) and a hard outer layer (with high hardness), in order to obtain a greater degree of flexibility for the hard outer surface of the roll cover [3].

From the information provided by the manufacturers of embossing rollers with rubber cover, depending on the type of rubber and its hardness, some advantages in the maintenance and lifetime of this cover can be achieved (Table 1).

Table 1. Range of hardness and advantages of rubber cover in the embossing process [4,5].

Product	Material	Hardness (Sh-A)	Cover Thickness (mm)	Advantages	Supplier
Skapa Mark Rubber	Rubber Standard	50–70	15–25	Abrasion resistance	Skapa
Skapa Mark Rubber plus	Rubber Premium	50–70	15–25	Better Abrasion resistance	Skapa
Skapa Mark Pur	Polyurethane Standard	50–70	15–25	Good Lifetime	Skapa
Skapa Mark Ultra	Polyurethane Premium	50–70	15–25	Optimized Lifetime; Marking Intensity	Skapa
EmboFlex Plus	Rubber Premium	60	12–20	Good resistance	Hannecard
EmboFlex XL	Rubber Premium	50–70	12–20	Good resistance	Hannecard
Multiplast	Rubber Premium	55	10–20	Demanding Applications	Hannecard
Resistoplast	Rubber Premium	45–98	10–20	Demanding Applications	Hannecard
Resistoplast-AS	Rubber Premium	55	10–20	Antistatic	Hannecard
XL Plast	Rubber Premium	50–95	10–20	Demanding Applications	Hannecard

To select a rubber cover for an embossing roll, the user cannot worry only about which material works best. If the operating and environmental conditions do not affect the performance of the roll cover, then the decision focuses only on economic reasons. In most situations, the process and environmental conditions limit the type of material that can be considered in the roll covers [6]. Each rubber has its own characteristics, as shown in Table 1. Some are great for temperature resistance, others for chemical resistance, others for abrasion resistance, and others have a good lifetime. Therefore, one type of rubber may not be suitable for all applications. For example, polyurethane covers are great for abrasion resistance (long lifetime). As they are casted, they do not leave joint marks in the roll manufacturing process. These characteristics make the choice of polyurethane very desirable. However, this material has a relatively low maximum operating temperature (starting to soften at 71 °C and becoming liquid at 81 °C) [6].

To determine the hardness of the roll cover, it must be static, and the measure is carried out with the assistance of a durometer. This hardness is never determined at the nip of the embossing process and is always carried out before the roll with the cover is put into service. With the embossing process, the stresses that the rubber suffers, both in terms of pressure and temperature increase, would change the hardness value if it would be measured during the process. Thus, the determination of hardness using a durometer, by itself, is not a good indicator of the rubber's performance under the conditions of embossing

operation. The modulus of elasticity of the rubber is an alternative method to evaluate the performance of the rubber during the process, as it gives us information about the stiffness or flexibility of the material when exposed to forces during the process. Each rubber has a characteristic modulus value that is directly related to its molecular structure [6]. High elastic modules indicate materials with a more crystalline structure and, consequently, more stiff materials. On the other hand, lower elastic modules, indicate materials with a more amorphous structure and, consequently, more flexible materials [6,7]. In brief, two different rubbers can have the same hardness value, but have a completely different nip compression behavior, due to value of elastic modulus [6]. It is important to underline that hardness is directly associated with strength and not stiffness [7]. This performance of the embossing roll cover will influence the properties of embossed tissue paper and directly the final product.

It has long been recognized that the most important physical characteristics of tissue paper products are their strength, thickness, softness, and absorption [1,8–10]. Research and development efforts by the tissue paper industry in this area have been directed to optimize each one of these parameters without seriously affecting the others [1]. In the conversion process a commitment is made to establish a balance of these parameters. The final quality required for the product results from a well-balanced combination of its final properties. If a tissue paper product, such as toilet paper, is not smooth enough, increasing the bulk or resistance would not add more value to the product, because softness is the most important property for the end consumer. On the other hand, if this product has an excess of bulk or resistance earlier, there are finishing processes that will improve the softness at the detriment of the loss of one or both properties. As a result, the balance and compromise of the final properties of papers can turn into an improvement in the quality and value for the final product, but generally, some properties are achieved to the detriment of others (see Table 2). With sufficient knowledge of these compensations, the transformation process can be optimized to meet the desired product requirements [2,11].

Table 2. Main effects of finishing processes on paper properties [11].

Type of Finishing Process	Scheme of Finishing Process	Gain Properties	Loss Properties
Calendering	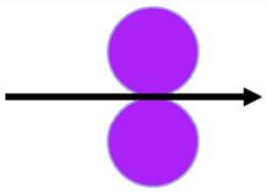	Softness	Bulk
Embossing	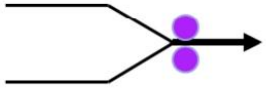	Bulk; Absorption Capacity; Softness	Tensile Strength; Softness
Ply Bonding and Laminating	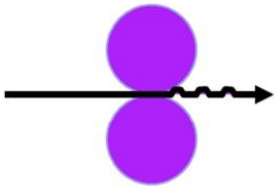	Absorption Capacity; Softness; Bulk (in some cases)	Softness

Table 2. *Cont.*

Type of Finishing Process	Scheme of Finishing Process	Gain Properties	Loss Properties
Lotionizing	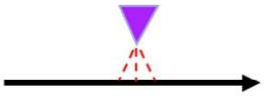	Softness	Absorption Capacity
Printing	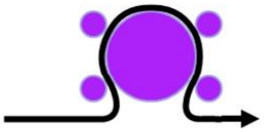	Aesthetic Appearance	Bulk

In this work we intend to study the evolution of mechanical and softness properties of tissue paper varying with the rubber hardness in a laboratory embossing process, using the same industrial base tissue paper. In addition, different combinations of double rubber layers were also studied. A finite element method (FEM) was used to analyze and validate this experiment.

2. Materials and Methods

2.1. Materials

To perform this work, an industrial base tissue paper (creped paper) from one Portuguese factory was used, as shown in Figure 1. The sample used is composed of a mixture of *eucalyptus globulus* (hardwood) and *pinus* (softwood) bleached kraft pulps, with hardwood content of about 30%, which is fully characterized as sample M in the data article from the authors [12]. This industrial base tissue paper, here designated by sample B, was produced on a machine with single headbox and ceramic creping blade with a grammage of 16.7 g/m^2.

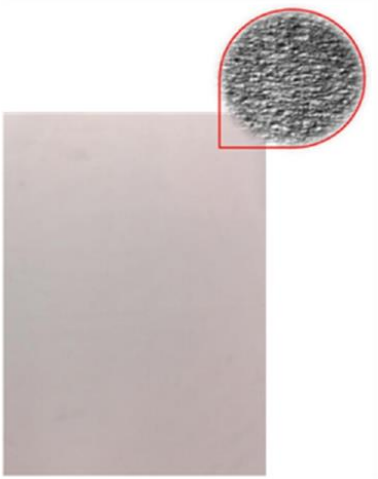

Figure 1. Image of the industrial base tissue paper and the inset showing the crepe structure in a small magnified area.

Additionally, for the execution of this work, 3 rubber plates with different hardness and a thickness of 11 mm were chosen, within the range mentioned by the suppliers 50–70 Sh-A. Figure 2 shows the aspect of these rubber plates.

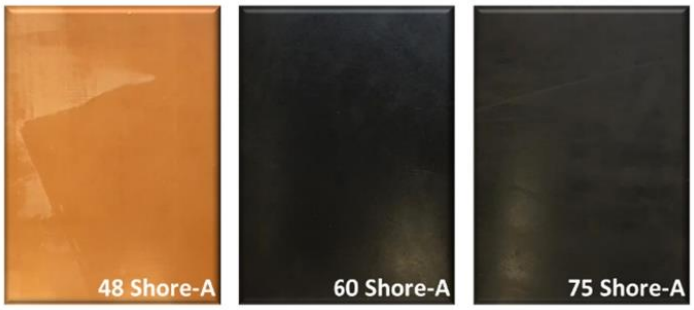

Figure 2. Images of the used rubber plates.

This work began with the determination of rubber hardness according to the specifications provided by the rubber's supplier. Table 3 presents the hardness results obtained for the rubbers used in this work, as well as other characteristics provided by the supplier.

Table 3. Rubber plates characterization results.

Rubber Characteristics	NR BG (45 ± 5 Sh-A)	SBR PR (65 ± 5 Sh-A)	CR PR (70 ± 5 Sh-A)
Hardness (Sh-A)	47.7 ± 0.55	60.3 ± 1.21	75.1 ± 1.98
Tensile Strength (MPa)	16.0	3.0	4.0
Density (g/cm^3)	1.05	1.6	1.5
Operation Temperature (°C)	−40 to +85	−20 to +100	−20 to +100

2.2. Methods

This work started by determining the hardness of the three chosen rubbers plates using a PCE-DDA durometer equipment (PCE Iberica S.L. Instrumentacíon, Albacete, Spain), where each rubber plate was divided in 10 sections, and 1 measurement was made in each section, comprising 10 measurements per plate.

Two embossing patterns were used to perform the embossing operation (deco and micro) engraved in steel plates. Furthermore, 3 different configurations of rubber plates were used in this operation, the configurations are exhibited in Figure 3. Configuration 1 consists of a set of the industrial base tissue paper over the embossing steel plate pressured against two rubber plates with same hardness, configuration 2 is the same set pressured against two rubber plates with different hardness (rubber plate with higher hardness in contact with the paper sample), and, finally, configuration 3 is also the same set, but now pressured against two rubber plates with different hardness (rubber plate with lower hardness in contact with the paper sample).

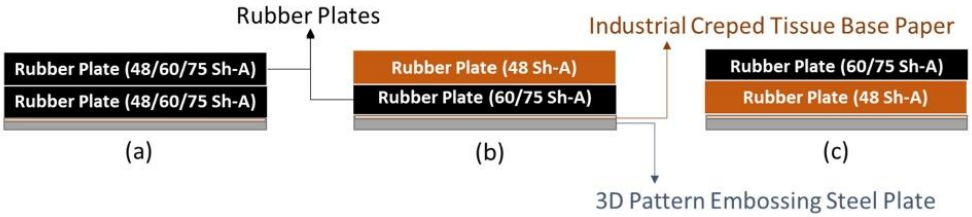

Figure 3. Schematic of the embossing process with different rubber plate hardness configurations: (**a**) configuration 1; (**b**) configuration 2; and (**c**) configuration 3.

The embossing operation conditions used were 2.8 bar during 1 min, for all combinations of 3 stacking configurations and 2 different steel plates, corresponding to the micro

and deco embossing patterns. These operating conditions were studied and optimized in a previous work developed by the authors [13]. The two embossing patterns used are shown in Figure 4.

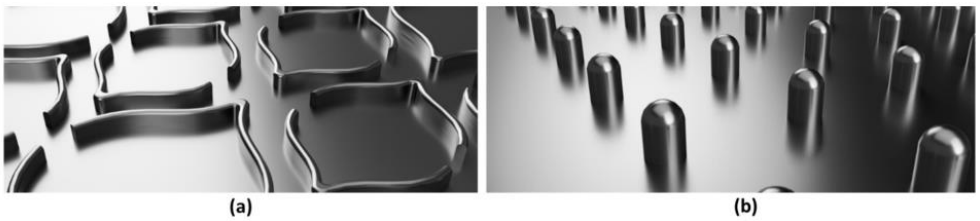

Figure 4. Embossing patterns: (**a**) deco embossing, and (**b**) micro embossing.

All the samples obtained using both patterns and the 3 rubber staking configurations were tested in terms of thickness/bulk and their mechanical tensile strength in machine direction (MD) and in transverse direction (CD). Tensile tests were performed in a Thwing-Albert® VantageNX Universal testing machine in accordance with the tissue standard ISO 12625-4:2005 [14]. Thickness and bulk were measured using a FRANK-TPI® Micrometer accordingly to tissue standard ISO 12625-3:2014 [15]. All samples produced were characterized in terms of softness using the Tissue Softness Analyzer (TSA) from EMTEC®. The TP II algorithm, and the QA I algorithm were used for the computation of the softness handfeel (HF), respectively.

The conducted experiments for surface image acquisition of paper samples engraved with the embossing patterns in the different considered combinations was carried out using a customized optical system [16–18]. This system has shown to be very versatile and useful in this kind of analysis and, therefore, it has already been considered in other related studies [8–10,19,20] concerning the visual inspection and quality control of tissue papers.

2.3. Finite Element Method (FEM)

A finite element model was proposed to improve the understanding of the effect of rubber stiffness, used in paper manufacturing process, on the mechanical properties. Two different die models were used for simulations (deco and micro) and their effects on the paper stress field and plasticity were analyzed, regarding the rubber stiffness used on the paper embossing process.

To model the paper plasticity, an orthotropic elastic-plastic material model [21] was implemented as a user material subroutine for explicit simulations (VUMAT) which is linked to the commercial finite element software ABAQUS™ version 6.14 (Waltham, MA, USA). This material model allows to account for the paper anisotropic behavior, since paper mechanical behavior is highly dependent of fiber orientation [21]. Since the library of commercial finite element software ABAQUS™ does not have a plasticity constitutive model for anisotropic materials, this VUMAT allows to implement a different constitutive relation based on the isotropic J_2 model. The model assumes the additive decomposition of the strain tensor into elastic strain tensor plus plastic strain tensor (Equation (1)), considering that volume is conserved:

$$\varepsilon_{ij} = \varepsilon^{e}_{ij} + \varepsilon^{p}_{ij}, \tag{1}$$

where ε_{ij} is the total strain, ε^{e}_{ij} is the elastic strain, and ε^{p}_{ij} is the plastic strain.

The model uses the concept of an isotropic plasticity equivalent [22] which is a fictitious material that relates the orthotropic stress state to the isotropic stress state. The relation between the actual Cauchy stress tensor and the isotropic plasticity equivalent (IPE) deviatoric tensor is given in Equation (2):

$$s_{ij} = L_{ijkl}\sigma_{kl}, \tag{2}$$

where s_{ij} is the deviatoric IPE stress tensor, σ_{kl} is the Cauchy stress and L_{ijkl} is the fourth order transformation tensor shown in Equation (3) for plane stress:

$$L = \begin{bmatrix} 2A & C-A-B & 0 \\ C-A-B & 2B & 0 \\ B-C-A & A-B-C & 0 \\ 0 & 0 & 3D \end{bmatrix}, \tag{3}$$

where parameters A, B, C, and D are obtained from the experiments using the following equations [21]:

$$A = \sqrt{1-12x^2}, \tag{4}$$

$$B = 3(y-x), \tag{5}$$

$$C = 3(y+x), \tag{6}$$

$$D = \frac{K_{12}^{\frac{n}{(n+1)}}}{\sqrt{3}}, \tag{7}$$

$$x = \sqrt{\frac{\alpha^2}{24(3\alpha^2+\beta^2-4\beta+4)}\left(\beta+1-\sqrt{6\beta-3\alpha^2-3}\right)}, \tag{8}$$

$$y = \frac{\alpha}{4x} - A, \tag{9}$$

$$\alpha = K_{33}^{\frac{2n}{(n+1)}} - K_{22}^{\frac{2n}{(n+1)}}, \tag{10}$$

$$\beta = K_{33}^{\frac{2n}{(n+1)}} + K_{22}^{\frac{2n}{(n+1)}}, \tag{11}$$

Parameters K_{ii} and n were obtained by curve fitting the experimental results, applying the Ramberg-Osgood methodology. For MD direction, the constitutive relation that models the tensile test was:

$$\varepsilon_{11} = \frac{\sigma_{11}}{E_{11}} + \left(\frac{\sigma_{11}}{E_0}\right)^n, \tag{12}$$

where for the CD direction was:

$$\varepsilon_{kk} = \frac{\sigma_{kk}}{E_{kk}} + \left(\frac{K_{kk}E_{kk}}{E_0}\right)^n, k = 2,3 \tag{13}$$

Note that in Equation (13) the repeated indices do not mean the usual summation rule used in the indicial notation. Finally, the parameter K_{12} is obtained using Equation (14).

$$\gamma_{12} = \frac{\sigma_{12}}{G_{12}} + \left(\frac{K_{12}\sigma_{12}}{E_0}\right)^n, \tag{14}$$

The Hooke's law for plane stress and small strain linear elastic orthotropic material is defined by Equation (15):

$$\sigma = C\varepsilon^e, \tag{15}$$

where σ is the Cauchy stress tensor, C is the plane stress linear elastic orthotropic constitutive law and ε^e is the small strain elastic tensor.

The implementation of this model is similar to the well know J_2 flow theory for isotropic materials using the backward-Euler algorithm. As mentioned before, this material model was implemented as a user material subroutine for explicit simulations linked to the commercial finite element software ABAQUS™. The explicit solver was used to overcome convergence issues that are usual when using the implicit solver. On the other hand, using the implicit solver, the stable time increment is very small, resulting in long time simulations. The simulations were performed using a workstation with two intel Xeon

E5-2630 8 cores (16 cores total with 32 threads) with 256 Gb ram. The finite element model dimensions and boundary conditions are presented in Figure 5. The die model dimensions are representative of the actual die dimensions to result in a reasonable computational cost and keeping the precision capability. The base dimension is the same, but it is thick enough to allow the deformation without severe interference in the die and paper kinematics. The paper follows the same dimensions of the die and the basis.

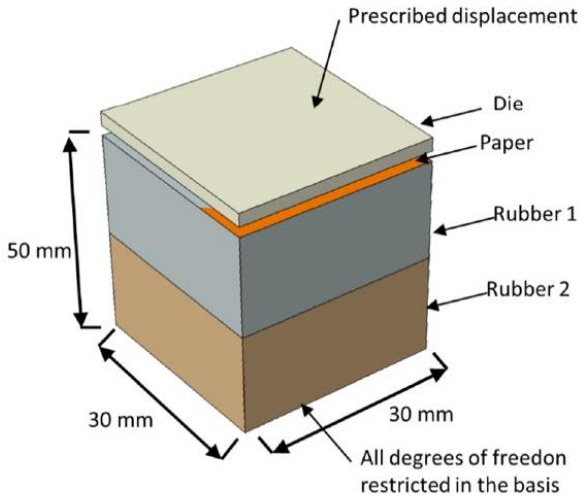

Figure 5. Model dimensions and boundary conditions.

To simulate the influence of the rubber hardness effect on the paper embossing process, the finite element model of the basis was split into two different parts, allowing to simulate the use of different rubber stacking configuration improving the understanding of the basis stiffness influence on the process.

Regarding the finite element boundary conditions, the bottom of the rubber base was recessed. A prescribed displacement was applied on the top of the die, in the downward direction, while the other degrees of freedom (displacements and rotations) were restricted. For the interactions between the model parts, hard contact for normal behavior and frictionless for tangential behavior was considered. The model has 473,694 elements for the simulation of micro die and 476,153 elements for the deco die. For both models, the paper was simulated using a 4-node reduced integration membrane element (M3D4R with a structured mesh with 250,000 elements. For micro die the 4-node reduced integration element (S4R) was used with total number of elements of 7694 elements. The same element was used for the deco die, but for this die, 10,314 elements were used. Finally, the rubber base was modeled using 8-node tridimensional elements (C3D8) using a total of 216,000 elements.

This model uses 5 different type of materials, steel for the die ($E = 200$ GPa, $\mu = 0.33$), a hyperelastic isotropic material model for each of the three different types of rubber, CR PR ($C10 = 1.8$ MPa and $D1 = 0.255746$ MPa^{-1}), SBR PR ($C10 = 0.810343$ MPa and $D1 = 0.56956$ MPa^{-1}), and NR BG ($C10 = 0.409852$ MPa and $D1 = 1.126109$ MPa^{-1}), the rubber mechanical properties was estimated relating the hardness with the Young Modulus as suggested by Larsson [23]. Finally, the paper was modeled as an orthotropic material ($E11 = 13.89$ MPa, $E22 = E33 = 4.23$ MPa, $\mu = 0.33$ and $G12 = 2.1$ MPa).

3. Results

3.1. Configuration 1

As explained in the previous section, in configuration 1 two rubber plates having the same hardness were stacked. In Figure 6, magnified images of the samples obtained for this configuration can be seen. The papers structure, as well as the engraved patterns performed during the embossing process with different hardness of the rubber plates, can easily be observed.

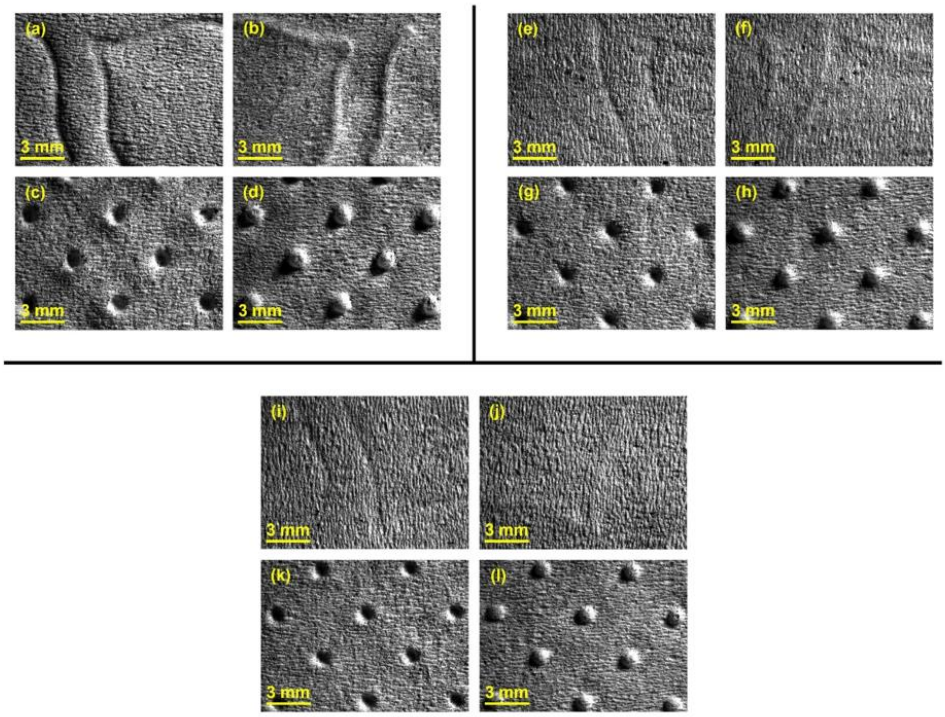

Figure 6. Global views of tissue paper embossed with the different rubber hardness using configuration 1: (**a**) 48 Sh-A (deco—front side); (**b**) 48 Sh-A (deco—back side); (**c**) 48 Sh-A (micro—front side); (**d**) 48 Sh-A (micro—back side); (**e**) 60 Sh-A (deco—front side); (**f**) 60 Sh-A (deco—back side); (**g**) 60 Sh-A (micro—front side); (**h**) 60 Sh-A (micro—back side); (**i**) 75 Sh-A (deco—front side); (**j**) 75 Sh-A (deco—back side); (**k**) 75 Sh-A (micro—front side); and (**l**) 75 Sh-A (micro—back side).

In Figures 7–9, the results obtained for the three main properties of tissue paper (bulk, tensile index, and softness, respectively) as a function of rubber hardness for this configuration and both patterns are presented.

3.2. Configuration 2

As mentioned before, in configuration 2 two rubber plates with different hardness were stacked, where the rubber plate with higher hardness was in direct contact with the sample. In Figure 10, it can be observed detailed images of the samples obtained for this configuration.

In Figures 11 and 12, are shown the results obtained for the three main properties of tissue paper (bulk, tensile index, and softness, respectively) for the two combinations of different rubber hardness plates in configuration 2 and both patterns (deco and micro, respectively).

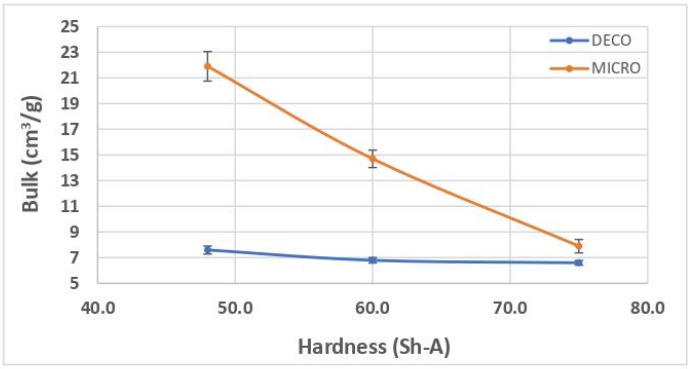

Figure 7. Bulk evolution with the increase in rubber hardness.

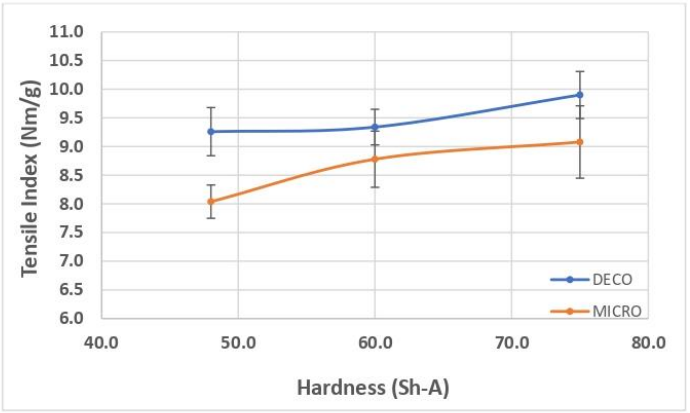

Figure 8. Tensile index behavior with the increase in rubber hardness.

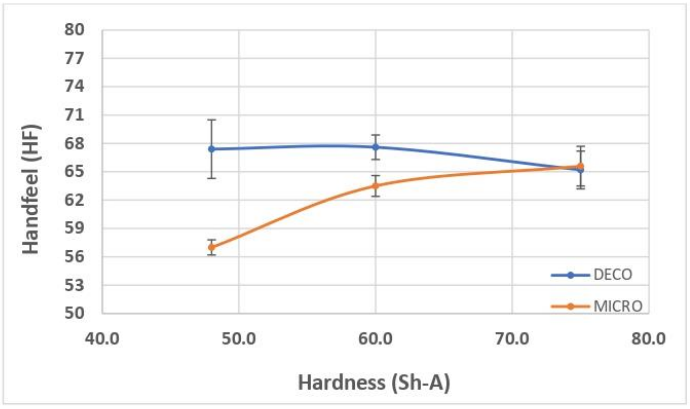

Figure 9. Handfeel comportment with the increase in rubber hardness.

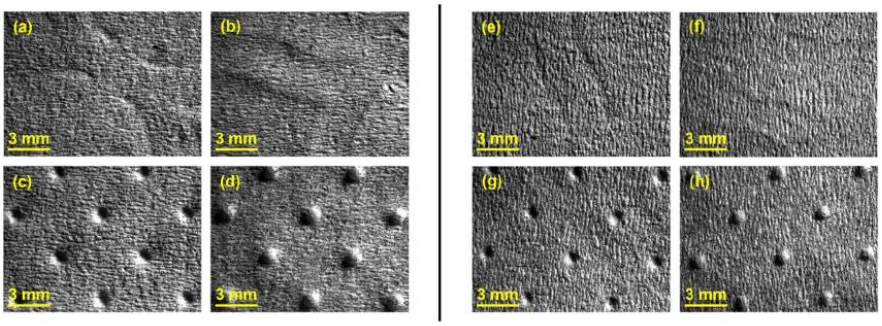

Figure 10. Global views of tissue paper embossed with the different combinations of rubber hardness of configuration 2: (**a**) 60_48 Sh-A (deco—front side); (**b**) 60_48 Sh-A (deco—back side); (**c**) 60_48 Sh-A (micro—front side); (**d**) 60_48 Sh-A (micro—back side); (**e**) 75_48 Sh-A (deco—front side); (**f**) 75_48 Sh-A (deco—back side); (**g**) 75_48 Sh-A (micro—front side); and (**h**) 75_48 Sh-A (micro—back side).

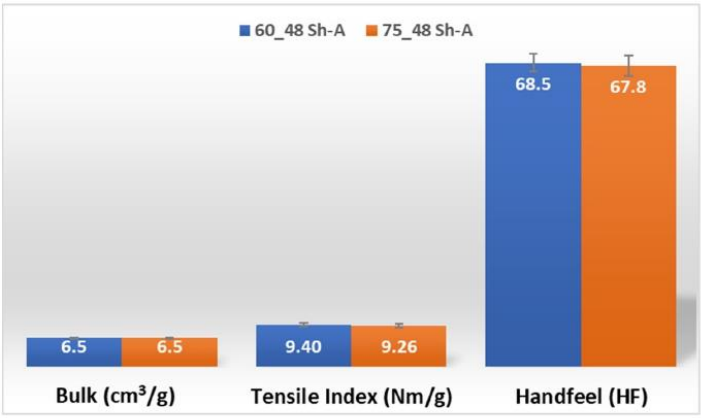

Figure 11. Bulk, tensile index, and handfeel results for deco embossing and configuration 2 rubber hardness conjugation.

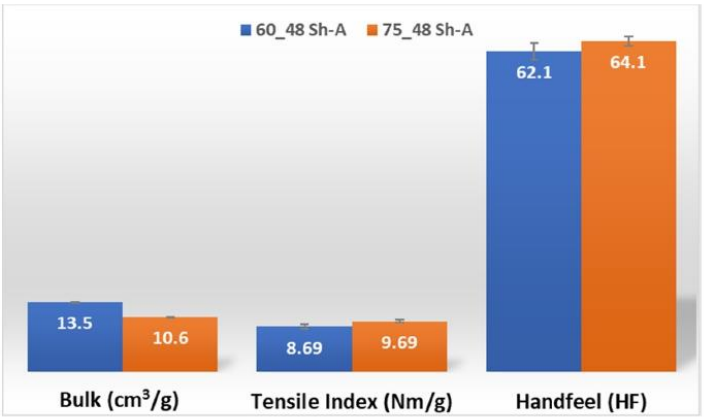

Figure 12. Bulk, tensile index, and handfeel results for micro embossing and configuration 2 rubber hardness conjugation.

3.3. Configuration 3

As stated before, in configuration 3 two rubber plates with different hardness were stacked, where the rubber plate with lower hardness was in direct contact with the sample. In Figure 13, detailed images of the samples obtained for this configuration can be seen.

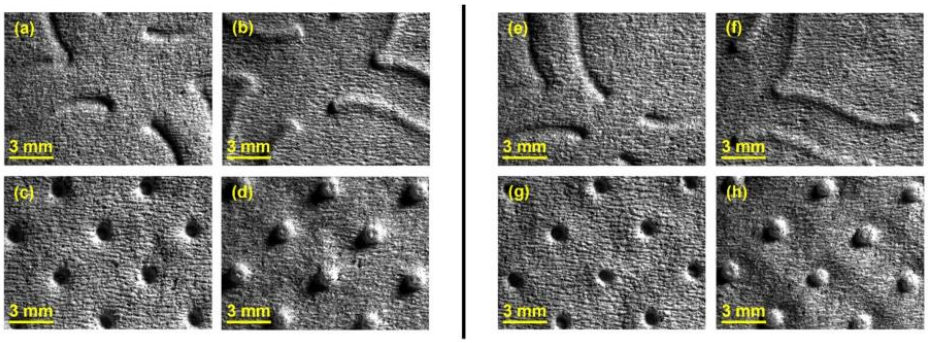

Figure 13. Global views of tissue paper embossed with the different combinations of rubber hardness of configuration 3: (**a**) 48_60 Sh-A (deco—front side); (**b**) 48_60 Sh-A (deco—back side); (**c**) 48_60 Sh-A (micro—front side); (**d**) 48_60 Sh-A (micro—back side); (**e**) 48_75 Sh-A (deco—front side); (**f**) 48_75 Sh-A (deco—back side); (**g**) 48_75 Sh-A (micro—front side); and (**h**) 48_75 Sh-A (micro—back side).

The results obtained for the three main properties of tissue paper (bulk, tensile index, and softness, respectively) are shown in Figures 14 and 15, for the two combinations of different rubber hardness plates in configuration 3 and both patterns (deco and micro, respectively).

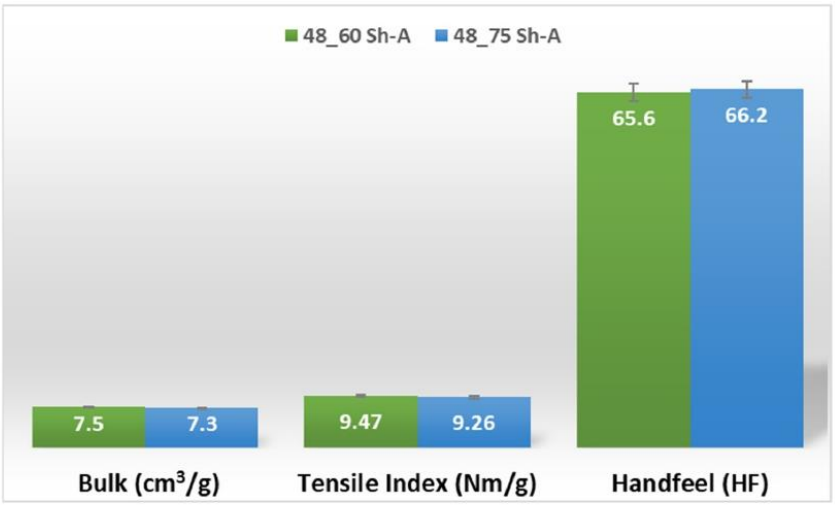

Figure 14. Bulk, tensile index, and handfeel results for deco embossing and configuration 3 rubber hardness conjugation.

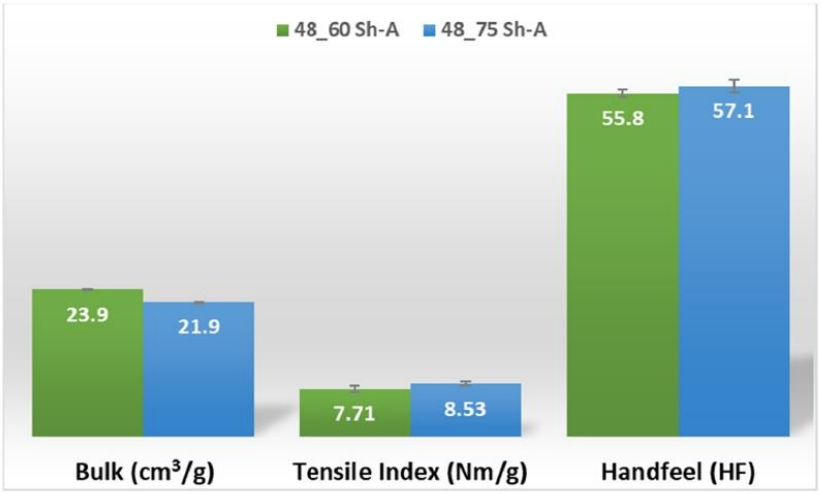

Figure 15. Bulk, tensile index, and handfeel results for micro embossing and configuration 3 rubber hardness conjugation.

Combining the deco embossed sheet with the micro embossed sheet for each rubber combination, in each of the three configurations, a prototype of a 2-ply finished product was obtained. With the aim of optimizing the softness as a function of the hardness of the rubber in the embossing process, the handfeel of each one of these prototypes was measured, and the results are shown in Figure 16.

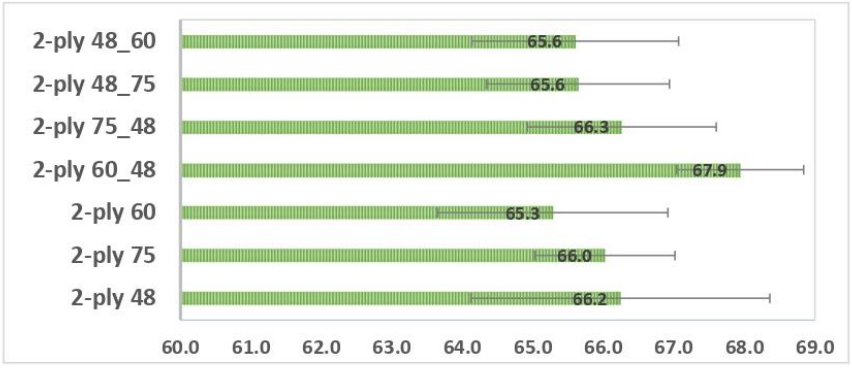

Figure 16. Results obtained for handfeel (HF) with the rubber hardness to the combined 2-ply deco and micro embossed samples.

3.4. Finite Element Method (FEM)

Several simulations were performed to investigate the effect of the basis rubber hardness regarding the different combinations of rubber and die used for the embossing process on the mechanical properties. This model was calibrated based on experimental results; tensile tests of tissue paper sample B, in both directions (MD and CD) and hardness of three different rubber plates, considering the isotropic Neo-Hookean constitutive model, using three different configurations. However, this model allows, with good precision, to digitally optimize future test with varying configurations and parameters combinations.

3.4.1. Configuration 1

As used in experiments, configuration 1, uses only one type of rubber in the basis. Thus, three different cases were simulated for the two die models, as showed from Figures 17–22.

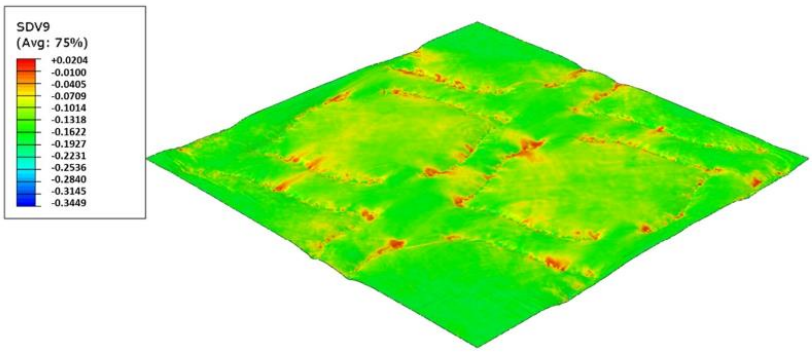

Figure 17. Deco die 75 Sh-A (CR PR), Plastic field.

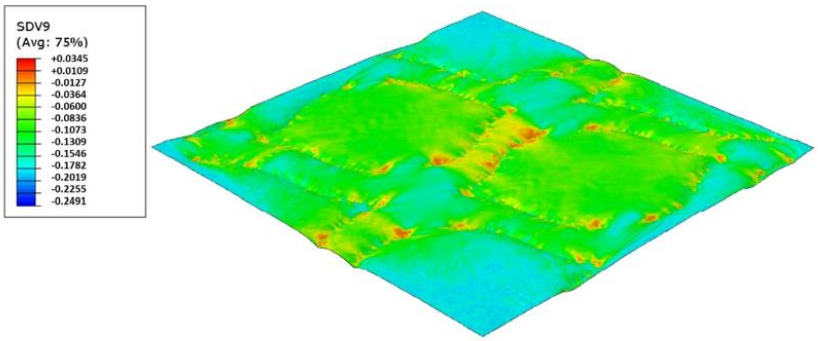

Figure 18. Deco die 60 Sh-A (SBR PR), Plastic field.

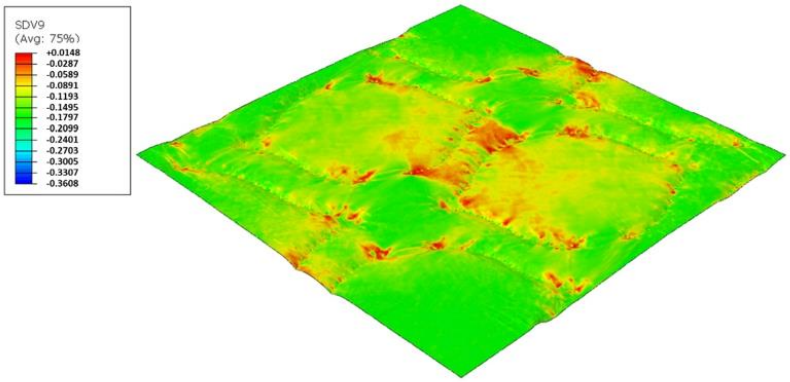

Figure 19. Deco die 48 Sh-A (NR BG), Plastic field.

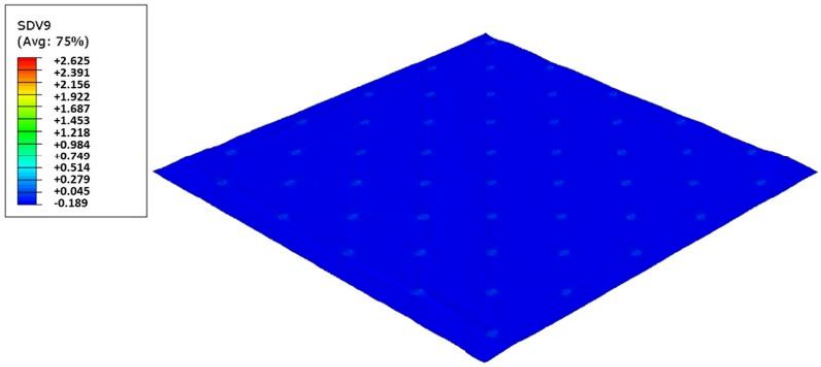

Figure 20. Micro die 75 Sh-A (CR PR), Plastic field.

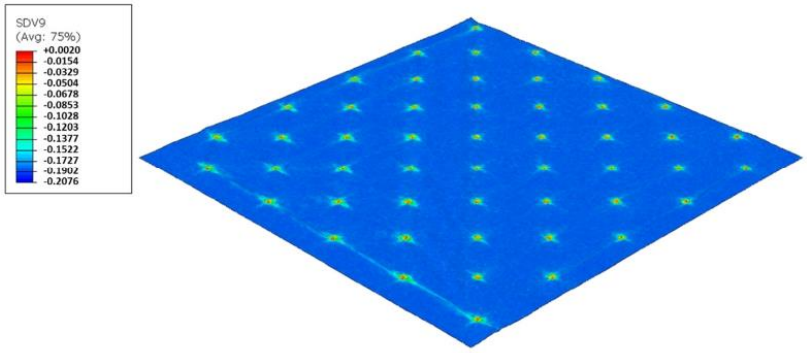

Figure 21. Micro die 60 Sh-A (SBR PR), Plastic field.

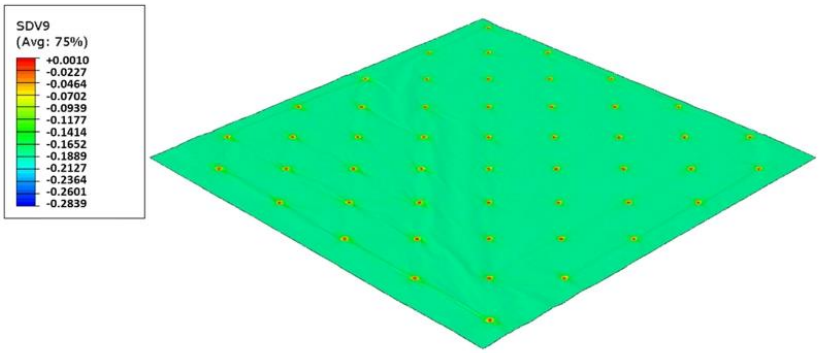

Figure 22. Micro die 48 Sh-A (NR BG), Plastic field.

3.4.2. Configuration 2

In this configuration, the harder rubber is placed on the top, in direct contact with the paper and the softer rubber is used in the bottom of the elastic basis. Figures 23–26 presents the simulation results for the rubber hardness conjugations of configuration 2.

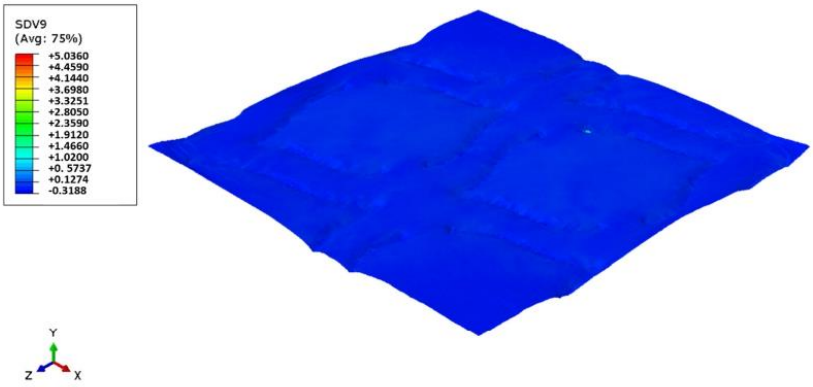

Figure 23. Deco die 75_48 Sh-A (CR PR/NR BG), Plastic field.

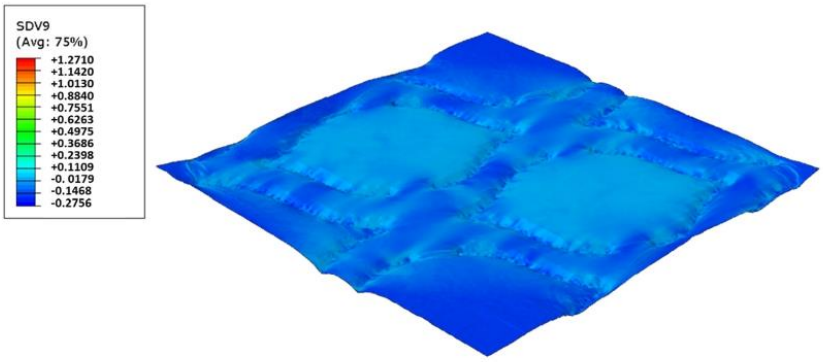

Figure 24. Deco die 60_48 Sh-A (SBR PR/NR BG), Plastic field.

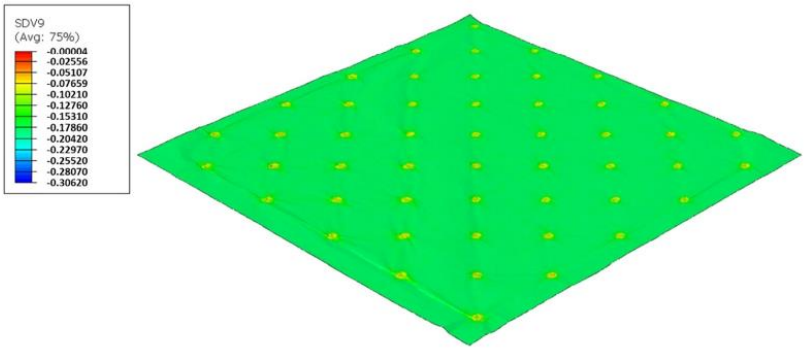

Figure 25. Micro die 75_48 Sh-A (CR PR/NR BG), Plastic field.

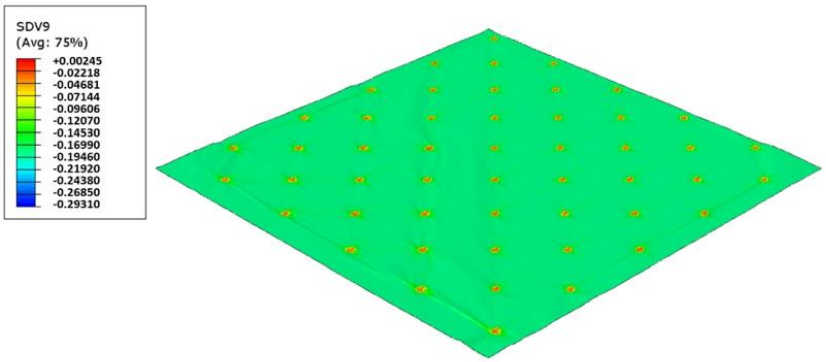

Figure 26. Micro die 60_48 Sh-A (SBR PR/NR BG), Plastic field.

3.4.3. Configuration 3

In this configuration, the softer rubber is placed on the top, in direct contact with the paper. Figures 27–30 presents the simulation results for the rubber hardness conjugations of configuration 3.

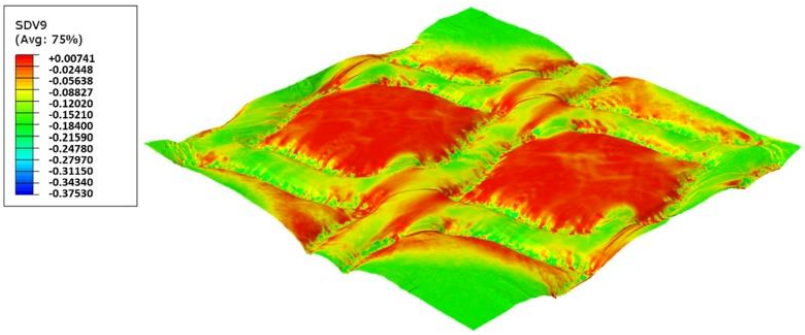

Figure 27. Deco die 48_75 Sh-A (NR BG/CR PR), Plastic field.

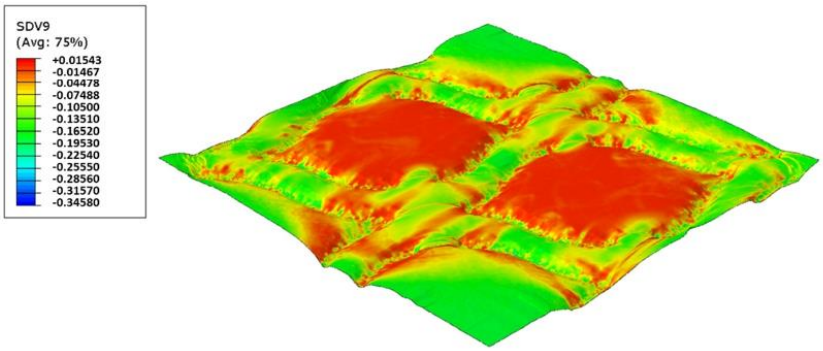

Figure 28. Deco die 48_60 Sh-A (NR BG/SBR PR), Plastic field.

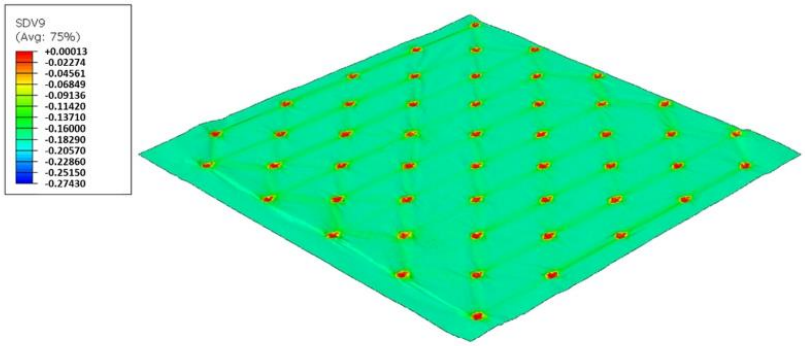

Figure 29. Micro die 48_75 Sh-A (NR BG/CR PR), Plastic field.

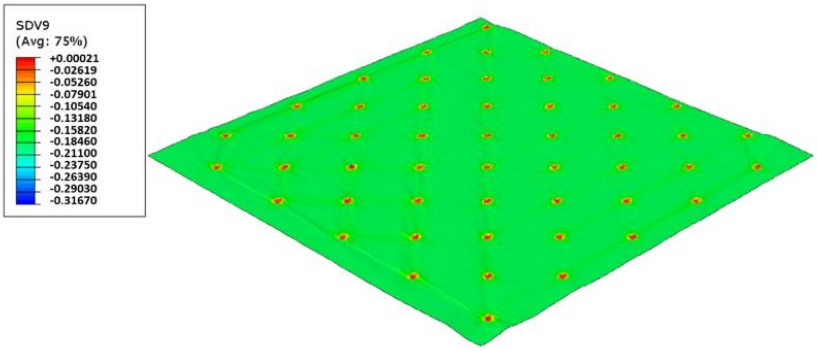

Figure 30. Micro die 48_60 Sh-A (NR BG/SBR PR), Plastic field.

4. Discussion

For configuration 1, analyzing the images presented in Figure 6, it can be seen that with the increase in rubber hardness, the marks engraved with the two used embossing patterns appear shallower in the surfaces of the paper. In particular, the marks obtained with the deco embossing are very similar and very dissimulated for the 60 Sh-A and 75 Sh-A hardness's and the same marks appear a lot more pronounced for the 48 Sh-A hardness. The same effect can also be noticed for the marks obtained with the micro embossing, on which deeper holes are engraved for the 48 Sh-A hardness, and shallower holes are engraved with the 60 Sh-A and 75 Sh-A hardness's. This effect can also be observed, not only by observation of the formed holes in the images shown in Figure 6c,g,k, but also considering the counter side of the paper surfaces engraved with the micro pattern, shown in the images of Figure 6d,h,l. According to the relations obtained in Figure 6, Figure 7 shows the same tendency for bulk, in which, for both embossing patterns, the bulk decreases with the increase in rubber hardness, and this decrease is more pronounced for the micro pattern. Contrary to bulk, the tensile index grows with the increase in rubber hardness as shown by the graph in Figure 8. From 48 Sh-A to 75 Sh-A rubber hardness, the tensile index has an increase of 6.5% for the deco pattern and 11.5% for the micro pattern. As expected, this increase is more pronounced for the micro pattern, since this pattern, by creating a deeper mark on the tissue paper sheet, it weakens the fibrous structure of the sheet, and, consequently, increases the difference obtained between the rubber hardness extremes. Looking at Figure 9, the handfeel for the deco pattern does not change greatly with increasing hardness of the rubber plates. Contrarily, for the micro pattern, it was verified that with the increase in the rubber plates hardness there is an increase in the handfeel value, since the structure of the paper sheet is less marked for higher hardness of

the rubbers. This is in line with the images in Figure 6. Having softness as the main property for the final consumer, and making a compromise between the different properties studied, for configuration 1, the best rubber plate hardness was 60 Sh-A. Figures 17–19 show the simulation results for the configuration with 75 Sh-A, 60 Sh-A and 48 Sh-A hardness for the deco pattern. The simulations show that the amount of plasticity found in the paper finite element model is related with the rubber hardness. For the harder rubber (Figure 17), the amount of plasticity (or permanent deformation) is smaller than that found for softer rubber (Figures 18 and 19). For the softer rubber the plastic field is much more visible. Those results corroborate the experiments showed in Figure 6, where the softer rubber allows deeper marks on the paper. Figures 20–22 show the simulation results for the configuration with 75 Sh-A, 60 Sh-A, and 48 Sh-A hardness for the micro pattern. As for the deco pattern, the simulations show that the amount of plasticity found in the paper finite element model is related with the rubber hardness. Those results also corroborate the experiments showed in Figure 6, where the softer rubber allows deeper marks on the paper.

For configuration 2, examining the pictures of Figure 10, it can be seen that for the deco embossing, both the considered cases, 60_48 Sh-A and 75_48 Sh-A, reveal marks that show to be engraved in the surfaces of the paper in a similar manner of the marks obtained with the rubber's hardness of 60 Sh-A and 75 Sh-A alone considered in the configuration 1. In particular, in Figure 6e,f,i,j and Figure 10a,b,e,f, one can observe that the marks reveal to be very shallow on all the mentioned examples. Concerning the micro embossing, the combination of rubbers 60_48 Sh-A, as shown in Figure 10c,d, reveals marks that are very similar with the ones obtained using the rubber 75 Sh-A alone, Figure 6k,l. It is the second combination of rubbers considered in configuration 3, 75_48 Sh-A, that shows the less engraved marks performed with the micro embossing pattern. The great difference of this example comparatively to all the others is remarkable and easily recognizable, as shown in Figure 10g,h. Analyzing the results of Figure 11, for the embossing deco pattern, it can be verified that for bulk, tensile index, and handfeel, the two combinations of rubber plates hardness show very similar values. In Figure 12, for the embossing micro pattern, the results show that for bulk, as expected, the rubber plate in contact with the sheet with less hardness has a higher value, on the other hand, for the tensile index and handfeel, the rubber plate in contact with the sheet with higher hardness originates higher values, since the sheet is less marked by the embossing pattern (see Figure 10) and, consequently, its structure is less affected. As the softness for the end consumer is the key property of the toilet paper, and making a compromise between the different properties studied, for configuration 2 and pattern of embossing deco, the best hardness was 60_48 Sh-A, while for the micro embossing pattern the best hardness was 75_48 Sh-A. In this configuration the plastic field is not detected for the configuration with the harder rubber on top (Figure 23) and a smaller plasticity in configuration with 60 Sh-A rubber on the top (Figure 24). Those results corroborate the experimental results showed in Figure 10 for the deco die. Thus, the basis with softer rubber allows deeper marks on the paper. As for the case of deco die, in the micro die, the plastic field is more pronounced for the case with the softer rubber on top (Figure 26) than for the harder rubber on the top (Figure 25). Those results also corroborate the experimental results showed in Figure 10 for micro die regarding the visual marks on the paper.

Considering configuration 3 and looking at the images presented in Figure 13, it can be seen that both the considered cases, 48_60 Sh-A and 48_75 Sh-A, reveal marks that show to be deeply engraved in the surfaces of the paper, in particular, the first one which results from the combination of the two of the softest rubbers. An interesting analogy can also be made by comparing the images of Figure 13 with the images of Figure 6, on which the marks obtained in the two considered cases of configuration 2 show great similarities with the marks obtained with the use of 48 Sh-A rubber alone in configuration 1. As in configuration 2, the analysis of Figure 14, for the embossing deco pattern, very similar values were found for both bulk and tensile index in the two combinations of rubber plates. Due to the fact that the rubber plate in contact with the sheet has a lower

hardness, it will imprint a deeper embossing pattern on the sheet (comparison of the images of Figure 10 with Figure 13) and consequently increases the bulk. Thus, the bulk of configuration 3 is higher than that of configuration 2. Since the operating conditions of the embossing process were optimized for this system in a previous work reported by the authors Vieira et al. 2022 [13], there is a maximization of the mechanical properties by the densification of the sheet structure. Therefore, despite verifying an increase in bulk there is no loss of mechanical strength. Regarding the handfeel, the results obtained in absolute value are lower than those obtained in configuration 2, thus being in accordance with the trend obtained for configuration 1. For the embossing micro pattern, Figure 15 presents a behavior very similar to configuration 2. In absolute value, the bulk was higher, while the tensile index and handfeel were lower. Likewise, this is justified, for the bulk, by the deeper marks of the embossing pattern on the sheet (comparing images of Figure 10 with Figure 13), and for the tensile index, by the densification of the sheet structure which results in the maximization of the mechanical properties. Once the sheet is more marked, there is an increase in the surface roughness decreasing the handfeel value. Since the manufacturer wants the highest softness value with the least loss of other properties, in this configuration of rubber plates, the combination chosen would be 48_75 Sh-A hardness for both embossing patterns. For this case, the simulation showed the results for the softer rubber placed on top of the basis in direct contact with the paper sheet. In this configuration, the plastic field is similar for both cases (Figures 27 and 28). For the case with micro pattern, the plastic field is similar for both cases, but the plasticity detected for the softer rubber configuration (Figure 30) is more pronounced than for the configuration with harder rubber on the bottom of the basis (Figure 29). In any case, when we combine rubbers of different hardness, using the lowest rubber hardness in contact with the paper sheet, this results in an embossed paper with lower softness values. Thus, configuration 3 is not an option for toilet paper production, since softness should be maximized.

From the results shown in Figure 16 it can be inferred that configuration 2 is the best rubber hardness configuration for the embossing process. This result agrees with what is mentioned in the bibliography [3], in which it is stated that the trend for future rubber embossing rollers will have an inner layer with low hardness and an outer layer with higher hardness. This is translated into configuration 2, where the rubber plate in contact with the paper sheet has higher hardness and the other plate has lower hardness. Furthermore, within configuration 2, the prototype 2-ply 60_48 Sh-A is the one that showed the best result for softness.

The finite element simulations results allow understanding the effect of the hardness of the rubber basis (and the combinations of rubbers) on the embossing process and linking the plastic field to the paper marks, where the combination of softer rubber results in deeper marks and, on the opposite, shallow marks (low plasticity) increase the paper strength. The validation of this numerical methodology to virtually optimize the process parameters is a subject for future works. In the present work, with a simple adaptation of the J_2 elastoplastic constitutive model that addresses orthotropy (and numerical implemented in Fortan^{TM} via VUMAT) for the paper, and the isotropic Neo-Hookean constitutive model for the rubbers (available in the library of ABAQUS^{TM}) were considered in the FEM model. The calibration of material parameters based on mechanical testing was also addressed. Hence, we can use this numerical methodology for any configuration of rubber laminates with varying thickness and hardness, or other papers based on tensile tests on MD and CD directions.

5. Conclusions

This work led us to conclude that configuration 2, is the best solution to obtain a maximum softness. In accordance with this statement the prototype 2-ply 60_48 Sh-A is the one that achieved the highest handfeel.

The obtained results point to an increase in softness with increasing rubber hardness. The mechanical property losses are more pronounced for the lower rubber hardness and

for the micro embossing pattern. In contrast, bulk is higher for lower rubber hardness and micro embossing pattern. Consequently, when the hardness of different rubbers is combined and the lower hardness rubber is in contact with the paper sheet, the final properties tend to those of the low hardness rubber alone.

The finite element simulations allow the understanding of how the embossing process and rubber hardness affect the paper characteristics. Thus, finite element models are shown to be a reliable tool to simulate the embossing process for paper industry and predict the final paper mechanical characteristics.

This research has highlighted the importance of the rubber hardness in the embossing process and its impact on the final properties of the tissue paper products.

The authors believe that these results improve the knowledge about the embossing process when the impact of each embossing parameter is studied separately, in this case the hardness of the rubber, and also the quality of the final product. In particular, these findings support the idea pointed out in the introduction that the future trend is the usage of embossing rubber rolls with a low hardness internal layer and a high hardness external layer. In future research other configurations considering the combination of different number of rubber plates will be studied, either by FEM simulation or experimentally.

Author Contributions: J.C.V.: Data acquisition and curation, Investigation, Writing—original draft, Writing—review and editing. A.d.O.M.: Image data acquisition and curation, Writing—original draft, Writing—review and editing. M.L.R.: FEM analysis, Writing—original draft, Simulation Supervision, Writing—review and editing. A.C.V.: FEM analysis, Writing—original draft, Simulation Supervision, Writing—review and editing. A.M.C.: Project Pivot, Writing—review and editing. P.T.F.: Supervision, Writing—review and editing. A.P.C.: Project supervisor, Writing—review and editing. All authors have read and agreed to the published version of the manuscript.

Funding: The authors gratefully acknowledge the funding of this work that was carried out under the Project InPaCTus—Innovative Products and Technologies from Eucalyptus, Project Nº 21874 funded by Portugal 2020 through European Regional Development Fund (ERDF) in the frame of COMPETE 2020 nº 246/AXIS II/2017. The authors are also very grateful for the support given by research unit Fiber Materials and Environmental Technologies (FibEnTech-UBI), on the extent of the project reference UIDB/00195/2020, and by the Center for Mechanical and Aerospace Science and Technologies (C-MAST-UBI), on the extent of the project reference UIDB/00151/2020, both funded by the Fundação para a Ciência e a Tecnologia, IP/MCTES through national funds (PIDDAC).

Institutional Review Board Statement: Not applicable.

Informed Consent Statement: Not applicable.

Data Availability Statement: Not applicable.

Acknowledgments: The authors would like to also thank the company PCE Iberica S.L. Instrumentacíon for the donation of the Durometer PCE-DDA equipment that was used in this work to determine the apparent hardness of the rubber plates. Finally, the authors acknowledge the materials, access to equipment and installations, and all the general support given by The Navigator Company, RAIZ, and the Optical Center, Department of Physics, Department of Textile Science and Technology, Department of Chemistry, and Nuno Santos from FABLAB of the Universidade da Beira Interior.

Conflicts of Interest: The authors declare no conflict of interest.

References

1. Hilbig, K.; Liplijn, M.; Reinheimer, H. Method of Making a Thick and Smooth Embossed Tissue. Available online: https://www.freepatentsonline.com/20050230069.pdf (accessed on 21 October 2020).
2. Lofink, B. Device for Applying an Embossing to a Web of Tissue Paper. Available online: https://patents.justia.com/patent/20030010228 (accessed on 21 October 2020).
3. Biagiotti, M. Tissue Embossing Developments | The Tissue Story. 2017. Available online: https://www.tissuestory.com/2017/11/21/tissue-embossing-developments/ (accessed on 8 January 2019).
4. Skapa Roll Covers for the Paper Industry-World of Roll Covers. 2020. Available online: http://vit-group.com/skapa/test/download/Produktprospekt_GB.pdf (accessed on 21 October 2020).

5. Hannecard Embossing Roll (Tissue). Available online: https://www.hannecard.com/en/industries/tissue/paper-tissue-converting/embossing-roll-tissue/ (accessed on 21 October 2020).
6. Huff, S.; Bell, J. *How Do You Know You^{TM}ve Got the Right Cover for Your*; Curran Associates, Inc.: Myrtle Beach, SC, USA, 2005; p. 8.
7. Schaefer, R.J. Chapter 33-mechanical properties of rubber. In *Harris' Shock and Vibration Handbook by Allan G. Piersol*; The McGraw-Hill Companies, Inc.: New York, NY, USA, 2002; p. 18.
8. Vieira, J.C.; Mendes, A.d.O.; Carta, A.M.; Galli, E.; Fiadeiro, P.T.; Costa, A.P. Impact of Embossing on Liquid Absorption of Toilet Tissue Papers. *BioResources* **2020**, *15*, 3888–3898. [CrossRef]
9. Mendes, A.d.O.; Vieira, J.C.; Carta, A.M.; Galli, E.; Simões, R.; Fiadeiro, P.T. Influence of Tissue Paper Converting Conditions on Finished Product Softness. *BioResources* **2020**, *15*, 7178–7190. [CrossRef]
10. Vieira, J.C.; Morais, F.; de Oliveira Mendes, A.; Ribeiro, M.L.; Carta, A.M.; Curto, J.; Amaral, M.E.; Fiadeiro, P.T.; Costa, A.P. Mechanical and softness characterization of "deco" and "micro" embossed tissue papers using finite element model (FEM) validation. *Cellulose* **2022**, *29*, 5895–5912. [CrossRef]
11. Ingalls, C. *Adding Quality Through Finishing Processes*; Paperloop: Miami, MIA, USA, 2002, Available online: http://www.embossingtechnologies.com/documents/TWA2002Ingalls/Finishing.htm (accessed on 21 October 2002).
12. Vieira, J.C.; Mendes, A.d.O.; Carta, A.M.; Fiadeiro, P.T.; Costa, A.P. Experimental dataset supporting the physical and mechanical characterization of industrial base tissue papers. *Data Brief.* **2020**, *33*, 106434. [CrossRef] [PubMed]
13. Vieira, J.C.; Mendes, A.d.O.; Ribeiro, M.L.; Vieira, A.C.; Carta, A.M.; Fiadeiro, P.T.; Costa, A.P. Embossing Pressure Effect on Mechanical and Softness Properties of Industrial Base Tissue Papers with Finite Element Method Validation. In Proceedings of the Materials Proceeding Materiais 2022-XX International Symposium on Materials, Marinha Grande, Leira, Portugal, 10–13 April 2022; Volume 8. [CrossRef]
14. *ISO 12625-4:2005*; Tissue Paper and Tissue Products-Part 4: Determination of Tensile Strength, Stretch at Break and Tensile Energy Absorption. International Organization for Standardization: Geneva, Switzerland, 2005.
15. *ISO 12625-3:2014*; Tissue Paper and Tissue Products-Part 3: Determination of Thickness, Bulking Thickness and Apparent Bulk Density and Bulk. International Organization for Standardization: Geneva, Switzerland, 2014.
16. Mendes, A.d.O.; Fiadeiro, P.T.; Costa, A.P.; Amaral, M.E.; Belgacem, M.N. Retro-Diffusion and Transmission of Laser Radiation to Characterize the Paper Fiber Distribution and Mass Density. *Proc. SPIE* **2013**, *8785*, 8785AY. [CrossRef]
17. Mendes, A.d.O.; Fiadeiro, P.T.; Costa, A.P.; Amaral, M.E.; Belgacem, M.N. Study of Repeatability of an Optical Laser System for Characterization of the Paper Fiber Distribution and Mass Density. *Proc. SPIE* **2014**, *9286*, 92862Y. [CrossRef]
18. Mendes, A.d.O.; Fiadeiro, P.T.; Costa, A.P.; Amaral, M.E.; Belgacem, M.N. Laser scanning for assessment of the fiber anisotropy and orientation in the surfaces and bulk of the paper. *Nord. Pulp Pap. Res. J.* **2015**, *30*, 308–318. [CrossRef]
19. Vieira, J.C.; Vieira, A.C.; Mendes, A.d.O.; Carta, A.M.; Fiadeiro, P.T.; Costa, A.P. Mechanical Behavior of Toilet Paper Perforation. *BioResources* **2021**, *16*, 4846–4861. [CrossRef]
20. Vieira, J.C.; Vieira, A.C.; Mendes, A.d.O.; Carta, A.M.; Fiadeiro, P.T.; Costa, A.P. Toilet Paper Perforation Efficiency. *BioResources* **2022**, *17*, 492–503. [CrossRef]
21. Mäkelä, P.; Östlund, S. Orthotropic elastic–plastic material model for paper materials. *Int. J. Solids Struct.* **2003**, *40*, 5599–5620. [CrossRef]
22. Karafillis, A.P.; Boyce, M.C. A general anisotropic yield criterion using bounds and a transformation weighting tensor. *J. Mech. Phys. Solids* **1993**, *41*, 1859–1886. [CrossRef]
23. Larsson, P.T.; Lindström, T.; Carlsson, L.A.; Fellers, C. Fiber length and bonding effects on tensile strength and toughness of kraft paper. *J. Mater. Sci.* **2018**, *53*, 3006–3015. [CrossRef]

polymers

MDPI

Article

Embossing Lines and Dots Geometry Effect on the Key Tissue Paper Properties with Finite Element Method Analysis

Joana Costa Vieira [1,*], António de O. Mendes [1], Marcelo Leite Ribeiro [1,2], André Costa Vieira [3], Ana Margarida Carta [4], Paulo Torrão Fiadeiro [1] and Ana Paula Costa [1]

[1] Fiber Materials and Environmental Technologies Research Unit (FibEnTech-UBI), Universidade da Beira Interior, R. Marquês D'Ávila e Bolama, 6201-001 Covilhã, Portugal
[2] Aeronautical Engineering Department, São Carlos School of Engineering, University of São Paulo, Av. João Dagnone de Melo, São Carlos 13565-120, SP, Brazil
[3] Center for Mechanical and Aerospace Science and Technologies (C-MAST-UBI), Universidade da Beira Interior, R. Marquês D'Ávila e Bolama, 6201-001 Covilhã, Portugal
[4] Forest and Paper Research Institute (RAIZ), R. José Estevão, Eixo, 3800-783 Aveiro, Portugal
* Correspondence: joana.costa.vieira@ubi.pt

Abstract: Embossing is a functional and strategic process for creating high-quality multi-sensory tissue-paper products. Embossing modifies the sheet surface by generating hill and/or valley designs, changing the third-dimension z with a compressive die. This research work specifically concerns the impact study of the engraving finishing geometry on the final properties of tissue paper. This work led us to conclude that, even though the sheets individually present a higher hand-feel (HF) value for the straight finishing geometry, the highest softness was obtained in the two-ply prototype for the round finishing geometry. Moreover, this study confirmed that the HF value reduces with the increase of the bulk, being more accentuated for the micropattern. Relevant differences could not be seen in the spreading kinetics of the liquid droplets over time. Thus, the finishing geometry of the 3D plates did not impact the absorption kinetics on these samples. The finite element model allows us to understand the effect of the plate pattern and its finishing geometry on the paper, and the simulation results were in accordance with the experimental results, showing the same trend where patterns with a round finishing geometry marked the tissue-paper sheet more than patterns with a straight finishing did.

Keywords: dots and lines geometry; embossing prototype; FEM simulation; mechanical properties; softness characterization; tissue paper

Citation: Vieira, J.C.; Mendes, A.d.O.; Ribeiro, M.L.; Vieira, A.C.; Carta, A.M.; Fiadeiro, P.T.; Costa, A.P. Embossing Lines and Dots Geometry Effect on the Key Tissue Paper Properties with Finite Element Method Analysis. *Polymers* **2022**, *14*, 3448. https://doi.org/10.3390/polym14173448

Academic Editor: Victor Tcherdyntsev

Received: 1 August 2022
Accepted: 19 August 2022
Published: 24 August 2022

1. Introduction

Enhancing both originality and creativity is often a brand's selling and advertising argument. Therefore, embossing is a key process for producing high-quality multi-sensory products. Embossing is a type of compressive action that is carried out during tissue-paper converting by creating a pattern/engraving on paper with different depths, thus altering the sheet topography [1]. In addition to engrave the paper with patterns for aesthetic purposes, these hills or valleys increase the volume of the paper sheet, improving various properties, such as porosity, absorption, and softness. On the contrary, there are often losses of mechanical strength due to the damage caused to the structure of the material [2–4]. During the embossing process, the cellulosic fibers are compressed into well-marked permanent patterns, using pressure as force [5]. Each sheet passes through a pair of rolls, a steel roll that has the desired embossing pattern engraved on it, and often a rubber roll of a predetermined hardness. A defined pressure is applied to the nip, as presented in Figure 1, so that the engravings fulfill the intended purpose [2,3].

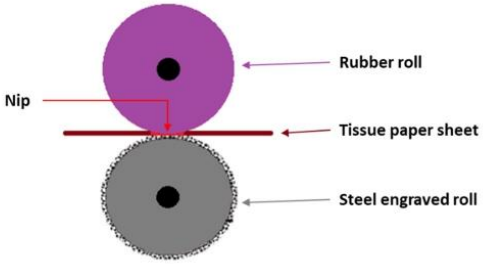

Figure 1. Schematic of the main performers in the tissue-paper-embossing process.

In theory, any kind of paper and/or cardboard can be embossed, considering the material properties, thickness, composition, fiber type, fiber length, and mechanical-strength properties (tensile strength, elongation, tear strength, delamination strength, compressive strength, and burst strength). Thus, bulkier materials will respond like a sponge, as they are more compressible, requiring higher pressure to make the engraving permanent. On the other hand, if this pressure exceeds the limit of the material, the embossing process will cause permanent damage to its structure, and this will appear on the surface of the sheet of paper [5].

A limitation of the embossing process is related to the dimensions and geometry of the embossing-pattern elements. Patterns with fine details, such as dots and fine lines, cannot be engraved to a high depth, as fine details are predisposed to tearing the sheet of paper. High-quality embossing is not only related to the engraving depth; the ability of the paper to stretch and adapt to the embosser is an equally important physical limitation [5]. There are no standardized embossing-pattern geometries and/or designs for an objective evaluation of the final properties of these structures with hills/valleys.

From the work developed by Khan [6], it was shown that different parameters of the geometry of the embossing pattern, such as the density of dots (number of dots/cm^2), height of the dots, and the angle that the dot makes with the base, affect the deformation of the sheet and, consequently, the mechanical properties of the embossed product. Thus, Khan [6] concluded that a higher density of dots and a higher height of the dots lead to a greater deformation of the tissue-paper sheet and, consequently, to a greater loss of mechanical properties. Conversely, a higher dot angle (cylindrical dot geometry) leads to less deformation and, consequently, to a lower loss of mechanical properties. In addition to the work developed by Khan [6], the novelty of our study was keeping those parameters constant and varying the finishing geometry of the lines and dots.

The influence of embossing pressure, time, and rubber hardness on the final properties of tissue paper is known from previous works [7,8]. In the present work, we intended to study the impact of engraving geometry on the final properties of tissue paper, using four customized 3D steel plates with different finishing geometries, and to confirm the obtained results by a finite element method (FEM) simulation.

2. Materials and Methods

2.1. Materials

To carry out this work, industrial creped toilet-base tissue paper from one Portuguese factory was used. The composition of the used paper was a mixture of 30% *Eucalyptus globulus* (hardwood) and 70% *Pinus pinaster* (softwood) bleached kraft pulps. This paper, denominated by B, had a grammage of 16.7 g/m^2 and was produced on a paper machine with a single layer headbox and with a ceramic creping blade. Moreover, for the execution of this work, four steel embossing plates were used, two of them with a deco pattern and the other two with a micropattern. Each steel plate presents dimensions of 210 × 297 mm and a different line or dot finishing geometry. In Figure 2, images of the four 3D steel embossing plates with the deco patterns and micropatterns are presented. The deco patterns were

composed only by lines, and the micropatterns were composed only by dots, using both straight and round finishing geometries.

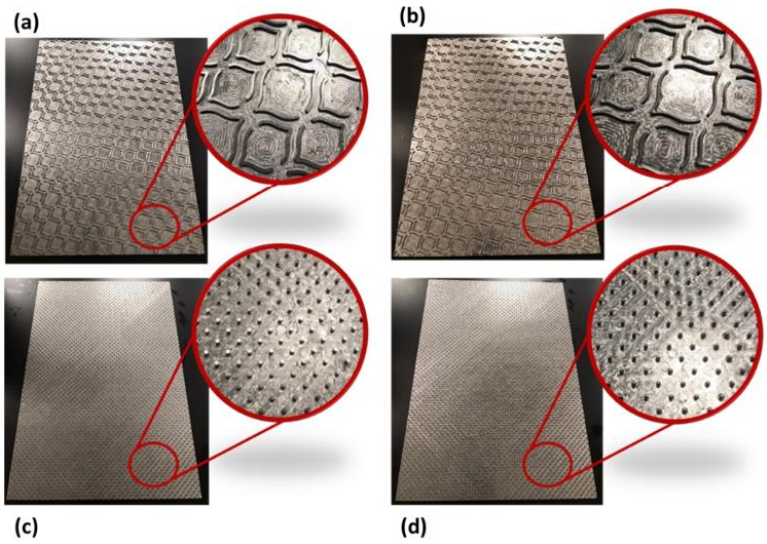

Figure 2. Images of the 3D steel embossing plates with the deco pattern and micropattern, and details of the respective finishing geometries: (**a**) deco pattern with straight lines, (**b**) deco pattern with round lines, (**c**) micropattern with straight dots, and (**d**) micropattern with round dots.

All the tissue samples are denominated according to each 3D steel-plate pattern and finishing geometry. Samples embossed with the deco pattern with straight lines are designated by adding the abbreviation d_{sl} to the paper denomination, and those with round lines are designated by d_{rl}. The samples embossed with the micropattern with straight dots are designated by adding the abbreviation m_{sd} to the paper denomination, and those with round dots by m_{rd}.

2.2. Methods

This work started by performing the embossing operation itself, with the four different embossing patterns engraved on steel plates. The two deco-pattern plates differ in the finishing geometry of the lines (straight or round), while the two micropattern plates differ in the finishing geometry of the dots (straight or round). Figure 3 shows the finishing geometry and dimensions of the lines and dots engraved in the 3D steel plates. The used operation conditions in the embossing process were 2.8 bar during 1 min and a variable rubber hardness of 60_48 Sh-A for the 4 types of 3D steel plates with the embossing patterns. These operating conditions were the same as those previously set by the authors in other related works [7,8].

All the tissue samples engraved with the four embossing patterns were tested in terms of thickness/bulk and their mechanical tensile strength in the machine direction (MD) and in the machine cross direction (CD). Tensile tests were performed in a Thwing-Albert® VantageNX Universal testing machine, in agreement with the tissue standard ISO 12625-4:2005, and thickness and bulk were determined by using a FRANK-TPI® Micrometer, fulfilling the tissue standard ISO 12625-3:2014. On all the embossed samples, the softness was tested with a Tissue Softness Analyzer (TSA) from EMTEC® equipment. For the computation of the handfeel (HF), the TP II and the QA I algorithms were used.

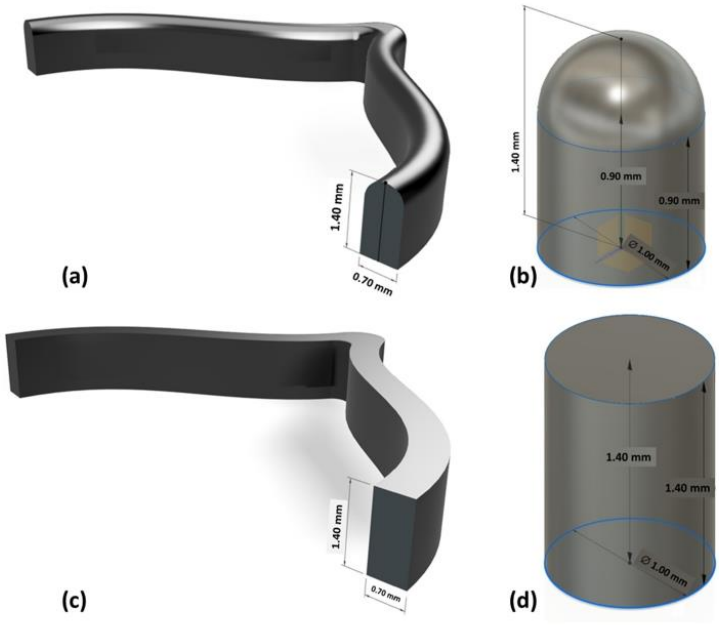

Figure 3. Finishing geometry and dimensions of the lines and dots engraved in the 3D steel plates: (**a**) line with a round finishing, (**b**) dot with a round finishing, (**c**) line with a straight finishing, and (**d**) dot with a straight finishing.

The samples were also analyzed by using three different modules of the customized optical system for the visual inspection of their surfaces, for the topographic reconstruction of the samples in three-dimensions, and also for the study of their interaction with liquid droplets. Specifically, the first module of the optical system [9–11] enables the image acquisition of the surfaces of the paper samples engraved with the different embossing patterns, considering highly detailed and magnified images, having shown to be very versatile in other similar studies [12–16]. The second module of the optical system, originally developed for the evaluation of topographic changes manifested on the surface of textiles [17–20], was used as a complement to the first module, to further explore the inspection of the paper samples, reconstructing their surfaces in 3D, enabling us to fully observe, in different views, the differences of the engraving marks obtained with the different considered embossing plates. Recently, this module has also been used in a study that was carried out regarding the characterization of the crepe microstructure in a set of different industrial tissue samples, on which the samples used in the current study were included. Finally, the third module of the optical system [21] enables the study of the spreading kinetics of liquid droplets, performing their ejection onto the surface of the samples and acquiring images of their interaction for a given period of time (from 35.7 ms to 3 s), and, similarly as for the other two modules, this third module was also used in other conducted studies by our research team [7,22–25].

2.3. Finite Element Method (FEM)

The effect of the plates' pattern geometry can be analyzed in terms of stress field and how the finishing geometry affects the plasticity after the embossing process, using the finite element models. Thus, different models were proposed to investigate in more detail these effects on the permanent deformations after the embossing process.

Since ABAQUS™ does not have a native constitutive law for orthotropic plasticity material, a user material subroutine for explicit simulations (VUMAT) linked to the

commercial finite element software ABAQUS™ was implemented, using an orthotropic elastic–plastic material model, proposed by Mäkelä and Östlund [26]. This material model allows users to simulate the paper anisotropic behavior, since the paper response is highly dependent on fiber orientation [26]. The model assumes the decomposition of the strain tensor into an elastic strain tensor plus a plastic strain tensor (Equation (1)), while volume is conserved:

$$\varepsilon_{ij} = \varepsilon_{ij}^{e} + \varepsilon_{ij}^{p} \tag{1}$$

where ε_{ij} is the total strain, ε_{ij}^{e} is the elastic strain, and ε_{ij}^{p} is the plastic strain.

The VUMAT subroutine was implemented by using the concept of an isotropic plasticity equivalent [27], considering an equivalent material that correlates the orthotropic stress state to an equivalent isotropic stress state. The relation between the actual Cauchy stress tensor and the isotropic plasticity equivalent (IPE) deviatoric tensor is given in Equation (2):

$$s_{ij} = L_{ijkl}\sigma_{kl} \tag{2}$$

where s_{ij} is the deviatoric IPE stress tensor, σ_{kl} is the Cauchy stress, and L_{ijkl} is the fourth-order transformation tensor shown in Equation (3) for plane stress:

$$L = \begin{bmatrix} 2A & C-A-B & 0 \\ C-A-B & 2B & 0 \\ B-C-A & A-B-C & 0 \\ 0 & 0 & 3D \end{bmatrix} \tag{3}$$

where the parameters A, B, C, and D were calibrated from tensile-test results by using the following Equations (4)–(11) [26]:

$$A = \sqrt{1-12x^2} \tag{4}$$

$$B = 3(y-x) \tag{5}$$

$$C = 3(y+x) \tag{6}$$

$$D = \frac{K_{12}^{\frac{n}{(n+1)}}}{\sqrt{3}} \tag{7}$$

$$x = \sqrt{\frac{\alpha^2}{24(3\alpha^2+\beta^2-4\beta+4)}\left(\beta+1-\sqrt{6\beta-3\alpha^2-3}\right)} \tag{8}$$

$$y = \frac{\alpha}{4x} - A \tag{9}$$

$$\alpha = K_{33}^{\frac{2n}{(n+1)}} - K_{22}^{\frac{2n}{(n+1)}} \tag{10}$$

$$\beta = K_{33}^{\frac{2n}{(n+1)}} + K_{22}^{\frac{2n}{(n+1)}} \tag{11}$$

The parameters K_{ii} and n were obtained by inverse parametrization, using the Ramberg–Osgood methodology to minimize the error between the tensile tests results and the model results. For the MD tensile test (Equation (12)):

$$\varepsilon_{11} = \frac{\sigma_{11}}{E_{11}} + \left(\frac{\sigma_{11}}{E_0}\right)^{n} \tag{12}$$

For the CD, the equation is as follows (Equation (13)):

$$\varepsilon_{kk} = \frac{\sigma_{kk}}{E_{kk}} + \left(\frac{K_{kk}E_{kk}}{E_0}\right)^{n}, k = 2,3 \tag{13}$$

Note that, for Equation (13), the repeated indices do not mean the usual summation rule used in the indicial notation. Finally, the parameter K_{12} was obtained by using Equation (14):

$$\gamma_{12} = \frac{\sigma_{12}}{G_{12}} + \left(\frac{K_{12}\sigma_{12}}{E_0}\right)^n \tag{14}$$

In the case of this study, it is possible to consider $K_{22} = K_{33}$, since the mechanical behavior in CD (direction 2) is similar to that on the thickness direction (direction 3). Thus, $A = 1$ for all models. For deco models, $B = 2.40$, $C = 2.40$, and $D = 1.38$, and for micro models, $B = 2.44$, $C = 2.44$, and $D = 1.40$. Since the tensile vs. strain curves had a similar shape, those parameters are almost the same in both MD (direction 1) and CD (direction 2).

The Hooke's law for plane stress, small strain, and linear elastic orthotropic material is given by using Equation (15):

$$\sigma = C : \varepsilon^e \tag{15}$$

where σ is the second-order Cauchy stress tensor; C is the four-order plane stress, linear elastic, orthotropic constitutive law tensor; and ε^e is the second-order small strain elastic tensor.

The implementation of this model is similar to the well-known J_2 flow theory for isotropic materials, using the backward-Euler algorithm. The explicit solver was used to overcome convergence issues that are usual when using the implicit solver for this type of simulations. On the other hand, the stable time increment is very small, which increases the computational costs. Simulations were performed by using a workstation with two intel Xeon E5-2630 8 cores (16 cores total with 32 threads) with 256 Gb ram.

The finite-element-model dimensions and boundary conditions are presented in Figure 4. The plate model dimensions are representative of the actual plate, resulting in a reasonable computational cost and accuracy. The rubber base dimensions were the same, but it was thick enough to allow the deformation without severe interference in the plate and paper kinematics. The paper had the same dimensions of the die and basis.

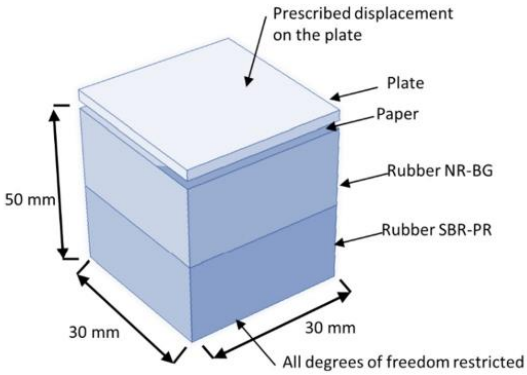

Figure 4. Model dimensions, characteristics, and boundary conditions.

The boundary conditions were imposed to represent the embossing process. Thus, all the displacements' degrees of freedom were restricted in the bottom of the rubber base, and a prescribed displacement was applied on the top of the plate, corresponding to a manufacture pressure of 2.8 bar applied during the embossing process. To model the contact interactions between each part of the model, hard contact was considered for normal behavior, and the tangential behavior was modeled by using penalty interaction with 0.3 for friction coefficient.

The model has 473,694 20-node hexahedral elements (C3D20) for the simulation of the micro die with round finishing dots, and 476,153 20-nodes hexahedral (C3D20) elements for the deco die with round finishing lines. To improve the simulation, the straight finishing

dots of the micro die was modeled with 443,206 10-node tetrahedral mixed-mode elements (C3D10M), and 1,491,454 10-node tetrahedral mixed-mode elements (C3D10M) for the straight finishing lines of the deco die.

For all models, paper was simulated by using a 4-node reduced integration membrane element (M3D4R). The structured mesh has a total of 250,000 elements. Finally, the rubber base was modeled by using a total of 216,000 8-node hexahedral elements (C3D8).

This model uses 3 different types of materials: steel for the die (E = 200 GPa, μ = 0.33); a hyper-elastic isotropic material model for the rubber basis, SBR-PR (C_{10} = 0.810343 MPa and D_1 = 0.56956 MPa^{-1}), and for NR-BG (C_{10} = 0.409852 MPa and D_1 = 1.126109 MPa^{-1}). Paper was modeled as a user orthotropic material (E_{11} = 13.89 MPa, $E_{22} = E_{33}$ = 4.23 MPa, μ = 0.33, and G_{12} = 2.1 MPa). As mentioned above, the parameters B, C, and D for the IPE model consider the different mechanical behavior for the deco pattern and micropattern.

The finite element model does not consider a compression force on the paper, since a plane stress constitutive relation was adopted in the used membrane element. On the other hand, the material parameters used for the simulations of the other materials (rubbers and dies) consider a manufacture pressure of 2.8 bar applied during the embossing process.

3. Results

This work began with the mechanical characterization and determination of the bulk of the previously embossed samples and the industrial base tissue paper. The results obtained are shown in Figure 5.

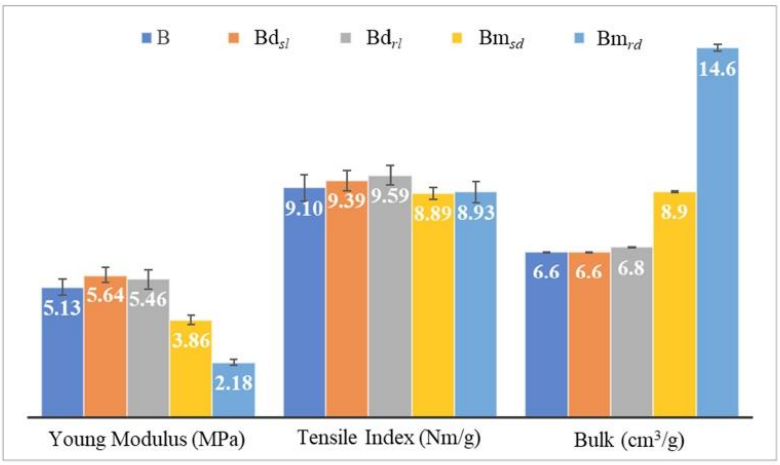

Figure 5. Results of mechanical characterization and bulk obtained for all the embossed samples and the reference paper, B, for the different finishing geometries of the 3D steel plates.

The images obtained by analysis with the first module of the optical system of the tissue samples embossed with the four different 3D steel plates are presented in Figure 6.

Figures 7–10 show the 3D maps created for each one of the studied cases, using the second module of the optical system.

Regarding the essays conducted with the third module of the optical system, the images and the results obtained for the study of the spreading dynamics of a liquid droplet on the surface of the tissue-paper samples engraved with the different embossing plates can be seen in Figures 11–15.

By combining the deco and micro embossed sheets for each finishing geometry, straight or round, a prototype of a two-ply finished product was obtained. With the aim of optimizing the softness as a function of the 3D steel-plate finishing geometry in the embossing

process, the handfeel (HF) of each one of these prototypes was measured, and the results are shown in Figure 16.

In order to better understand the effect of embossing on softness, Figure 17 shows the behavior of handfeel (HF) as a function of bulk.

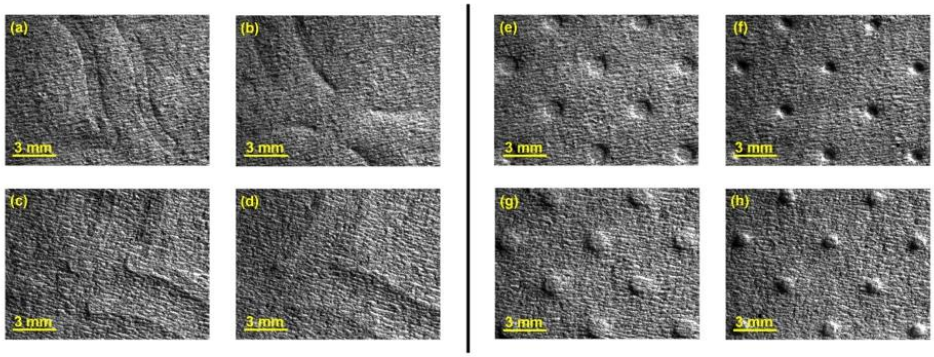

Figure 6. Global views of the tissue-paper samples engraved with the different considered embossing plates: (**a**) Bd_{sl} (front side), (**b**) Bd_{rl} (front side), (**c**) Bd_{sl} (back side), (**d**) Bd_{rl} (back side), (**e**) Bm_{sd} (front side), (**f**) Bm_{rd} (front side), (**g**) Bm_{sd} (back side), and (**h**) Bm_{rd} (back side).

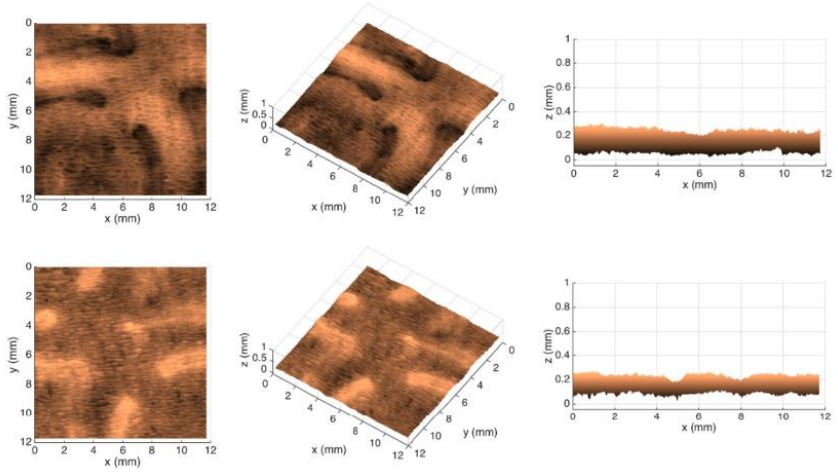

Figure 7. Different views of the 3D maps created for the front and back sides of the tissue-paper sample Bd_{sl}.

Finite Element Method (FEM)

The finite element models can predict the effect of the die finishing geometry on the paper. Figures 18 and 19 shows the plastic stress field (J_2 invariant) model results for the round- and straight-line finishing of the deco pattern, respectively, as well as the deformed shape, and Figures 20 and 21 shows the results for the round- and straight-dot finishing for the micro die.

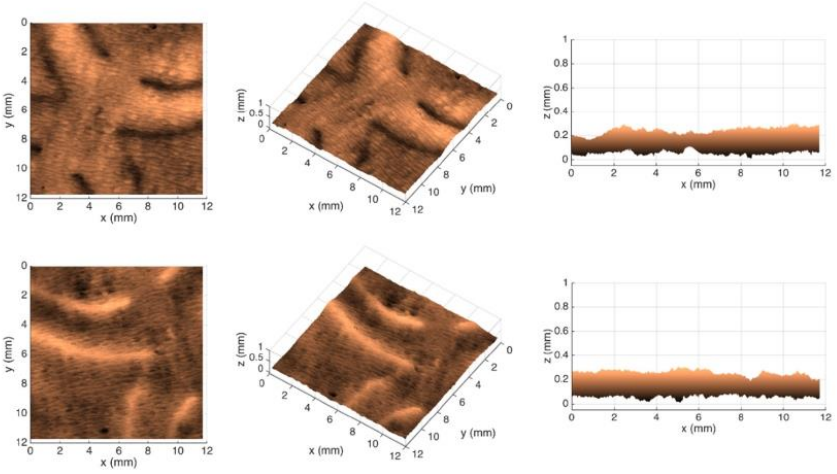

Figure 8. Different views of the 3D maps created for the front and back sides of the tissue-paper sample Bd_H.

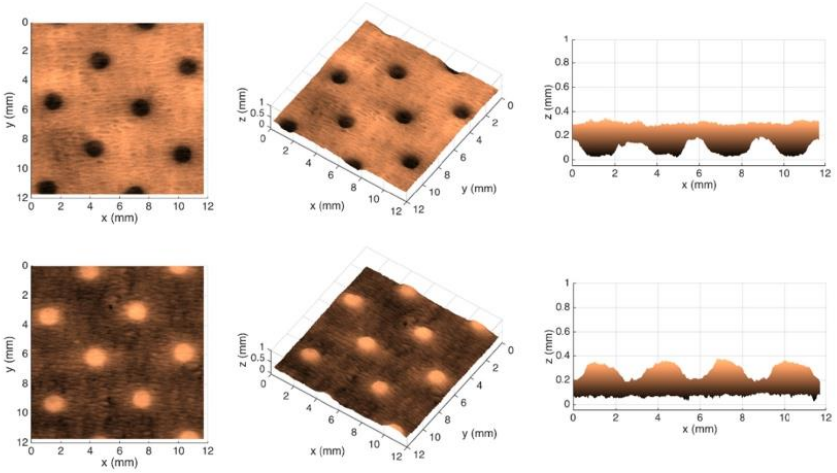

Figure 9. Different views of the 3D maps created for the front and back sides of the tissue-paper sample Bm_{sd}.

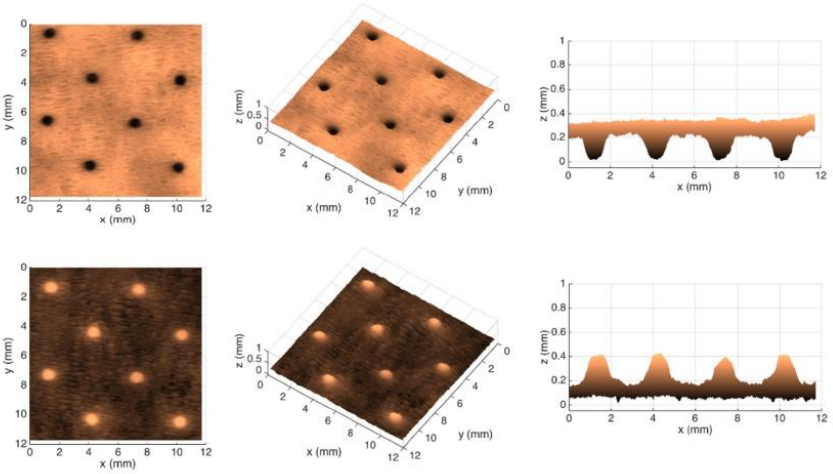

Figure 10. Different views of the 3D maps created for the front and back sides of the tissue-paper sample Bm_{rd}.

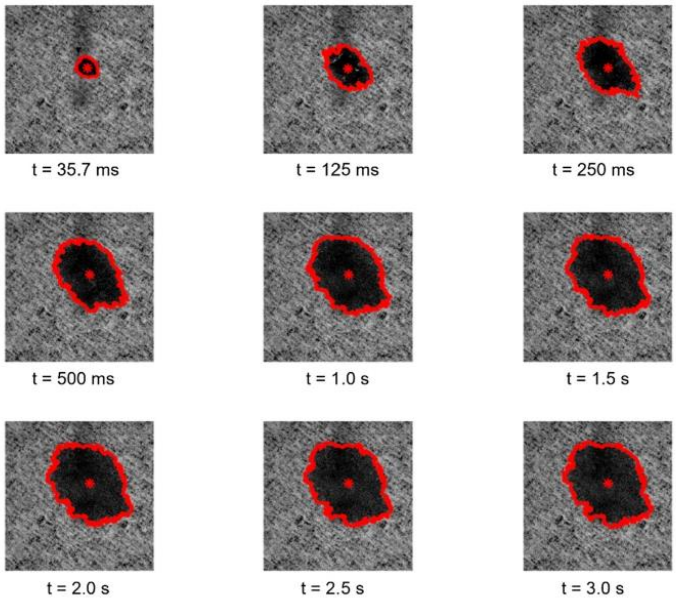

Figure 11. Spreading dynamics of a liquid droplet from t = 35.7 ms to 3 s for the tissue-paper sample Bd_{sl}.

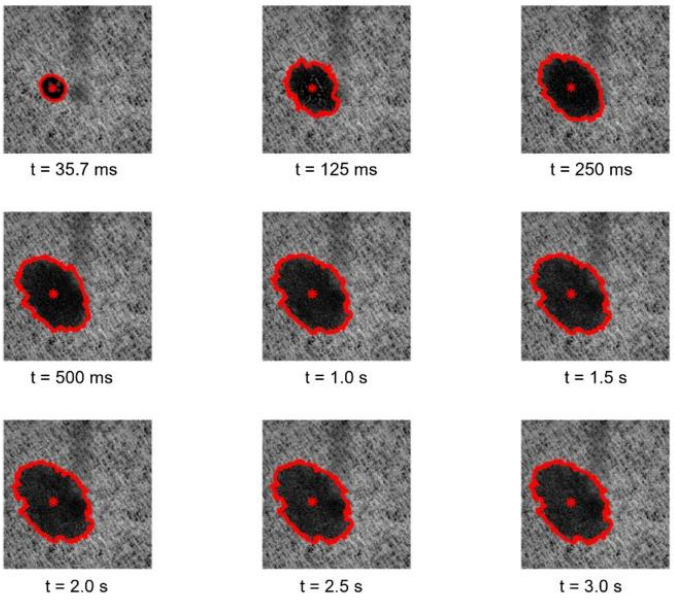

Figure 12. Spreading dynamics of a liquid droplet from t = 35.7 ms to 3 s for the tissue-paper sample Bd_{rl}.

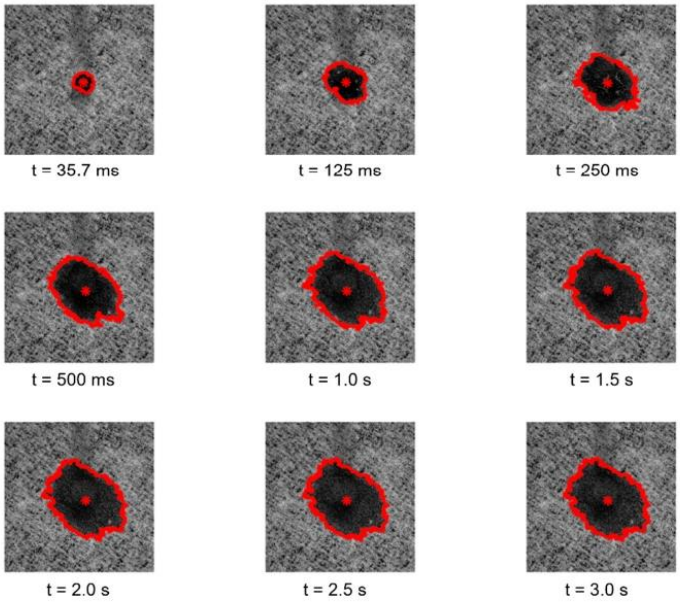

Figure 13. Spreading dynamics of a liquid droplet from t = 35.7 ms to 3 s for the tissue-paper sample Bm_{sd}.

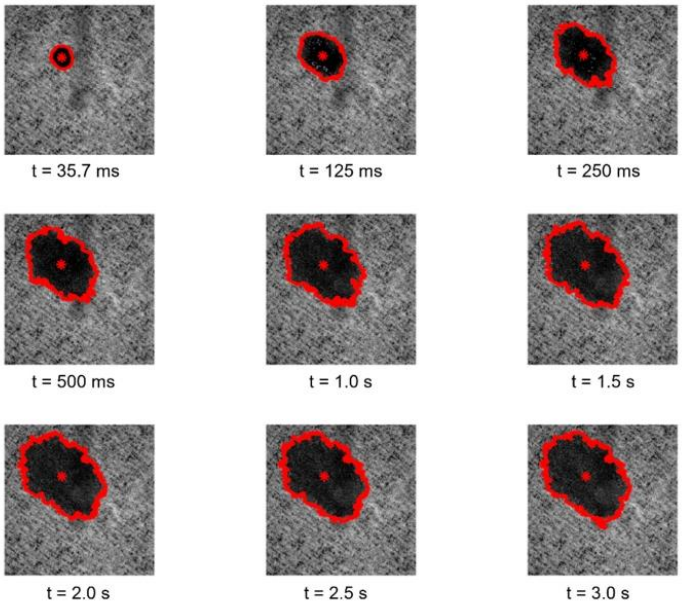

Figure 14. Spreading dynamics of a liquid droplet from t = 35.7 ms to 3 s for the tissue-paper sample Bm_{rd}.

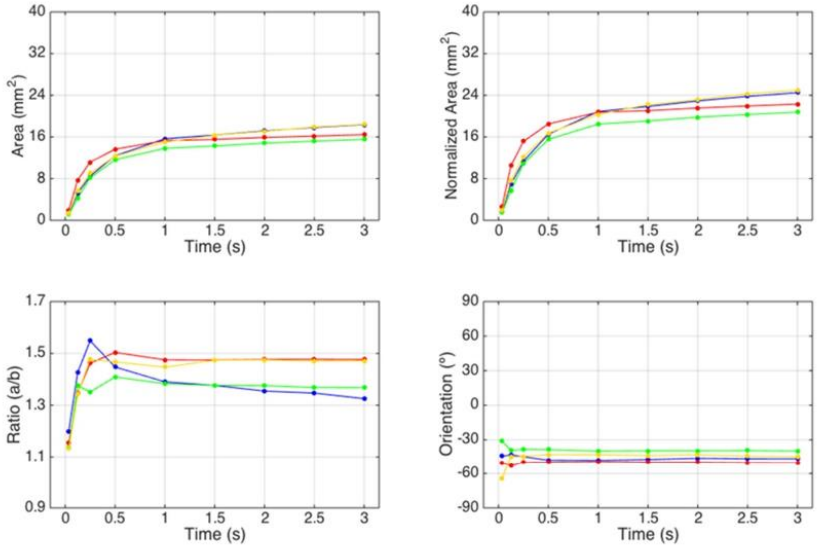

Figure 15. Comparative graphs of the spreading dynamics of a liquid droplet for the tissue-paper samples Bd_{sl} (in blue), Bd_{rl} (in red), Bm_{sd} (in green), and Bm_{rd} (in yellow).

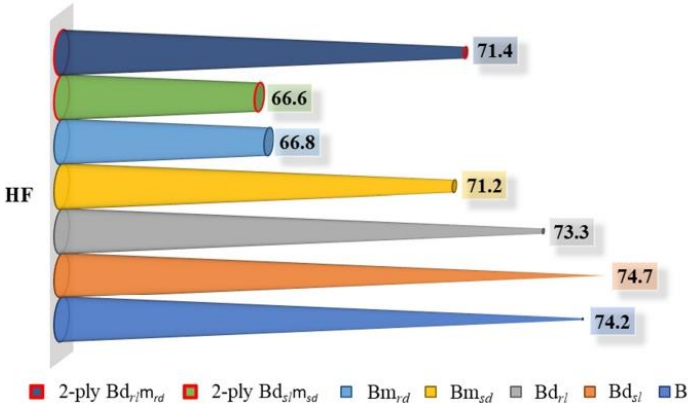

Figure 16. Results obtained for handfeel (HF) for all the embossed samples and the reference paper, B, for the different finishing geometries of the 3D steel plates.

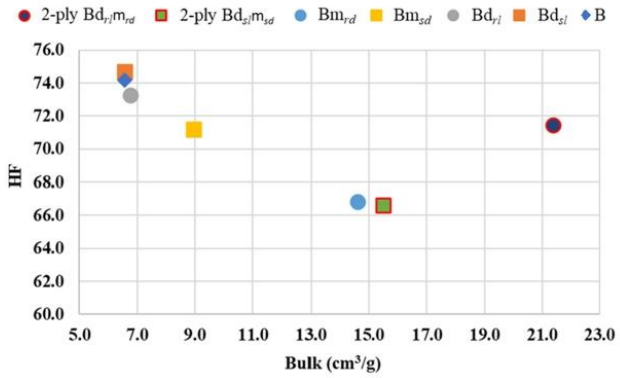

Figure 17. Handfeel (HF) behavior as a function of bulk.

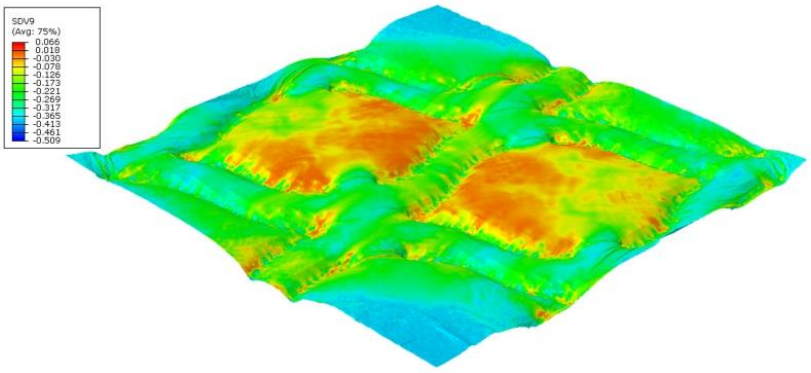

Figure 18. Plastic-stress-field finite-element results for deco pattern with round finishing.

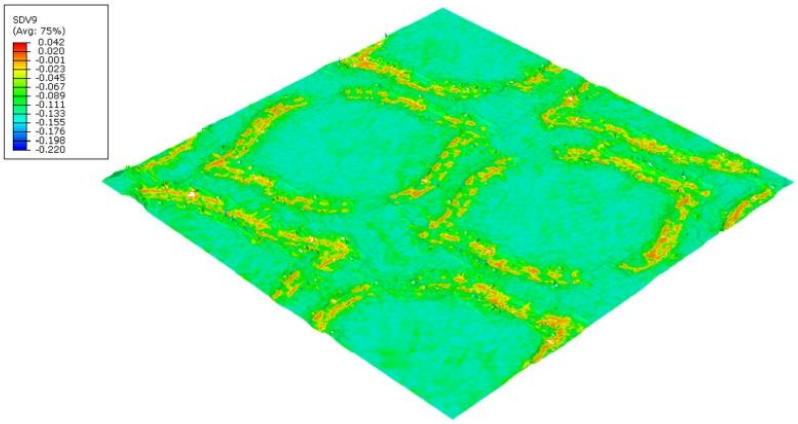

Figure 19. Plastic-stress-field finite-element results for deco pattern with straight finishing.

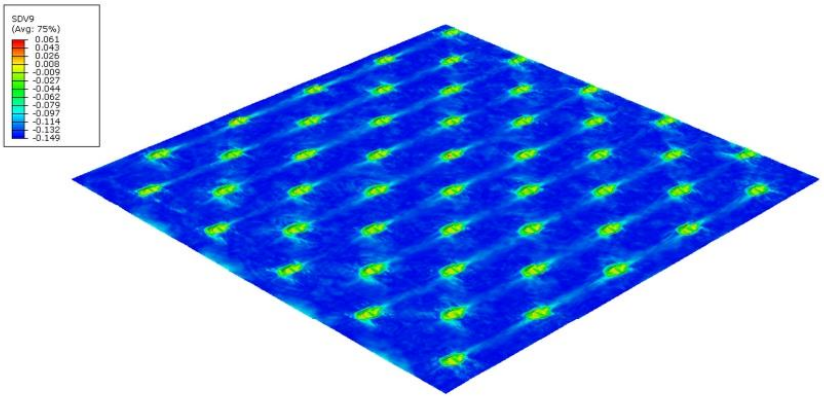

Figure 20. Plastic-stress-field finite-element results for micropattern with round finishing.

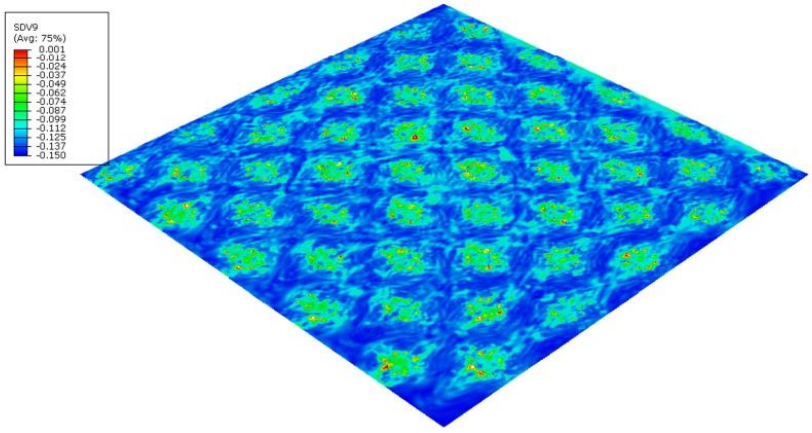

Figure 21. Plastic-stress-field finite-element results for micropattern with straight finishing.

4. Discussion

Looking at Figure 5, in terms of sheet rigidity, we see that the micropattern affects this property of the sheet more than the deco pattern. Within each pattern (deco and micro) the round finishing geometry is the one that impacts the structure of the sheet the most. On the other hand, and bearing in mind that the embossing was carried out at the optimum pressure of the embossing system [7,8], when compared to the industrial base tissue paper, the losses and gains in mechanical strength are not very excessive, being within the standard deviation, despite, and as expected, the micropattern presenting the highest loss of mechanical strength. In both embossing patterns, the straight finishing geometry is the one with the greatest loss of this property. Moreover, as expected and in line with the results obtained for the mechanical properties, the bulk is quite superior in the micropattern when compared to the deco pattern. In terms of the line and dot finishing geometry of the embossing patterns, the round finishing stands out again, doubling the bulk value when compared to the industrial base tissue paper.

From the images shown in Figure 6, it can be seen that, in fact, the micropatterns affect the surface of the tissue-paper samples more extensively than the deco patterns do. It can also be seen from the images that the marks engraved with the deco pattern and micropattern with straight finishing appear larger than the marks engraved with the deco pattern and micropattern with round finishing. However, the marks engraved with the round finishing geometry appear to be deeper than the first ones. This can also be observed in Figures 7–10, which show the 3D maps created for each one of the studied cases, using the second module of the optical system. The 3D maps confirm that the marks (lines and dots) engraved with the straight finishing geometry are larger in area than the marks engraved with the round finishing geometry. They also confirm that the same marks are deeper for the engravings performed with the round comparatively to the straight finishing geometries. This is very clear by observation of the above figures, especially for the micropatterns. This means that the steel plates that were manufactured with the round finishing geometry, because of their characteristic design, provide a higher penetration of the engravings in the paper structure. Therefore, they provide a higher impact in the depth of the paper sheets, especially in the paper sample engraved with the micropattern, on which the marks are the deepest, with the highest values in the z direction.

By observing the images seen in the Figures 11–14, it can be noticed that there are no relevant differences in the spreading of the liquid droplets over time, when comparing the four considered cases. In particular, it can be seen that the droplets spread wider over time, and then they tend to stabilize around t = 1.0 to 1.5 s. In all cases, the droplets assume elliptical shapes, following the creping lines present in the surface of the tissue samples that are aligned approximately with the diagonal of the images. Globally, the areas occupied by the droplets and their shapes are very similar in the four cases. The comparative graphs shown in the Figure 15 confirm exactly the same, revealing evolutions over time very close and in the same range of values in all the considered cases for the parameters "Area", "Normalized Area", and "Orientation". The only parameter that shows some differences is the "Ratio" of the shape assumed by the droplets, as it was revealed to be more elliptical for the tissue-paper sample engraved with the deco pattern with round finishing (in red) and for the tissue-paper sample engraved with the micropattern with round finishing (in yellow). The other two cases, namely the tissue-paper sample engraved with the deco pattern with straight finishing (in blue) and the tissue-paper sample engraved with the micropattern with straight finishing (in green), revealed lower values of ellipticity; however, they still show very pronounced elliptical shapes (see images of Figures 11–14). From the images and the third graph of Figure 15, it can also be noted that there is a high peak that appeared for the instant of time t = 250 ms for the case of the tissue-paper sample engraved with the deco pattern with straight finishing (in blue). In terms of the "Orientation" of the droplets spreading (fourth graph of Figure 15), it can be seen that all cases are contained in the same range, as already stated earlier, coincident with the diagonal of the images (approximately −45°), which is the angle at which the creping lines are seen. In sum,

the results obtained for the spreading dynamics of liquid droplets have shown to be very similar for all the considered cases, meaning that the finishing geometry of the elements contained in the steel plates did not have a significant impact on the assays conducted with the third optical system.

By analyzing Figure 16 and looking at the finishing geometry of the lines and dots individually, we can see that, for the two embossing patterns, the straight finish of the 3D steel plates results in a higher HF value. This result is mainly associated with the low effect of the surface roughness of the sheet, very close to the non-embossed industrial base tissue paper. On the other hand, when we analyze the two-ply prototypes, it is possible to verify that this trend is reversed, with the prototype with a round finish having the highest HF value. Observing Figure 17 and considering the sheets individually embossed with the 3D plates of steel, it is verified that, with the increase of the bulk, there is a decrease of the HF, and this decrease is more accentuated for the micropattern. Looking at the two-ply prototypes, and as mentioned before, we can see that the prototype with a round finish is the one that has the highest HF value, and this happens due to the contribution of bulk softness. In a two-ply prototype, the HF is measured at the top surface, where the deco pattern embossing is found. This pattern, as seen, is the one that least affects the softness, so the parameter that is contributing to the increase in the HF value is the bulk. Thus, to optimize the final softness of the toilet paper, the round finishing of the deco and micro embossing patterns would be the best choice for the producer.

Figures 18–21 show the amount of plasticity obtained in the paper, using these models, due to the embossing process. In these figures, it is possible to observe the regions where the plastic deformations were detected and their distribution over the paper's surface. When we compared Figures 18 and 19, for the deco pattern, the plastic stress field for the round finishing showed that the plastic stress field is more spread over the paper's surface (Figure 18), while for the straight finishing, the plastic stress field is concentrated in the regions near the edges, where the peaks of the plate touch the paper (Figure 19). On the other hand, when we compared Figures 20 and 21, for the micropattern, we noted that the plastic stress field for the round finishing is concentrated in the regions where the die peaks touch the paper (Figure 20), while the plastic stress field for the straight finishing is more spread over the paper surface (Figure 21). Hence, the simulations enable us to show that a round finishing produces a concentrated plastic-stress-field distribution over the paper's surface, as well as higher stresses, in accordance with experimental results where the round finishing produces a more marked pattern compared to the straight finishing. This trend is observed in both deco patterns and micropatterns. The simulation of the embossing process shows that the finishing of the patterns influences the plastic-stress-field distribution, more or less concentrated; the maximum stress; and the regions where higher stress values occur. For the plates with straight finishing, the plastic field is more pronounced on the top of the pattern along the contact edge, but with the plates with round finishing, the plastic field is more pronounced on the base contact region of the pattern.

5. Conclusions

The study of the impact of the finishing geometry of the line and dots (straight or round) of steel 3D plates in the embossing process led us to conclude that, although the sheets individually present a higher HF value for straight finishing geometry, in the two-ply prototype, the highest softness was obtained for the prototype with the round finishing geometry. Moreover, for the sheets embossed individually, it was verified that the HF value decreases with the increase of the bulk, and this was more accentuated for the micropattern.

It was also concluded that there are no relevant differences in the spreading kinetics of the liquid droplets over time. Thus, the finishing geometry of the steel 3D plates does not affect the absorption kinetics of these products.

The finite element model allowed to understand the effect of the plate patterns' finishing geometry on the paper due to the embossing process changing the plastic stress field. The simulation results were in accordance with the experimental results. These were able to

show a trend where patterns with round geometry marked the tissue-paper sheet more than patterns with straight finishing did. This increase of the marks corresponds to an increase of bulk. Furthermore, this tool enables the optimization of process parameters; —in this work, particularly in regard to the pattern's finishing geometry—in a virtual environment, thus avoiding a costly trial–error approach.

This study highlighted the importance of the patterns' finishing geometry and its impact on the final properties of tissue-paper products. The authors consider that the obtained results contribute to creating a better understanding of the embossing process when analyzing the impact of each embossing operation condition separately—in this case, the finishing geometry of the lines and dots in the finish of steel 3D plates.

Author Contributions: J.C.V. data acquisition and curation, investigation, writing—original draft, and writing—review and editing; A.d.O.M. image data acquisition and curation, writing—original draft, and writing—review and editing; M.L.R. FEM analysis, writing—original draft, simulation supervision, and writing—review and editing; A.C.V. FEM analysis, writing—original draft, simulation supervision, and writing—review and editing; A.M.C. project pivot, writing—review and editing; P.T.F. supervision, writing—review and editing; A.P.C. project supervisor and writing—review and editing. All authors have read and agreed to the published version of the manuscript.

Funding: The authors gratefully acknowledge the funding of this work that was carried out under the Project InPaCTus—Innovative Products and Technologies from Eucalyptus, Project Nº 21874, funded by Portugal 2020 through European Regional Development Fund (ERDF) in the frame of COMPETE 2020 nº 246/AXIS II/2017. The authors are also very grateful for the support given by research unit Fiber Materials and Environmental Technologies (FibEnTech-UBI), to the extent of the project reference UIDB/00195/2020, and by the Center for Mechanical and Aerospace Science and Technologies (C-MAST-UBI), to the extent of the project reference UIDB/00151/2020, both funded by the Fundacão para a Ciência e a Tecnologia, I.P./MCTES through national funds (PIDDAC).

Institutional Review Board Statement: Not applicable.

Informed Consent Statement: Not applicable.

Data Availability Statement: Not applicable.

Acknowledgments: The authors would like to also thank the company PCE Iberica S.L. Instrumentacíon for the donation of the Durometer PCE-DDA equipment that was used in this work to determine the apparent hardness of the rubber plates. Finally, the authors acknowledge the materials, access to equipment, and installations, as well as all the general support given by The Navigator Company; RAIZ; and the Optical Center, Department of Physics, Department of Textile Science and Technology, Department of Chemistry, and Nuno Santos from FABLAB of the Universidade da Beira Interior.

Conflicts of Interest: The authors declare no conflict of interest.

References

1. Delić, G.; Vladić, G.; Pál, M.; Banjanin, B.; Dedijer, S. Performance evaluation of paper embossing tools produced by fused deposition modelling additive manufacturing technology. *J. Graph. Eng. Des.* **2017**, *8*, 47–54. [CrossRef]
2. Spina, R.; Cavalcante, B. Characterizing Materials and Processes Used on Paper Tissue Converting Lines. *Mater. Today Commun.* **2018**, *17*, 427–437. [CrossRef]
3. Biagiotti, M. Tissue Embossing Developments | The Tissue Story. 2017. Available online: https://www.tissuestory.com/2017/11/21/tissue-embossing-developments/ (accessed on 8 January 2019).
4. Wilhelm, L. Embossing Roll and Embossed Substract. WO2005065928A1, 30 June 2005.
5. Pál, M.; Banjanin, B.; Dedijer, S.; Vladić, G.; Bošnjaković, G. Preliminary analysis of image processing-based evaluation of embossing quality. In Proceedings of the Tenth International Symposium GRID 2020, Kashan, Iran, 16–17 December 2020; University of Novi Sad, Faculty of Technical Sciences, Department of Graphic Engineering and Design: Novi-Sad, Serbia, 2020; pp. 269–279. [CrossRef]
6. Khan, A.A. Development of Model to Simulate Embossing of Tissue Paper: Effect of Embossing on Mechanical Performance of Tissue. Thesis for Master of Science (M.Sc.) in Engineering Mechanics, KTH Royal Institute of Technology. 2021. Available online: https://www.diva-portal.org/smash/get/diva2:1590118/FULLTEXT01.pdf (accessed on 14 November 2021).

7. Vieira, J.C.; Mendes, A.d.O.; Ribeiro, M.L.; Vieira, A.C.; Carta, A.M.; Fiadeiro, P.T.; Costa, A.P. Embossing Pressure Effect on Mechanical and Softness Properties of Industrial Base Tissue Papers with Finite Element Method Validation. *Materials* **2022**, *15*, 4324. [CrossRef] [PubMed]
8. Vieira, J.C.; Mendes, A.d.O.; Ribeiro, M.L.; Vieira, A.C.; Carta, A.M.; Fiadeiro, P.T.; Costa, A.P. FEM Analysis Validation of Rubber Hardness Impact on Mechanical and Softness Properties of Embossed Industrial Base Tissue Papers. *Polymers* **2022**, *14*, 2485. [CrossRef] [PubMed]
9. Mendes, A.d.O.; Fiadeiro, P.T.; Costa, A.P.; Amaral, M.E.; Belgacem, M.N. Retro-diffusion and transmission of laser radiation to characterize the paper fiber distribution and mass density. In Proceedings of the 8th Iberoamerican Optics Meeting and 11th Latin American Meeting on Optics, Lasers, and Applications, Porto, Portugal, 22–26 July 2013; p. 8785. [CrossRef]
10. Mendes, A.d.O.; Fiadeiro, P.T.; Costa, A.P.; Amaral, M.E.; Belgacem, M.N. Study of repeatability of an optical laser system for characterization of the paper fiber distribution and mass density. In Proceedings of the Second International Conference on Applications of Optics and Photonics, Aveiro, Portugal, 26–30 May 2014; p. 9286. [CrossRef]
11. Mendes, A.d.O.; Fiadeiro, P.T.; Costa, A.P.; Amaral, M.E.; Belgacem, M.N. Laser scanning for assessment of the fiber anisotropy and orientation in the surfaces and bulk of the paper. *Nord. Pulp Pap. Res. J.* **2015**, *30*, 308–318. [CrossRef]
12. Vieira, J.C.; Mendes, A.d.O.; Carta, A.M.; Galli, E.; Fiadeiro, P.T.; Costa, A.P. Impact of Embossing on Liquid Absorption of Toilet Tissue Papers. *BioResources* **2020**, *15*, 3888–3898. [CrossRef]
13. Mendes, A.d.O.; Vieira, J.C.; Carta, A.M.; Galli, E.; Simões, R.; Fiadeiro, P.T. Influence of Tissue Paper Converting Conditions on Finished Product Softness. *BioResources* **2020**, *15*, 7178–7190. [CrossRef]
14. Vieira, J.C.; Vieira, A.C.; Mendes, A.d.O.; Carta, A.M.; Fiadeiro, P.T.; Costa, A.P. Mechanical Behavior of Toilet Paper Perforation. *BioResources* **2021**, *16*, 4846–4861. [CrossRef]
15. Vieira, J.C.; Vieira, A.C.; Mendes, A.d.O.; Carta, A.M.; Fiadeiro, P.T.; Costa, A.P. Toilet Paper Perforation Efficiency. *BioResources* **2021**, *17*, 492–503. [CrossRef]
16. Vieira, J.C.; Morais, F.; Mendes, A.d.O.; Ribeiro, M.L.; Carta, A.M.; Curto, J.; Amaral, M.E.; Fiadeiro, P.T.; Costa, A.P. Mechanical and softness characterization of "deco" and "micro" embossed tissue papers using finite element model (FEM) validation. *Cellulose* **2022**, *29*, 5895–5912. [CrossRef]
17. Mendes, A.d.O.; Fiadeiro, P.T.; Miguel, R.A.L. Three-dimensional surface reconstruction for evaluation of the abrasion effects on textile fabrics. In Proceedings of the SPIE—The International Society for Optical Engineering, San Jose, CA, USA, 15–19 January 2006. [CrossRef]
18. Mendes, A.d.O.; Fiadeiro, P.T.; Pereira, M.J.T.; Miguel, R.A.L. Dual-scanning System for Optical Estimation of Pilling Formation. *Text. Res. J.* **2010**, *80*, 1201–1213. [CrossRef]
19. Mendes, A.d.O.; Fiadeiro, P.T.; Miguel, R.A.L.; Lucas, J.M.; Silva, M.J.d.S. Three-dimensional surface reconstruction for evaluation of wrinkling on textile fabrics. In Proceedings of the Fourth International Conference on Applications of Optics and Photonics, SPIE, Lisbon, Portugal, 31 May–4 June 2019; p. 7. [CrossRef]
20. Mendes, A.d.O.; Fiadeiro, P.T.; Miguel, R.A.L.; Lucas, J.M.; Silva, M.J.d.S. Optical 3D-system for fabric pilling assessment: A complementary tool to avoid evaluation errors. *J. Text. Inst.* **2020**, *112*, 921–927. [CrossRef]
21. Mendes, A.d.O.; Fiadeiro, P.T.; Ramos, A.M.M.; de Sousa, S.C.L. Development of an optical system for analysis of the ink–paper interaction. *Mach. Vis. Appl.* **2013**, *24*, 1733–1750. [CrossRef]
22. Curto, J.M.R.; Mendes, A.O.; Conceição, E.L.T.; Portugal, A.T.G.; Fiadeiro, P.T.; Ramos, A.M.M.; Simões, R.M.S.; Silva, M.J.S. Development of an Innovative 3D Simulator for Structured Polymeric Fibrous Materials and Liquid Droplets. In *Mechanical and Materials Engineering of Modern Structure and Component Design*; Öchsner, A., Altenbach, H., Eds.; Springer International Publishing: Cham, Switzerland, 2015; pp. 301–321. [CrossRef]
23. Fiadeiro, P.T.; Mendes, A.d.O.; Ramos, A.M.M.; de Sousa, S.C.L. Study of the ink-paper interaction by image analysis: Surface and bulk inspection. In Proceedings of the 8th Iberoamerican Optics Meeting and 11th Latin American Meeting on Optics, Lasers, and Applications, Porto, Portugal, 22–26 July 2013; p. 8785. [CrossRef]
24. Sousa, S.C.L.; Mendes, A.d.O.; Fiadeiro, P.T.; Ramos, A.M.M. Dynamic Interactions of Pigment-Based Inks on Chemically Modified Papers and Their Influence on Inkjet Print Quality. *Ind. Eng. Chem. Res.* **2014**, *53*, 4660–4668. [CrossRef]
25. Morais, F.P.; Vieira, J.C.; Mendes, A.O.; Carta, A.M.; Costa, A.P.; Fiadeiro, P.T.; Curto, J.M.R.; Amaral, M.E. Characterization of absorbency properties on tissue paper materials with and without "deco" and "micro" embossing patterns. *Cellulose* **2021**, *29*, 541–555. [CrossRef]
26. Mäkelä, P.; Östlund, S. Orthotropic elastic–plastic material model for paper materials. *Int. J. Solids Struct.* **2003**, *40*, 5599–5620. [CrossRef]
27. Karafillis, A.P.; Boyce, M.C. A general anisotropic yield criterion using bounds and a transformation weighting tensor. *J. Mech. Phys. Solids* **1993**, *41*, 1859–1886. [CrossRef]

Cellulose
https://doi.org/10.1007/s10570-022-04618-2

ORIGINAL RESEARCH

Mechanical and softness characterization of "deco" and "micro" embossed tissue papers using finite element model (FEM) validation

Joana Costa Vieira · Flávia Morais · António de Oliveira Mendes · Marcelo Leite Ribeiro · Ana Margarida Carta · Joana Curto · Maria Emília Amaral · Paulo Torrão Fiadeiro · Ana Paula Costa

Received: 4 March 2022 / Accepted: 24 April 2022

Abstract An innovative approach of using a laboratory embossing prototype was carried out to develop and optimize tissue papers, to quantify the influence of "deco" and "micro" embossing. A comparison between non-embossed and embossed tissue papers was conducted to investigate the effect of this process, on industrial and laboratory-made structures, evaluated by mechanical and softness properties. To identify the influence of the embossing patterns, the fiber composition and the creping process, a creped industrial base tissue paper, a disintegrated fibrous suspension obtained from this one, and an industrial never-dried bleached eucalyptus kraft pulp, were used as samples. These last two materials were used to produce similar industrial base tissue paper, in other words, handsheets with a grammage of 17 g/m^2 and unpressed. The end-use tissue properties were evaluated on the non-embossed and embossed structures. The results indicated that the embossing process produced bulkier and more porous structures, at the expense of reduced mechanical and softness properties, more intensified in the "micro" embossing than in the "deco" embossing. The effect of fiber composition shows that the mechanical properties were increased with an adverse effect on the structures' TSA-softness. Furthermore, these properties are enhanced for the structures where creping process effects are presents. The performance of structures with and without embossing allowed to quantify the functional properties of softness and strength, combining ISO experimental methods and computational approaches that benefit from modeling strategies considering its structural hierarchy at the fiber and structure levels, and the shape pattern used in the embossing process. Finite Element Model (FEM) analysis enabled a better understanding of how the embossing patterns affect the mechanical properties during the embossing process. The experimental results were validated using FEM simulation, which proved that "micro" pattern has a higher stress field value, and consequently a lower mechanical strength. Overall, the results indicate that the embossing prototype can be used as an opportunity to investigate

J. C. Vieira (✉) · F. Morais · A. de Oliveira Mendes · M. L. Ribeiro · J. Curto · M. E. Amaral · P. T. Fiadeiro · A. P. Costa
Fiber Materials and Environmental Technologies (FibEnTech-UBI), R. Marquês de D'Ávila E Bolama, Universidade da Beira Interior, 6201-001 Covilhã, Portugal
e-mail: joana.costa.vieira@ubi.pt

M. L. Ribeiro
Aeronautical Engineering Department, São Carlos School of Engineering, University of São Paulo, São Carlos, SP, Brazil

A. M. Carta
Forest and Paper Research Institute (RAIZ), R. José Estevão, 3800-783 Eixo, Aveiro, Portugal

J. Curto
Chemical Process Engineering and Forest Products Research Centre (CIEPQPF), Universidade de Coimbra, R. Sílvio Lima, Polo II, 3004-531 Coimbra, Portugal

Published online: 22 May 2022

the embossing process at laboratory scale and to optimize the final end-use tissue properties due to the controlled process parameters implemented in this methodology.

Keywords "deco" and "micro" Embossing prototypes · Eucalyptus-based fibrous materials · Finite element model simulation · Fiber modeling · Mechanical properties · Softness · Tissue paper

Introduction

Tissue papers presents various thicknesses and textures and are used mainly to produce facial tissues, toilet paper, paper towels, and napkins. The first step in the tissue paper manufacturing process is pulp production, which can be generated from wood fiber, recycled fiber, or a mixture of both (Fišerová et al. 2019). Tissue paper manufacturers produce their fibrous suspension by mixing properly treated cellulosic fiber with a large amount of water. The mixture of fibers and additives depends on the desired final product. While the fibrous suspension is in the mixing tank, the manufacturer can at this stage, add any additives that may be needed to soften, strengthen, or color the paper (Stankovská et al. 2020). During paper production at the tissue paper machine, paper residues are produced (e.g., during paper sheet breaks) these are called broke and are collected, recirculated to a re-pulper, and introduced again in the process by mixing it into the suspension.

As a result of using a fiber mixture to produce tissue papers, its three-dimensional (3D) structure is directly influenced by the fiber's morphological properties, consequently affecting the performance of these materials. Therefore, the concept of structural hierarchy applied to tissue papers is essential to establish the role of fibers in the structure made by them. Due to strong competition, the tissue industry is engaged in innovative methods to analyze materials behavior and production processes. 3D fiber modeling studies were proposed to realistically simulate tissue structures and, consequently, optimize their properties (Morais et al. 2020a, b). Hence, the development of advanced characterization and simulation tools, specifically developed for tissue papers, presents itself as an advantage for process optimization. These approaches are important for the tissue paper industry, but also from a researcher's perspective.

Once the fibrous suspension is ready, it is deposited uniform and consistently across the width of the web (2–6 m), on a fast-moving web and the formation of the sheet itself occurs (paper formation zone). A large quantity of the water is drained (95% water removed), leaving only the fibers, thus forming a kind of delicate tissue (pressing zone). The sheet is transferred to a huge, heated roller called the Yankee dryer (drying zone). The Yankee dryer is very hot, and the tissue sheet dries almost instantly (Boudreau and Germgård 2014). The tissue paper is then detached from the Yankee dryer by a blade called a creping blade, producing a more flexible and wrinkled creped sheet (Assis et al. 2018; Ramasubramanian et al. 2011; Wang et al. 2019). The creping process in the Yankee dryer is one of the key operations in the production of tissue paper, since this operation influences the softness, absorbency, and elongation of the sheet (Assis et al. 2018). However, because of this operation, the paper loses considerably its mechanical strength (Anukul et al. 2015). The creping process consists of uninterrupted folding and occurs in the final zone of the Yankee dryer, leading to an apparent decrease of about 15 to 20% of the length of the sheet (Hollmark 1984). The creped tissue paper (base tissue paper) is winded into the pope reel (winding zone). By adjusting the sheet extraction speed in the Yankee dryer and the winding speed of the pope reel, a thicker or thinner tissue paper can be obtained, according to the requirements of the final product (Assis et al. 2018; Ramasubramanian et al. 2011; Wang et al. 2019).

The main differences between the industrial base sheet and the laboratory-made sheet (handsheet) are the crepe and the fiber orientation. The creping operation gives volume and elongation to the industrial paper sheet, that is not found in the laboratory-made (Assis et al. 2018). The anisotropy effect also results from the creping lines and fiber orientation, while the isotropy effect is visible on the laboratory sheets. Therefore, the analysis of these operations separately is possible by comparing both structures. Additionally, this random deposition of fibers in laboratory structures is also considered in the 3D fiber and structure modeling (Conceição et al. 2010; Curto et al. 2011).

The tissue paper converting process occurs when the mother reel (single or combined pope reels) from

the tissue papermaking machine goes through the embossing process, perforation, rewinding, log cutting, packaging, and the palletization of the final product (Vieira et al. 2020). Embossing is a key process at the converting process, it is a mechanical operation which influences the tissue paper properties, and additionally, provides the physical bond between the different paper sheets, engraves a pattern, by application of localized pressure, that contributes to the improvement of the product properties namely softness, bulk, and liquid absorption capacity (Spina and Cavalcante 2018).

The quality of the finished tissue paper depends on various physical parameters of this process such as temperature, humidity, and pressure (DeMaio and Patterson 2008), in addition to allowing to identify and distinguish tissue papers from different industrial competitors, through the production of papers with aesthetically pleasing designs ("deco" embossing on the top layers and "micro" embossing on the bottom layers). The properties resulting from a product having more than one layer are not the same obtained on a single layer paper (Digby 2012). Despite the embossing process being able to improve some tissue paper properties, it may deteriorate others, such as tensile strength. The embossing operation itself is the passage of the base tissue paper sheet through a nip aligned between two rolls. One of them is made of steel with a pattern engraved on its surface, and the other is often a roll of steel with a rubber coating with a hardness between 50 and 70 Shore-A (Hilbig et al. 2005; Lofink 2003; Skapa 2020). According with information provided by a Portuguese tissue paper mill, linear pressure applied to the nip is in the range of 26–28 kg/cm for “deco” embossing and 16–18 kg/cm for “micro” embossing.

The properties of tissue paper are more influenced by the requirements imposed by the final consumer and its production process is adapted to meet those requests. Table 1 presents qualitatively the relevance of tissue paper properties in the European market due to its functionality (Assis et al. 2018; Bai et al. 2019).

The structural-mechanical properties of the single layer of virgin paper are usually evaluated in terms of basis weight, thickness, and elongation, as well as tensile strength in the machine direction (MD) and cross direction (CD). These values change from supplier to supplier due to the tissue paper machine roll (Spina and Cavalcante 2018). Softness, bulk, liquid absorbency, and mechanical strength are important and differentiating properties for tissue paper products. It is a challenge to understand how they relate and in what sense changing one property can affect others.

In our previous work, the influence of “deco” and “micro” embossing was studied on absorbency properties, such as water absorption capacity, Klemm capillary rise, and liquid spreading kinetics. It was proved that the type of 3D structure, the effect of anisotropy and isotropy, and the creping and embossing process operations are key parameters on the interaction of liquids with tissue materials, including industrial and laboratory-made structures (Morais et al. 2022). To the best of our knowledge, the influence of these embossing patterns on mechanical and softness properties for industrial and laboratory samples has not been investigated in the literature. In this context, the goal of the present work was to compare the performance of un-embossed and embossed materials, made with eucalyptus fibrous based, to study the effect of fibrous composition, and the influence of “micro” and “deco” embossing on these structures. To reproduce its effects a methodology was proposed using a laboratory-made prototype, which constitutes an innovative approach to identify the influence of the embossing patterns, in a controlled way, on the structural-mechanical properties, and TSA softness of the tissue products, considering different tissue materials.

Table 1 Summary of the main properties of tissue papers in the European Union (EU) and in the United States of America (USA) markets (Assis et al. 2018; Bai et al. 2019)

Products and properties	Strength		Wet strength		Softness		Absorption capacity		Brightness and color	
Toilet tissue		×			×	××			×	
Facial tissue		×			××	××			×	
Hand towels	×	××	×	××			××	××		
	EU	USA	EU	USA	EU	USA	EU	USA	EU	USA

Materials and methods

Materials

In this study 3 types of tissue paper sheets were used in which the embossing process was performed. The first type was an industrial base tissue paper sheet produced with an approximate composition of hardwood (49%) and softwood (27%) bleached pulps, and broke (24%), supplied by Portuguese tissue paper manufacturers. The second type was obtained by the disintegration of the previous tissue paper. Finally, the third type used in this study was a never-dried bleached eucalyptus kraft pulp laboratory tissue sheet. The two-last type of samples were used to produce isotropic handsheets. Table 2 shows the abbreviations and their meaning for each tissue paper samples with and without embossing process. These abbreviations will be used throughout this manuscript.

Fiber and suspension characterization and modeling

The industrial tissue paper samples, I_{hs}/$HD_{Ihs,}$ and the never-dried eucalyptus pulp, H_h were all disintegrated following ISO 5263-1:1995 standard. The fibers morphological properties of these samples were evaluated using of MorFi® analyzer (LB-01) (Techpap SAS, Grenoble, France). These properties were assessed by image analysis of a diluted suspension (20 mgL^{-1}) flowing in a transparent chamber equipped with a CCD video camera (Tourtollet et al. 2003). The assays were repeated three times for each sample.

The fibers and structures were modeled in 3D according to their dimensions and properties using a 3D simulator of fibrous materials, the *voxelfiber* (https://github.com/eduardotrincaoconceicao/voxelfiber) (Conceição et al. 2010; Curto et al. 2011; Morais et al. 2020a). Computational studies were carried out using Matlab® (R 2020a, 9.8.0.1323502, MathWorks, Natick, MA, USA).

The intrinsic viscosity was achieved by dissolving the samples in a cupriethylenediamine (CED) solution as a solvent, followed by flow time measurement on a capillary tube viscometer, according to the ISO 5351:2010 standard. The polymerization degree (DP_v) was calculated from viscosity (Sihtola et al. 1963). The carboxyl group's content of the samples was determined according to the TAPPI T 237 cm-08 standard, and calculated using Eq. 1,

$$\text{COOHcontent(mmol/100g)} = \left(b - a - \frac{C_W \times a}{V_{NaHCO3/NaCl}}\right) \times \left(\frac{V_{NaHCO3/NaCl}}{V_{filtrate} \times W}\right) \quad (1)$$

where a is the HCl volume spent on titration (mL), b is the HCl volume spent on standard titration (mL), C_W is the water mass that was in the sample after filtration (g), $V_{NaHCO3/NaCl}$ is the volume added of $NaHCO_3$/NaCl solution, $V_{filtrate}$ is the filtrate volume used in the titrations and W is the sample dry mass (g). The assays were performed in duplicate. The water retention value, WRV, was assessed using the centrifugation method described by Silvy et al. (1968). The wet pulp samples were centrifuged by 3000×g for 10 min after they were weighed and recorded as W_1. The samples were oven drying at 105 °C overnight followed by sequential

Table 2 Abbreviations of the tissue paper samples used in this work

Abbreviation	Description
I_{hs}	Industrial Sheet (hardwood + softwood) – Embossing none
$I_{hs}E_d$	Industrial Sheet (hardwood + softwood) – Embossing "deco"
$I_{hs}E_m$	Industrial Sheet (hardwood + softwood) – Embossing "micro"
HD_{Ihs}	Handsheet Disintegration of Industrial Sheet – Embossing none
$HD_{Ihs}E_d$	Handsheet Disintegration of Industrial Sheet – Embossing "deco"
$HD_{Ihs}E_m$	Handsheet Disintegration of Industrial Sheet – Embossing "micro"
H_h	Handsheet (hardwood) – Embossing none
H_hE_d	Handsheet (hardwood) – Embossing "deco"
H_hE_m	Handsheet (hardwood) – Embossing "micro"

weighing, up to constant weight, and recorded as W_2. The assays were performed in triplicate. The *WRV* (%) was calculated by using the Eq. 2,

$$WRV(\%) = 100 \times \left(\frac{W_1 - W_2}{W_2} \right) \quad (2)$$

The drainability of the samples suspensions was determined in terms of °SR (Schöpper Riegler degree), according to the ISO 5267-1:1999. The assays were performed in triplicate.

Isotropic handsheets preparation and innovative embossing operation

To simulate the grammage of the industrial tissue paper, isotropic handsheets with a grammage between 16.5 and 17.7 g/m^2 were prepared in a conventional sheet-former with an adaptation of the ISO 5269-1:1998, i.e., produced without the pressing process. The ensuing handsheets were conditioned at 23 ± 1 °C with a relative humidity of 50 ± 2%, according to ISO 187:1990.

An innovative laboratory embossing prototype was carried out using 3D plates with "deco" and "micro" embossing patterns. The rubber hardness of the rolls was determined. This hardness was determined with the assistance of a PCE-DDA durometer (PCE Iberica S.L. Instrumentacíon, Albacete, Spain), where each roll was divided in 3 sections, and in each section were made 3 measurements, always perpendicular to the roll axis. The apparent hardness is the mean of the 9 measures made in each roll, accordingly with ISO 48-7:2018. To perform the embossing were used a rolls speed of 1.0 m/min, and a nip pressure of 2.2 bar (≈ 26.4 kg/cm) for "deco" embossing and 1.5 bar (≈ 18.0 kg/cm) for "micro" embossing, at room temperature.

For a detailed observation of the studied samples and the modifications performed on their surfaces, after usage of the previously described embossing methodology, a customized optical system (Mendes et al. 2013, 2014, 2015) was considered in this work as a complementary inspection tool. In particular, the system used a higher magnification for observation of the fibers structure of the different paper samples composing the chosen set of samples to be studied and used a lower magnification (3 × lower than the first) for a global observation of the modifications that were performed on them.

Structural, mechanical and softness properties characterization

All samples were characterized in terms of their structural (grammage, thickness, bulk, apparent density, and apparent porosity), mechanical, and TSA softness properties. Grammage (in g/m^2) was determined with the assistance of a Mettler Toledo PB303 Delta Range analytical balance, accordingly with ISO 12625-6:2005. Thickness was determined with the equipment FRANK-TPI® Micrometer following the ISO 12625-3:2014. Apparent density and bulk could be determined by applying the same standard as before. Apparent porosity (P) was calculated using Eq. 3,

$$P(\%) = 100 \times \left(1 - \frac{\rho_{sample}}{\rho_{cellulose}} \right) \quad (3)$$

where $\rho_{cellulose}$ is the density of the cellulose (assumed to be 1.6 g/cm^3) and ρ_{sample} is the density of the sample (g/cm^3) (Henriksson et al. 2008; Costa et al. 2016; Vieira et al. 2020).

Tensile tests were performed in MD and CD directions for industrial base tissue paper samples, and in a single direction for the remaining samples, since handsheets are isotropic. A Thwing-Albert® VantageNX Universal Testing Machine was used for the measurements following the ISO 12625-4:2005. The Tissue Softness Analyzer (TSA) from EMTEC® was used to determine the TSA-softness properties of the tissue paper samples. All samples were prepared accordingly to the machine specifications. TSA uses specific algorithms to combine several measurements on the samples to obtain a global quantification, handfeel (HF), of tissue papers softness. The algorithms QAI and TPII were used for the softness calculation of the HF for the tissue-based paper analysis. These algorithms considered for the calculation a set of measured parameters on the tissue paper sample, such as the "real" softness (TS7), the roughness/smoothness (TS750), and the stiffness (D). To study the impact of the embossing on the tissue paper samples, the authors decided to use the same algorithm,

QAI, to avoid another variable in the analysis keeping the same test conditions in the methodology.

Finite element model (FEM)

A finite element model was proposed to improve the understanding of the paper manufacturing process and its implication on paper strength. The two different dies are used for simulations that corresponds to 3D patterns "deco" and "micro" and their effects on the paper stress field, as well as their strength are analyzed.

The ABAQUS™ explicit solver was used to overcome convergence issues that are usual for the implicit solver, on the other hand the stable time increment is very small resulting in simulations long time. The simulations were performed using a workstation with two intel Xeon E5-2630 8 cores (16 cores, 32 threads) with 128 Gb RAM.

The finite element model dimensions and boundary conditions are presented in Fig. 1. The die model dimensions are smaller than the actual die dimensions to reach a reasonable computational cost and keeping the precision for the embossing process. The base dimension follows the die dimensions, but it is thick enough to allow the deformation without severe interference in the die and paper kinematics. The paper follows the same dimensions of the die and basis.

The boundary conditions are applied to simulate the embossing process of paper, thus all the displacements degree of freedom are restricted in the bottom of the elastic base and a prescribed displacement is applied on the top of the die to move it against the paper and the paper and the elastic base. Additionally, all other degrees of freedom of the die are restricted avoiding the die to rotate or undesirable displacements.

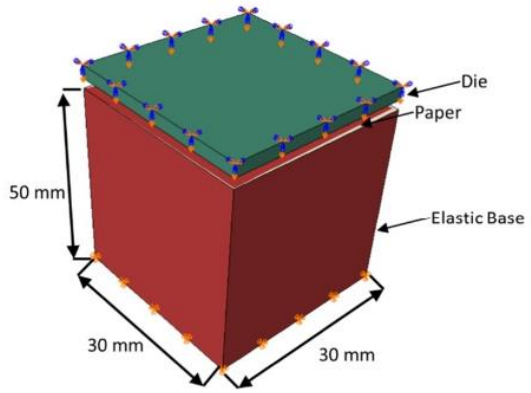

Fig. 1 Finite element model dimensions and boundary conditions

The interactions are essential to model the contact between the different parts of the model thus the finite element model accounts for hard contact for normal behavior and a 0.3 penalty factor for tangential behavior.

As the element size is an important parameter for finite element model accuracy, finer mesh (small element size) ensures the model accuracy. On the other hand, it increases the computational costs. Thus, to keep a reasonable computational cost without accuracy lost, it is important to employ finer meshes in some specific parts, for this case the paper must have a fine and a coarse mesh can be employed for the other parts. The die models for the "micro" and "deco" patterns use a total of 473,694 and 476,153 elements, respectively.

For both models, the paper uses a four-node reduced integration element (ABAQUS™ S4R) regarding only membrane stiffness (no bending stiffness) to better simulate the paper behavior. A structured mesh with 250,000 elements is used for this part.

As the die is not an interesting part for this analysis, a coarse mesh is used for "micro" and "deco" die. A four-node reduced integration element (ABAQUS™ S4R) was used with a total 7694 elements for "micro" and 10,314 elements for "deco".

The elastic base was modeled using 8 nodes fully integrated tridimensional elements (ABAQUS™ C3D8) with 216,000 elements.

Finally, both die parts are modelled using an isotropic material with same properties as for steel materials (E=200 GPa, μ=0.33), the paper was modeled as orthotropic material (E_{11}=10 MPa, E_{22}=5 MPa, G_{12}=2.5 MPa, G_{13}=2.5 MPa, G_{23}=1.5 MPa, μ_{12}=0.3) and the elastic base was modeled as a soft rubber material (E=0.5 MPa, μ=0.1). Where E is the Young Modulus, μ is the Poisson coefficient and the subscripts used in the paper properties stands for the paper fiber direction (E_{11}), fiber transverse direction (E_{22}), in-plane shear modulus (G_{12}), out of plane shear modulus (G_{13} and G_{23}).

Results and discussion

Fiber and suspension characterization and modeling

It is of great relevance to underline that the tissue products properties are a result of fiber composition

and their morphological characteristics, beyond the creping and embossing processes.

In Table 3 the morphological properties of the I_{hs} and HD_{Ihs} samples are the same, since the HD_{Ihs} sample derives from the disintegration of the I_{hs} sample. The samples I_{hs}/HD_{Ihs} present a lower fiber population than the H_h, whose composition is 100% eucalyptus fibers. In previous publications of Assis et al. (2018) and Morais et al. (2019), is also shown, that pulps with high fiber population will provide a uniform paper structure and this property is related to the fiber length and fiber coarseness. For the length weighted by length I_{hs}/HD_{Ihs} samples have higher values than the H_h sample, contributing directly to the development of mechanical properties, more notable in I_{hs}/HD_{Ihs}, as well as, to a potential improvement in the runnability of the paper machine. In the sample H_h, the coarseness is lower. This property involves the fiber width, wall thickness and density therefore, promoting tissue products with better surface softness, and higher water retention (Axelsson 2001). The kink and curl properties are related to the fiber deformations that may arise during the pulp production process. The I_{hs}/HD_{Ihs} samples showed kinks and curl higher when compared to the H_h sample. Additionally, the same trend is verified for the properties of broken ends and fine elements. The obtained differences can be translated into gains in the mechanical properties of the structures since the fine elements contribute to the inter-fiber bonds, and consequently, to a more organized and closed structure.

Table 3 Mean values and standard deviations of the results for morphological, chemical, and suspensions properties for all types of samples

Properties	I_{hs}/HD_{Ihs}		H_h	
	$\bar{x}$	$\pm\sigma$	$\bar{x}$	$\pm\sigma$
Morphological characterization				
Number of fibers (million/g)	17.3	0.2	25.3	0.1
Length weighted by length (mm)	0.784	0.003	0.729	0.003
Width (μm)	20.7	0.1	19.1	0.0
Coarseness (mg/100 m)	9.25	0.06	6.31	0.04
Kink fibers (%)	48.4	0.2	44.2	0.3
Curl (%)	10.3	0.0	9.7	0.0
Broken ends (%)	26.3	0.4	21.3	0.3
Fine elements (% in length)	47.0	0.1	38.5	0.4
Fine elements (% in area)	14.4	0.1	13.7	0.2
Chemical characterization				
Intrinsic viscosity (mL/g)	607		469	
DP_v [a]	3827		3634	
Carboxyl group content (mmol/100 g)	6.27	0.06	5.08	0.05
Suspensions characterization				
°SR	26		25	
WRV(%)	103.1	1.6	135.3	0.7

[a] $DP_v = (0.75(954\log\eta - 325))^{1.105}$ (Sihtola et al. 1963)

At the molecular level, the intrinsic viscosity of cellulose chains is directly related to the average degree of polymerization of polysaccharides, mainly cellulose. As can be seen in Table 3, the DP_v, shows that I_{hs}/HD_{Ihs} exhibits a higher DP_v than the H_h sample. These obtained values are within the range reported by Costa et al. (2016). The lower values of the intrinsic viscosity may be related to the severe cooking and bleaching process used to obtain the eucalyptus pulps, that caused a more degraded fibers, and consequently, a loss in their intrinsic strength, which negatively influences the strength properties (Sjöholm et al. 1997). The carboxyl group content in pulps contributes to the establishment of bonds between fibers and water, providing more interaction points with water molecules. In our study, all the samples exhibit similar carboxyl content.

Regarding the suspensions drainability measured by °SR, the I_{hs}/HD_{Ihs} samples showed a slightly higher °SR compared to the H_h sample, with our

Additionally, these results of fiber properties and dimensions were considered to simulate the 3D structures with different fiber compositions, enhancing a more realistic computational representation. The fibers were modeled individually, and the simulated 3D structure was built by sequential and random fiber deposition, representing a good estimative of the handheets. The tissue structures were simulated according to fiber length/width ratio, fiber flexibility, fiber wall thickness, lumen thickness, and resolution (Morais et al. 2020a, b), predicting their structural properties. Figure 2 presents a comparison between the H_h and HD_{Ihs} samples. The different structures were modeled computationally with the same fibrous elements. The structures were simulated by random fiber deposition in space according to their furnish distribution. The H_h structure was obtained by modeling 100% of eucalyptus fibers (Fig. 2a), while the HD_{Ihs} structure was obtained with a mixture of eucalyptus, softwood, and broke fibers (Fig. 2b).

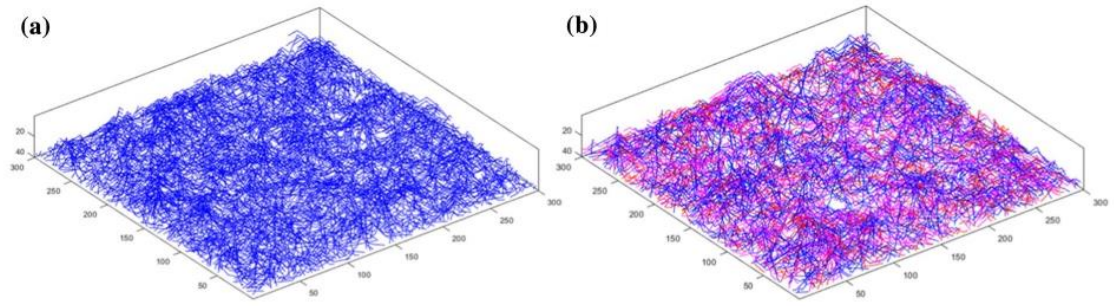

Fig. 2 Example of 3D structures H_h (**a**) and HD_{Ihs} (**b**), obtained by computational simulation, with different fibrous compositions. Structure H_h presents a composition of 100% eucalyptus fibers (blue), while structure HD_{Ihs} presents a mixture of eucalyptus fibers (blue), softwood fibers (magenta), and fibers from broke (red)

values being within the recommended range for producing high quality tissue papers (Assis et al. 2018). The amount of water retained by fiber or fibrils measured by *WRV*, gives for the H_h sample a 27.8% higher *WRV* compared to the I_{hs}/HD_{Ihs} samples, which can be explained by the absence of the effect of hornification caused by drying softwood pulp operation (Giacomozzi and Joutsimo 2015).

Innovative embossing operation

The apparent hardness of the calender rubber rolls is similar. The front rubber roll presents an apparent hardness of 72.2 ± 2.1 Shore-A and the back rubber roll of 71.4 ± 2.8 Shore-A, contributing in the same way to the NIP pressure and to the embossing engraving. As mentioned in the introduction this value of apparent hardness is on the superior limit of the rubber hardness of an industrial embossing rubber roll.

Figure 3 illustrates the samples with "deco" and "micro" embossing in which the structural-mechanical characterization was carried out. As it can be seen, the same "deco" and "micro" embossing pattern has always been used, simplifying the analysis of the impact of this effect on tissue paper.

In addition to the previous presented photos, more detailed images of the samples in study can be seen in the Figs. 4, 5, 6, 7, 8, and 9, on which the structure itself of the papers as well as the engraved patterns performed during the embossing process can easily

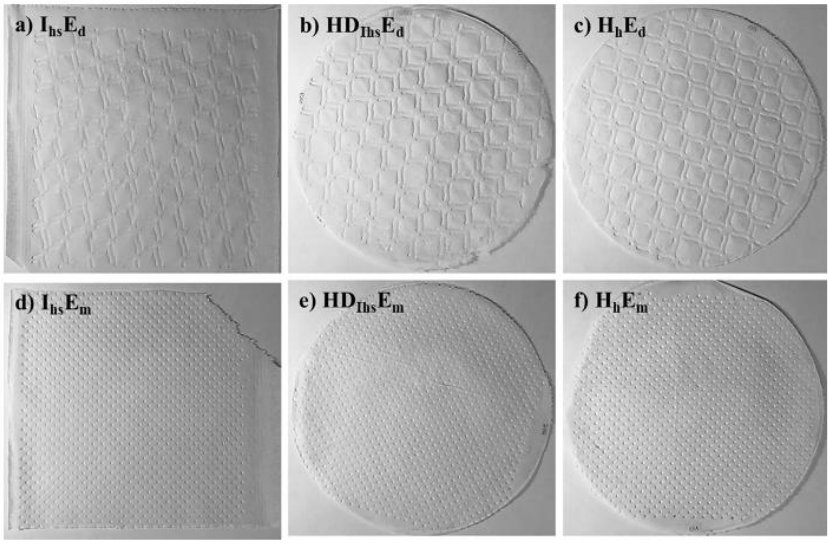

Fig. 3 Photos of "deco, E_d" and "micro, E_m" embossing on **a**, **d** industrial base tissue paper sheet, **b**, **e**, handsheet produced from the industrial sheet, and **c**, **f** 100% eucalyptus handsheet

be observed, which allow a proper discrimination and differentiation of the entire set of samples used in this work.

Structural properties

Table 4 presents the structural properties of all tissue paper samples. In a first approach, the samples without the embossing process (I_{hs}, $HD_{Ihs,}$ and H_h)

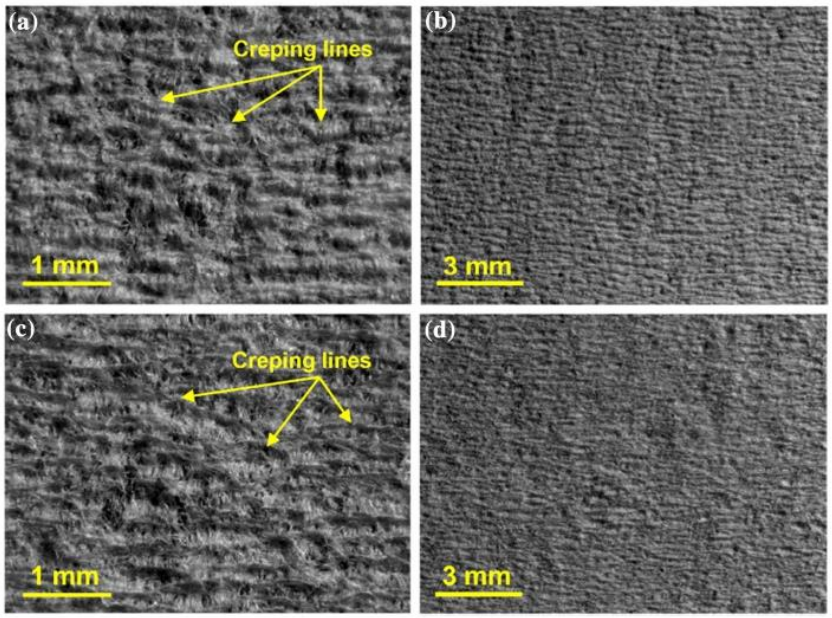

Fig. 4 Magnified and global views of the front surface (**a**, **b**) and back surface (**c**, **d**) for the industrial base tissue paper (I_{hs})

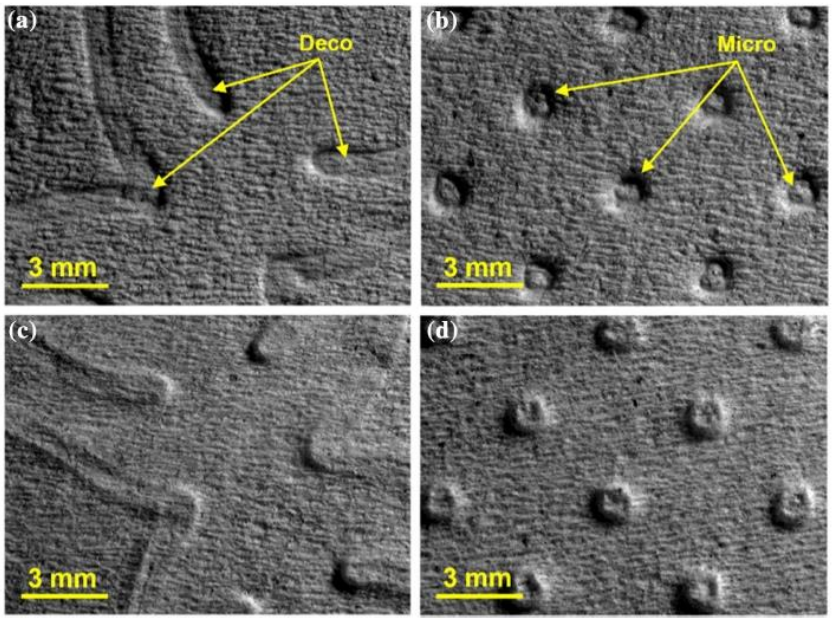

Fig. 5 Global views of the "deco" ($I_{hs}E_d$) and "micro" ($I_{hs}E_m$) embossing on the front surface (a and b) and back surface (**c**, **d**) for the industrial base tissue paper

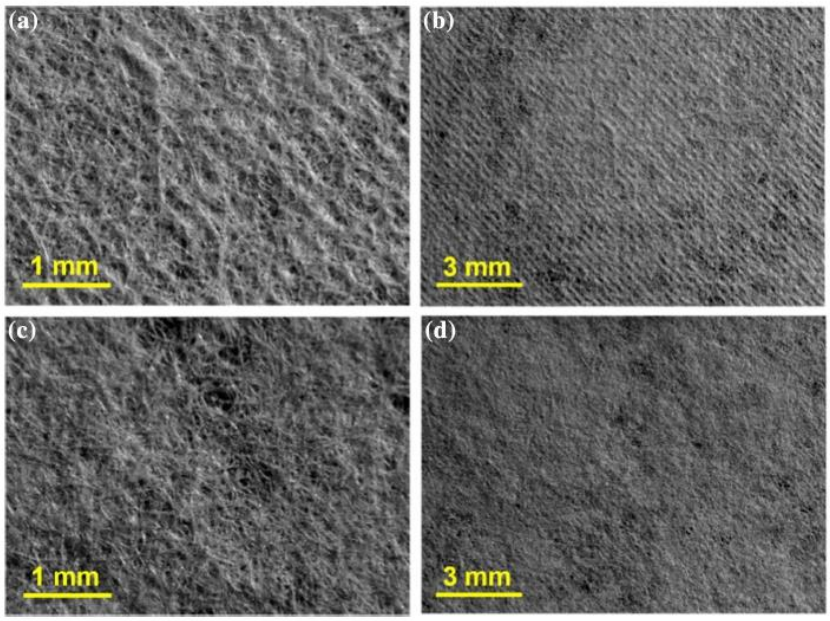

Fig. 6 Magnified and global views of the front surface (a and b) and back surface (c and d) for the handsheet produced from the industrial sheet (HD_{Ihs})

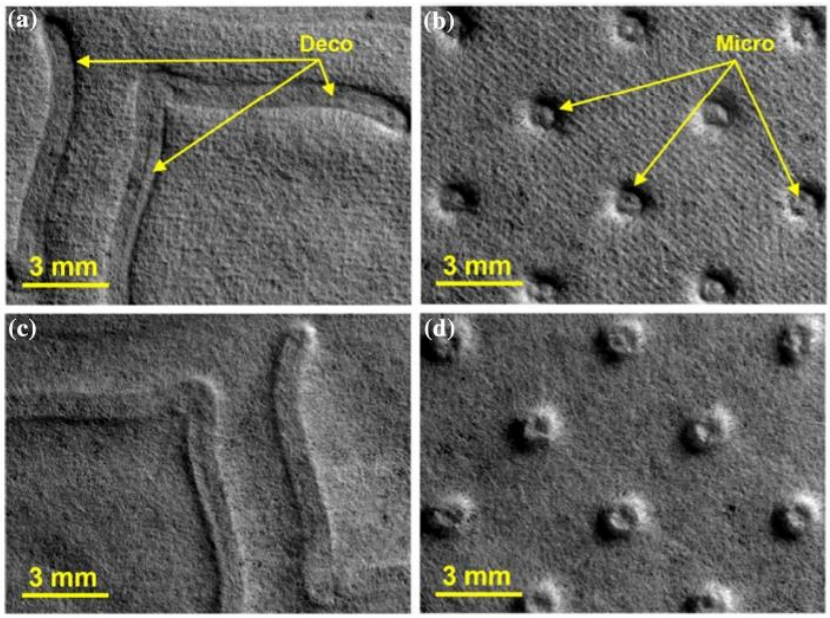

Fig. 7 Global views of the "deco" ($HD_{Ihs}E_d$) and "micro" ($HD_{Ihs}E_m$) embossing on the front surface (a and b) and back surface (c and d) for the handsheet produced from the industrial sheet

were analyzed. The I_{hs} sample is an industrial base tissue paper sheet, so the creping process is present, and its main effects will be giving bulk to the sheet and creating a more porous structure (Boudreau and Germgård 2014). In the HD_{Ihs} sample the creping is suppressed by its disintegration, as seen by comparison of the Figs. 3 and 5. The results indicated that the creping process and the fiber compositions influence the structural properties. As expected, comparing the samples with and without the

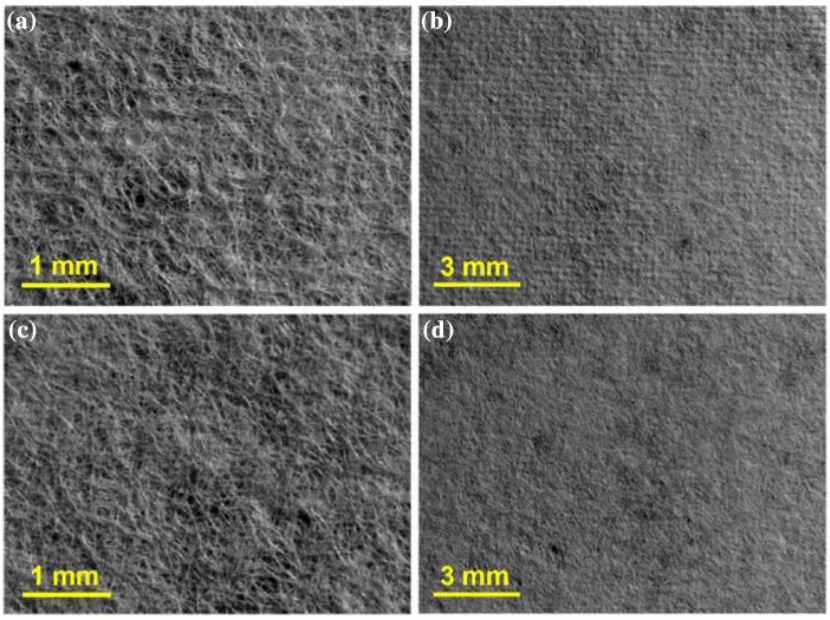

Fig. 8 Magnified and global views of the front surface (a and b) and back surface (c and d) for the 100% eucalyptus handsheet (H_h)

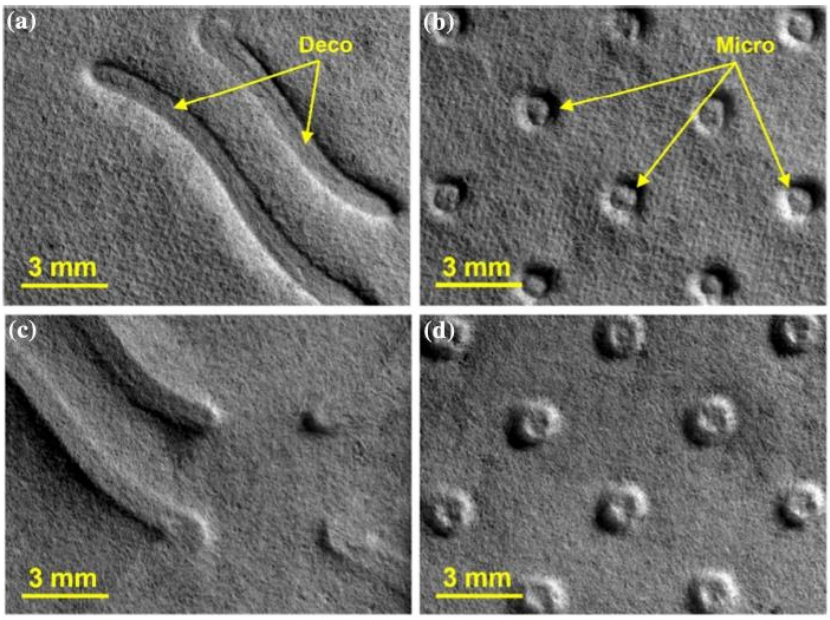

Fig. 9 Global views of the "deco" (H_hE_d) and "micro" (H_hE_m) embossing on the front surface (a and b) and back surface (c and d) for the 100% eucalyptus handsheet

creping process and same fiber composition (I_{hs} and HD_{Ihs}), the tissue paper thickness increases by 20.9%, and consequently, the bulk and apparent porosity properties are also increased by 22.8% and 2.6%, respectively. Additionally, comparing the H_{hs} sample (100% eucalyptus) with HD_{Ih}, the thickness increases 11.2%, the bulk 5%, and finally the apparent porosity slightly increases.

In a second approach, the samples with the creping and embossing process (I_{hs}, $I_{hs}E_d$ and $I_{hs}E_m$)

Table 4 Mean values and standard deviations of the results from structural characterization for all tissue paper samples

Tissue paper sample	Grammage (g/m^2)		Thickness (μm)		Bulk (cm^3/g)		Apparent density (g/cm^3)		Apparent porosity (%)	
	$\bar{x}$	±σ	$\bar{x}$	±σ	$\bar{x}$	±σ	$\bar{x}$	±σ	$\bar{x}$	±σ
I_{hs}	17.3	0.2	131.4	2.3	7.62	0.11	0.131	0.006	91.3	0.4
$I_{hs}E_d$	16.7	0.0	133.4	2.6	7.99	0.16	0.125	0.003	91.7	0.2
$I_{hs}E_m$	16.7	0.0	220.0	27.8	13.18	1.66	0.077	0.011	94.9	0.7
HD_{ihs}	17.7	0.2	104.0	3.3	5.88	0.18	0.170	0.005	88.9	0.3
$HD_{Ihs}E_d$	17.8	0.2	109.5	3.9	6.20	0.25	0.161	0.007	89.5	0.4
$HD_{Ihs}E_m$	17.8	0.2	186.0	18.5	10.48	1.13	0.095	0.011	93.8	0.7
H_h	16.7	0.3	93.5	3.6	5.60	0.15	0.179	0.005	88.1	0.3
H_hE_d	16.9	0.2	135.3	21.5	7.99	1.23	0.128	0.019	91.5	1.3
H_hE_m	16.8	0.2	326.5	33.2	19.39	1.86	0.052	0.005	96.5	0.3

were analyzed. The results indicated that "micro" embossing presents a higher relevance in structural properties than "deco" embossing, as seen by comparison of the different patterns shown in Fig. 4. Handsheets with the same industrial paper fibrous composition, results with “deco” and “micro” embossing, present the same behavior, being the most accentuated in the “micro” pattern (see Fig. 6). For 100% eucalyptus handsheets, the effect of embossing operation on structural properties shows that the “micro” pattern reveals the highest impact than the “deco” pattern, as shown in Fig. 8. This occurs according with mentioned above about the fiber morphology of 100% eucalyptus, with a uniform and more flexible structure.

Mechanical properties

Mechanical characterization in MD and CD were analyzed for industrial base tissue paper samples and these results are presented in Table 5. The first observation that can be made is that the value of the CD tensile index is less than half the value in MD. In both directions, “micro” embossing presents the lower tensile index, indicating a higher damage in the fibrous structure of the paper than the "deco" embossing. Regarding elongation, in MD there was an elongation 86% higher than the CD for the I_{hs} and $I_{hs}E_d$ samples and 6% higher for the $I_{hs}E_m$ sample. These results can be explained by the crepe waves, as they are perpendicular to the MD, when stretched, they give a bigger elongation to the paper sample (see Figs. 3 and 4). In the sample with "micro" embossing, the smallest difference obtained in the elongation value is due to the higher fragility of the fibrous structure via this type of embossing, blocking the elongation effect due to the creping process.

The Fig. 10 presents the evolution of the load on the paper samples I_{hs} and HD_{Ihs} as a function of the elongation. As expected, these curves are well fitted and confirming the previous findings by Hollmark (1984) and Park et al. (2020).

Table 5 Mean Values and Standard Deviations of the results from mechanical characterization (MD and CD) for industrial base tissue paper samples

Tissue paper sample	Maximum tensile force (N)		Elongation at break (%)		Tensile strength (N/m)		Tensile index (Nm/g)	
	$\bar{x}$	±σ	$\bar{x}$	±σ	$\bar{x}$	±σ	$\bar{x}$	±σ
I_{hs} (MD)	8.4	0.3	23.0	1.0	168.1	6.4	10.0	0.4
$I_{hs}E_d$ (MD)	8.3	0.6	20.8	1.2	166.5	11.0	9.8	0.7
$I_{hs}E_m$ (MD)	3.4	0.2	3.6	0.4	67.8	4.2	4.1	0.3
I_{hs} (CD)	3.7	0.2	3.3	0.3	74.2	2.8	4.4	0.2
$I_{hs}E_d$ (CD)	3.7	0.2	2.9	0.3	73.3	3.3	4.4	0.2
$I_{hs}E_m$ (CD)	3.4	0.1	3.4	0.2	69.0	2.9	4.1	0.2

The fiber composition of the analyzed samples is the same, which enables us to evaluate separately the influence of the creping and the embossing processes. The results shown in Fig. 10 indicate that the creping operation increases drastically the elongation for the tissue paper samples (I_{hs}) in MD when compared with the uncreped handsheet sample (HD_{Ihs}). It should be noted that this increase is consequence of the orientation of the folds/wrinkles from the creped structure in the tissue paper machine (Figs. 4, 5). Relatively to the embossing, the "deco" and the "micro" patterns have a similar effect on CD as shown in Fig. 10b, c, having a small effect when compared with the non-embossed sample (creped CD) in Fig. 10a. As expected, in MD the effect of the "micro" embossing has a negative impact in both the load and elongation properties due to the damage of the creping folds/wrinkles.

Table 6 presents the mechanical characterization results for the isotropic paper samples. As expected, H_h present a smaller tensile index than HD_{Ihs} which can be explained by the presence of softwood fibers. For handsheets the embossing process promoted a loss of the mechanical properties. In the case of HD_{Ihs} that loss was about 25% and for H_h was 10%. The elongation in these samples is practically nonexistent due to the absence of creping (Figs. 6, 8).

The simulations results allow understand the stress field during the embossing process and how it can affect the paper strength. Figure 11 shows the stress in fiber direction (direction 1) for "deco" die and Fig. 12 also shows the stress in fiber direction (direction 1) for "micro" die. It is important to mention that this stress values are for the same die displacement in the paper (0.57 mm).

The stress field are considerable different for each model. The "deco" model stress field are more homogeneous with an average value 0.056 MPa (Fig. 11), on the other hand, the stress field for "micro" die shows several points of stress concentration, around 0.082 MPa (Fig. 12). It explains the effect of the embossing die on the mechanical properties, once

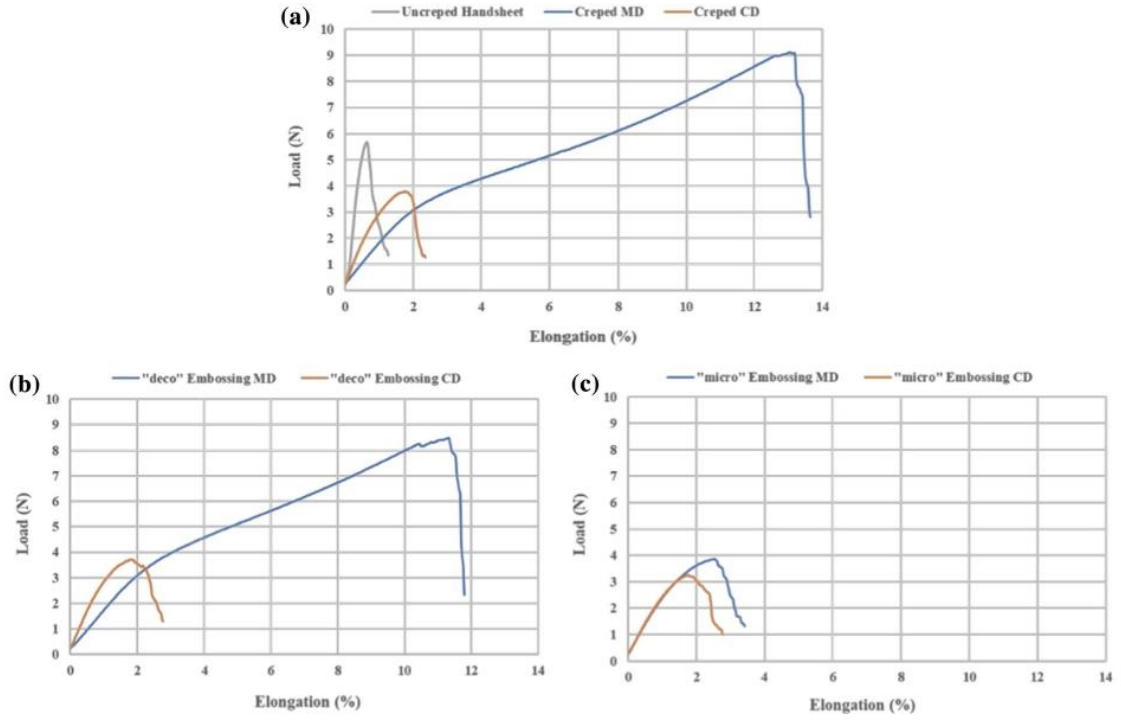

Fig. 10 **a** Load-Elongation curves of the I_{hs} (creped CD and MD) and HD_{Ihs} (uncreped) tissue paper samples, **b** the $I_{hs}E_d$ ("deco" embossing CD and MD), **c** the $I_{hs}E_m$ ("micro" embossing CD and MD)

Table 6 Mean Values and Standard Deviations of the results from mechanical characterization in one direction for tissue paper samples

Tissue paper sample	Maximum tensile force (N)		Elongation at break (%)		Tensile strength (N/m)		Tensile index (Nm/g)	
	$\bar{x}$	$\pm\sigma$	$\bar{x}$	$\pm\sigma$	$\bar{x}$	$\pm\sigma$	$\bar{x}$	$\pm\sigma$
HD_{ihs}	6.1	0.4	1.4	0.2	121.5	8.1	6.9	0.5
$HD_{ihs}E_d$	5.4	1.0	1.5	0.3	108.2	17.1	6.1	1.1
$HD_{ihs}E_m$	4.6	0.6	1.4	0.1	92.2	7.1	5.2	0.6
H_h	5.1	0.6	0.5	0.1	103.4	13.4	5.2	0.7
H_hE_d	4.0	1.1	0.4	0.2	79.8	21.1	4.7	1.2
H_hE_m	4.0	0.5	0.6	0.2	80.9	9.8	4.8	0.6

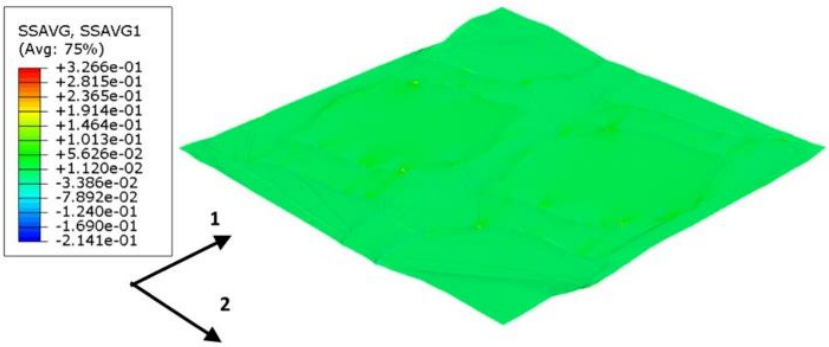

Fig. 11 Membrane stress in fiber direction (1) for "deco" die

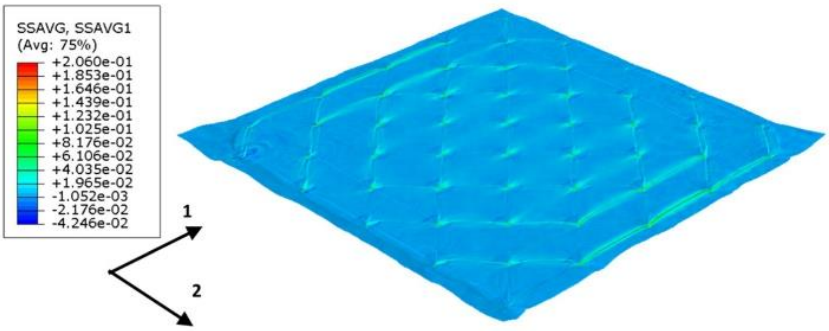

Fig. 12 Membrane stress in fiber direction (1) for "micro" die

there are much more points high loaded than for the "deco" pattern.

Despite the peak values of the "deco" higher (legend of Fig. 11) than "micro", this values are much localized (only two elements in the model) and are related with numerical issues due to contact algorithm between die and paper and basis which leads to as excessive element rotations and convergence problems.

Finally, the same pattern is observed for the other stress directions as for fiber transverse stress (direction 2), in plane shear and out of plane shear (1–3 and 2–3).

Softness properties

Figure 13 shows the results obtained with TSA-Tissue Softness Analyzer for all tissue samples, respectively, the parameters of HF, TS7, TS750, and D. From the results presented in Fig. 10, similar overall trends can

be easily identified for each measured TSA parameter. In particular, the samples I_{hs} and HD_{Ihs} show comparable results for the handfeel HF on Fig. 13a, the "real" softness TS7 on Fig. 13b, and the roughness/smoothness TS750 on Fig. 13c in all the cases of non-embossed, "deco" embossing, and "micro" embossing. This happens because both samples have the same fiber composition being the only difference between them the presence of creping in the sample I_{hs} and the absence of creping in the sample HD_{Ihs}. Nevertheless, this aspect appears to have little effect in the results. Moreover, the samples HD_{Ihs} and H_h also show comparable results for the stiffness D on Fig. 13d. This occurs because both these samples are laboratory handsheets and therefore, have a very similar structure, but different from the first industrial sample I_{hs}.

In Fig. 13 it can also be seen that the performed embossing process ("deco" and "micro") on the studied samples clearly affect the TSA-softness results. From Fig. 13a a decrease in the HF can be noted for all samples, meaning that the global handfeel of the non-embossed samples was somehow damaged (blue bars). It should be noted that the "micro" embossing had a bigger effect than the "deco" embossing on the HF decrease. Concerning the parameter TS7 it can be observed that the performed embossing process ("deco" and "micro") increase relatively to the results of the non-embossed samples, indicating a lower "real" softness inherent to the material. At the same time, the parameter TS750 also displays a slight decrease with embossing, which agrees with implies a rougher and irregular surface, as a result of the engraved patterns. Regarding the D parameter, it can also be seen that the embossing process ("deco" and "micro") influenced the stiffness of the samples, increasing slightly for all the samples, favoring the flexibility of the samples. One last note that can be highlighted from the Fig. 13 is related to the fact that the sample H_h has better results on HF, TS7 and TS750, due to the fact of being composed by 100% eucalyptus fibers, which favors the overall softness of the paper sample. Particularly, the HF value shows an increase of 21% when compared with the HD_{Ihs} and I_{hs} samples, while the TS7 and the TS750 values show a decrease of 43% and 38%, respectively. Concerning the D parameter, this sample does not show the best results because it corresponds to a handsheet sample. A comparison with the result obtained for the industrial sample I_{hs} show a decrease of 79% on this parameter due to the lack of the creping on this handsheet sample. If the sample HD_{Ihs} was indeed an industrial sample with crepe, it would be expected higher bars in Fig. 13d, and it would be also the sample with the best results for each one of the TSA parameters HF, TS7, TS750, and D.

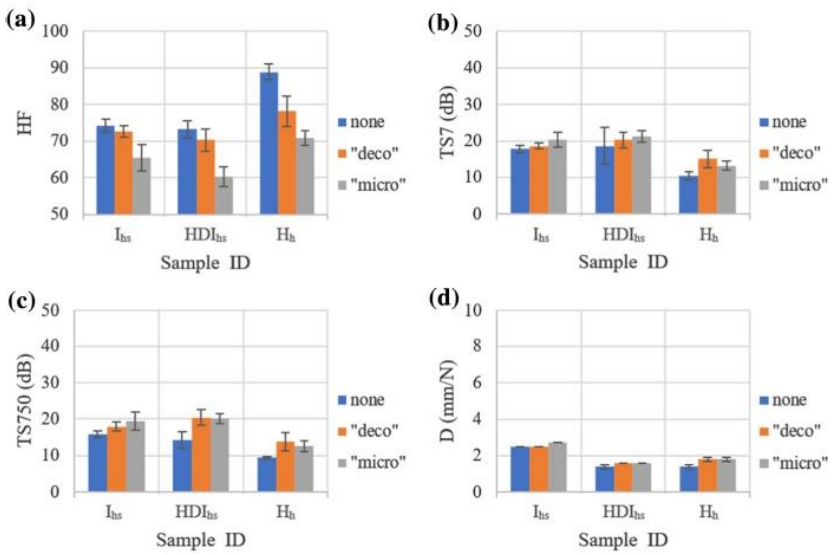

Fig. 13 TSA-softness properties of the tissue paper samples using the QAI algorithm. The calculated **a** handfeel HF, and the measured parameters **b** TS7, **c** TS750, and **d** D for the different samples with and without embossing

Conclusions

Our research highlights the influence of non-embossed and embossed tissue structures on mechanical and softness properties. With an innovative laboratory embossing prototype was possible to obtain important data to study and quantify this effect on eucalyptus-based tissue papers.

This work demonstrated that embossing has a negative impact on mechanical properties, being this effect more accentuated with the "micro" embossing pattern. This converting operation, on the other hand, increases the thickness in the *Z* direction, and consequently increases the bulk, with a higher impact obtained by the "micro" embossing. The effect of the presence of softwood fiber, in samples I_{hs} and HD_{Ihs} translates in a gain in the tensile strength.

The creping operation gives to the industrial paper a high elongation capacity being practically nonexistent in handsheets. Also, due to this operation, the industrial samples present a higher apparent porosity than handsheets samples. From the comparison between the HD_{Ihs} and H_h handsheets, the latter with a composition of 100% eucalyptus presents a higher softness than the first whose composition is a mixture of hardwood and softwood.

The samples I_{hs} and HD_{Ihs} have the same fibrous composition and similar TSA-softness results, except for the parameter D of flexibility due to the creping process. The embossing process generally impairs the softness results of the samples but improves flexibility. The 100% eucalyptus sample showed to have the best softness except for the TSA parameter D due to the absence of crepe on the surface.

The modelling strategy is based in the 3D fiber model and the FEM simulations. The computational results contribute for the understanding of how the shape pattern used in the embossing process affect the paper stress field and the final paper mechanical properties as paper strength.

Acknowledgments The authors would like to also thank the company PCE Iberica S.L. Instrumentacíon for the donation of the Durometer PCE-DDA equipment that was used in this work to determine the apparent hardness of the rubber rollers. Finally, the authors acknowledge the materials, access to equipment and installations, and all the general support given by The Navigator Company, RAIZ, and the Optical Center, Department of Physics, Department of Textile Science and Technology, and Department of Chemistry of the Universidade da Beira Interior.

Funding The authors gratefully acknowledge the funding of this work that was carried out under the Project InPaCTus – Innovative Products and Technologies from Eucalyptus, Project Nº 21874 funded by Portugal 2020 through European Regional Development Fund (ERDF) in the frame of COMPETE 2020 nº 246/AXIS II/2017. The authors are very grateful for the support given by research unit Fiber Materials and Environmental Technologies (FibEnTech-UBI), on the extent of the project reference UIDB/00195/2020, funded by the Fundação para a Ciência e a Tecnologia, IP/MCTES through national funds (PIDDAC).

Data availability The raw/processed data required to reproduce the above findings cannot be shared at this time as the data also forms part of an ongoing study.

Declarations

Conflict of interest The author(s) declare(s) that they have no competing interests.

References

Anukul P, Khantayanuwong S, Somboon P (2015) Development of laboratory wet creping method to evaluate and control pulp quality for tissue. Tappi J 14(5):339–345

Axelsson B (2001) Pulp for high absorption tissue products. Pap Technol 42(7):24–26

Bai B, Folorunso M, Berglund M (2019) Perceived vs recorded quality of tissue paper. Master's Thesis, Linköping University, Linköping, Östergötland, Sweden

Boudreau J, Germgård U (2014) Influence of various pulp properties on the adhesion between tissue paper and Yankee cylinder surface. BioResources 9(2):2107–2114. https://doi.org/10.15376/biores.9.2.2107-2114

Costa VLD, Costa AP, Amaral ME, Oliveira C, Gama M, Dourado F, Simões RM (2016) Effect of hot calendering on physical properties and water vapor transfer resistance of bacterial cellulose films. J Mater Sci 51:9562–9572. https://doi.org/10.1007/s10853-016-0112-4

Crescent Former, or Conventional, Tissue Machine TechnologyIThe Tissue Story (2017)

Curto JMR, Conceição ELT, Portugal ATG, Simões RMS (2011) Three dimensional modeling of fibrous materials and experimental validation. Materwiss Werksttech 42:370–374. https://doi.org/10.1002/mawe.201100790

de Assis T, Reisinger L, Pal L, Pawlak J, Jameel H, Gonzalez R (2018) Understand the effect of machine technology and cellulosic fibers on tissue properties—a review. BioResources 13(2):4593–4629. https://doi.org/10.15376/biores.13.2.DeAssis

DeMaio A, Patterson T (2008) Similarities in bonding influence between pre-failure tensile creep and stress–strain behavior of paper. Mech Mater 40(3):133–149. https://doi.org/10.1016/j.mechmat.2007.06.007

Digby, P. "pd-Tissues - Trees to Paper" (2012) http://pd-tissues.co.uk/trees-to-paper.aspx Accessed 13 Feb 2019

Conceição ELT, Curto JMR, Simões RMS, Portugal ATG (2010) Coding a simulation model of the 3D structure

of paper. In: Barneva RP, Brimkov VE, Hauptman HA, Natal Jorge RM, Tavares JMRS (eds) Computational modeling of objects represented in images, CompIMAGE 2010. Lecture notes in computer science. Springer, Berlin, pp 299–310. https://doi.org/10.1007/978-3-642-12712-0_27

Fišerová M, Gigac J, Stankovská M, Opálená E (2019) Influence of bleached softwood and hardwood kraft pulps on tissue paper properties. Cellul Chem Technol 53(5–6):469–477. https://doi.org/10.35812/CelluloseChemTechnol.2019.53.47

Giacomozzi DE, Joutsimo O (2015) Drying temperature and hornification of industrial never-dried Pinus Radiata Pulps. 1. Strength, optical, and water holding properties. Bioresources 10(3):5791–5808. https://doi.org/10.15376/biores.10.3.5791-5808

Henriksson M, Berglund LA, Isaksson P, Lindström T, Nishino T (2008) Cellulose nanopaper structures of high toughness. Biomacromol 9:1579–1585. https://doi.org/10.1021/bm800038n

Hilbig K, Liplijn M, Reinheimer H (2005) Method of making a thick and smooth embossed tissue. Cincinnati, OH (2005)

Hollmark H (1984) Mechanical properties of tissue. In: Handbook of physical and mechanical testing of paper and paperboard, New York, pp 497–521

ISO 187:1990 Paper, board and pulps—Standard atmosphere for conditioning and testing and procedure for monitoring the atmosphere and conditioning of samples (1990) INTERNATIONAL STANDARD ISO.

ISO 5263-1:1995 Pulps—Laboratory wet disintegration (1995) INTERNATIONAL STANDARD ISO

ISO 5269-1:1998 Pulps — Preparation of laboratory sheets for physical testing—Part 1: Conventional sheet-former method (1998) INTERNATIONAL STANDARD ISO

ISO 5267-1:1999 Pulps — Determination of drainability—Part 1: Schopper-Riegler method. (1999) INTERNATIONAL STANDARD ISO

ISO 12625-4:2005a Tissue Paper and Tissue Products - Part 4: Determination of tensile strength, stretch at break and tensile energy absorption (2005a) INTERNATIONAL STANDARD ISO

ISO 12625-6:2005b Tissue Paper and Tissue Products - Part 6: Determination of Grammage (2005b) INTERNATIONAL STANDARD ISO.

ISO 5351:2010 Pulps — Determination of limiting viscosity number in cupri-ethylenediamine (CED) solution (2010) INTERNATIONAL STANDARD ISO.

ISO 12625-3:2014 Tissue Paper and Tissue Products—Part 3: Determination of Thickness, Bulking Thickness and Apparent Bulk Density and Bulk (2014). INTERNATIONAL STANDARD ISO

ISO 48-7:2018 Rubber, vulcanized or thermoplastic—Determination of hardness—Part 7: Apparent hardness of rubber-covered rollers by Shore-type durometer method" (2018) INTERNATIONAL STANDARD ISO

Lofink B (2003) Device for applying an embossing to a web of tissue paper. Justia Patents, USA, Patent N° 6729869 (2003)

Mendes AO, Fiadeiro PT, Costa AP, Amaral ME, Belgacem MN (2015) Laser scanning for assessment of the fiber anisotropy and orientation in the surfaces and bulk of the paper. Nord Pulp Pap Res J 30(2):308–318. https://doi.org/10.3183/npprj-2015-30-02-p308-318

Mendes AO, Fiadeiro PT, Costa AP, Amaral ME, Belgacem MN (2013) Retro-diffusion and transmission of laser radiation to characterize the paper fiber distribution and mass density. In: Proceedings Volume 8785: 8th Ibero American optics meeting and 11th latin american meeting on optics, lasers, and applications, Porto, Portugal, pp 8785AY-1/8785AY-8. https://doi.org/10.1117/12.2022367

Mendes AO, Fiadeiro PT, Costa AP, Amaral ME, Belgacem MN (2014). "Study of repeatability of an optical laser system for characterization of the paper fiber distribution and mass density. In: Proceedings Volume 9286: second international conference on applications of optics and photonics, Aveiro, Portugal, pp 92862Y-1/92862Y-8. https://doi.org/10.1117/12.2062697

Morais FP, Bértolo RAC, Curto JMR, Amaral MECC, Carta AMMS, Evtyugind DV (2019) Comparative characterization of eucalyptus fibers and softwood fibers for tissue papers applications. Mater. Lett. X 4:100028. https://doi.org/10.1016/j.mlblux.2019.100028

Morais FP, Carta AMMS, Amaral ME, Curto JMR (2020a) 3D fiber models to simulate and optimize tissue materials. BioResources 15:8833–8848. https://doi.org/10.15376/biores.15.4.8833-8848

Morais FP, Carta AMMS, Amaral ME, Curto JMR (2020b) Experimental 3D fibre data for tissue papers applications. Data Brief 30:105479. https://doi.org/10.1016/j.dib.2020.105479

Morais FP, Vieira JC, Mendes AO, Carta AM, Costa AP, Fiadeiro PT, Curto JMR, Amaral ME (2022) Characterization of absorbency properties on tissue paper materials with and without "Deco" and "Micro" embossing patterns. Cellulose. https://doi.org/10.1007/s10570-021-04328-1

Park NY, Ko YC, Melani L, Kim HJ (2020) Mechanical properties of low-density paper. Nord Pulp Pap Res J 35(1):61–70. https://doi.org/10.1515/npprj-2019-0052

Ramasubramanian MK, Sun Z, Chen G (2011) A mechanics of materials model for the creping process. J Manuf Sci Eng 133(5):051011. https://doi.org/10.1115/1.4004925

Sihtola H, Kyrklund B, Laamanen L, Palenius L (1963) Comparison and conversion of viscosity and DP values by different methods. Pap Puu 45(4a):225–232

Silvy J, Romatier G, Chiodi R (1968) Méthodes pratiques de controle du raffinage. ATIP 22:31–53

Sjöholm E, Gustafsson K, Norman E, Colmsjö A (1997) The effect of degradation on the strenght of hardwood kraft pulp fibers. In: Proceedings of the 9th international symposium wood and pulping chemistry, Montréal, vol 106, pp 1–4

Skapa. Roll covers for the paper industry (2020) http://vit-group.com/skapa/test/download/Produktprospekt_GB.pdf. Accessed 21 Oct. 2020

Spina R, Cavalcante B (2018) Characterizing materials and processes used on paper tissue converting lines. Mater Today Commun 17:427–437. https://doi.org/10.1016/j.mtcomm.2018.10.006

Stankovská M, Gigac J, Fišerová M, Opálená E (2020) Blending impact of hardwood pulps with softwood pulp on tissue paper properties. Wood Res 65:447–458. https://doi.org/10.37763/wr.1336-4561/65.3.447458

TAPPI T237 cm-08 Carboxyl Content of Pulp. Technical Association of the Pulp and Paper Industry (2008)

Tourtollet GEP, Cottin F, Cochaux A, Petit-Conil M (2003) The use of MorFi analyser to characterise mechanical pulps, Quebec City, Canada

Vieira JC, de Oliveira Mendes A, Carta AM, Galli E, Fiadeiro PT, Costa AP (2020) Impact of embossing on liquid absorption of toilet tissue papers. BioResources 15(2):3888–3898. https://doi.org/10.15376/biores.15.2.3888-3898

Wang Y, Assis TD, Zambrano F, Pal L, Venditti R, Dasmohapatra S, Pawlak J, Gonzalez R (2019) Relationship between human perception of softness and instrument measurements. BioResources 14(1):780–795. https://doi.org/10.15376/biores.14.1.780-795

Impact of Embossing on Liquid Absorption of Toilet Tissue Papers

Joana Costa Vieira,[a,*] António de Oliveira Mendes,[a] Ana Margarida Carta,[b] Enrico Galli,[c] Paulo Torrão Fiadeiro,[a] and Ana Paula Costa [a]

Absorption capacity is a key feature of toilet tissue papers. Several parameters can affect their final absorption capacities, such as pulp composition, stock preparation, number of sheets, additives, bulk, grammage, and converting process parameters, such as the embossing operation. In this work, the absorption capacities of four different 2-ply industrial toilet tissue papers, as well as the respective base papers from the mother-reel was compared using the immersion method according to ISO 12625-8 (2010). Previously, these samples were characterized in terms of morphology, grammage, thickness, and bulk. It was concluded that the embossing operation noticeably increased the thickness and bulk of toilet tissue paper. Furthermore, it was also verified that among the various toilet tissue paper samples there was not a noticeable variation in the time of water absorption because the samples revealed similar morphology and porosity. However, it was found that the bulk increased more than 150%, resulting in an increase of water absorption capacity over 60%.

Keywords: Tissue paper; Embossing; Paper morphology; Liquid absorption capacity; Porosity

Contact information: a: Universidade da Beira Interior, Fiber Materials and Environmental Technologies (FibEnTech-UBI), Rua Marquês de Ávila e Bolama, 6201-001, Covilhã, Portugal; b: RAIZ - Instituto de Investigação da Floresta e Papel, Quinta de S. Francisco, Apartado 15, 3801-501, Eixo, Portugal; c: The Navigator Company, R. dos Bombeiros da Celulose, 3800-536, Cacia, Portugal;
** Corresponding author: joana.costa.vieira@ubi.pt*

INTRODUCTION

Tissue papers, namely toilet paper, kitchen towels, and napkins, have distinctive characteristics from printing and writing papers. Tissue paper is characterized by its physical and mechanical properties, namely softness, low grammage, bulk, high flexibility, and liquid absorption capacity. In contrast to printing and writing papers, in which the finishing process, the calendering operation, is the most important step, in tissue paper the key processing operations include creping and embossing, which are lesser studied.

Embossing is the mechanical process of sculpturing tissue paper during converting. Moreover, providing the physical connection between the different sheets of paper, it embosses (by applying a localized pressure) a decoration pattern that contributes to the bulk increase, compressibility, liquid absorption capacity, and softness (Spina and Cavalcante 2018). Currently, various types of embossing technologies are used. In general only pressure is applied, but the usage and control of temperature and humidity are emerging, resulting in various products (DeMaio and Patterson 2008; Biagiotti 2017).

Figure 1 shows the steps of the converting process, starting from the unwinding of the paper mother-reel produced in the tissue paper machine, passing through the embossing process, until the final product is palletized (Kimari 2000).

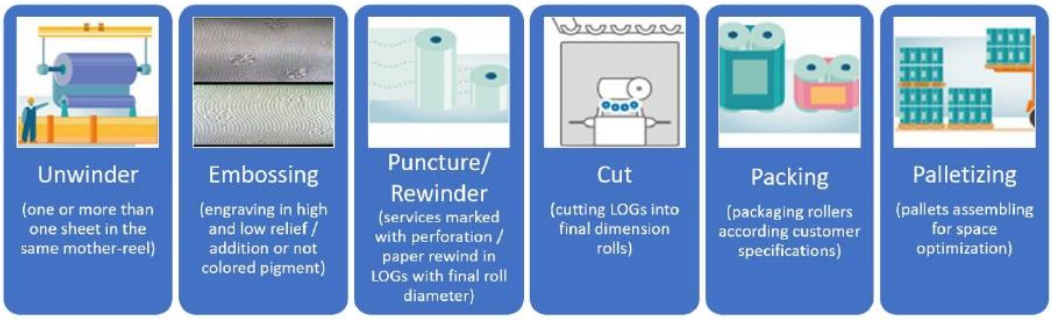

Fig 1. Steps of tissue paper converting process to the finished product

Embossing the top layer of tissue papers (with one or more plies), is known as deco (decorative) embossing. In contrast, embossing the bottom layer is known as micro embossing. This is usually the case of toilet paper products. The resulting product with more sheets/plies has properties that cannot be achieved by a single paper layer finished product (Digby 2012).

Although the embossing process improves some properties of tissue papers, it can impair other properties. Thus, certain properties, such as tensile strength and thickness, may be reduced. Liquid absorption is a key property for most tissue paper products and its main purpose is to improve cleaning and liquid absorption. It is generally better defined as absorption capacity, and absorption rate or absorption time (Hollmark 1983; Tutuş *et al.* 2016). Absorption capacity reflects the maximum amount of water the paper can absorb until its saturation and is expressed in gram of water per gram of fiber, while the absorption rate measures how quickly tissue products absorb water (Hollmark 1983; Kullander 2012). In the tissue world, both water absorption time and water absorption capacity are important parameters used to compare different tissue papers (Tutuş *et al.* 2016).

Beyond embossing, liquid absorption capacity and absorption rate/time can also be controlled by fiber type, fines content, refining, fiber network structure, pressing, creping, number of sheets, additives, bulk, grammage, and porosity (Kullander 2012; De Assis *et al.* 2018).

The porosity of base and final tissue papers is an important parameter for liquid absorption. Absorption measurements indicate the ability of a paper to hold a liquid. The pores in the paper/fibrous network influence water passages by capillarity action in all directions. In addition, the amount/volume of pores influences the amount of water the paper is able to accommodate. To enhance water absorption, the porosity should not be too high, because this would lead to fewer contact points with the liquid and thus less absorption. In contrast, if porosity is too low, this increases the resistance to capillary transport of liquids and thus decreases absorption. The optimal porosity must enable the liquid to be absorbed by cohesive forces but, at the same time, it must hinder its removing due to gravity without impairing the penetration rate. Porosity is influenced by pore size, which in turn depends on fiber size, degree of collapse resistance, and interfiber bonding (Milanez and Rost 2005). Hydroxyl groups on cellulose surface form hydrogen bonds with water, which directly affects water absorption (Bracken 2014).

Bulk also influences absorption. Papers with higher bulk values, *i.e.*, less dense with a more porous structure, will reveal higher absorption values, because paper will exhibit more sites for water accommodation. In addition to these aspects, factors such as surface energy of the phases involved (water, paper, and water vapor), contact angle,

roughness, topography, and position of the paper (pro or against gravity), influence the paper absorption (Milanez and Rost 2005).

Absorption properties are also strongly dependent on the surface chemistry of the fibers. In this context, to optimize absorption of tissue paper, the main elements that directly influence this characteristic should be well controlled and balanced, such as the type of pulp used, white water chemistry, and added additives. In summary, paper absorption is influenced by the manufacturing process, the composition of the raw materials, and the bulk of the paper (Milanez and Rost 2005; De Assis *et al.* 2018).

Specifically, the ability to absorb water more quickly is a key attribute of tissue paper. Gigac and Fiserová (2008) found that absorption decreased, when comparing different pulps with increased refining. Pulps that were less sensitive to refining maintained the highest levels of absorption. Although with low refining levels, kraft pulp showed a higher absorption.

Absorption also depends on the pulp's chemical composition. Pulps containing a high lignin content indicated a low absorption of liquids (De Assis *et al.* 2018). Thus, mechanical pulps (high lignin content) absorb approximately 1.0 g water/g fiber. Tissue products based on recycled fibers typically absorb approximately 4.0 g water/g fiber, while bleached kraft pulps (residual lignin contents) absorb between 5.0 and 10.0 g water/g fiber. Premium tissue products can achieve absorption capacities of up to 18.0 g water/g fiber (Kullander 2012; Hubbe *et al.* 2013; De Assis *et al.* 2018).

This work presents the results of a study regarding the impact of embossing on the absorption capacity of industrial toilet papers using the immersion method according to ISO 12625-8 (2010). A set of six base and the respective four toilet paper samples were directly collected in the converting line. The base papers were produced in the same tissue paper machine using a mixture of hardwood and softwood bleached kraft pulps and were compared in terms of water absorption before and after the embossing operation carried out in the same embossing conditions. The embossing pattern designs used in our samples are those available on the industrial converting line through steel engraving embossing rolls against rubber rolls.

EXPERIMENTAL

Materials

In this study, four different 2-ply toilet papers as well as the respective base paper mother-reels were used, supplied by a Portuguese tissue paper manufacturer. These industrial base tissue papers have been produced with a grammage range 16 to 19 g/m^2, being the mother-reels and toilet papers composed by 2 sheets. Papers were organized according to Table 1. The designation of A1, B1, and C1 correspond to the base paper mother-reels on the unwinder-1 of the converting machine (top sheet of the final toilet papers A, B, C, and D, respectively), and A2, B2, and C2 correspond to the base paper mother-reels on the unwinder-2 of the same machine (bottom sheet of the final toilet papers A, B, C, and D, respectively). All essays on the mother-reels were completed with two sheets, one from unwinder-1 and the other from unwinder-2. Toilet papers A and B were produced from different mother-reels, and different deco/micro embossing patterns. The others toilet papers C and D were produced from the same mother-reels, but with different deco and the same micro embossing patterns. Table 1 shows the images of both surfaces of each paper, on which the differences between them in terms of embossing (deco and

micro) can be observed. In particular, global views of the paper services are presented on the 3rd and 7th rows of Table 1, whereas magnified views of the embossed patterns are presented on the 4th and 8th rows of the same table.

Table 1. Sample Organization and Images of the Paper Services and Embossed Patterns (Size of Global Views ≈ 77 × 77 mm^2, Magnified Views ≈ 10 × 10 mm^2)

Mother-reel	A1+A2	B1+B2
2-ply Paper	A	B
Global View of Paper Service (Deco / Micro)	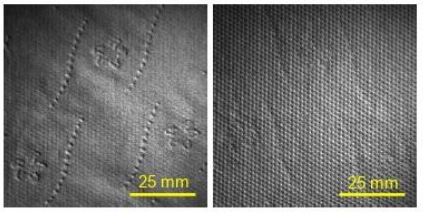	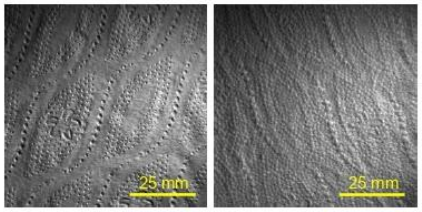
Magnified View of Embossing (Deco / Micro)	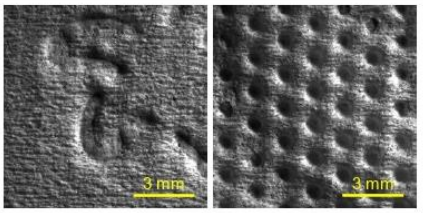	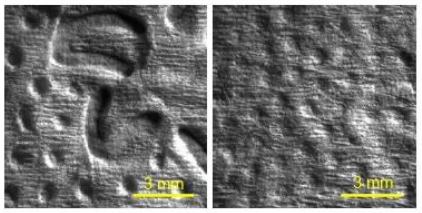
Mother-reel	C1 + C2	C1 + C2
2-ply Paper	C	D
Global View of Paper Service (Deco / Micro)	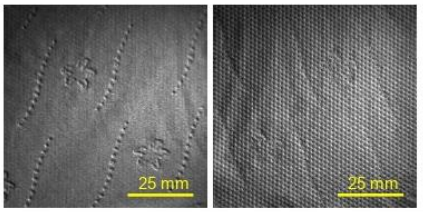	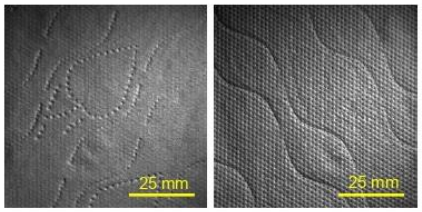
Magnified View of Embossing (Deco / Micro)	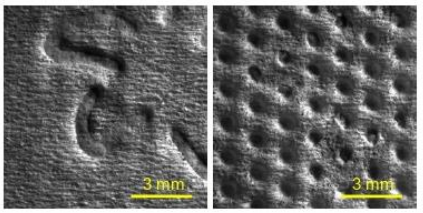	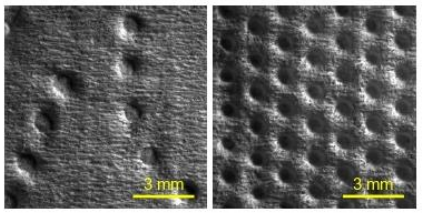

Methods

First, the fibers morphology of both final toilet papers and respective base paper mother-reels were determined. This was evaluated using the MORFI® system (Fiber and Shive Analyser; Techpap SAS, Grenoble, France) that provides fiber length and width, curl, kink fibers, coarseness, long and short fiber distribution, broken ends, and fines percentage.

Then, the grammage, defined as the mass per unit paper area, was determined and expressed in g/m^2. It was determined by weighing the tissue paper sample to a known area in accordance with ISO 12625-6 (2005) and using a Mettler Toledo PB303 Delta range analytical balance (Mettler Toledo, Columbus, OH, USA). The thickness was also determined using a FRANK-PTI® Micrometer (FRANK-PTI GMBH, Birkenau, Germany), where a sheet of tissue paper or a stack of sheets of tissue paper was compressed at a given pressure between two parallel plates according to ISO 12625-3 (2014). Finally, the bulk, which is the inverse of density, was determined by using the grammage and thickness according to ISO 12625-3 (2014).

Then, the porosity was determined for all the toilet paper and base mother-reels samples using a Micromeritics AccuPyc II 1340 helium pycnometer (Micromeritics, Norcross, GA, USA). Apparent porosity (theoretical) was calculated using Eq. 1,

$$P\ (\%) = 100 \times \left(1 - \frac{\rho_{sample}}{\rho_{cellulose}}\right) \quad (1)$$

where ρ_{sample} is the sample density (g/cm^3) and $\rho_{\text{cellulose}}$ is the cellulose density (which is assumed to be 1.6 g/cm^3) (Costa *et al.* 2016).

Finally, the absorption capacity and the absorption time were measured by the immersion method according to ISO 12625-8 (2010) using a FRANK-TPI® tissue absorption tester (FRANK-PTI GMBH, Birkenau, Germany). The industrial toilet paper samples were cut according to the above standard. The mother-reel paper samples were prepared and cut following the toilet paper dimensions, in machine direction, according the same standard. The samples have a width of 76±1 mm and a length of the respective toilet paper service in sufficient number to achieve a mass of 5.0±0.2 g.

In terms of image acquisition, a customized optical system (Prototype, University of Beira Interior, Covilhã, Portugal) previously used in research for other purposes (Mendes *et al.* 2013, 2014, and 2015) was conveniently configured for inspection of the papers' surfaces using specific conditions of illumination and magnification. The images were captured with fields of view of approximately 77×77 mm^2 and 10×10 mm^2, a resolution of 1024 × 1024 pixels, and a bit depth of 10 bits (1024 gray levels).

RESULTS AND DISCUSSION

The fibers morphological characterization of the industrial tissue paper samples used are presented in Tables 2, 3, and 4. It can be verified that both the mother-reels and the finished paper product were comparable, with no relevant variation of their values. Knowing that the samples were produced on the same industrial tissue paper machine under similar conditions, one can say that their networks of fibrous structure are analogous and consequently the porosity will not be an influencing factor in these tests of absorption capacity and water absorption time.

From the results presented in the following tables, one can state that the fiber composition of all the samples was similar, and it did not have any influence on the study of the embossing impact on the liquid absorption.

Table 2. Mean Values and Standard Deviations of the Morphological Results Obtained for the Mother-reels A1 and A2, and the Toilet Paper A

Morphology	Mother-reel A1		Mother-reel A2		Paper A	
	$\bar{x}$	σ	$\bar{x}$	σ	$\bar{x}$	σ
Fibers (million / g)	16.7	± 0.2	18.6	± 0.5	17.1	± 0.2
Length Weighted in Length (mm)	0.860	± 0.006	0.828	± 0.007	0.835	± 0.006
Width (µm)	20.1	± 0.1	20.0	± 0.2	19.9	± 0.2
Coarseness (mg/100 m)	8.80	± 0.00	8.10	± 0.00	8.70	± 0.00
Kink Fibers (%)	47.9	± 0.6	47.9	± 0.1	46.5	± 0.4
Curl (%)	10.2	± 0.0	10.4	± 0.0	10.2	± 0.1
Broken Ends (%)	24.8	± 0.2	25.4	± 1.8	24.7	± 0.2
Fines (% Area)	16.1	± 0.7	16.1	± 1.8	14.1	± 0.4

Table 3. Mean Values and Standard Deviations of the Morphological Results Obtained for the Mother-reels B1 and B2, and the Toilet Paper B

Morphology	Mother-reel B1		Mother-reel B2		Paper B	
	$\bar{x}$	σ	$\bar{x}$	σ	$\bar{x}$	σ
Fibers (million / g)	18.0	± 1.1	14.7	± 0.2	16.1	± 0.5
Length Weighted in Length (mm)	0.850	± 0.007	0.930	± 0.004	0.889	± 0.003
Width (µm)	19.5	± 0.1	20.8	± 0.2	20.0	± 0.2
Coarseness (mg/100 m)	8.04	± 0.00	9.47	± 0.00	8.82	± 0.00
Kink Fibers (%)	40.1	± 0.2	43.7	± 0.2	42.4	± 0.3
Curl (%)	9.2	± 0.0	10.0	± 0.0	9.6	± 0.1
Broken Ends (%)	23.2	± 0.3	26.8	± 0.3	24.2	± 0.3
Fines (% Area)	14.1	± 0.1	14.3	± 0.3	13.0	± 0.8

Table 4. Mean Values and Standard Deviations of the Morphological Results Obtained for the Mother-reels C1 and C2, and the Toilet Papers C and D

Morphology	Mother-reel C1		Mother-reel C2		Paper C		Paper D	
	$\bar{x}$	σ	$\bar{x}$	σ	$\bar{x}$	σ	$\bar{x}$	σ
Fibers (million / g)	16.8	± 0.4	17.4	± 0.2	16.3	± 0.6	16.3	± 0.2
Length Weighted in Length (mm)	0.862	± 0.010	0.859	± 0.002	0.862	± 0.007	0.870	± 0.009
Width (µm)	20.0	± 0.1	20.3	± 0.3	19.8	± 0.1	19.9	± 0.1
Coarseness (mg/100 m)	8.73	± 0.26	8.48	± 0.12	9.00	± 0.34	8.94	± 0.14
Kink Fibers (%)	130.8	± 0.3	130.7	± 0.2	130.6	± 0.3	130.4	± 0.3
Curl (%)	10.1	± 0.0	10.4	± 0.0	10.0	± 0.0	10.0	± 0.1
Broken Ends (%)	25.3	± 0.1	26.3	± 1.9	24.6	± 0.3	24.6	± 0.4
Fines (% Area)	14.7	± 0.1	16.1	± 1.9	13.9	± 0.6	13.9	± 0.1

Table 5 shows the grammage, thickness, and bulk results for the samples under study, determined according to the above-referred standards.

Table 5. Results Obtained on the Determination of Grammage, Thickness, and Bulk of Mother-reels (A1 + A2), (B1 + B2), (C1 + C2), and the Toilet Papers A, B, C, and D

	Mother-reels (A1 + A2)	Paper A	Mother-reels (B1 + B2)	Paper B	Mother-reels (C1 + C2)	Paper C	Paper D
Grammage (g/m^2)	33.2	32.4	37.9	37.3	32.4	31.4	32.1
Thickness (μm)	241	619	259	477	243	611	612
Bulk (cm^3/g)	7.3	19.1	6.8	12.8	7.5	19.5	19.1

Looking at the results in Table 5 it can be seen that the grammage has values that correspond to a composition of two sheets, hence showing values in the range of 31.4 to 37.9 g/m^2. The differences of grammage evidenced for the analyzed samples are related with the individual grammage of each sheet (16 to 19 g/m^2) but yet, within the allowed industrial tolerance. Comparing the results before and after the embossing operation, the thickness and bulk values increased with this process.

Table 6 shows the apparent and the measured porosity for all samples under study.

Table 6. Results of the Apparent and the Measured Porosities of Mother-reels (A1 + A2), (B1 + B2), (C1 + C2), and the Toilet Papers A, B, C, and D

	Apparent Porosity (%)	Porosity (%)
Mother-reel (A1 + A2)	91.0	91.0
Paper A	96.6	96.2
Mother-reel (B1 + B2)	90.5	89.8
Paper B	94.9	92.4
Mother-reel (C1 + C2)	91.3	90.9
Paper C	96.7	95.2
Paper D	96.6	94.9

Table 6 shows the results and comparison of the apparent porosities of the toilet papers and the respective mother-reels. The apparent porosity and the measured porosity were similar for all samples; meanwhile the toilet papers revealed a higher porosity in comparison with the corresponding mother-reels, due to the embossing process impact. The porosity differences between mother-reels and papers is due to the increase of the air gap volume between the 2 sheets during the embossing operation, given more bulk to the papers, which will allow a greater liquid retention.

Finally, Table 7 summarizes the mean values and standard deviations for the achieved results on water absorption time and the absorption capacity tests of all samples under study, according to the above-referred standard.

In Fig. 2, it can be seen that the water absorption time, determined for the various papers (mother-reels and final tissue paper products), was close in value, which also justified an equivalent fibrous structural network and a similar porosity. In such way, the embossing operation itself does not influence the absorption time results.

Table 7. Mean Values and Standard Deviations of the Results from Water Absorption Time and Absorption Capacity Tests of Mother-reels (A1 + A2), (B1 + B2), (C1 + C2), and the Toilet Papers A, B, C, and D

	Water Absorption Time (s)		Absorption Capacity (g/g)	
	$\bar{x}$	σ	$\bar{x}$	σ
Mother-reels (A1 + A2)	3.82	± 0.23	8.71	± 0.37
Paper A	3.80	± 0.30	13.94	± 0.27
Mother-reels (B1 + B2)	4.59	± 0.38	7.97	± 0.24
Paper B	4.63	± 1.11	9.38	± 0.26
Mother-reels (C1 + C2)	3.92	± 0.46	8.21	± 0.21
Paper C	4.73	± 0.52	13.72	± 0.30
Paper D	4.24	± 0.40	14.10	± 0.18

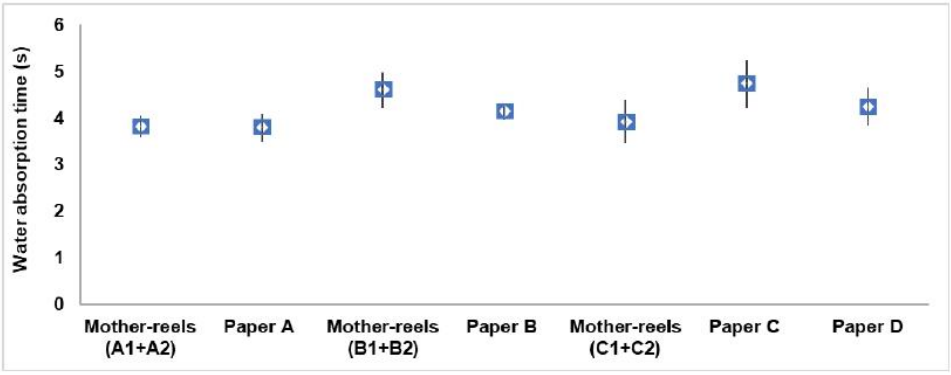

Fig. 2. Water absorption time of the tested samples

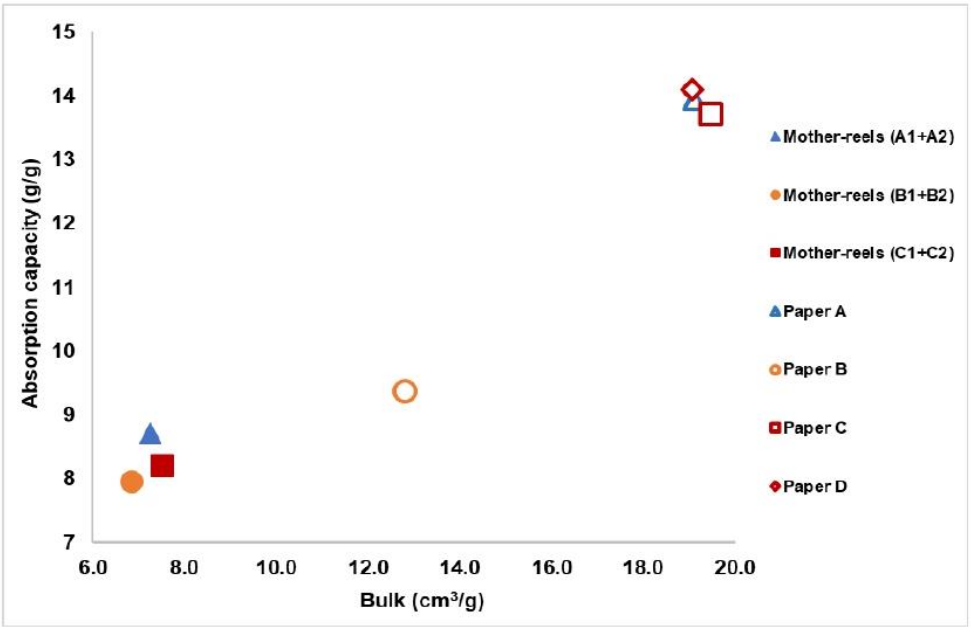

Fig. 3. Variation of water absorption capacity with bulk of the tested samples

Based on Fig. 3 (water absorption capacity *vs.* bulk), with the increase of the bulk there was an increase in water absorption capacity. Due to the embossing processes, bulk increases of 163%, 87%, 159%, and 154% for the toilet papers A, B, C, and D, respectively, were observed. This led to an increase in water absorption capacity of 60%, 18%, 67%, and 72% for the same toilet papers. Thus, a greater bulk and porosity increase led to a greater water absorption capacity. This bulk increment results from the thickness gain induced by the embossing process, and it will be more pronounced as deeper the embossing pattern is engraved.

CONCLUSIONS

1. In this study, a set of tissue paper samples (base mother-reels and the corresponding finished toilet papers), exhibited a similar morphological characterization. Because the base papers were produced on the same industrial paper machine under the same conditions, the fibrous networks were equivalent. This was also demonstrated by the apparent and the measured porosity results of the base paper mother-reels (approximately 91% in all cases). In contrast, the apparent and the measured porosity results of the toilet papers increased relative to the corresponding mother-reels (between 92% and 97%). This was attributed to the results from the embossing process because the fibrous networks were similar.
2. It was concluded that the embossing operation substantially increased the thickness and the bulk of the toilet papers. The differences in percentage of increase were dependent on the embossing pattern and the operation conditions of the converting machine.
3. Moreover, the embossing operation had no relevant implication on the time of water absorption, when comparing the paper mother-reels with the toilet papers, because they presented similar values with small variations. Additionally, there was not a relevant variation in the time of water absorption because the tissue paper samples were morphologically similar. However, the embossing operation had a major impact on water absorption capacity, promoting water absorption, due to the bulk increase.
4. With the embossing operation, bulk increased more than 150%, resulting in an increase of water absorption capacity over 60%.

ACKNOWLEDGMENTS

This work was carried out under the Innovative Products and Technologies project from Eucalyptus, Project No. 21874, funded by Portugal 2020 through European Regional Development Fund (ERDF) in the frame of COMPETE 2020 No. 246/AXIS II/2017.

The authors are also very grateful for the support given by Fiber Materials and Environmental Technologies (FibEnTech-UBI) on the extent of the project reference UIDB/00195/2020.

REFERENCES CITED

Biagiotti, M. (2017). "Tissue embossing developments - the tissue story," Tissue Story, (https://www.tissuestory.com/2017/11/21/tissue-embossing-developments/), Accessed 8 Jan 2019.

Bracken, L. (2014). *Potential for Utilization of Novel Modified Pulps in Tissue Paper Grades*, Master of Chemical Engineering Dissertation, Miami University, Oxford, OH, USA.

Costa, V. L. D., Costa, A. P., Amaral, M. E., Oliveira, C., Gama, M., Dourado, F., and Simões, R. M. (2016). "Effect of hot calendering on physical properties and water vapor transfer resistance of bacterial cellulose films," *Journal of Materials Science* 51(21), 9562–9572. DOI: 10.1007/s10853-016-0112-4

De Assis, T., Reisinger, L., Pal, L., Pawlak, J., Jameel, H., and Gonzalez, R. (2018). "Understand the effect of machine technology and cellulosic fibers on tissue properties - A review," *BioResources* 13(2), 4593-4629. DOI: 10.15376/biores.13.2.

DeMaio, A., and Patterson, T. (2008). "Similarities in bonding influence between pre-failure tensile creep and stress–strain behavior of paper," *Mechanics of Materials* 40(3), 133-149. DOI: 10.1016/j.mechmat.2007.06.007

Digby, P. (2012). "pd-Tissues - Trees to paper," (http://pd-tissues.co.uk/trees-to-paper.aspx), Accessed 13 Feb 2019.

Gigac, J., and Fišerová, M. (2008). "Influence of pulp refining on tissue paper properties," *TAPPI Journal* 7(8), 27-32.

Hollmark, H. (1983). *Handbook of Physical and Mechanical Testing of Paper and Paperboard: Chapter 20 - Absorbency of Tissue and Towelling*, (R. E. Mark, ed.), Dekker, New York.

Hubbe, M. A., Ayoub, A., Daystar, J. S., Venditti, R. A., and Pawlak, J. J. (2013). "Enhanced absorbent products incorporating cellulose and its derivatives: A review," *BioResources* 8(4), 6556-6629–6629. DOI: 10.15376/biores.8.4.6556-6629

ISO 12625-3 (2014). "Tissue paper and tissue products - Part 3: Determination of thickness, bulking thickness and apparent bulk density and bulk," International Organization for Standardization, Geneva, Switzerland.

ISO 12625-6 (2005). "Tissue paper and tissue products - Part 6: Determination of grammage," (2005). International Organization for Standardization, Geneva, Switzerland.

ISO 12625-8 (2010). "Tissue paper and tissue products - Part 8: Water-absorption time and water-absorption capacity, Basket-immersion test method," International Organization for Standardization, Geneva, Switzerland.

Kimari, O. (2000). *Papermaking Science and Technology: 18 - Paper and Board Grades by Hannu Paulapuro*, (J. Gullichsen, H. Paulapuro, Suomen Paperi-Insinöörien Yhdistys, and Technical Association of the Pulp and Paper Industry, eds.), Fapet Oy, Helsinki.

Kullander, J. (2012). *Evaluation of Furnishes for Tissue Manufacturing*, Ph.D. Thesis, Karlstads Universitet, Karlstad, Sweden.

Mendes, A. O., Fiadeiro, P. T., Costa, A. P., Amaral, M. E., and Belgacem, M. N. (2013). "Retro-diffusion and transmission of laser radiation to characterize the paper fiber distribution and mass density," in: *Proceedings of the 8th Iberoamerican Optics Meeting and 11th Latin American Meeting on Optics, Lasers, and Applications*, Volume 8785, Porto, Portugal, Paper Number 8785AY. DOI: 10.1117/12.2022367

Mendes, A. O., Fiadeiro, P. T., Costa, A. P., Amaral, M. E., and Belgacem, M. N. (2014). "Study of repeatability of an optical laser system for characterization of the paper fiber distribution and mass density," in: *Proceedings of the Second International Conference on Applications of Optics and Photonics*, Volume 9286, Aveiro, Portugal, Paper Number 92862Y. DOI: 10.1117/12.2062697

Mendes, A. O., Fiadeiro, P. T., Costa, A. P., Amaral, M. E., and Belgacem, M. N. (2015). "Laser scanning for assessment of the fiber anisotropy and orientation in the surfaces and bulk of the paper," *Nordic Pulp & Paper Research Journal* 30(2), 308-318. DOI: 10.3183/npprj-2015-30-02-p308-318

Milanez, A. F., and Rost, É. (2005). *Tissue Paper - Revisão Tecnológica* (Report No. P&D 306-05), Suzano Papel E Celulose SA, Suzano-SP, Brazil. DOI: 10.13140/2.1.1629.4726

Spina, R., and Cavalcante, B. (2018). "Characterizing materials and processes used on paper tissue converting lines," *Materials Today Communications* 17, 427-437. DOI: 10.1016/j.mtcomm.2018.10.006

Tutuş, A., Çiçekler, M., and Çali, A. (2016). "Tissue papers in Turkey and some physical and optical properties," *Journal of Natural and Applied Sciences* 20(1), 98-102.

Article submitted: November 12, 2019; Peer review completed: March 8, 2020; Revised version received and accepted: March 21, 2020; Published: April 7, 2020.
DOI: 10.15376/biores.15.2.3888-3898

Impact of 5-Ply Toilet Paper Configuration on Its Mechanical and Absorption Properties

Joana Costa Vieira,[a,*] António de Oliveira Mendes,[a] Ana Margarida Carta,[b] Paulo Torrão Fiadeiro,[a] and Ana Paula Costa [a]

Several physical and mechanical properties can characterize tissue papers. In particular, low grammage but high values of bulk, flexibility, liquid absorption capacity, and softness are common properties for tissue papers. These properties must be adapted to meet the requirements of the final consumer, which can vary greatly in different countries. This work resulted from a study regarding the impact of two different stacking sequences of 5-ply toilet paper with configurations 1 and 2 (deco:micro embossing of 3:2 and 2:3 plies, respectively), which had the same base tissue papers in each mother reel, on their mechanical behavior and absorption capacity. The stacking sequence of the plies influenced the properties of the finished toilet paper. For configurations 1 and 2, after the embossing process, bulk increases of 46% and 40%, respectively, and water absorption capacity increases of 2% and 17%, respectively, were registered. In this case, the bulk increase was not the key property that influenced the water absorption capacity. Regarding mechanical properties, both configurations showed a higher negative impact caused by the deco embossing. For commercial purposes and to adhere to the final consumers' preferences for toilet paper, configuration 1 was more suitable for mechanical strength, and configuration 2 was more suitable for absorption capacity.

Keywords: Tissue toilet paper; Paper stacking sequence; Paper morphology; Liquid absorption capacity; Mechanical properties

Contact information: a: Universidade da Beira Interior, Fiber Materials and Environmental Technologies (FibEnTech-UBI), Rua Marquês de Ávila e Bolama, 6201-001, Covilhã, Portugal; b: RAIZ - Instituto de Investigação da Floresta e Papel, Quinta de S. Francisco, Apartado 15, 3801-501, Eixo, Portugal;
** Corresponding author: joana.costa.vieira@ubi.pt*

INTRODUCTION

Tissue paper is produced from the deposition of a mixture of short cellulosic fibers with a lower percentage of long cellulosic fibers, and sometimes starch is added to increase dry strength. The mixture of ingredients is present in an aqueous suspension at consistency of approximately 0.8% as a moving wet-web of fibers on a forming fabric. Through a filtration process 95% of the water is then removed. After the forming zone, the base paper is carried to the pressing zone. The purpose of pressing is to remove the water and consolidate the paper structure. This promotes contact between fibers in the presence of water as a binder to establish inter-fiber connections. The drying section, which is the final step, removes the remaining water from the tissue structure. In this part of the paper machine, water is evaporated by heat transfer and consequent condensation of steam within a large steel dryer cylinder called the Yankee dryer. With the introduction of TAD (Through-Air Drying) technology in the drying section of the tissue paper machine, the manufacturers were able to produce final products with higher bulk, softness, and liquid

absorption. This technology is more advantageous to produce premium tissue papers, but at the expense of greater energy consumption (De Assis *et al.* 2018; Wang *et al.* 2019). The tissue paper is detached from the surface of this cylinder with the aid of a creping blade, as schematically shown in Fig. 1, which ultimately produces the creped base paper. Finally, the produced base paper is wound up to form the reel. This paper reel will then generate multiple mother reels to feed the converting machine to produce the finished product (Ramasubramanian *et al.* 2011; Das 2019).

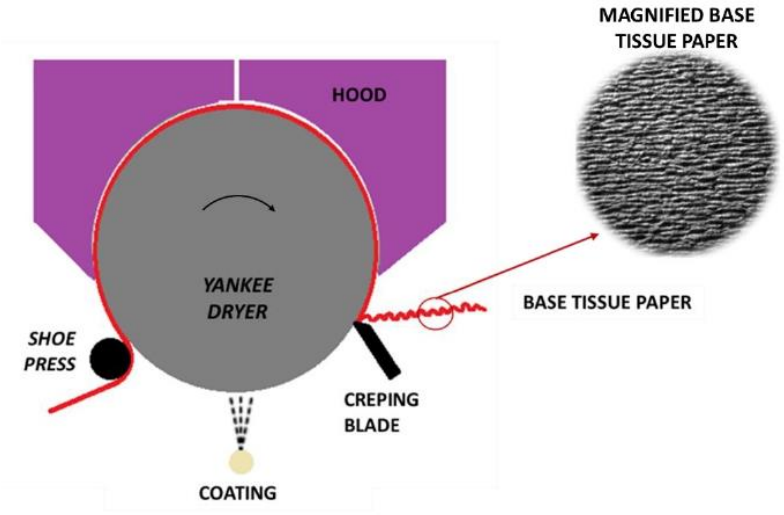

Fig. 1. Scheme of the tissue paper detachment from the surface of Yankee cylinder (creping process)

Converting machines include several processes, such as unwinding, embossing, lamination, printing, punching, packaging, and palletization, to produce multilayer tissue papers (Spina and Cavalcante 2018; Vieira *et al.* 2020). Embossing is a method of paper-compressive formation in the converting lines. Deco embossing is performed in the top surface of toilet paper product having one or more plies. Its main purpose is related to decoration and marketing. Micro embossing is engraved in the bottom surface of the toilet paper, and its main purpose will be to give bulk to the paper. Both surfaces will be assembled using the embossing details to glue them together. Embossing is used to modify the properties of the finished product, such as water absorption capacity, softness, and bulk. Despite improving some properties, this process deteriorates others, such as tensile strength (Spina and Cavalcante 2018; Vieira *et al.* 2020).

The properties of tissue papers are generally influenced by the requirements of the consumer. Therefore, the production process must be adapted to meet these requirements. Such properties differ depending on destination country, which requires that they must be evaluated with consideration to each market (De Assis *et al.* 2018). The physical-mechanical properties of the base tissue paper are usually evaluated in terms of grammage, thickness, bulk, and tensile strength in the machine direction (MD) and cross direction (CD). These values change according to the manufacturing machine and suppliers (Spina and Cavalcante 2018).

Bulk, which is the inverse of its apparent density, is an important property of tissue papers that defines the volume occupied by a given grammage. Strategies to improve the

bulk of tissue paper include lowering the pressure in the wet pressing zone and/or using a low refining level in the fibers, changing the creping process itself, using a composition rich in fibers with high coarseness (mg/100 m), keeping low flexibility of fibers, or orienting paper in the MD (Kullander 2012; De Assis *et al.* 2018).

The most relevant and differentiating physical-mechanical properties of the finished toilet paper products are bulk, liquid absorption, mechanical strength, and softness. Understanding how they are related, and how changing one property affects the others remains a challenge.

The liquid absorption of toilet paper products is usually divided into absorption capacity and absorption time. Absorption capacity reflects the maximum amount of water that it can absorb and is the ratio between the mass of absorbed water:mass of fibers (g:g), whereas the absorption time measures how quickly the product absorbs that amount of water (s) (Kullander 2012). These properties are influenced by the type of fibers, content of fines and inorganic additives, refining, fibrous network structure, pressing, creping, number of plies, grammage, bulk, and porosity. Common toilet papers present a range of water absorption between 6 to 13 g of water per g of fiber, while premium/ultra toilet paper products can absorb up to 18 g of water per g of fiber (Kullander 2012; Hubbe *et al.* 2013; De Assis *et al.* 2018; Wang *et al.* 2019). Absorption measurements reflect the ability of a toilet paper to hold a liquid. Hydroxyl groups on the cellulose surface promote hydrogen bonds with water, which directly affects water absorption (Bracken 2014). In European and International trades, both water absorption capacity and water absorption time are important requirements used to compare different tissue papers (Tutuş *et al.* 2016).

The papermaking process modifies the physical-mechanical properties of tissue papers. These properties are influenced by the intrinsic strength of the fibers and the inter-fiber bonds. Long fibers and various additives (carboxymethylcellulose and starch) are employed to increase dry tensile strength (Hollmark 1984; De Assis *et al.* 2018). The refining of the fibrous suspension, due to internal and external fibrillation, also increases the tensile strength as the fibers become more flexible and accommodated, which improves their fiber-fiber bonding abilities. However, the fibers can be damaged due to the refining process (Kullander 2012; Boudreau 2013). The strength of the tissue paper is reduced by the creping process and further reduced in the converting lines by the embossing process, as the inter-fiber bonds are broken (Kullander 2012; Boudreau 2013). Creping increases maximum deformation and toughness and decreases strength and stiffness, in both the MD and CD, with a particularly major impact on the MD (Das 2019). However, the elongation in the CD is important so that the operability in the converting occurs successfully, as in the case of embossing. The Young's modulus of the dried crepe tissue paper influences the softness of the bulk (compressibility). Therefore, a better understanding of the main mechanisms that influence the tissue paper response to tensile loading (characterized by tensile index and related to strength), Young's modulus, and maximum strain, is necessary to successfully design a tissue paper geared to consumer needs that can be produced at an efficient speed (Das 2019).

This work presents the results of a study on the impact of two different stacking sequences of 5-ply toilet paper with the same base tissue papers on their mechanical behavior and absorption capacity. Adjusting and control of the plies stacking sequence might represent an alternative to produce toilet tissue papers, because that will have a direct impact on the final properties of them. Toilet papers with two different configurations, which were produced by two different mother reels forming two different stacking

sequences, were compared in terms of water absorption (before and after the embossing process) and tensile strength.

EXPERIMENTAL

Materials

For this study 5-ply commercial toilet papers, which were assembled by two different mother reels (one mother reel with 2-ply and the other with 3-ply), forming two different stacking sequences (configurations 1 and 2), were used. In configuration 1, the 3-ply mother reel was on top (deco embossing), and the 2-ply mother reel was on the bottom (micro embossing). In configuration 2, the inverse of configuration 1 was applied, the 2-ply mother reel was on top (deco embossing), and the 3-ply mother reel was on the bottom (micro embossing). The configurations are presented in Fig. 2. The two commercial toilet papers and the corresponding mother reels were collected at a Portuguese factory line that were produced using a mixture of 85% hardwood eucalyptus and 15% softwood pine and spruce European virgin bleached kraft pulps. The tissue base paper was produced in a DCT (dry crepe technology) paper machine. All the tissue papers samples were conditioned according to the standard ISO 187 (1990).

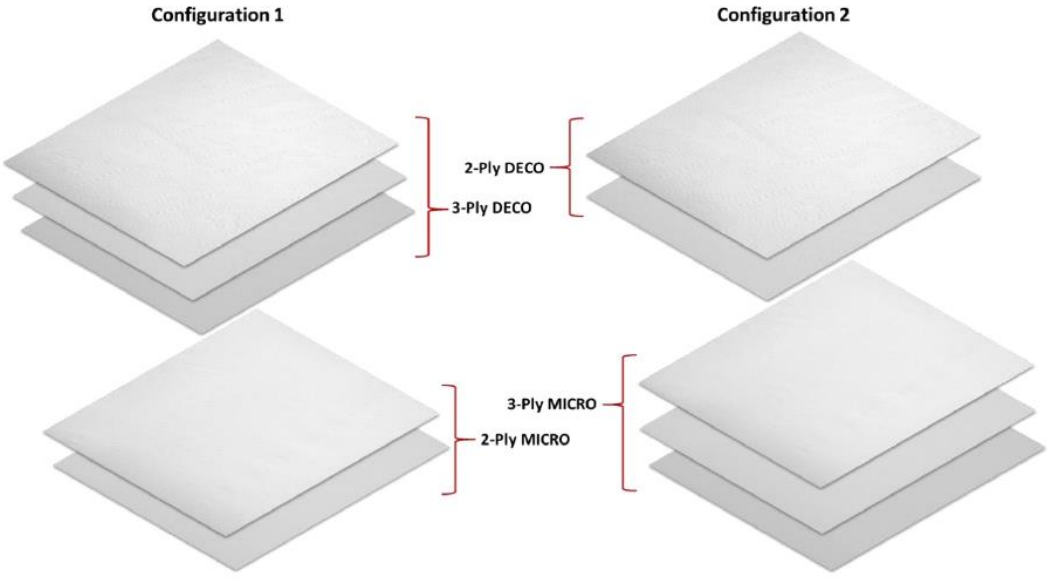

Fig. 2. Stacking sequences of the two configurations of the 5-ply toilet papers

Methods

First, the morphology of both the finished toilet papers and the mother reels that produced them were determined. These tests were conducted using the MORFI® Fiber and Shive Analyser (Techpap SAS, Grenoble, France), and the values for fiber length and width, curl, kink fibers, coarseness, long and short fiber distribution, broken ends, and fines percentage were obtained. Then, the grammage, was determined and expressed in g/m^2, which is defined as the mass per unit of paper area. A PB303 Delta Range analytical balance (Mettler Toledo, Columbus, OH, USA) was used to weigh the paper samples of a known area in accordance with ISO 12625-6 (2005). The thickness was determined

according to ISO 12625-3 (2014) with a FRANK-TPI Micrometer (Birkenau, Germany) for tissue paper. The measure of the assembled mother reels (without embossing) were done using the stacking sequences. Finally, the bulk, which is the inverse of density, was determined according to ISO 12625-3 (2014) with known thickness and grammage.

Absorption time and absorption capacity were then measured using a tissue absorption tester (FRANK-PTI GMBH, Birkenau, Germany) according to ISO 12625-8 (2010) *via* the immersion method. Toilet paper samples were cut according to ISO 12625-8 (2010), and the mother reel samples were cut along MD width according to the standard and along length according to the service length of the toilet paper from which they were originated (Vieira *et al.* 2020). The assembled mother reel samples (without embossing) were prepared using the stacking sequences until obtain 5 g of total base tissue paper mass.

Tensile tests were performed on a VantageNX universal testing machine (Thwing-Albert Instrument Company, West Berlin, NJ, USA) in accordance with ISO 12625-4 (2005). In a tensile test, tensile strength is the maximum tensile force per unit width that a test piece can withstand before breaking. These tests were performed on both finished toilet papers and mother reels that produced them.

The porosity for all the base mother reels and toilet papers samples was determined using a Micromeritics AccuPyc II 1340 helium pycnometer (Micromeritics, Norcross, GA, USA).

RESULTS AND DISCUSSION

Table 1 presents the morphological characteristics of the 2-ply mother reel, the 3-ply mother reel, and the 5-ply toilet paper samples. Figure 3 shows the percentages of the fibrous distribution in relation to the length weighted in length and in relation to the width of the fibers.

Table 1. Mean Values and Standard Deviations of the Morphological Results Obtained for the 2-ply Mother Reel, 3-ply Mother Reel, and 5-ply Toilet Paper

Morphology	2-ply Mother Reel		3-ply Mother Reel		5-ply Toilet Paper	
	$\bar{x}$	σ	$\bar{x}$	σ	$\bar{x}$	σ
Fibers (million/g)	17.6	± 0.2	19.5	± 0.3	18.3	± 0.3
Length Weighted in Length (mm)	0.817	± 0.006	0.736	± 0.004	0.768	± 0.004
Width (µm)	19.5	± 0.1	19.6	± 0.1	19.6	± 0.1
Coarseness (mg/100 m)	8.52	± 0.12	8.53	± 0.13	8.73	± 0.11
Kink Fibers (%)	46.7	± 0.5	49.8	± 0.1	48.3	± 0.1
Curl (%)	9.9	± 0.0	11.1	± 0.0	10.6	± 0.0
Broken Ends (%)	23.2	± 0.3	24.6	± 0.5	24.8	± 0.7
Fines (% Area)	14.2	± 0.3	16.1	± 0.3	15.9	± 0.6

Analysis of the morphological properties presented in Table 1 verified that the fibrous composition of the 5-ply finished toilet paper had an average value similar to the values of the mother reels from which they were produced. These results showed a fiber composition that consisted mainly of short fiber (hardwood), which was in line with reference literature (Niskanen *et al.* 1998), to obtain a better formation and softness of the tissue paper base sheet. Because the two finished toilet paper configurations were produced

from the same base paper (only the mother reels were changed in the converting machine), the morphological composition was not an influencing factor on the results obtained in the remaining tests. Figure 3 confirms the existence of a major quantity of short fiber. The distributions presented in Figs. 3a and 3b show that there was a slightly higher percentage of long fiber (softwood) in terms of length (> 2.000 mm) and width (>30 µm) for the 2-ply mother reel. As expected, for both mother reels, the small percentage of long fiber was used to increase the strength properties of the papers and ensure process runnability.

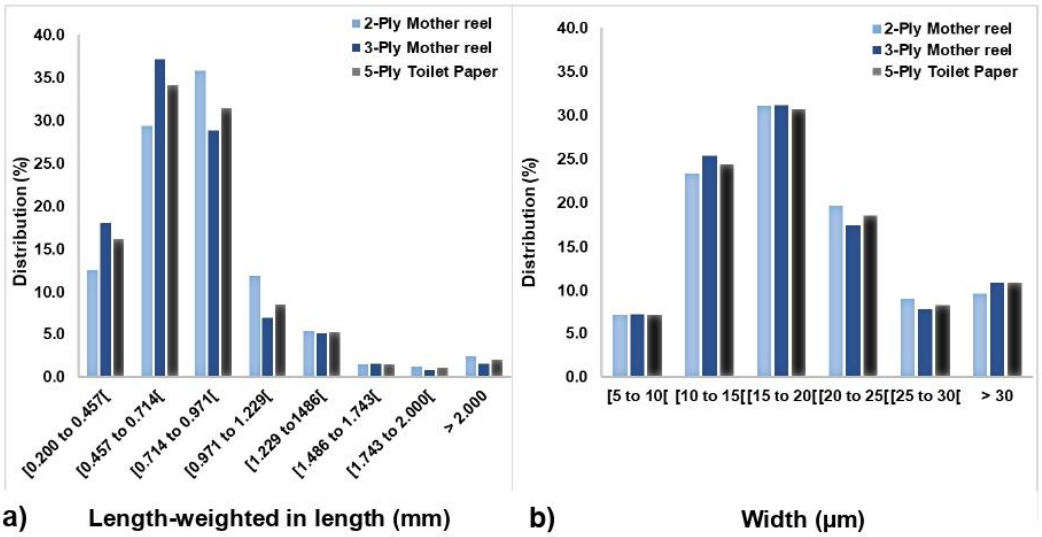

Fig. 3. Percentages of fibrous distribution for the 2-ply and 3-ply mother reels and the 5-ply toilet paper in relation to the: a) length weighted in length and b) width

Table 2 shows the tissue paper structural properties, namely grammage, thickness, and bulk for the studied samples.

Table 2. Structural Properties of Grammage, Thickness, and Bulk of the Mother Reels (2-Ply + 3-Ply) and the 5-ply Toilet Papers in Configurations 1 and 2

	Mother Reels (2-ply + 3-ply)	Toilet Paper Configuration 1	Toilet Paper Configuration 2
Grammage (g/m^2)	78.9	76.0	76.4
Thickness (µm)	514	725	695
Bulk (cm^3/g)	6.5	9.5	9.1

Table 2 shows that the grammage of the finished toilet papers decreased slightly relative to the mother reels. Due to the converting process thickness and bulk increased with these operations. The measure of the thickness of the assembled mother reels (2-ply + 3-ply or 3-ply + 2-ply) was the same because there is no contribution of the embossing process.

Table 3 summarizes the mean values and standard deviations of the results for the porosity tests of all tissue samples under study. The tabulated data shows that the porosity obtained for the different papers (mother reels and finished toilet papers) was very high. It

also shows that the porosity with the embossing was increased, being higher in configuration 2.

Table 3. Mean Values and Standard Deviation of the Porosity Tests of the Mother Reels (2-ply + 3-ply) and the 5-ply Toilet Papers in Configurations 1 and 2

	Porosity (%)	
	$\bar{X}$	σ
Mother Reels (2-ply + 3-ply)	89.39	± 0.01
Toilet Paper Configuration 1	90.17	± 0.01
Toilet Paper Configuration 2	90.52	± 0.01

Table 4 summarizes the mean values and standard deviations of the results for the water absorption time and absorption capacity tests of all samples under study.

Table 4. Mean Values and Standard Deviation of the Results of the Water Absorption Time and Absorption Capacity Tests of the Mother Reels (2-ply + 3-ply) and the 5-ply Toilet Papers in Configurations 1 and 2

	Water Absorption Time (s) MD		Absorption Capacity (g/g) MD	
	$\bar{X}$	σ	$\bar{X}$	σ
Mother Reels (2-ply + 3-ply)	4.54	± 0.23	8.33	± 0.16
Toilet Paper Configuration 1	4.53	± 0.27	8.49	± 0.20
Toilet Paper Configuration 2	3.76	± 0.44	9.74	± 0.16

Table 4 shows that the water absorption time obtained for the different papers (mother reels and finished toilet papers) was practically the same, which indicates that the porosities and fibrous structural networks were similar. The small changes in the absorption capacity are in accordance with the porosity results obtained, being higher in configuration 2 in both tests (Vieira *et al.* 2020).

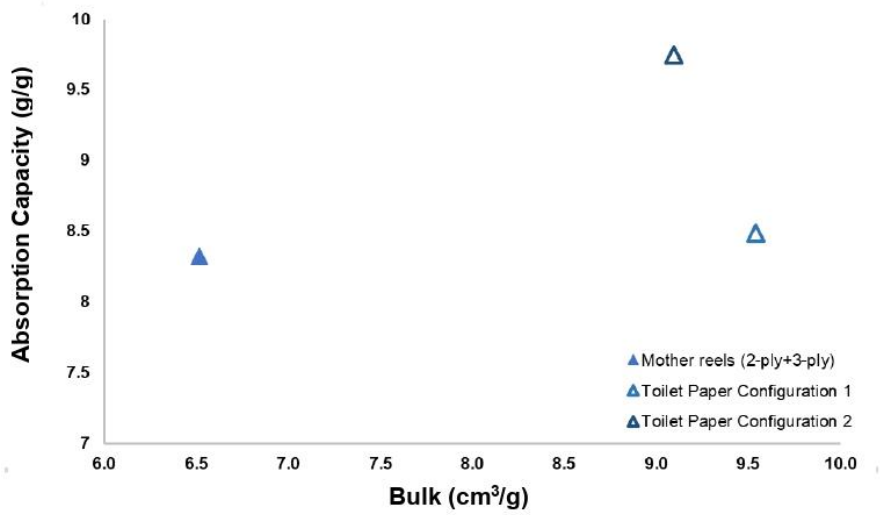

Fig. 4. Variation of water absorption capacity with bulk of the tested samples

Figure 4 shows that the water absorption capacity increased as bulk increased. Due to the embossing process, bulk increases of 46% and 40% were observed for toilet paper configurations 1 and 2, respectively. This led to an increase in water absorption capacity of 2% and 17% for configurations 1 and 2, respectively. The rearrangement of the mother reels (2-ply + 3-ply and 3-ply + 2-ply) in the finished paper configuration influenced the water absorption capacity and porosity. A larger number of micro-embossed sheets (configuration 2) promoted a higher water absorption capacity due to the creation of a larger number of empty spaces (high porosity) for liquid retention (Vieira *et al.* 2020).

Finally, Tables 5, 6, and 7 present the average results obtained for the tissue paper mechanical properties, which included tensile index, maximum strain, and Young's modulus in MD and CD.

Table 5. Tensile Test Results (Tensile Index, Maximum Strain, and Young's Modulus) of the Two Mother Reels (2-ply and 3-ply) in the MD and the CD

	2-ply Mother Reel		3-ply Mother Reel	
	CD	MD	CD	MD
Tensile Index (Nm/g)	4.9	10.1	4.9	9.6
Maximum Strain (%)	4.2	24.2	4.0	27.5
Young Modulus (MPa)	24.5	11.9	31.4	9.3

Table 6. Tensile Test Results (Tensile Index, Maximum Strain, and Young's Modulus) for Configuration 1 of the 5-ply Toilet Paper and the Corresponding 3-ply Deco Embossing Paper and 2-ply Micro Embossing Paper

Configuration 1	2-ply MICRO Paper		3-ply DECO Paper		5-ply Toilet Paper	
	CD	MD	CD	MD	CD	MD
Tensile Index (Nm/g)	4.6	8.9	2.2	6.8	3.6	7.9
Maximum Strain (%)	4.9	18.6	5.9	18.5	6.4	19.9
Young Modulus (MPa)	11.9	7.7	3.4	3.2	7.7	5.1

Table 7. Tensile Test Results (Tensile Index, Maximum Strain, and Young's Modulus) for Configuration 2 of the 5-ply Toilet Paper and the Corresponding 2-ply Deco Embossing Paper and 3-ply Micro Embossing Paper

Configuration 2	2-ply DECO Paper		3-ply MICRO Paper		5-ply Paper	
	CD	MD	CD	MD	CD	MD
Tensile Index (Nm/g)	1.6	5.0	4.5	9.2	3.5	6.8
Maximum Strain (%)	3.7	11.9	4.2	20.8	4.5	16.1
Young Modulus (MPa)	2.8	3.0	21.6	9.3	11.8	6.6

Figure 5 shows that the mechanical properties decreased and bulk increased due to the embossing process. In addition, a higher bulk increase value was observed for the 2-ply mother reel than for the 3-ply mother reel. The tensile index decreased more in configuration 2 than in configuration 1. The same trend was observed for the maximum strain and the Young's modulus. The deco embossing pattern used was more pronounced with deeper engraving details, as the authors showed in previous work with samples of the same 5-ply commercial toilet papers (Mendes *et al.* 2020). For this particular study, this deco embossing had a more negative impact on the mechanical properties than the micro embossing in both configurations. However, this impact was more noticeable in the 2-ply

deco and micro embossing's. As expected, the embossing process negatively affected the mechanical properties of the tissue paper (Hollmark 1984).

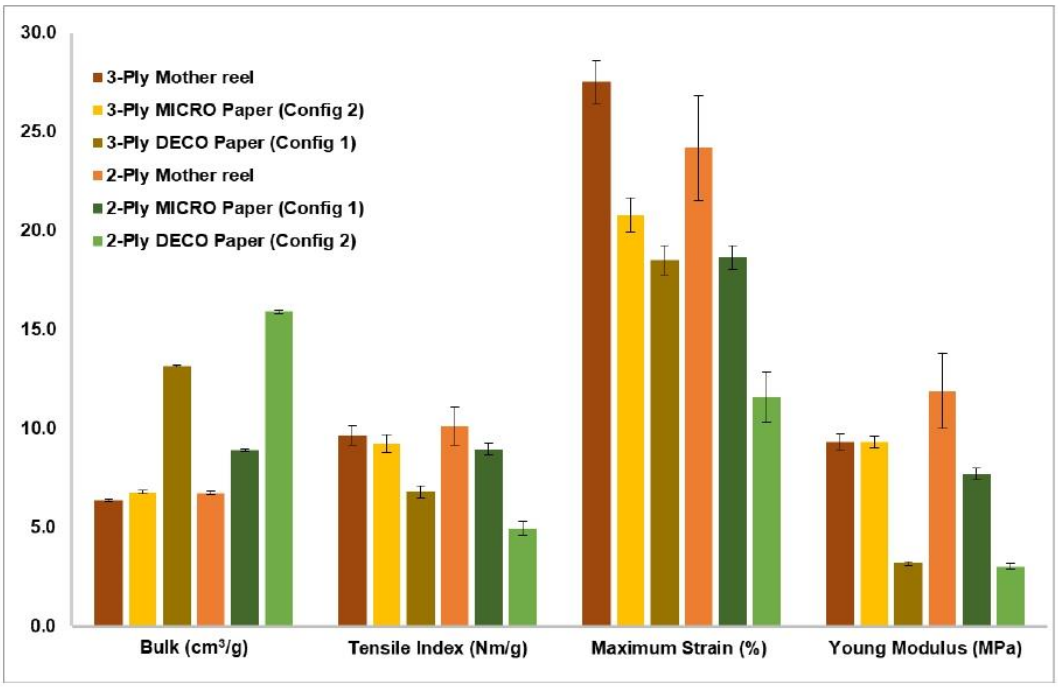

Fig. 5. Comparison of the mechanical properties (MD) of 2-ply and 3-ply mother reels with the corresponding deco and micro embossed papers

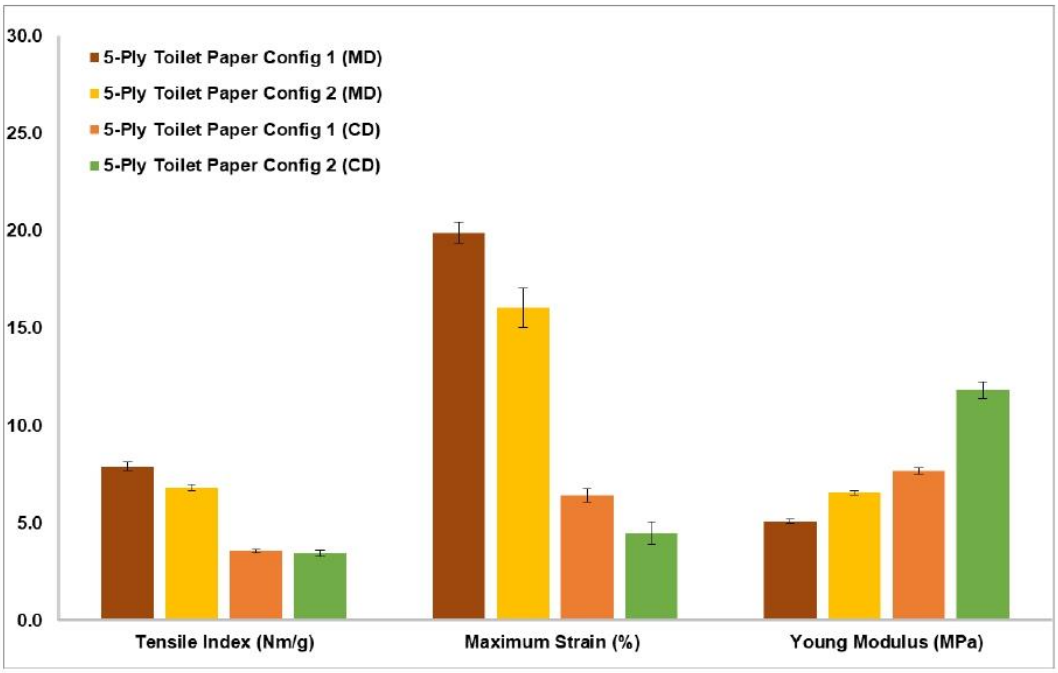

Fig. 6. Comparison of mechanical properties of the 5-ply toilet papers with configurations 1 and 2

Figure 6 shows the comparison of the mechanical properties of the two studied configurations. Configuration 2 had lower tensile index and maximum strain values than configuration 1. However, configuration 2 had a higher Young's modulus value than configuration 1. This was true both for both MD and CD. Configuration 2 had lower mechanical property values because it had 1-ply less in the deco embossing, which further weakened the structure.

CONCLUSIONS

1. In this study, the morphological compositions of the finished toilet papers were characterized to identify the average values of the compositions of the base papers from which they were produced.
2. The thickness and bulk of the toilet papers increased due to the embossing process.
3. The water absorption times were similar without notable variation, so the embossing process had little impact on these values. As bulk increased 46% and 40% for configurations 1 and 2, respectively, water absorption capacity increased 2% and 17% for configurations 1 and 2, respectively. Therefore, the stacking sequence of the finished toilet paper sheets influenced water absorption capacity.
4. The embossing process changed the mechanical properties of the toilet papers. The tensile index, maximum strain, and Young's modulus decreased considerably due to the embossing process. Configuration 1 had minor losses in tensile index and maximum strain. However, configuration 1 had a higher loss in Young's modulus than configuration 2. The negative impact on the mechanical properties was higher for deco embossing than for micro embossing in both configurations.
5. This study found that the stacking sequence of the sheets in the finished toilet papers influenced its final characteristics. For commercial purposes and to attend the final consumer preferences for toilet paper, configuration 1 was more suitable for mechanical strength, and configuration 2 was more suitable for absorption capacity.

ACKNOWLEDGMENTS

This work was carried out under Project InPaCTus – Innovative Products and Technologies from Eucalyptus (Project No. 21874) funded by Portugal 2020 through the European Regional Development Fund (ERDF) in the frame of COMPETE 2020 (No. 246/AXIS II/2017). In addition, the authors thank Fiber Materials and Environmental Technologies (FibEnTech-UBI) for their support (Grant No. UIDB/00195/2020).

REFERENCES CITED

Boudreau, J. (2013). *New Methods for Evaluation of Tissue Creping and the Importance of Coating, Paper and Adhesion*, Master's Dissertation, Karlstads Universitet, Karlstad, Sweden.

Bracken, L. (2014). *Potential for Utilization of Novel Modified Pulps in Tissue Paper Grades*, Master's Dissertation, Miami University, Oxford, OH, USA.

Das, R. (2019). *Experimental Studies on Creping and Its Influence on Mechanical Properties of Tissue Paper Products*, Master's Dissertation, The University of British Columbia, Vancouver, Canada.

De Assis, T., Reisinger, L. W., Pal, L., Pawlak, J., Jameel, H., and Gonzalez, R. W. (2018). "Understand the effect of machine technology and cellulosic fibers on tissue properties - A review," *BioResources* 13(2), 4593-4629. DOI: 10.15376/biores.13.2.

Hollmark, H. (1984). "Mechanical properties of tissue," in: *Handbook of Physical and Mechanical Testing of Paper and Paperboard*, R. E. Mark (eds.), Marcel Dekker Inc., New York City, NY, USA, pp. 497-521.

Hubbe, M. A., Ayoub, A., Daystar, J. S., Venditti, R. A., and Pawlak, J. J. (2013). "Enhanced absorbent products incorporating cellulose and its derivatives: A review," *BioResources* 8(4), 6556-6629. DOI: 10.15376/biores.8.4.6556-6629

ISO 187 (1990). "Standard atmosphere for conditioning and testing and procedure for monitoring atmosphere and conditioning of samples," International Organization for Standardization, Geneva, Switzerland.

ISO 12625-3 (2014). "Tissue paper and tissue products - Part 3: Determination of thickness, bulking thickness and apparent bulk density and bulk," International Organization for Standardization, Geneva, Switzerland.

ISO 12625-4 (2005). "Tissue paper and tissue products - Part 4: Determination of tensile strength, stretch at break and tensile energy absorption," International Organization for Standardization, Geneva, Switzerland.

ISO 12625-6 (2005). "Tissue paper and tissue products - Part 6: Determination of grammage," International Organization for Standardization, Geneva, Switzerland.

ISO 12625-8 (2010). "Tissue paper and tissue products - Part 8: Water-absorption time and water-absorption capacity, basket-immersion test method," International Organization for Standardization, Geneva, Switzerland.

Kullander, J. (2012). *Evaluation of Furnishes for Tissue Manufacturing*, Master's Thesis, Karlstads Universitet, Karlstad, Sweden.

Mendes, A. de O., Vieira, J. C., Carta, A. M., Galli, E., Simões, R., Silva, M., Costa, A. P., and Fiadeiro, P. T. (2020). "Influence of tissue paper converting conditions on finished product softness." *BioResources* 15(3), 7178-7190. DOI: 10.15376/biores.15.3.7178-7190

Niskanen, K., Gullichsen, J., and Paulapuro, H. (1998). *Papermaking Science and Technology. 16, Paper Physics*, Fapet Oy, Helsinki, Finland.

Ramasubramanian, M. K., Sun, Z., and Chen, G. (2011). "A mechanics of materials model for the creping process," *Journal of Manufacturing Science and Engineering* 133(5), Article ID 051011. DOI: 10.1115/1.4004925

Spina, R., and Cavalcante, B. (2018). "Characterizing materials and processes used on paper tissue converting lines," *Materials Today Communications* 17, 427-437. DOI: 10.1016/j.mtcomm.2018.10.006

Tutuş, A., Çiçekler, M., and Çali, A. (2016). "Tissue papers in turkey and some physical and optical properties," *Süleyman Demirel Universit Journal of Natural and Applied Sciences* 20(1), 98-102. DOI: 10.19113/sdufbed.98003

Wang, Y., Zambrano F., Venditti R., Dasmohapatra S., De Assis T., Reisinger L., Pawlak J., and Gonzalez R. (2019). "Effect of pulp properties, drying technology, and

sustainability on bath tissue performance and shelf price," *BioResources* 14(4), 9410-9428. DOI: 10.15376/biores.14.4.9410-9428

Vieira, J. C., De Oliveira Mendes, A., Carta, A. M., Galli, E., Torrão Fiadeiro, P., and Costa, A. P. (2020). "Impact of embossing on liquid absorption of toilet tissue papers," *BioResources* 15(2), 3888-3898. DOI: 10.15376/biores.15.2.3888-3898

Article submitted: June 4, 2020; Peer review completed: July 25, 2020; Revised version received and accepted: August 6, 2020; Published: August 12, 2020.
DOI: 10.15376/biores.15.4.7475-7486

Chapter 4 – Perforation Study

1. National Patent II Draft – Laboratorial Perforation System (Sistema Laboratorial de Perfuração)

Vieira, J.C., Vieira, Mendes, A.O., A.C., Carta, A.M., Fiadeiro, P.T., Costa, A.P. (in preparation)

A detailed description of the perforation system developed is provided in this draft of the national Patent II. Each component that composes this laboratory system is identified and its main advantages and disadvantages are also pointed out. Additionally, it delivers the main results that validate the use of the laboratory perforation system developed. The developed laboratory perforation system presented by Patent II draft, proved to be a useful tool for small scale studies, with a lower cost before moving on to pilot scale studies.

The overall contribution in the development of Patent II of Joana Costa Vieira was 65% to the concept development, analysis, drafting and revising the final submission; André Costa Vieira contributed 10% in the concept development, drafting and revising the final submission; Paulo Torrão Fiadeiro contributed 10% in the transformation of cutting blades into perforation blades and revising the final submission; António de Oliveira Mendes, Ana Margarida Carta and Ana Paula Costa contributed in reviewing, editing, and providing important technical inputs by 5%, respectively.

2. Article VIII – Toilet Paper Perforation Efficiency

Vieira, J.C., Vieira, A.C., de O. Mendes, A., Carta, A.M., Fiadeiro, P.T., Costa, A.P.
BioResources, 2022, 17(1), pp. 492–503
https://doi.org/10.15376/biores.17.1.492-503

With Article VIII, it was intended to understand how the cut distances of perforation acted on the tearing efficiency by separating a service from a roll of tissue paper. This study made it possible to verify that the perforation efficiency tends to a limit value on which the maximum value is reached. The developed laboratory perforation system, proved to be a useful tool for this study, allowing the variation of different cut distances. On the other hand, both the optical system and the FEM simulation proved to be very useful auxiliary tools for a better understanding of the effects that occurred in this study.

The overall contribution in Article VIII of Joana Costa Vieira was 70% to the concept development, analysis, drafting and revising the final submission; André Costa Vieira contributed 8% with the FEM analysis, drafting and revising the final submission; António de Oliveira Mendes contributed 7% with the optical system data, drafting and revising the final submission; Ana Margarida Carta, Paulo Torrão Fiadeiro and Ana Paula Costa contributed in reviewing, editing, and providing important technical inputs by 5%, respectively.

3. Article IX – Mechanical Behavior of Toilet Paper Perforation

Vieira, J.C., Vieira, A.C., de O. Mendes, A., Carta, A.M., Fiadeiro, P.T., Costa, A.P.
BioResources, 2021, 16(3), pp. 4846–4861
https://doi.org/10.15376/biores.16.3.4846-4861

To understand better how acts the mechanical behavior of toilet paper perforation, in the study presented in Article IX, the perforation efficiencies and respective cut distances were evaluated in different commercial toilet papers in terms of number of plies, composition and cut distances. This study made it possible to verify that cutting distances less or equal to 2 mm should not be used, as for this limit the separation of the paper roll service is carried out outside the perforation line. Both the optical system and the FEM simulation proved to be very useful auxiliary tools for a better understanding of the effects that occurred in this study.

The overall contribution in Article IX of Joana Costa Vieira was 70% to the concept development, analysis, drafting and revising the final submission; André Costa Vieira contributed 8% with the FEM analysis, drafting and revising the final submission; António de Oliveira Mendes contributed 7% with the optical system data, drafting and revising the final submission; Ana Margarida Carta, Paulo Torrão Fiadeiro and Ana Paula Costa contributed in reviewing, editing, and providing important technical inputs by 5%, respectively.

RESUMO

"SISTEMA LABORATORIAL DE PERFURAÇÃO PARA PAPEL *TISSUE*"

A perfuração em produtos de papel *tissue* é empregue com a intenção de facilitar o porcionamento dos serviços de produtos de papel *tissue*. A presente invenção descreve um sistema laboratorial de perfuração que permite testar novos tipos de perfuração à escala laboratorial, permitindo transpor os resultados à escala industrial, avaliar problemas associados com a perfuração dos produtos *tissue*, bem como testar novos padrões de perfuração e a sua eficiência. O sistema compreende uma guilhotina rotacional (1) que compreende uma lâmina giratória de perfuração amovível de corte (2) e uma base de perfuração (3), onde está acoplado um suporte de encaixe linear (4) do eixo (5) da lâmina giratória de perfuração amovível de corte que desliza sobre uma calha (6) ao longo do eixo vertical (Y), guiando o deslizamento do suporte de encaixe linear (4) e numa direção perpendicular ao eixo (5) da lâmina, paralelo ao eixo horizontal (X) da base de perfuração (3), de forma a que a lâmina giratória de perfuração amovível de corte (2) gire e perfure uma folha de papel (7) colocada entre a base de perfuração (3) e a calha(6), pela ação de uma força normal à folha de forma a pressionar o eixo da lâmina (5) e a lâmina giratória de perfuração amovível de corte (2) contra a folha (7).

DESCRIÇÃO

"SISTEMA LABORATORIAL DE PERFURAÇÃO PARA PAPEL *TISSUE*"

Área da Invenção

A presente invenção refere-se a um sistema de perfuração laboratorial para papel *tissue* dotado de uma guilhotina rotacional com lâminas de corte circulares giratórias, lisas ou padronizadas, que podem perfurar uma ou mais folhas de papel, para criar o padrão da perfuração, com um determinado comprimento de corte e outro por cortar, que se repetem sequencialmente.

Estado da arte

A perfuração em produtos de papel *tissue* é utilizada com o propósito de facilitar o particionamento das folhas de papel. Os principais produtos em que este processo é utilizado são: papel higiénico, papel de cozinha e lenços faciais [1-3]. Na área do papel *tissue*, isto estimulou os fabricantes a produzirem os seus produtos com a capacidade para serem particionados. O recurso à perfuração do papel, permite ao consumidor dispensar convenientemente uma determinada quantidade do produto conforme sua necessidade.

Estes tipos de papel são semelhantes e normalmente são perfurados para facilitar o seu particionamento, de acordo com as necessidades do consumidor. As perfurações facilitam esse particionamento, promovendo a separação das folhas ou serviços, pelo perfurado sem os rasgar. Porém, o papel perfurado tem de ser suficientemente forte para se manter unido sob uma certa tensão, quando o consumidor desejar utilizar mais do que uma folha, mas por outro lado tem de ser fraco o suficiente para que a folha ou serviço possa ser destacado do rolo de modo fácil, sem o rasgar, com pouco esforço e ao longo de uma linha horizontal reta ou padronizada. Este equilíbrio é dado pela eficiência de perfuração. Quanto maior a eficiência da perfuração, mais fácil será a separação do serviço.

A adequada geometria da lâmina de perfuração deve ser levada em consideração. O perfurador é também o responsável pela aparência visual da borda livre do rolo de papel

remanescente. O consumidor final pretende uma borda livre esteticamente agradável (mais lisa e menos irregular entre as áreas cortadas e não cortadas) após destacar a quantidade de papel pretendida.

Quando a resistência à tração do papel perfurado é muito forte, a folha de papel é dividida fora da linha de perfuração. Por outro lado, quando a resistência à tração é muito fraca, a folha, ao ser puxada do rolo de papel, não é bem controlada saindo mais do que um comprimento predeterminado entre perfurações. Este equilíbrio é dado pela eficiência de perfuração. Quanto maior a eficiência da perfuração, mais fácil será a separação do serviço. A baixa resistência à tração também pode prejudicar a *runnability* da máquina de *converting*, causando quebras sucessivas da folha após a operação de perfuração. Portanto, a fim de tudo isto ser evitado, a resistência à tração na direção transversal da perfuração tem de ser controlada de modo a cair dentro de uma faixa predeterminada. Por outro lado, a resistência à tração do papel perfurado é muito influenciada pela resistência à tração da própria folha na direção máquina (composição fibrosa, formação e orientação das fibras na folha de papel). Estes problemas associados à separação dos serviços por parte do consumidor, podem ter um impacto negativo na lealdade e satisfação deste com a marca do produto em questão. Assim, o estudo da eficiência de perfuração de um papel *tissue* revela-se de extrema importância para os produtores deste tipo de produtos, tanto a nível de desenvolvimento de produto como para resolver problemas de reclamações de clientes. Para tal, existe a necessidade da existência de um equipamento laboratorial, de fácil uso, que permita levar acabo os estudos necessários.

Atualmente, não se encontram disponíveis no mercado sistemas de perfuração laboratorial com características de versatilidade, portabilidade e de baixo custo.

Referências

[1] Ogg, R. G., and Habel, M. A. (1992). “Perforator blade for paper products and products made therefrom” USA, Patent N°: US 5114771.

2

[2] Schulz, G., and Gracyalny, D. (1998). "Method and Apparatus for Pinch Perforating Multiply Web Material" USA, Patent N°: US 5755654.

[3] Baggot, J., Gropp, R. F., and Wojcik, S. (2006). "System and Method for Severing or Perforating a Web" USA, Patent N°: US 2006/0014616.

Sumário da Invenção

A presente invenção diz respeito a um sistema de perfuração laboratorial para papel *tissue* que compreende uma guilhotina rotacional (1) que compreende uma lâmina giratória de perfuração amovível de corte (2) e uma base de perfuração (3), onde está acoplado um suporte de encaixe linear (4) do eixo (5) da lâmina giratória de perfuração amovível de corte que desliza sobre uma calha (6) ao longo do eixo vertical (Y), guiando o deslizamento do suporte de encaixe linear (4) e numa direção perpendicular ao eixo (5) da lâmina, paralelo ao eixo horizontal (X) lado da base de perfuração (3), de forma a que a lâmina giratória de perfuração amovível de corte (2) gire e perfure uma folha de papel (7) colocada entre a base de perfuração (3) e a calha(6), pela ação de uma força normal à folha de forma a pressionar o eixo da lâmina (5) e a lâmina giratória de perfuração amovível de corte (2) contra a folha (7).

Numa forma preferencial da invenção, a base de perfuração (3) apresenta marcas de réguas para auxiliar de auxílio do processo de posicionamento do papel.

Numa forma preferencial da invenção, a lâmina giratória de perfuração amovível de corte (2) apresenta um perfil liso ou padronizado.

Numa forma preferencial da invenção, a calha (6) compreende meios de acionamento automático de avanço pelo eixo vertical (Y) linearmente ao longo da calha (6).

Numa forma preferencial da invenção, os meios de acionamento automático são selecionados do grupo que consiste em motor elétrico acoplado a um parafuso sem-fim, motor elétrico

acoplado a uma cremalheira, cilindro pneumático e cilindro hidráulico com pressão controlada.

Breve Descrição das Figuras

A Figura 1 descreve o sistema de perfuração laboratorial para papel *tissue* da presente invenção, que inclui uma guilhotina rotacional (1) que inclui uma lâmina giratória de perfuração amovível de corte (2), uma base de perfuração (3), um suporte de encaixe linear (4) do eixo (5) da lâmina giratória de perfuração amovível de corte (2), e uma calha (6) onde o suporte de encaixe linear desliza.

A Figura 2 representa o mecanismo e posicionamento da lâmina giratória de perfuração amovível de corte (2) e de uma folha de papel (7) no sistema de perfuração. É também representado, pelas setas apresentadas, o sentido de rolamento da lâmina (8), a força da lâmina contra o papel (9) e o sentido de avanço do eixo da lâmina (10).

A Figura 3 representa uma possível geometria da lâmina giratória de perfuração amovível de corte e seus respetivos raios (11), ângulos de corte (12) e passos angulares (13).

A Figura 4 representa a comparação entre uma perfuração de 3 mm industrial e uma laboratorial para papéis higiénicos de 2, 3 e 4 folhas.

A Figura 5 representa as imagens ampliadas de uma perfuração de 3 mm industrial e uma laboratorial para um papel higiénico de 2 folhas.

Descrição Detalhada da Invenção

A presente invenção refere-se a um sistema de perfuração que compreende uma guilhotina rotacional (1) com lâminas giratórias de perfuração amovível de corte (2), lisas ou padronizadas, que podem perfurar uma ou mais folhas de papel (7), para criar o padrão da perfuração, com um determinado comprimento de corte e outro por cortar, que se repetem sequencialmente. As lâminas giratórias de perfuração amovível de corte (2) são maquinadas de forma a criar um disco com segmentos de corte cujo comprimento de arco corresponde ao comprimento a cortar e o espaço maquinado corresponde ao comprimento não cortado no papel.

Este sistema de perfuração aplica-se a produtos de papel *tissue*, tais como papel de cozinha ou papel higiénico. Neste contexto, a presente invenção descreve um sistema de perfuração laboratorial que permite testar novos tipos de perfuração à escala laboratorial, permitindo transpor os resultados à escala industrial, avaliar problemas associados com a perfuração dos produtos, bem como testar novos padrões de perfuração e a sua eficiência.

A presente invenção tem como principais vantagens ser um sistema de pequeno tamanho pequeno, leve, portátil e de baixo custo; ser um sistema versátil, pois que permite utilizar vários tipos de lâminas (lisas ou padronizadas) que podem ser adaptáveis ao tipo de perfuração pretendido; e ser um sistema que permite a sua utilização em vários tipos de papéis, nomeadamente o papel *tissue*.

O sistema de perfuração laboratorial para papel *tissue* da presente invenção é composto por uma guilhotina rotacional (1) apresentada na Figura 1, que compreende uma base de perfuração (3), onde está acoplado um suporte de encaixe linear (4) do eixo (5) de uma lâmina giratória de perfuração amovível de corte (2), que desliza sobre uma calha (6) permitindo à lâmina giratória de perfuração amovível de corte (2) girar e perfurar uma folha de papel (7), enquanto o eixo (5) avança livremente na calha (6).

A base de perfuração (3) pode estar marcada com réguas que permitem auxiliar o processo de posicionamento do papel,

para que a perfuração seja efetuada exatamente a meio ou na posição pretendida da amostra. A folha de papel é colocada entre a base (3) e a calha (6) de modo que a lâmina giratória de perfuração amovível de corte (2) ao rolar sobre a folha, a consiga perfurar devido à ação de uma força normal à folha no sentido de pressionar o eixo (5), e a lâmina (2), contra a folha (7).

A Figura 2 mostra uma possível geometria da lâmina giratória de perfuração amovível de corte (2), com o sentido da força aplicada na lâmina contra o papel (9), assim como a direção e o sentido do avanço de rolamento da lâmina ao longo do eixo na calha (10).

A geometria da lâmina giratória de perfuração amovível de corte é definida pelo ângulo de corte (12) e o passo angular (13), como apresentado na Figura 3. O ângulo de corte (12) está relacionado com o comprimento de corte de cada perfuração, medido na reta de perfuração, considerando que o comprimento de arco correspondente ao comprimento de corte é o produto entre o ângulo de corte (em radianos) (12) e o raio do disco (11). O passo linear, que é a distância medida na reta de perfuração entre duas perfurações consecutivas, está relacionado com o passo angular (13), considerando que o comprimento de arco correspondente ao passo é o produto entre o passo angular (em radianos) (13) e o raio do disco (11).

Na Figura 4 é possível verificar que os resultados obtidos com o sistema de perfuração laboratorial foram capazes de reproduzir as distâncias de corte obtidas numa máquina industrial de transformação de papel *tissue*, para Papéis Higiénicos (PH) comerciais de 2, 3, 4 e 5 folhas, com diferenças muito pequenas. Estes resultados são também corroborados visualmente através das imagens da Figura 5, em que se compara o corte de 3 mm de um Papel Higiénico comercial de 2 folhas tanto pelo processo industrial como com o processo laboratorial.

Reivindicações

1. Um sistema de perfuração laboratorial para papel *tissue* caracterizado por compreender uma guilhotina rotacional (1) que compreende uma lâmina giratória de perfuração amovível de corte (2) e uma base de perfuração (3), onde está acoplado um suporte de encaixe linear (4) do eixo (5) da lâmina giratória de perfuração amovível de corte que desliza sobre uma calha (6) ao longo do eixo vertical (Y), guiando o deslizamento do suporte de encaixe linear (4) e numa direção perpendicular ao eixo (5) da lâmina, paralelo ao eixo horizontal (X) da base de perfuração (3), de forma a que a lâmina giratória de perfuração amovível de corte (2) gire e perfure uma folha de papel (7) colocada entre a base de perfuração (3) e a calha(6), pela ação de uma força normal à folha de forma a pressionar o eixo da lâmina (5) e a lâmina giratória de perfuração amovível de corte (2) contra a folha (7).

2. Sistema de acordo com a reivindicação anterior, caracterizado por a base de perfuração (3) apresentar marcas de réguas de auxílio do processo de posicionamento do papel.

3. Sistema de acordo com qualquer uma das reivindicações anteriores, caracterizado por a lâmina giratória de perfuração amovível de corte (2) apresentar um perfil liso ou padronizado.

4. Sistema de acordo com qualquer uma das reivindicações anteriores, caracterizado por a calha (6) compreender meios de acionamento automático de avanço pelo eixo vertical (Y) linearmente ao longo da calha (6).

5. Sistema de acordo com qualquer uma das reivindicações anteriores caracterizado pelos meios de acionamento automático serem selecionados do grupo que consiste em motor elétrico acoplado a um parafuso sem-fim, motor elétrico acoplado a uma cremalheira, cilindro pneumático e cilindro hidráulico com pressão controlada.

1

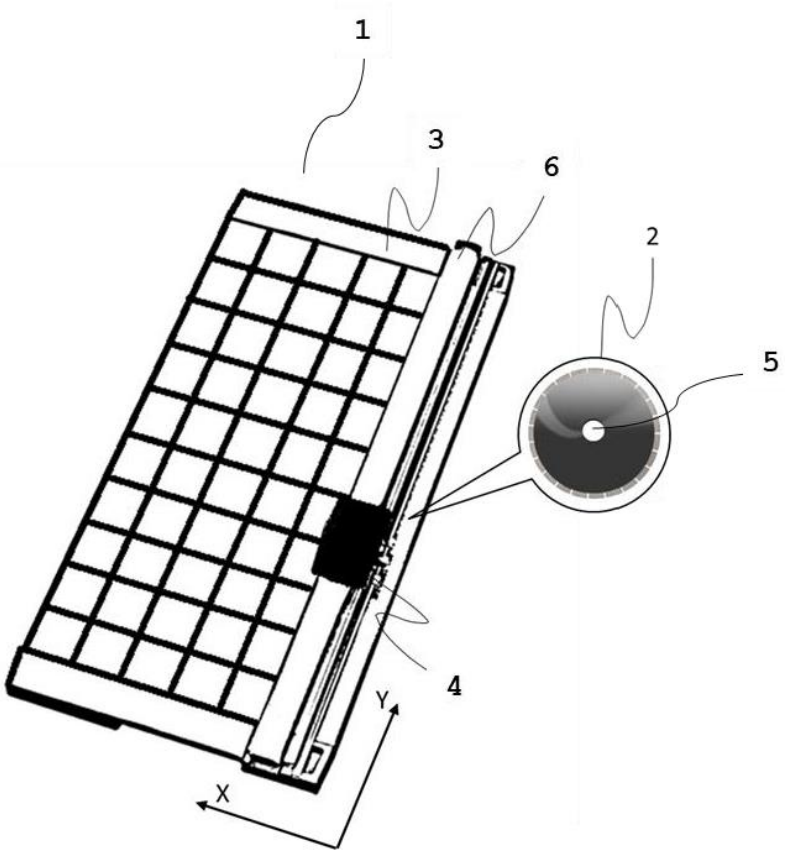

Figura 1

1/5

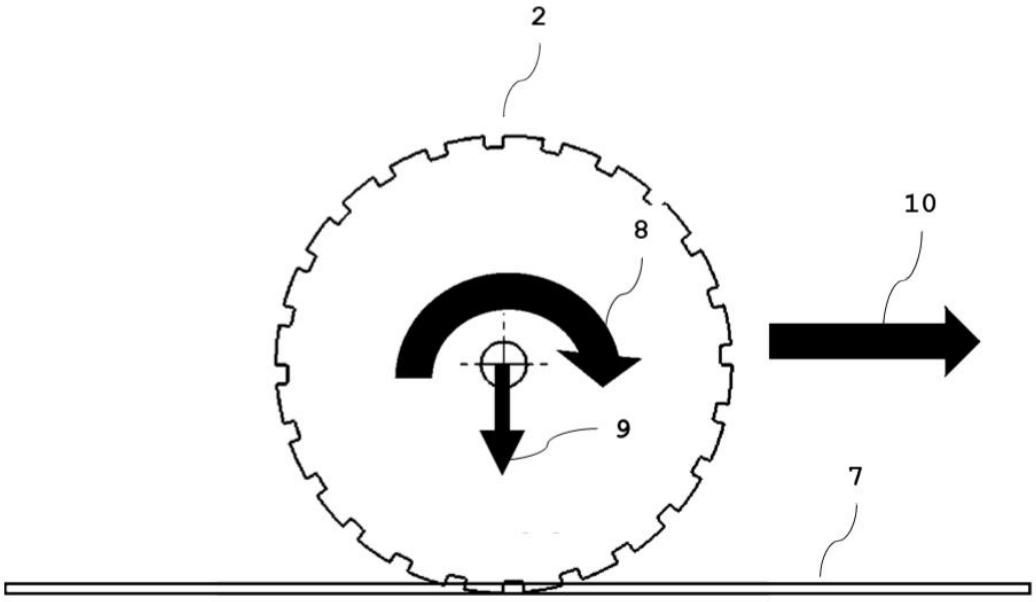

Figura 2

2/5

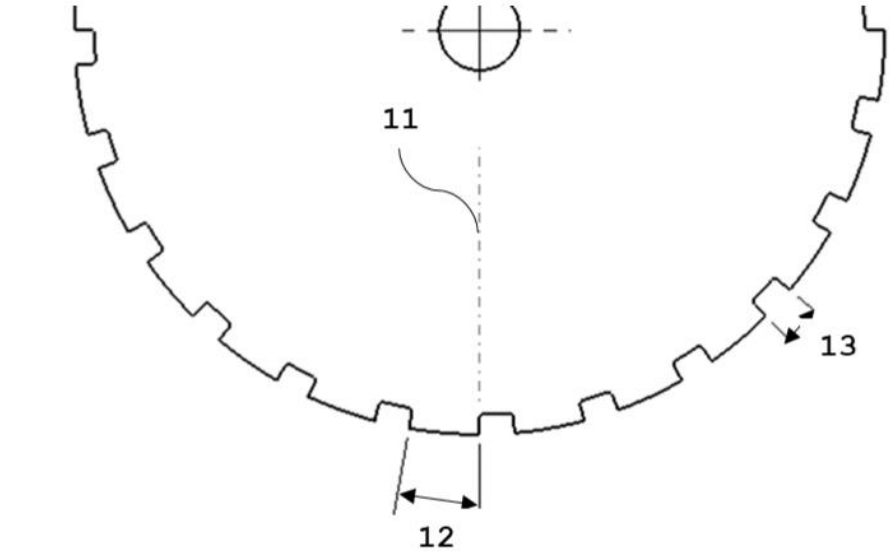

Figura 3

3/5

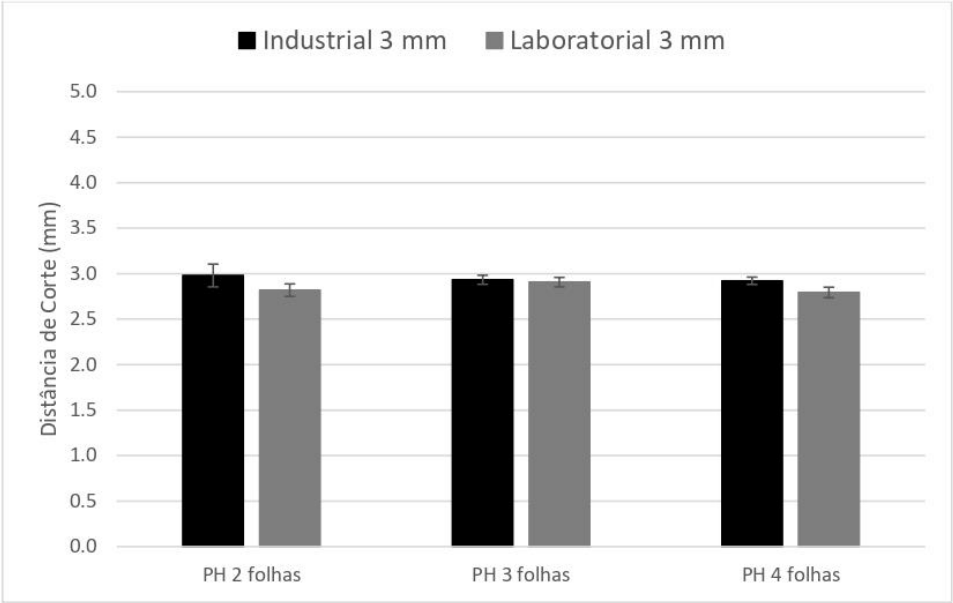
Industrial 3 mm
Laboratorial 3 mm
Distância de Corte (mm)
5.0
4.5
4.0
3.5
3.0
2.5
2.0
1.5
1.0
0.5
0.0
PH 2 folhas
PH 3 folhas
PH 4 folhas

Figura 4

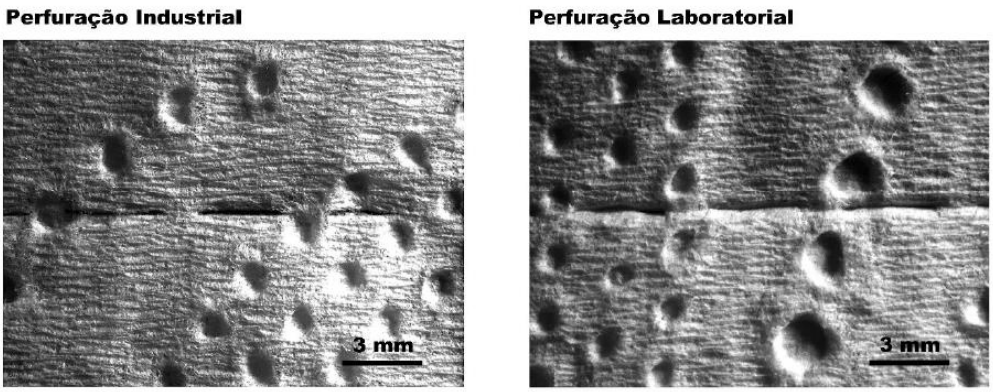

Figura 5

5/5

Toilet Paper Perforation Efficiency

Joana C. Vieira,[a,*] André C. Vieira,[b] António de O. Mendes,[a] Ana M. Carta,[c] Paulo T. Fiadeiro,[a] and Ana P. Costa [a]

Today, the toilet paper market offers product types with varying number of plies, providing better mechanical strength and liquid absorption. Several tissue paper perforation systems exist, and the best commonly applied is a top-cutting mechanism that includes an oblique blade, a combined oblique blade, or a simple spiral blade. The perforation efficiency must be high to have an easy sheet separation from the roll of the toilet paper, which does not always occur. Hence, consumer satisfaction can depend on the perforation performance. To study this, a laboratory perforation system was used to perforate different commercial toilet papers (in brands and number of plies) and evaluate their perforation efficiency. A finite element method (FEM) was used to simulate the curve of the progression of perforation efficiency as a function of the cut distance. The main findings were a stabilization of the perforation efficiency from a cut distance of 6 mm and a 15% increase in the cut distance for the laboratory blade to match the industrial perforation efficiency. The FEM analysis confirmed the behavior of the evolution of perforation efficiency with the increase of the cut distance.

DOI: 10.15376/biores.17.1.492-503

Keywords: Tissue toilet paper; Perforation efficiency; Finite element method (FEM); Mechanical behavior

*Contact information: a: Fiber Materials and Environmental Technologies (FibEnTech-UBI), Universidade da Beira Interior, R. Marquês D'Ávila e Bolama, 6201-001 Covilhã, Portugal; b: Center for Mechanical and Aerospace Science and Technologies (C-MAST-UBI), Universidade da Beira Interior, R. Marquês D'Ávila e Bolama, 6201-001 Covilhã, Portugal; c: RAIZ - Instituto de Investigação da Floresta e Papel, Aveiro, 3801-501, Portugal; *Corresponding author: joana.costa.vieira@ubi.pt*

INTRODUCTION

The use of toilet paper was first recorded in China in 851 AD (Bennett 2009). The perforated roll toilet paper known today originated in the 19th century, with the patent of Seth Wheeler in 1894 (Wheeler 1894). The toilet paper market presents this product with a diverse number of plies (1 to 6 plies). A greater number of plies increases the thickness, which provides greater strength and liquid absorption. Globally, tissue paper, with toilet paper is included, is the fastest growing sector of the paper industry, where each person in the world consumes an average of 4.4 kg per year (Haggith and Martin 2018). From the specifications of a 3-ply toilet paper roll with 150 sheets, it weighs about 78 g. This means that each person in the world consumes about 56.5 rolls per year (more than 1 roll per week per person). Between 2010 and 2015, tissue paper production increased 3.5% annually, and it is expected to grow almost 6% per year between 2018 and 2022. The environmental benefit that has been seen, despite this rapid evolution of the tissue market, especially in developing countries, is to compensate the increase of digitization and the decline in the use of printing and writing paper (Skene and Vinyard 2019).

Today, the use of disposable products is high, but many consumers are concerned with the level of resources needed to produce these products. Thus, the development of environmentally friendly disposable products remains an important work (Olson *et al.* 2016). Tissue paper products, such as kitchen, toilet, and facial papers, are similar and usually perforated to facilitate portioning (Ogg and Habel 1992; Schulz and Gracyalny 1998; Baggot *et al.* 2006). In a roll of perforated toilet paper, the holes with a certain cut distance along a line are called perforation lines. These lines of weakness are parallel to the axis on which the toilet paper is rolled and aim to divide the roll of toilet paper into portions with a predefined length. This predefined length between two perforation lines is known as a "sheet" (Ogg and Habel 1992; Chih 2018). Figure 1 shows a scheme that presents these concepts.

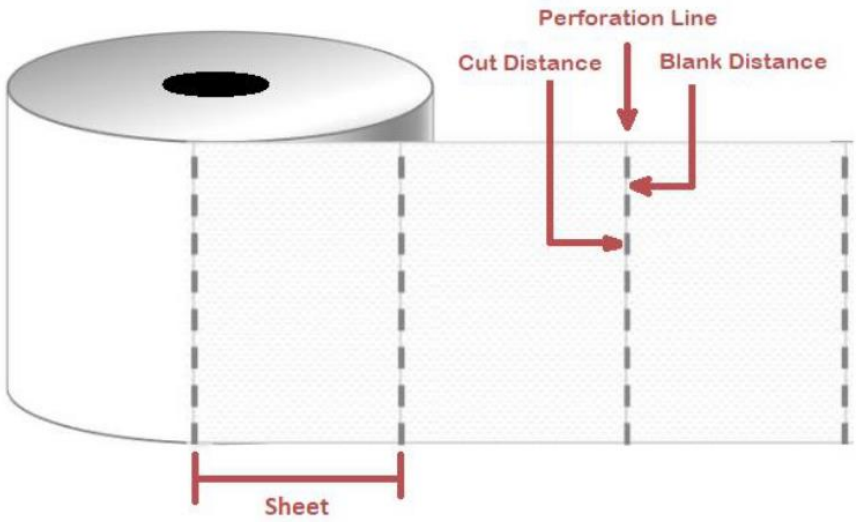

Fig. 1. Diagram of the concepts associated with toilet paper perforation

In the existing tissue paper perforation techniques, an upper cutting blade and a lower roll are generally used. Currently, the most widely used top-cutting mechanism includes an oblique blade, a combined oblique blade, or a simple spiral blade (Shiang 2012). Because the perforation blade operates in a rotating spiral, the contact between the blade and the paper sheet is theoretically at one point, which reduces the impact of this on the sheet. The soft contact (low impact) between the perforation blade and the paper sheet increases its lifetime and decreases the failure phenomena, such as the break of the blade (Chih 2018). There are disadvantages in the methods currently known for perforating tissue paper sheets. The forces generated in this operation cause vibrations that are harmful to the general processing of the sheet. In addition, there must be well-defined speed limitations, because high processing speeds cause high levels of vibration, causing imperfections in sheet cuts, sheet breaks, and/or machine malfunction (Baggot *et al.* 2006).

When the tensile strength of the perforated toilet paper is strong, the paper sheet is split off the perforation line. In contrast, when the tensile strength is weak, the sheet when pulled out from the toilet paper roll is not well controlled, leaving more than a predetermined number of sheets (Schulz and Gracyalny 1998; Mukai and Shimizu 2003). This low tensile strength can also impair the runnability of the converting machine, causing successive breaks of the sheet after the perforation process. Therefore, for all of this to be

avoided, the tensile strength in the machine direction (MD) of the perforation must be controlled so that it falls within a predetermined range. In contrast, the tensile strength of perforated toilet paper is greatly influenced by the tensile strength of the base paper itself in MD (fibrous composition, formation, and orientation of the paper sheet) (Mukai and Shimizu 2003). These problems, which are associated with the separation of the sheets by the consumer, can have a negative impact on the customer's loyalty and satisfaction with the brand of the product in question (Schulz and Gracyalny 1998). Thus, the study of the perforation efficiency, by definition "the difference between the tensile strengths of non-perforated and perforated material from the same sample divided by the tensile strength of non-perforated material," of a toilet paper is extremely important for the producers of this type of product (ISO 12625-1:2019). To have an easy sheet detachment from the toilet paper roll, the perforation efficiency must be high. Equation 1 is used to evaluate the perforation efficiency according to the standard ISO 12625-12 (2010),

$$E_p = 100 \times [1 - (\overline{S}_p / \overline{S}_{np})] \quad (1)$$

where E_p is the perforation efficiency (%); $\overline{S}_p$ is the average tensile strength of perforated papers (N/m); and $\overline{S}_{np}$ is the average tensile strength of unperforated papers (N/m).

In this context, the objective of the present work is to evaluate the perforation efficiency for different cut distances in commercial papers of 2, 3, 4, and 5 plies, using a laboratory perforation system and comparing them with the industrial perforation of each one of these.

EXPERIMENTAL

Materials

Eight commercial toilet papers with a minimum service length of 125 mm were selected. This set is composed by two samples of each 2-ply, 3-ply, 4-ply, and 5-ply papers. These toilet papers were identified according to the following legend: XP_i, where X is the commercial toilet paper sample brand, P_i is the number of plies, and XP_iC_j where C_j is the cut distance (mm) of the perforation. The values of $i = 2, 3, 4$, and 5 represents the number of plies, and $j = 2, 3, 4, 5, 6, 7$, and 8 mm represents the cut distances performed.

Methods

To start this work, samples of commercial toilet paper with sheet length of 125 mm minimum were selected, meeting the ISO 12625-12 (2010) standard requirement of the 100 mm gauge length. Then, the samples were prepared to perform the tensile tests according to the above referred standard (width of 50 mm and a length of a minimum of 125 mm up to 150 mm). These samples were then perforated in the laboratory with the repeated cutting distances of 2, 3, 4, 5, 6, 7, and 8 mm. All the perforations were performed in the center of each sample along the cross direction (CD).

All samples were subjected to tensile tests along the MD on a Thwing-Albert® VantageNX universal testing machine (Thwing-Albert Instrument Company, West Berlin, NJ, USA) at a rate of elongation of 50 mm/min, in accordance with the standard mentioned above. Samples tensile tests were performed with and without perforation as illustrated in Fig. 2.

A customized optical system (Mendes *et al.* 2013, 2014, and 2015) was used to record the measurements of the cut distance of the toilet paper samples. The image

acquisition of the performed cut distances was carried out with precise requirements of lighting and magnification. After it was properly configured for the application in hand, the optical system allowed the observation of the elements to be measured using processing tools for this task. In this work, four different measurements were considered of each sample, which were used for the calculation of the corresponding mean and standard deviation for all the studied paper samples.

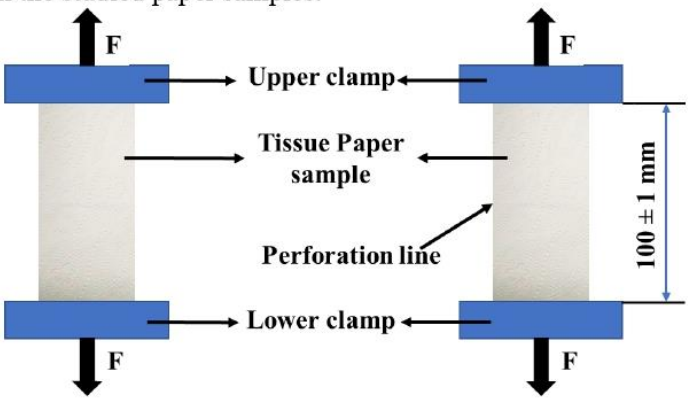

Fig. 2. Set-up of the tensile tests without and with perforation (Vieira *et al.* 2021)

All toilet paper samples were stored and tested at a temperature of 23 ± 1 °C and a relative humidity of 50 ± 2% according to ISO 187 (1990).

Numerical Model

In this work for the 2-ply toilet paper (BP_2) the influence of the cut distance was studied using mechanical simulation tools. The aim was to evaluate how the tensile strength decreases with the cut distance and how it affects the perforation efficiency. A simpler model was used to verify the stabilization of the perforation efficiency from a cut distance of 6 mm.

A finite element model (FEM) was executed in the software Abaqus/Standard finite element (Dassault Systèmes®, version 14.1, Vélizy-Villacoublay, France), using a linear elastic constitutive model to replicate the tensile tests on the 2-ply toilet paper BP_2 with 2, 3, 4, 5, 6, 7, and 8 mm of cut distances. The Young's modulus used, 1.38 MPa, was obtained by the tensile test performed in the sample without perforation and calculated as the slope between two specific points in the initial linear part of the load-elongation curve. An estimated value of 0.3 was used for the Poisson coefficient assuming that volume does not change. The sample geometry was a single shell with a width of 50.0 mm, a length of 100.0 mm, and a thickness of 0.3 mm. An axial load was employed by controlling a uniform elongation of 10.0 mm of the top surface. The lower surface was constrained to move and rotate in all directions. The CPS4R elements used in these models were 23503, 16043, 15252, 13222, 13165, 12158, and 12139 for the cut distances of 2, 3, 4, 5, 6, 7, and 8 mm, respectively. An ellipse was used for the cut's geometry with 0.01 mm to the smaller diameter and the longer diameter was matched to each cut distance. Perforation efficiency was calculated based on the tensile strength of the toilet paper sample without perforation. Load was increased iteratively, in several simulations, until this tensile strength value ($\overline{S}_{np}$ = 265.89 MPa in accordance with Table 1 for BP_2) was reached in the most critical element. The procedure was the same for each cut distance.

RESULTS AND DISCUSSION

From the previous work by Vieira *et al.* (2021), these toilet papers (with the same notation) were morphologically characterized. The fiber composition of the samples is mostly composed by hardwood short fibers. However, small differences were found in softwood long fibers content.

Tables 1 and 2 show the results for determining the perforation efficiency, as well as the measurements of the cut and blank distances laboratory performed for the 2-, 3-, 4-, and 5-ply toilet papers.

In Fig. 3, the cut distance measurements made on all toilet paper samples by cut blade size are shown. All the effective cuts were inferior to the target cuts. Comparing all the cuts for the same cut blade, they had an average coefficient of variation of 2.1% which indicates that this is a good mechanical method of laboratory perforation for this kind of tissue paper sample.

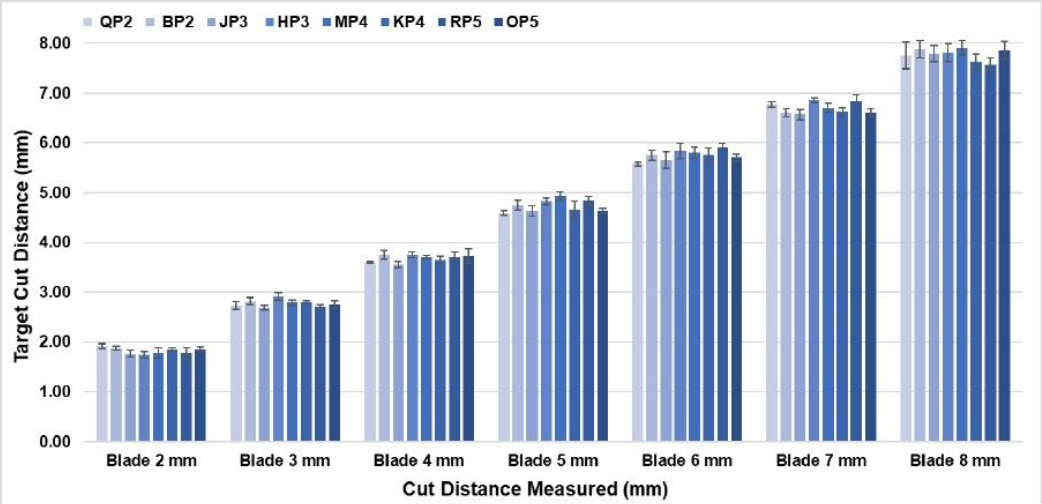

Fig. 3. Evaluation of the cut distances for all study samples

The evolution of perforation efficiency with the variation of the cut distances is presented in Fig. 4, by number of plies of toilet paper. It can be confirmed that for all samples there was a stabilization of the perforation efficiency above a cut distance of 6 mm. Therefore, for cutting distances higher than this value, perforation efficiency is not gained, which may impair the runnability of the paper sheet in the converting machine. In the previous work Vieira *et al.* (2021), the authors concluded that with the increase of the cut distance, stress concentration factor tends to increase asymptotically, physically meaning that the stress gets more homogenously distributed. Because the samples are from commercial papers of different brands, they have different fibrous compositions, which justifies the gap between the curves for the toilet papers with the same number of plies. Images obtained by the customized optical system are shown in Fig. 5, which represents the 6 mm cut distance of the 2-, 3-, 4-, and 5-ply toilet papers. The figure verifies that samples had uniform and clean cuts, and that with the increase of the number of plies the cut was not affected.

Table 1. Perforation Efficiency and Cut Distance for 2-ply and 3-ply Toilet Papers

Toilet Paper ID	Tensile Index (Nm/g)		Tensile Strength (N/m)	Perforation Efficiency (%)	Target Cut Distance (mm)	Cut Distance Measured (mm)		Blank Distance Measured (mm)	
	$\bar{x}$	$\pm\sigma$				$\bar{x}$	$\pm\sigma$	$\bar{x}$	$\pm\sigma$
QP_2	5.87	0.19	175.38						
QP_2C_2	3.49	0.24	104.34	40.5	2	1.92	0.05	1.15	0.03
QP_2C_3	2.58	0.20	77.26	55.9	3	2.73	0.08	1.21	0.06
QP_2C_4	2.13	0.16	63.65	63.7	4	3.60	0.02	1.27	0.04
QP_2C_5	1.73	0.19	51.80	70.5	5	4.59	0.05	1.22	0.03
QP_2C_6	1.37	0.10	41.09	76.6	6	5.58	0.04	1.18	0.05
QP_2C_7	1.34	0.15	40.08	77.1	7	6.77	0.05	1.19	0.03
QP_2C_8	1.00	0.10	39.85	77.3	8	7.75	0.27	1.21	0.03
BP_2	7.13	0.44	265.89						
BP_2C_2	3.65	0.28	136.05	48.8	2	1.87	0.04	1.11	0.02
BP_2C_3	2.83	0.26	105.72	60.2	3	2.82	0.07	1.20	0.05
BP_2C_4	2.14	0.31	79.67	70.0	4	3.75	0.09	1.19	0.06
BP_2C_5	1.78	0.19	66.33	75.1	5	4.75	0.10	1.17	0.07
BP_2C_6	1.23	0.13	46.82	82.4	6	5.75	0.10	1.12	0.05
BP_2C_7	1.22	0.12	45.51	82.9	7	6.60	0.08	1.20	0.03
BP_2C_8	1.12	0.13	41.82	84.3	8	7.88	0.17	1.14	0.07
HP_3	7.00	0.22	305.25						
HP_3C_2	3.35	0.35	146.01	52.2	2	1.76	0.06	1.15	0.09
HP_3C_3	2.78	0.14	121.19	60.3	3	2.69	0.07	1.22	0.06
HP_3C_4	2.12	0.09	92.53	69.7	4	3.55	0.06	1.22	0.04
HP_3C_5	1.85	0.23	80.65	73.6	5	4.63	0.07	1.21	0.07
HP_3C_6	1.32	0.10	57.39	81.2	6	5.65	0.16	1.09	0.07
HP_3C_7	1.20	0.14	52.54	82.8	7	6.57	0.05	1.22	0.01
HP_3C_8	1.13	0.15	50.06	83.6	8	7.79	0.18	1.19	0.07
JP_3	6.86	0.21	360.10						
JP_3C_2	3.38	0.16	177.61	50.7	2	1.74	0.07	1.18	0.07
JP_3C_3	2.69	0.26	141.22	60.8	3	2.91	0.05	1.21	0.04
JP_3C_4	2.15	0.21	113.04	68.6	4	3.75	0.06	1.19	0.05
JP_3C_5	1.69	0.13	88.53	75.4	5	4.82	0.11	1.15	0.06
JP_3C_6	1.19	0.13	62.46	82.7	6	5.83	0.17	1.11	0.06
JP_3C_7	1.21	0.16	63.63	82.3	7	6.86	0.10	1.13	0.06
JP_3C_8	1.29	0.18	63.60	82.3	8	7.81	0.17	1.15	0.06

Table 2. Perforation Efficiency and Cut Distance for 4-ply and 5-ply Toilet Papers

Toilet Paper ID	Tensile Index (Nm/g)		Tensile Strength (N/m)	Perforation Efficiency (%)	Target Cut Distance (mm)	Cut Distance Measured (mm)		Blank Distance Measured (mm)	
	$\bar{x}$	± σ				$\bar{x}$	± σ	$\bar{x}$	± σ
KP_4	**6.78**	0.29	**410.05**						
KP_4C_2	**3.71**	0.22	**224.70**	**45.2**	**2**	**1.85**	0.03	**1.17**	0.04
KP_4C_3	**2.88**	0.19	**174.33**	**57.5**	**3**	**2.80**	0.03	**1.10**	0.06
KP_4C_4	**2.29**	0.10	**138.44**	**66.2**	**4**	**3.64**	0.08	**1.25**	0.07
KP_4C_5	**1.85**	0.21	**111.97**	**72.7**	**5**	**4.66**	0.17	**1.16**	0.05
KP_4C_6	**1.48**	0.18	**89.47**	**78.2**	**6**	**5.75**	0.15	**1.12**	0.04
KP_4C_7	**1.29**	0.08	**78.30**	**80.9**	**7**	**6.62**	0.08	**1.14**	0.04
KP_4C_8	**1.20**	0.18	**74.81**	**81.8**	**8**	**7.63**	0.16	**1.17**	0.04
MP_4	**8.89**	0.40	**611.07**						
MP_4C_2	**4.44**	0.33	**305.24**	**50.0**	**2**	**1.78**	0.10	**1.18**	0.07
MP_4C_3	**3.55**	0.10	**243.75**	**60.1**	**3**	**2.79**	0.06	**1.13**	0.04
MP_4C_4	**2.97**	0.09	**204.28**	**66.6**	**4**	**3.71**	0.03	**1.18**	0.02
MP_4C_5	**2.26**	0.24	**155.20**	**74.6**	**5**	**4.93**	0.09	**1.11**	0.06
MP_4C_6	**1.71**	0.15	**117.25**	**80.8**	**6**	**5.80**	0.12	**1.10**	0.08
MP_4C_7	**1.64**	0.12	**112.73**	**81.6**	**7**	**6.70**	0.09	**1.16**	0.06
MP_4C_8	**1.52**	0.21	**108.33**	**82.3**	**8**	**7.91**	0.14	**1.11**	0.08
OP_5	**7.53**	0.27	**572.06**						
OP_5C_2	**3.60**	0.31	**273.28**	**52.2**	**2**	**1.85**	0.05	**1.13**	0.08
OP_5C_3	**2.63**	0.20	**200.22**	**65.0**	**3**	**2.75**	0.08	**1.10**	0.05
OP_5C_4	**1.92**	0.19	**146.03**	**74.5**	**4**	**3.72**	0.14	**1.21**	0.03
OP_5C_5	**1.73**	0.16	**131.60**	**77.0**	**5**	**4.63**	0.06	**1.13**	0.03
OP_5C_6	**1.32**	0.11	**100.28**	**82.5**	**6**	**5.70**	0.07	**1.05**	0.01
OP_5C_7	**1.21**	0.10	**91.79**	**84.0**	**7**	**6.60**	0.08	**1.24**	0.07
OP_5C_8	**1.08**	0.16	**87.97**	**84.6**	**8**	**7.86**	0.18	**1.15**	0.05
RP_5	**5.54**	0.35	**423.59**						
RP_5C_2	**3.39**	0.24	**258.71**	**38.9**	**2**	**1.78**	0.11	**1.12**	0.06
RP_5C_3	**2.60**	0.22	**198.85**	**53.1**	**3**	**2.71**	0.04	**1.18**	0.04
RP_5C_4	**2.06**	0.21	**157.46**	**62.8**	**4**	**3.71**	0.09	**1.20**	0.03
RP_5C_5	**1.53**	0.16	**116.95**	**72.4**	**5**	**4.84**	0.08	**1.14**	0.07
RP_5C_6	**1.31**	0.10	**100.43**	**76.3**	**6**	**5.92**	0.07	**1.14**	0.06
RP_5C_7	**1.30**	0.06	**99.09**	**76.6**	**7**	**6.84**	0.12	**1.13**	0.09
RP_5C_8	**1.12**	0.12	**95.90**	**77.4**	**8**	**7.57**	0.13	**1.13**	0.07

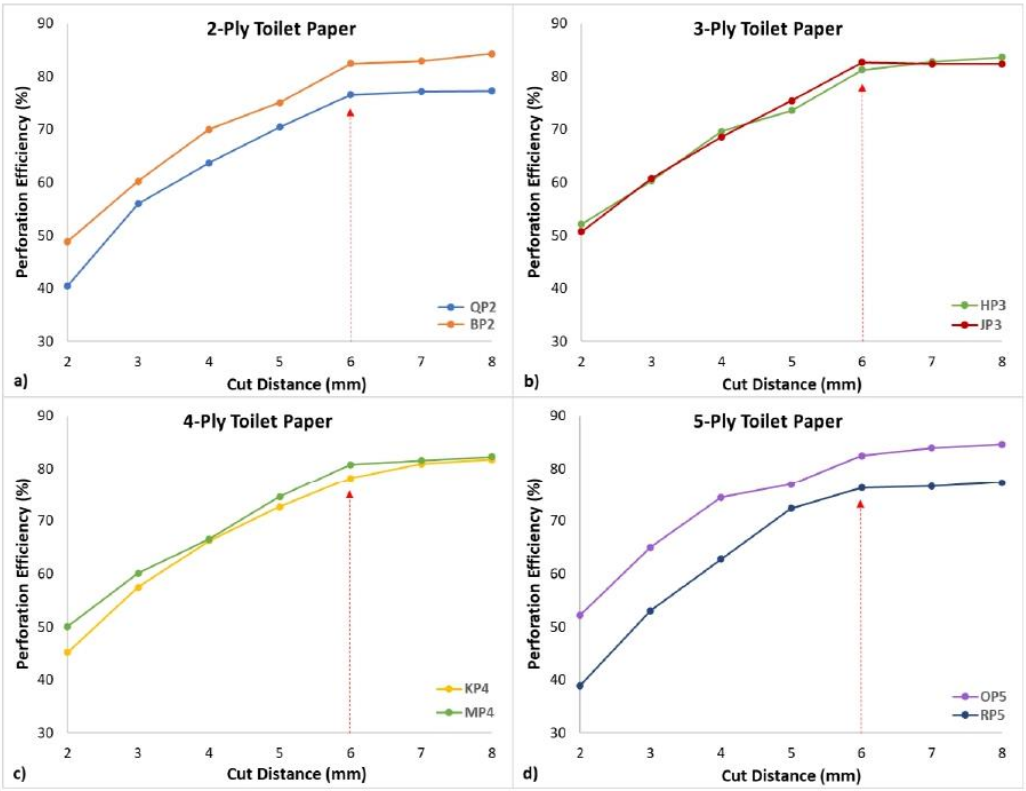

Fig. 4. Evolution of perforation efficiency with the variation of the cut distances: a) 2-ply toilet paper; b) 3-ply toilet paper; c) 4-ply toilet paper, and d) 5-ply toilet paper

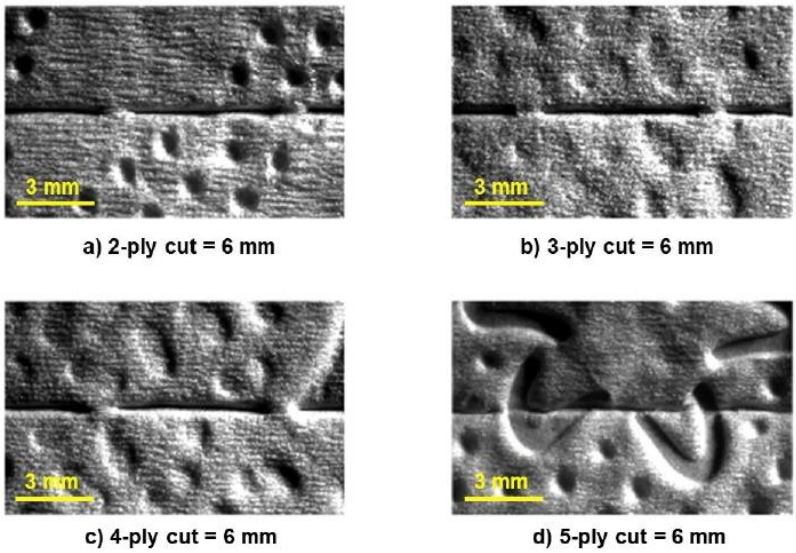

Fig. 5. Optical images of the 6 mm cut distance from: a) 2-ply toilet paper; b) 3-ply toilet paper; c) 4-ply toilet paper; and d) 5-ply toilet paper

Figure 6 presents the confirmation of the perforation efficiency stabilization to a cut distance of 6 mm by the FEM simulation. This curve shows the same behavior as the curves related to experimental data. The gap between the curves of simulation and experimental data is due to the parameters assumed for the simulation, *i.e.*, despite the Young's modulus and the sample dimensions being the same, it was considered to be one homogeneous and isotropic shell (although 2-plies in toilet paper), not considering the fibrous orientation, friction between plies, volume changes due to creping, and embossing. Another justification is the fact that the FEM simulation is performed for an exact cut distance (target dimension) and the cut distance performed in the laboratory is always smaller than the target dimension (according to the values presented in Tables 1 and 2).

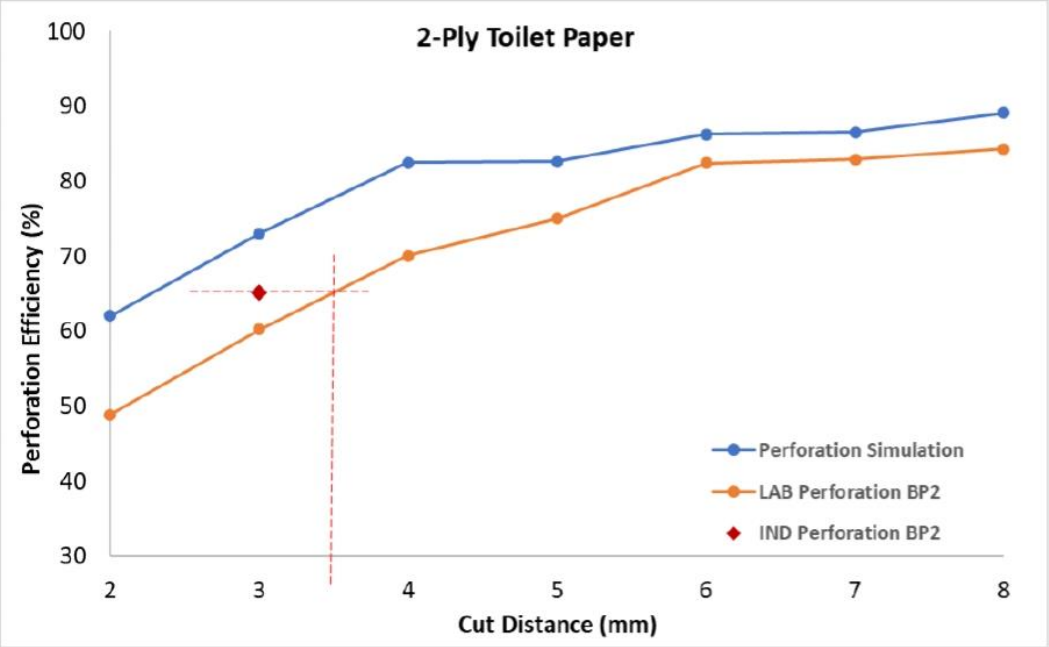

Fig. 6. Comparison of the evolution of perforation efficiency with the variation of the cut distances of the FEM simulation, laboratory (LAB) perforation, and industrial (IND) perforation results for a 2-ply toilet paper (BP_2)

Figure 6 shows the industrial perforation of the same commercial toilet paper. Comparing laboratory perforation with the same industrial perforation, the first achieves a higher perforation efficiency; this can be justified by looking at Figs. 7(b) and 7(c), respectively. Figure 7(c) shows a thinner and less marked cut, without affecting the fibrous structure adjacent to the cut. In contrast, Fig. 7(b) shows a thicker and more marked cut, weakening the structure nearby the cut. To achieve the same perforation efficiency of the industrial 3 mm cut, a 3.5 mm cutting blade would need to be used. Therefore, to equalize the efficiency of industrial perforation with laboratory perforation the cut distance of the laboratory blade must be increased 15% when compared to the industrial cut distance.

In addition to the qualitative comparison of industrial and laboratory cuts, Fig. 7 illustrates the sequence of all cut distances (2 mm to 8 mm) that were laboratory performed in this work, keeping the blank distance constant (1 mm).

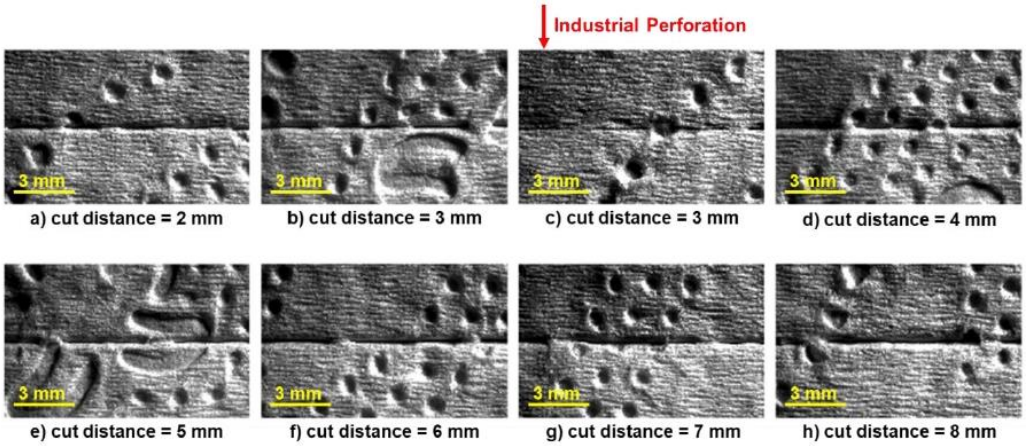

Fig. 7. Optical images of the different laboratory cut distances for the BP_2 toilet paper and the industrial perforation for the same toilet paper

Figure 8 compares the industrial and laboratory perforations in different commercial toilet papers from the measurements of the cuts by the optical system. Analyzing this figure, it is confirmed that the dimensions of the laboratory cuts are always smaller than the industrial ones. In addition, both types of cut are inferior to the target measure.

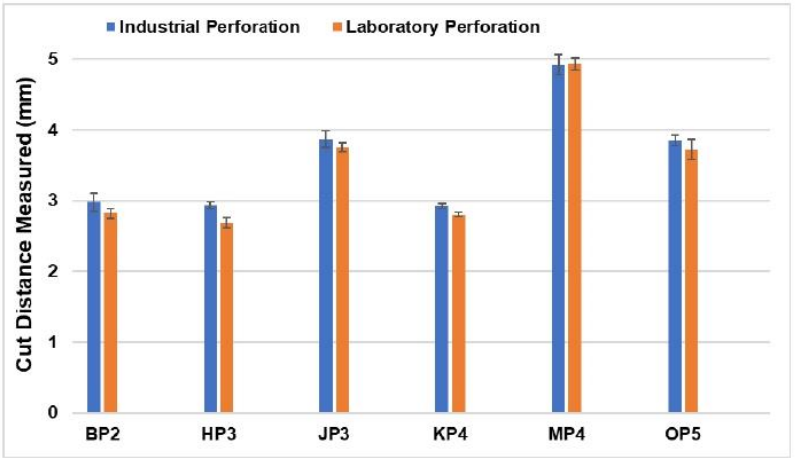

Fig. 8. Comparison of industrial *vs* laboratory cut distances for different toilet papers

In agreement with what was previously presented in Fig. 4, the stabilization for a 6 mm laboratory cut, and because this cut was inferior to the industrial one, it can be assumed that industrially this stabilization will occur for a 5 mm industrial cut. In brief, industrially, the maximum cut to obtain an optimized perforation efficiency without impairing the runnability of the converting machine is 5 mm. Of the analyzed papers, the one with the best perforation efficiency was a 4-ply paper with a cut distance of 5 mm (MP_4). The findings of this study suggest that the fibrous composition and the number of plies had a small contribution in the perforation efficiency results. The cut distance had the biggest impact in the results of the perforation efficiency.

CONCLUSIONS

1. The optimization of the perforation efficiency was obtained for a 6 mm laboratory cut distance, corresponding to an industrial cut distance of 5 mm.
2. The evidence from this study suggests that the major impact on perforation efficiency is related to the dimensions of the perforation cuts and not the fibrous composition and number of plies of the toilet paper samples.
3. In general, the results of the finite element method (FEM) simulation analysis support the idea that the value of perforation efficiency tends towards an establishment from a specific cut distance of 6 mm.
4. The described laboratory approach applied to this set of samples, has the potential to explain the perforation behavior on the converting machine, although for that a blade with a cut distance 15% higher than the industrial cut distance must be used.

ACKNOWLEDGMENTS

The authors gratefully acknowledge the funding of this work that was carried out under the Project InPaCTus – Innovative Products and Technologies from Eucalyptus (Project Nº 21874) funded by Portugal 2020 through the European Regional Development Fund (ERDF) in the frame of COMPETE 2020 nº246/AXIS II/2017.

The authors are also very grateful for the support given by research unit Fiber Materials and Environmental Technologies (FibEnTech-UBI), on the extent of the project reference UIDB/00195/2020, and by the Center for Mechanical and Aerospace Science and Technologies (C-MAST-UBI), on the extent of the project reference UIDB/00151/2020, both funded by the Fundação para a Ciência e a Tecnologia, IP/MCTES through national funds (PIDDAC).

REFERENCES CITED

Baggot, J., Gropp, R. F., and Wojcik, S. (2006). "System and method for severing or perforating a web," U.S. Patent No. 2006/0014616.

Bennett, H. (2009). "Ever wondered about the history of toilet paper?," *Washington Post* (http://www.washingtonpost.com/wp-dyn/content/article/2009/05/31/AR2009053102217.html), Accessed 14 July 2019.

Chih, C.-K. (2018). "Perforation design & calculation of toilet paper rewinder," *China Pulp and Paper* 37(9), 38-42. DOI: 10.11980/j.issn.0254-508X.2018.09.007

Haggith, M., and Martin, J. (2018). *The State of the Global Paper Industry*, The Environmental Paper Network (EPN), Asheville, NC, USA.

ISO 187 (1990). "Paper, board and pulps - Standard atmosphere for conditioning and testing and procedure for monitoring the atmosphere and conditioning of samples," International Organization for Standardization, Geneva, Switzerland.

ISO 12625-1 (2019). "Tissue paper and tissue products - Part 1: Vocabulary," International Organization for Standardization, Geneva, Switzerland.

ISO 12625-12 (2010). "Tissue paper and tissue products - Part 12: Determination of tensile strength of perforated lines - calculation of perforation efficiency," International Organization for Standardization, Geneva, Switzerland.

Mendes, A. O., Fiadeiro, P. T., Costa, A. P., Amaral, M. E., and Belgacem, M. N. (2013). "Retro-diffusion and transmission of laser radiation to characterize the paper fiber distribution and mass density," in: *Proceedings Volume 8785: 8th Ibero American Optics Meeting and 11th Latin American Meeting on Optics, Lasers, and Applications*, Porto, Portugal, pp. 8785AY-1/8785AY-8. DOI: 10.1117/12.2022367

Mendes, A. O., Fiadeiro, P. T., Costa, A. P., Amaral, M. E., and Belgacem, M. N. (2014). "Study of repeatability of an optical laser system for characterization of the paper fiber distribution and mass density," in: *Proceedings Volume 9286: Second International Conference on Applications of Optics and Photonics*, Aveiro, Portugal, pp. 92862Y-1/92862Y-8. DOI: 10.1117/12.2062697

Mendes, A. O., Fiadeiro, P. T., Costa, A. P., Amaral, M. E., and Belgacem, M. N. (2015). "Laser scanning for assessment of the fiber anisotropy and orientation in the surfaces and bulk of the paper," *Nordic Pulp & Paper Research Journal* 30(2), 308-318. DOI: 10.3183/npprj-2015-30-02-p308-318

Mukai, T., and Shimizu, Y. (2003). "Toilet paper roll with perforated line," JPO Patent No. 2003061861A.

Ogg, R. G., and Habel, M. A. (1992). "Perforator blade for paper products and products made therefrom," U.S. Patent No. 5114771.

Olson, S. R., Hoadley, D. A., and Daul, T. A. (2016). "Partitionable paper towel," U.S. Patent No. US20160345786A1.

Schulz, G., and Gracyalny, D. (1998). "Method and apparatus for pinch perforating multiply web material," U.S. Patent No. 5755654.

Shiang, T. T. (2012). "Tissue paper cutting mechanism having upper knife with variable spiral curve angle and upper knife structure therefor," EPO Patent No. EP2095917B1.

Skene, J., and Vinyard, S. (2019). *The Issue with Tissue: How Americans are Flushing Forests Down the Toilet* (R: 19-01-A), Natural Resources Defense Council and Stand.earth, New York, NY, USA.

Vieira, J. C., Vieira, A. C., Mendes, A. O., Carta, A. M., Fiadeiro, P. T., and Costa, A. P. (2021). "Mechanical behavior of toilet paper perforation," *BioResources* 16(3), 4846-4861. DOI: 10.15376/biores.16.3.4846-4861

Wheeler, S. (1894). "Wrapping or toilet paper," U.S. Patent No. 511983A.

Article submitted: August 6, 2021; Peer review completed: October 17, 2021; Revised version received and accepted: November 18, 2021; Published: November 24, 2021.
DOI: 10.15376/biores.17.1.492-503

Mechanical Behavior of Toilet Paper Perforation

Joana C. Vieira,[a,*] André C. Vieira,[b] António de O. Mendes,[a] Ana M. Carta,[c] Paulo T. Fiadeiro,[a] and Ana P. Costa [a]

Perforation is used in multilayer tissue products, such as toilet and kitchen papers, as part of the converting process. Perforation facilitates the detachment of consecutive sheets by the user. The compromise between the strength required to detach a perforated sheet and the strength required to break a sheet affects the perforation efficiency. In this work, the mechanical behaviors of 15 commercial papers from different European producers were studied. A morphological analysis of the materials was performed, followed by the determination of their perforation efficiency (through tensile tests). A qualitative analysis of the cuts quality, along with a quantitative analysis of the same cuts dimensions was performed through an optical system. Finally, the stress concentration in the holes and the influence of the cuts distance were analyzed using a finite element model implemented in Abaqus/Standard finite element software. The results showed that a cut distance of 2.0 mm should not be used in these types of papers, and the perforation efficiency increased with the cut distance, regardless of the number of plies in the toilet paper. The stress concentration factor was also determined to have a limit value of 0.11. Papers above this limit value tear at the perforation line, as desired.

Keywords: Tissue paper; Perforation; Finite element methods (FEM); Mechanical behavior

*Contact information: a: Fiber Materials and Environmental Technologies (FibEnTech-UBI), Universidade da Beira Interior, R. Marquês D'Ávila e Bolama, 6201-001 Covilhã, Portugal; b: Center for Mechanical and Aerospace Science and Technologies (C-MAST-UBI), Universidade da Beira Interior, R. Marquês D'Ávila e Bolama, 6201-001 Covilhã, Portugal; c: RAIZ - Instituto de Investigação da Floresta e Papel, Aveiro, 3801-501, Portugal; *Corresponding author: joana.costa.vieira@ubi.pt*

INTRODUCTION

Prior to the invention of toilet paper, people across the world had different methods for personal hygiene. The first record of toilet paper took place in China around 851 AD. Thereafter, no document was found on the use of toilet paper until the 14th century. During the Ming Dynasty (1368 AD to 1644 AD), special sheets of toilet paper were made for the Imperial court. These toilet paper sheets were made of soft fabric that was cut into 2 ft by 3 ft squares (Bennett 2009).

Joseph C. Gayetty invented the first packaged toilet paper in the United States in 1857. "Gayetty Medicated Paper" was sold in flat-leaf packages, and it contained a hemorrhoid medicine and watermark with its name (Hendrickson 2000). In 1871 Seth Wheeler became the official inventor of toilet roll as it is known today. From this invention, Wheeler held the first patent of the perforated toilet paper roll (Wheeler 1894).

Converting technology produces consumable, finished products from large paper rolls. Converting equipment can perform lamination, printing, embossing, perforation, and packaging operations to produce multi-layer bathroom papers and towels, table napkins, and other disposable products (de Assis *et al.* 2018).

When a multilayer or single layer paper product such as toilet paper is produced, a perforation process is generally used. Multilayer or single layer tissue papers should be perforated to allow easy dispensing of the paper sheets (pieces of laminated paper between two consecutive perforations) so that a consumer can use it incrementally. This process allows a consumer to detach and use one or more sheets from a toilet paper roll (Schulz and Gracyalny 1998; Paulapuro 2000).

Perforations are formed using a roll with several diagonally arranged blades to perforate the paper sheet. This process occurs at a high speed in the converting machine. Within the perforation line there exist bonding areas, *i.e.* the uncut area of the perforation process. As the blade is pressed against the paper sheet, it cuts any point of contact. The slots in the blade prevent certain areas of the paper sheet from being cut. The uncut areas of the paper prevent the sheet from tearing prematurely (Baggot *et al.* 2006). Figure 1 shows a diagram of a perforation blade creating a perforated tissue paper sheet.

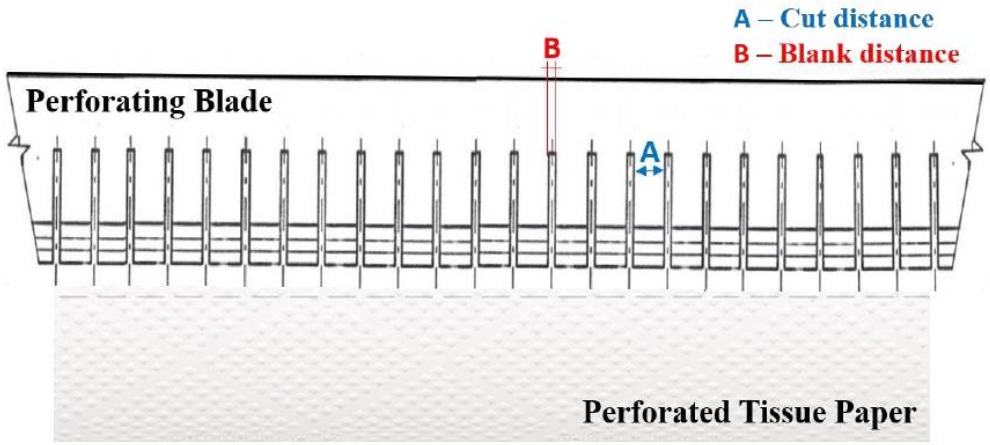

Fig. 1. The tissue paper perforation scheme

The tensile strength of perforation is the strength that is required to ensure that the paper separates through its perforation zone. The tensile strength of the perforation should be optimized to allow high-speed production of the multi-layer tissue paper product and to allow the consumer to easily separate individual sheets. In a multilayer tissue paper, the perforation must be done in all layers at the same time to facilitate the detachment of paper sheets by the consumer (Schulz and Gracyalny 1998).

In converting operations, the machine is required to perforate the tissue paper under consistent conditions. The machine should run without vibration or equipment failure and at high processing speeds to reduce the maintenance requirements. In addition, a system capable of changing the adhesion patterns, the sheet length, and the weight in a short time is desirable (Baggot *et al.* 2006).

The perforation zones must be strong enough to hold together under a certain tension when the consumer wishes to use more than one sheet. The perforation zone must also be weak enough to enable detachment from the roll easily and in a straight horizontal line. This balance is measured using the perforation efficiency. A higher perforation efficiency allows for easier separation of the sheets. The perforation efficiency is determined according to the ISO standard 12625-12 (2010), as seen in Eq. 1,

$$E_p = 100 \times \left[1 - \frac{\overline{S}_p}{\overline{S}_{np}}\right] \quad (1)$$

where E_p is the perforation efficiency (%), $\overline{S}_p$ is the average tensile strength of the perforated papers (N/m), and $\overline{S}_{np}$ is the average tensile strength of the unperforated papers (N/m).

A hole will affect the stress field near the geometrical discontinuity, and the maximum stress depends on the hole geometry. Therefore, the stress concentration factor geometry due to the perforation geometry will affect the final efficiency. The stress concentration factor is defined as the ratio between the highest value at a geometrical discontinuity and the nominal stress at the minimum cross-section (Carvill 2015).

In this work, several commercial toilet papers with approximately the same blank distance (theoretically 1.0 mm) and different cut distances were tested. The perforation design was studied in terms of its final efficiency. To the authors knowledge, there have been no other studies on this subject.

EXPERIMENTAL

Materials

Fifteen toilet papers with different cut distances were selected. Six of the toilet papers were 2-ply, four of the toilet papers were 3-ply, four of the toilet papers were 4-ply paper, and one of the toilet papers was 5-ply. These toilet papers were identified according to the following legend: XP_i, where X is the commercial toilet paper brand, P_i is the number of plies, and XP_iC_j, where C_j is the cut distance (mm) of the perforation. The values of i = 2, 3, 4, and 5 represent the number of plies, and j = 2, 3, 4, and 5 mm represent the cut distances.

It was previously verified that three of the 2-ply papers tear at other locations than the perforation when they were loaded manually (toilet papers C, D, and E). All the other papers tear at the perforation when they were loaded manually.

Methods

All the toilet tissue samples, and all performed tests were equilibrated in a conditioned room according to ISO 187 (1990) (temperature of 23 ± 1 °C and relative humidity of 50 ± 2%). The grammage of the toilet papers, defined as the mass per unit paper area, was determined and expressed in g/m^2. The grammage was determined by weighing the paper sample of a known area in agreement according to the ISO standard 12625-6 (2005) using a Mettler Toledo PB303 Delta range analytical balance (Mettler Toledo, Columbus, OH, USA). The thickness was also determined using a FRANK-PTI micrometer for tissue paper (FRANK-PTI GMBH, Birkenau, Germany), where a sheet of paper or a stack of sheets of paper was compressed at a given pressure between two parallel plates according to the ISO standard 12625-3 (2014). The bulk, which is the inverse of the density, was determined by using the grammage and thickness according to the ISO standard 12625-3 (2014).

The morphology of all the commercial toilet papers was evaluated using the MorFi Fiber and Shive Analyzer from Techpap SAS (Gières, France). The morphology analysis provided the fiber length, the fiber width, the fiber distribution, the fiber coarseness, and the fines percentage for the toilet paper samples.

The tensile tests were performed with a Thwing-Albert Vantage^{NX} universal testing machine (West Berlin, NJ, USA), according to the ISO standard 12625-12 (2010). Each sample was prepared with the perforation in the center. The un-perforated area of the other samples were also prepared and tested (Fig. 2). Both type of samples had a width of 50 mm and a length of 150 mm, to allow a gauge length of 100 mm to carry out the tensile tests and a rate of elongation of 50 mm/min, according to above referred standard.

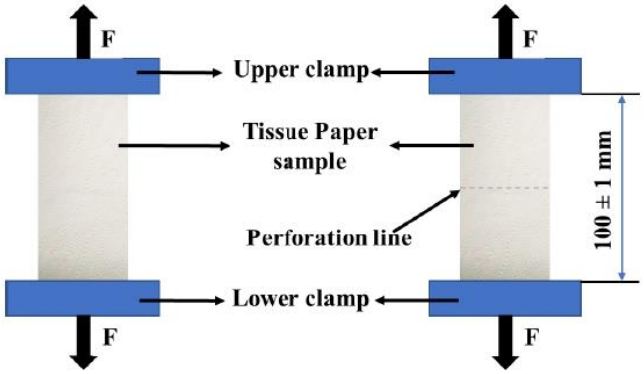

Fig. 2. The experimental set-up to test the non-perforated and perforated toilet papers

For the distance measurements of the papers, a customized optical system (Mendes *et al.* 2013, 2014, and 2015) was used. This system consisted in the image acquisition of the surface of the studied papers, with specific conditions of illumination and magnification. After it was properly configured for the application in hand, the optical system allowed for the observation of the elements to be measured using processing tools for this task. In this work, the elements in study (cut and blank distances) were carried out considering 10 different measurements, which were used for the calculation of the corresponding average and standard deviation for all the studied papers.

Numerical Model

In this work, the influence of the cut distance was studied using mechanical simulation tools. The aim was to evaluate how the increased cut distance affected the mechanical strength and the stress concentration around the cuts.

A finite element model was implemented in Abaqus/Standard finite element software (Johnston, RI, USA), using the linear elastic constitutive model to simulate the tensile test on samples with 2, 3, 4, and 5 cut distances. Two Young's moduli were used, 1.38 and 0.95 MPa, which represented the mechanical properties of the papers with different behaviors AP_2 (tear at the perforation) and CP_2 (tear at other location than perforation). The Young's modulus values were determined from the respective tensile tests without perforation, as the slope between two specific points in the initial linear part of the load-elongation curve. The coefficient of Poison was estimated to the value of 0.3. The sample geometry was 50.0 mm in width, 100.0 mm in length, and 0.3 mm in thickness. An axial load was applied by controlling a uniform displacement of 10.0 mm of the top surface. The lower surface was constrained to move and rotate in all directions. The CPS4R elements used in these models were 7266, 6085, 5437, and 5194 for the cut distances of 2, 3, 4, and 5 mm, respectively. The geometry of the cuts was an ellipse with a smaller diameter of 0.01 mm and the longer diameter corresponded to each cut distance.

RESULTS AND DISCUSSION

The commercial toilet papers samples were first subjected to a physical and morphological characterization. Table 1 shows the grammage, thickness, and bulk results for all the toilet papers, which were determined according to the previously mentioned standards.

Table 1. Characterization of the Toilet Papers in Terms of the Number of Plies, Grammage, Thickness, and Bulk

Toilet Paper ID	No. Plies	Grammage (g/m^2)	Thickness (μm)	Bulk (cm^3/g)
AP_2	2	44.9	345	7.7
BP_2	2	37.3	477	12.8
CP_2	2	33.5	423	12.6
DP_2	2	36.6	384	10.5
EP_2	2	35.4	305	8.6
FP_2	2	32.4	619	19.1
GP_3	3	43.9	419	9.5
HP_3	3	43.6	464	10.6
IP_3	3	50.1	429	8.6
JP_3	3	52.5	482	9.2
KP_4	4	60.5	486	8.0
LP_4	4	63.6	375	5.9
MP_4	4	68.7	394	5.7
NP_4	4	64.2	519	8.1
OP_5	5	76.0	725	9.5

The grammage ranged from 32.4 g/m^2 to 76.0 g/m^2. These values corresponded to a composition of the number of plies. The thickness and bulk values varied by 58% and 70%, respectively, due to the embossing type and the number of plies. Also, as can be seen in Table 1, an increase in the number of plies did not imply an increase in thickness and / or bulk. The highest bulk was found for the toilet paper (FP_2) with the low number of plies, the smallest grammage value, and the major thickness. On the other hand, the smallest bulk was found for a 4-ply toilet paper (MP_4), with the second largest grammage, and one of the thicknesses with the lowest value. This analysis reinforces the impact that the embossing operation has in the *z*-direction. Most of the lowest bulk values were found for the toilet papers with a higher number of plies, and this reveals that the final structure of the toilet paper is more compact, with a small expansion in the *z*-direction. Hermans *et al.* (2009) explain how the empty space between the different sheets on a toilet paper can be maximized by the way they are combined. The combination of the plies with deco and the micro embossing patterns, is where the greatest void volume is achieved, because between layers with the same embossing pattern, the voids are mainly due to the creping of each ply. The points of contact between them prevent the structure from collapsing when compressed or wet. This is in line with the results obtained.

The morphological characterization and the fiber distribution, by length weighted

in length and width, of the commercial toilet papers samples are presented in Table 2 and Fig. 3. Analyzing the different morphological characteristics revealed that all the toilet paper samples were composed mainly of short, hardwood fibers. These results are in agreement with those found in the literature (Niskanen 1998). As a complement to the information obtained in Table 2, Fig. 3 illustrates the percentages of the short and long fibers in the toilet paper samples. As expected, this small percentage of long fiber is used to improve the paper strength and machine runnability during the tissue paper production process.

The toilet paper CP_2 stood out from the others for its higher average value of width (23.2 μm) and coarseness (9.98 mg/100 m) of fibers. In addition, the CP_2 sample also had a notable width distribution, particularly above 30 μm (Fig. 3). The CP_2 sample was not the sample with the highest length distribution (>2000 μm); it can be inferred that the CP_2 paper was composed of some recycled fiber, which contributed to the sample's low Young's modulus value (0.95 MPa).

Table 2. Toilet Papers Morphological Characterization

	Length Weighted in Length (mm)		Width (μm)		Coarseness (mg/100 m)		Fines (% Area)	
Toilet Paper ID	$\bar{x}$	± σ	$\bar{x}$	± σ	$\bar{x}$	± σ	$\bar{x}$	± σ
AP_2	0.871	0.009	20.7	0.0	8.47	0.45	11.9	1.1
BP_2	0.889	0.003	20.0	0.2	8.82	0.34	13.0	0.8
CP_2	0.813	0.010	23.2	0.1	9.98	0.39	14.3	0.6
DP_2	0.745	0.003	19.9	0.1	7.93	0.09	15.4	0.4
EP_2	0.795	0.005	20.2	0.1	7.83	0.13	14.1	0.2
FP_2	0.862	0.007	19.8	0.1	9.00	0.34	13.9	0.6
GP_3	0.745	0.002	20.1	0.1	8.28	0.04	14.7	0.2
HP_3	0.761	0.009	20.2	0.1	8.53	0.07	14.0	0.3
IP_3	0.796	0.005	20.1	0.1	7.61	0.14	13.4	0.5
JP_3	0.878	0.011	20.8	0.1	9.31	0.94	12.4	1.2
KP_4	0.729	0.004	20.4	0.2	8.32	0.11	15.4	0.6
LP_4	0.840	0.001	21.6	0.1	9.00	0.04	13.4	0.2
MP_4	0.781	0.002	20.4	0.1	7.90	0.12	14.7	0.6
NP_4	0.754	0.007	20.4	0.1	7.86	0.03	14.8	0.4
OP_5	0.768	0.004	19.6	0.1	8.73	0.11	15.9	0.6

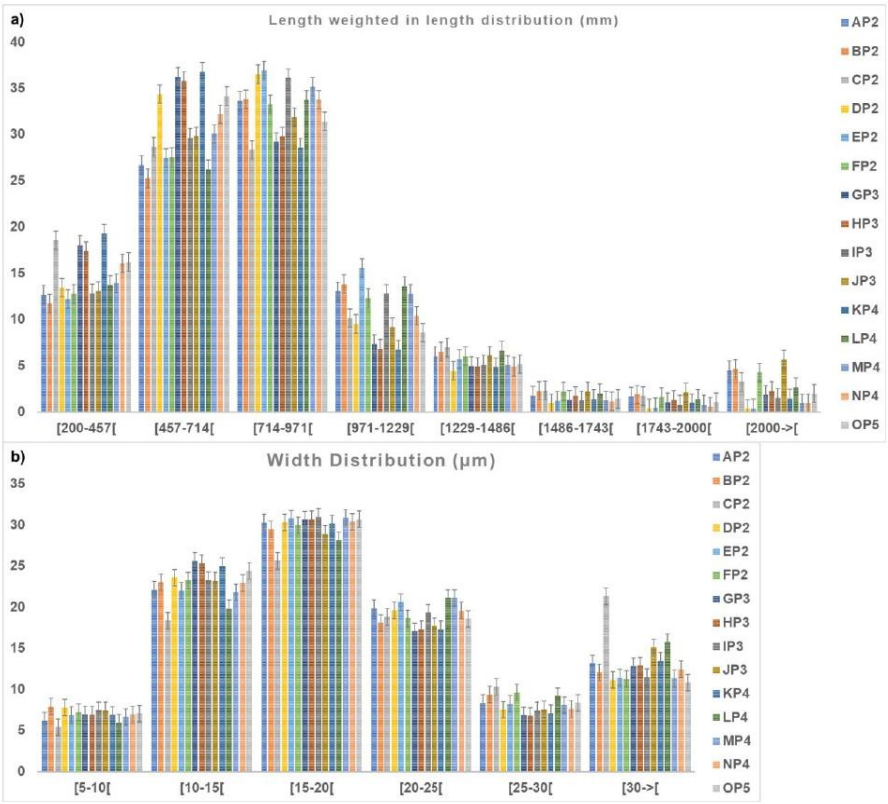

Fig. 3. The fiber distribution by a) length weighted in length (mm) and b) width (µm)

As shown in Table 3, the MP_4 paper had the highest perforation efficiency and the longest cut distance, at 79.4% and 4.92 mm, respectively. The DP_2 paper had the lowest perforation efficiency and the shortest cut distance, at 46.4% and 1.48 mm, respectively. In general, for papers with the same number of plies, a greater cut distance yielded a higher perforation efficiency. Of the studied papers, only the CP_2, DP_2, and EP_2 papers tore at other locations than the perforation, as mentioned above. These papers had the lowest cut distance, as did the AP_2 paper, which did not tear at the perforation. Although the AP_2 and CP_2 papers had the same cut distance (2.31 mm), they had different Young's modulus values of 1.38 MPa and 0.95 MPa, respectively. The CP_2 paper had the lowest Young's modulus value.

Table 3. The Perforation Efficiency and Cut Distance for the Toilet Paper Samples

Toilet Paper ID	Tensile Index (Nm/g)		Tensile Strength (N/m)	Perforation Efficiency (%)	Target Cut Distance (mm)	Cut Distance Measured (mm)		Blank Distance Measured (mm)	
	$\bar{x}$	$\pm\sigma$				$\bar{x}$	$\pm\sigma$	$\bar{x}$	$\pm\sigma$
AP_2C_2	**1.36**	0.08	**61.19**	**66.2**	**2**	**2.31**	0.07	**0.99**	0.07
AP_2C_0	**4.04**	0.23	**181.26**						
BP_2C_3	**2.65**	0.19	**98.96**	**65.1**	**3**	**2.98**	0.13	**1.04**	0.08
BP_2C_0	**7.61**	0.68	**283.69**						
CP_2C_2	**1.97**	0.25	**65.87**	**65.7**	**2**	**2.31**	0.09	**0.88**	0.08
CP_2C_0	**5.74**	0.32	**192.28**						
DP_2C_2	**2.90**	0.22	**106.25**	**46.4**	**2**	**1.48**	0.05	**1.06**	0.04
DP_2C_0	**5.42**	0.35	**198.22**						
EP_2C_2	**3.19**	0.22	**113.00**	**55.7**	**2**	**1.86**	0.06	**1.19**	0.11
EP_2C_0	**7.21**	0.25	**255.21**						
FP_2C_4	**1.75**	0.33	**56.72**	**79.3**	**4**	**3.99**	0.06	**1.03**	0.05
FP_2C_0	**8.45**	0.55	**273.65**						
GP_3C_3	**2.37**	0.17	**104.25**	**67.8**	**3**	**2.95**	0.05	**1.07**	0.07
GP_3C_0	**7.37**	0.37	**323.59**						
HP_3C_3	**2.67**	0.20	**116.61**	**63.2**	**3**	**2.93**	0.05	**1.08**	0.05
HP_3C_0	**7.28**	0.29	**317.24**						
IP_3C_4	**2.27**	0.16	**113.83**	**73.7**	**4**	**3.81**	0.19	**1.17**	0.12
IP_3C_0	**8.64**	0.33	**433.00**						
JP_3C_4	**1.68**	0.17	**88.53**	**75.5**	**4**	**3.87**	0.12	**0.99**	0.10
JP_3C_0	**6.87**	0.10	**361.17**						
KP_4C_3	**2.52**	0.18	**152.54**	**62.4**	**3**	**2.92**	0.04	**1.08**	0.05
KP_4C_0	**6.71**	0.30	**405.89**						

LP_4C_3	**2.61**	0.24	**165.94**	**67.9**	**3**	**2.96**	0.04	**1.04**	0.03
LP_4C_0	**8.13**	0.25	**517.01**						
MP_4C_5	**2.19**	0.15	**150.13**	**79.4**	**5**	**4.92**	0.14	**1.13**	0.16
MP_4C_0	**10.59**	0.36	**727.52**						
NP_4C_3	**2.35**	0.17	**150.83**	**69.6**	**3**	**2.89**	0.05	**0.93**	0.05
NP_4C_0	**7.73**	0.35	**496.37**						
OP_5C_4	**1.63**	0.20	**123.96**	**79.0**	**4**	**3.85**	0.07	**1.13**	0.05
OP_5C_0	**7.78**	0.41	**591.11**						

Figure 4 shows the representative images of the four cut distances that were obtained from the studied toilet papers.

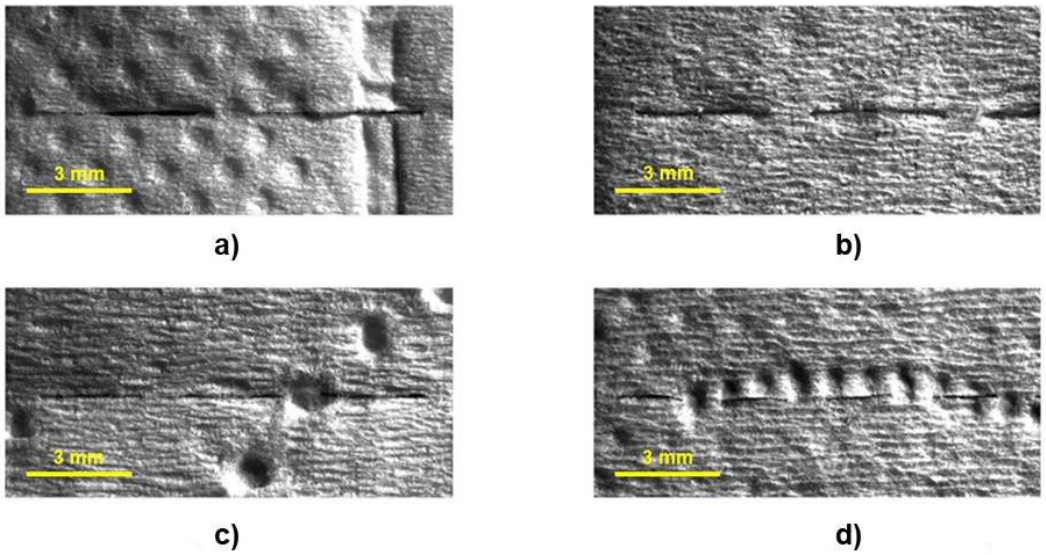

Fig. 4. Images of the a) C_5, b) C_4, c) C_3, and d) C_2 cut distances that were obtained with the customized optical system

During the perforation process, the blade passes through the paper sheet. The perforating blade becomes dull during the process because of its physical contact with the paper. This will cause incorrectly perforated or absent holes, so that when the user separates a sheet from the toilet paper roll, tearing is likely to go off the designated pattern of perforation, as illustrated in Fig. 5. The cellulose fibers are not cut but mashed and piled up at the bottom of the perforated hole. This layer of mashed fibers closes the back of the holes between the two services of the toilet paper. If the perforation is done with too much pressure, it can damage the bonding areas. These experiments are in line with the previous results of Gattuso (1989).

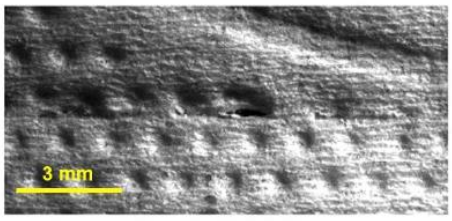

Fig. 5. Image of an incorrect perforation

The cutting efficiency (measured cutting distance) was compared to the target cutting distance if it was made with a perfect blade (without abrasion), as shown in Fig. 6.

As shown in Fig. 6, the cuts were effective despite some variability for the 2-ply samples. This variability can be justified by the low mechanical resistance of its structure, because of the reduced number of plies.

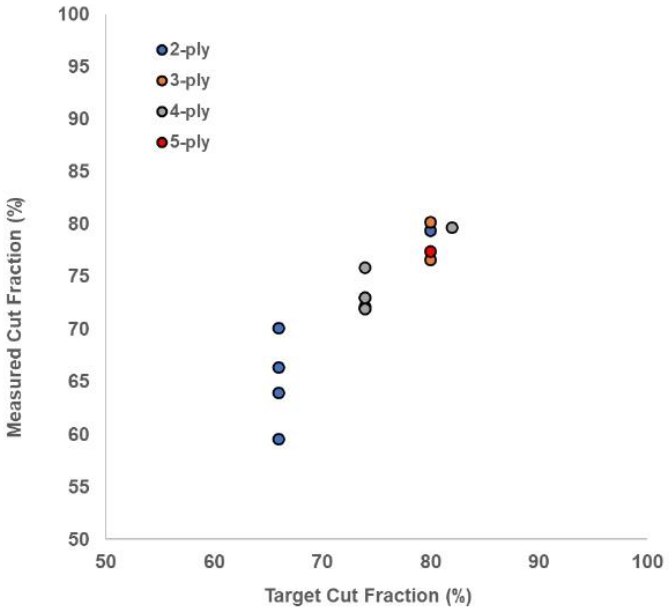

Fig. 6. Effectiveness of the cutting

Another important factor to understand is the perforation efficiency evolution with the measured cut fraction, as shown in Fig. 7.

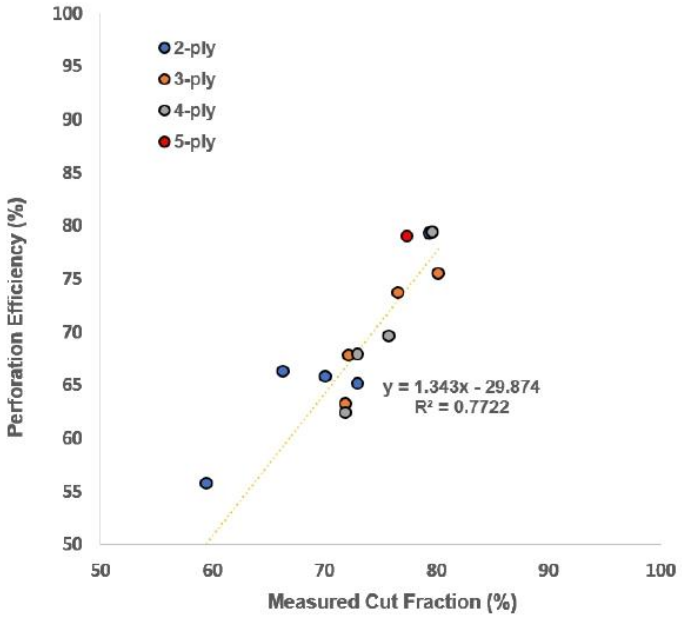

Fig. 7. Perforation efficiency against the measured cut fraction of the toilet papers

Figure 7 shows the impact that the cutting distance had on the perforation efficiency. Overall, the samples with a larger cutting distance had a greater perforation efficiency. As mentioned before, the 2-ply papers negatively influenced this correlation because the cutting distance was the smallest and some toilet papers had a tear at other location than perforation.

When holes were present, they effectively reduced the cross-sectional area. Instead of the full width, the resistant width was smaller. The nominal stress (N/m), which considered the load per unit width, is the ratio between the average maximum force of non-perforated papers $\bar{F}_{np}$ and the resistant length, as seen in Eq. 2,

$$\sigma_n = \frac{\bar{F}_{np}}{L - CD \times NH} \quad (2)$$

where σ_n is the nominal stress (N/m), $\bar{F}_{np}$ is the average maximum force of non-perforated papers (N), L is the resistant width (mm) of the tensile test samples, CD is the cut distance (mm), and NH is the average number of holes in the same test sample. Since the tensile strength of non-perforated paper is higher than that of perforated paper due to a smaller resistant width, it follows that the paper will tear along cross sections where holes are present. While this correctly calculates the average stress, it assumes that the stress between holes is uniform (and equal to the nominal stress). However, the stress field between holes is not uniform. It is well known that a hole will lead to a heterogeneous stress field around the geometrical discontinuity and this depends on the geometry of the hole (*i.e.* the ratio between the width and the hole diameter). Therefore, the geometry of the cut will influence the maximum stress near the hole. Stress concentrations describe the stress state at abrupt changes in geometry, where the stress field is non-uniform. Figure 8 shows the effect of the stress concentration where, analogous to lines of pressure in a fluid flow around an immersed body, lines of force (or "flow") around the holes become concentrated, where the absence of material is unable to transmit force.

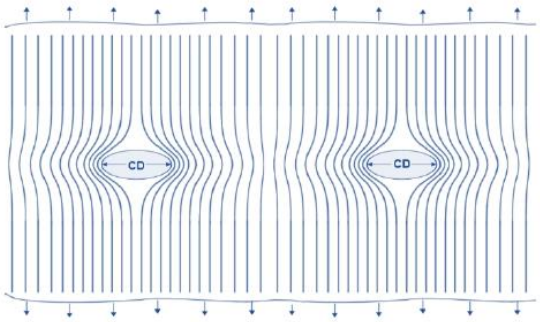

Fig. 8. Effect of stress concentration

A stress concentration factor (k) is applied to the nominal stress (σ_n) to calculate the maximum stress (σ_{max}), as seen in Eq. 3,

$$\sigma_{max} = k\,\sigma_n \quad (3)$$

When the stress at any location in the paper exceeds the paper's strength ($\overline{S}_p$), a tear is initiated and follows the line of highest stress, as seen in Eq. 4,

$$\sigma_{max} \geq \overline{S}_p \quad (4)$$

The resistant width is given by Eq. 5,

$$(L - CD \times NH) = L \times BD \times NH \quad (5)$$

where BD is the blank distance, which in this case is equal to 1.0 mm, and the stress concentration factor is given by Eq. 6:

$$k = \frac{\overline{S}_p}{\overline{F}_{np/NH}} \quad (6)$$

In Fig. 9, the stress concentration factor, calculated according to Eq. 5 based on the results presented in Table 3, is presented as function of the cut distance. The perforated papers that had a stress concentration above 0.11 were prone to tear at other location than perforation.

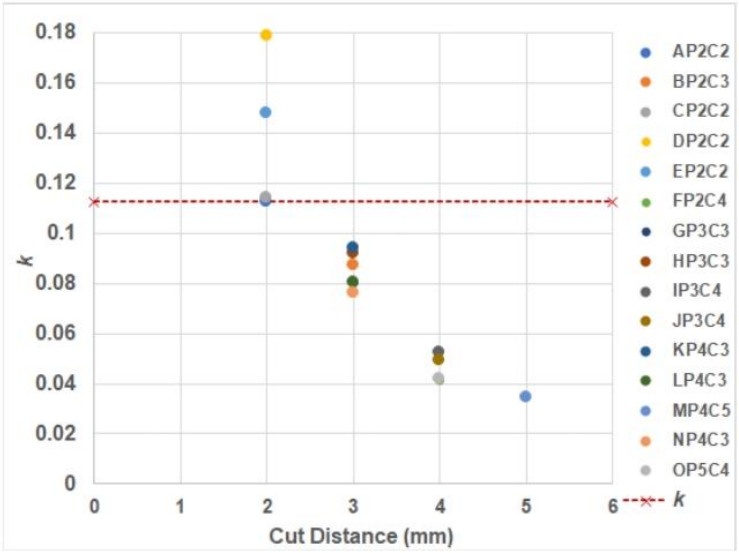

Fig. 9. Stress concentration factor (k) *vs.* the cut distance (mm)

The red line in Fig. 9 illustrates the stress concentration limit of 0.11. The AP_2 toilet paper is the limiting case in this set of samples, as it is on the red line. The papers below the red line tear at the perforation, as they were supposed to.

More accurate solutions can be obtained by Finite Element Methods (FEM), where analytic solutions are not possible with complex geometries. Considering the elliptic dimensions mentioned in the Numerical Model section, the software calculates the von-Mises stress field.

In Fig. 10, the colored scale shows the regions in red that correspond to higher equivalent von-Mises stress. The blue regions are the lower equivalent von-Mises stresses, equal to the nominal stresses present in non-perforated stresses. As the cut distance increased, the region of stress heterogeneity became wider due to a sharper geometry. Hence, the transition from higher stresses to lower stresses is cushioned. In Figs. 10a, 10b, 10c, and 10d, the material was less rigid. This transition from higher stresses to lower stresses was also more softened when compared to a stiffer material (Figs. 10e, 10f, 10g, and 10h). Furthermore, for higher cut distances for the regions of higher stress (in red) were visible, which indicates that this paper will preferably cut on this perforated region.

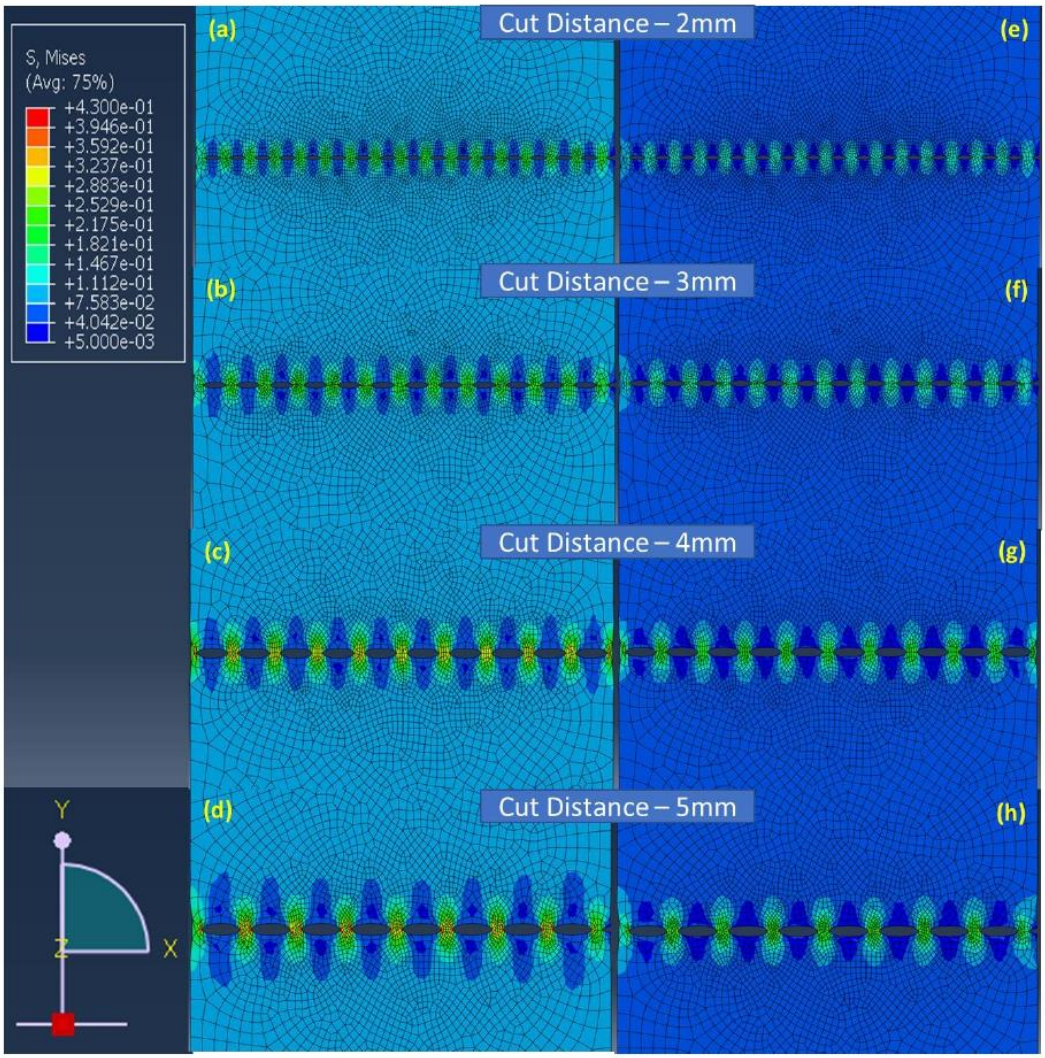

Fig. 10. The von-Mises Stress fields where the tear at perforation of the AP_2 paper is represented by a), b), c), and d) at the cut distances of 2, 3, 4, and 5, respectively. The tear at perforation of the CP_2 paper is represented by e), f), g), and h) at the cut distances of 2, 3, 4, and 5, respectively.

CONCLUSIONS

1. In this work, 15 commercial toilet papers from different European suppliers with various numbers of plies and cut distance were selected. The morphological analysis of the papers revealed that they present several fibrous compositions that resulted in different mechanical responses.
2. An optical method was used to measure the cut distance, the blank distance, and the quality of the perforation for the toilet paper samples.
3. In general, the cut distance had a great influence on the result of the perforation efficiency. The sample with the highest cut distance (4.92 mm) also had the greatest

perforation efficiency (79.4%). It was also determined that a cut distance of 2.0 mm should not be used in this type of paper, in order to minimize the tearing of the paper away from the perforation.

4. The toilet paper samples with a stress concentration factor above 0.11 experienced tear at other locations than at the perforation. The toilet paper samples with a stress concentration factor below 0.11 tore at the perforation.
5. The FEM analysis revealed that the region of stress heterogeneity became wider due to a sharper geometry, as the cut distance increased. Moreover, regions of higher stress were visible for the upper cut distance, which indicated that the paper will preferably cut on this perforated region.

ACKNOWLEDGMENTS

The authors gratefully acknowledge the funding of this work that was carried out under the Project InPaCTus – Innovative products and technologies from eucalyptus, Project No. 21874 funded by Portugal 2020 through European Regional Development Fund (ERDF) in the frame of COMPETE 2020 nº246/AXIS II/2017.

The authors also acknowledge UID Fiber Materials and Environmental Technologies (FibEnTech-UBI) on extent of the project UIDB/00195/2020, funded by the Fundação para a Ciência e a Tecnologia (FCT).

REFERENCES CITED

Baggot, J. L., Gropp, R. F., and Wojcik, S. (2006). "System and method for severing or perforating a web," U. S. Patent No. 20060014616.

Bennett, H. (2009). "Ever wondered about the history of toilet paper?" *Washington Post* (https://www.washingtonpost.com/wp-dyn/content/article/2009/05/31/AR2009053102217_2.html), Accessed 14/01/2019.

Carvill, J. (2015). *Mechanical Engineer's Data Handbook*, Butterworth Heinemann, Oxford, United Kingdom.

de Assis, T., Reisinger, L. W., Pal, L., Pawlak, J., Jameel, H., and Gonzalez, R. (2018). "Understanding the effect of machine technology and cellulosic fibers on tissue properties - A review," *BioResources* 13(2), 4593-4629. DOI: 10.15376/biores.13.2.DeAssis

Gattuso, C. F. (1989). "Laser perforation for computer paper," Rochester Institute of Technology, Rochester, NY, USA.

Hendrickson, R. (2000). *The Facts on File dictionary of American Regionalisms*, Facts on File, New York, NY.

Hermans, A., Perkins, J., Ko, Y., Kainth, A., Boudrie, L., Baggot, J., and Smith, M. (2009). "Multiple ply tissue products having enhanced interply liquid capacity," Neenah, WI, U. S. Patent No. 7,524,399 B2.

ISO 12625-3 (2014). "Tissue paper and tissue products – Part 3: Determination of thickness, bulking thickness and apparent bulk density and bulk," International Organization for Standardization, Geneva, Switzerland.

ISO 12625-6 (2005). "Tissue paper and tissue products – Part 6: Determination of

grammage," International Organization for Standardization, Geneva, Switzerland.
ISO 12625-12 (2010). "Tissue paper and tissue products – Part 12: Determination of tensile strength of perforated lines – Calculation of perforation efficiency," International Organization for Standardization, Geneva, Switzerland.
ISO 187 (1990). "Paper, board and pulps — Standard atmosphere for conditioning and testing and procedure for monitoring the atmosphere and conditioning of samples." International Organization for Standardization, Geneva, Switzerland.
Mendes, A. O., A., Fiadeiro, P. T., Costa, A. P., Amaral, M. E., and Belgacem, M. N. (2013). "Retro-diffusion and transmission of laser radiation to characterize the paper fiber distribution and mass density," in: *Proceedings Volume 8785: 8th Ibero American Optics Meeting and 11th Latin American Meeting on Optics, Lasers, and Applications*, Porto, Portugal.
Mendes, A. O., A., Fiadeiro, P. T., Costa, A. P., Amaral, M. E., and Belgacem, M. N. (2014). "Study of repeatability of an optical laser system for characterization of the paper fiber distribution and mass density," in: *Proceedings Volume 9286: Second International Conference on Applications of Optics and Photonics*, Aveiro, Portugal.
Mendes, A. O., Fiadeiro, P. T., Costa, A. P., Amaral, M. E., and Belgacem, M. N. (2015). "Laser scanning for assessment of the fiber anisotropy and orientation in the surfaces and bulk of the paper," *Nordic Pulp & Paper Research Journal* 30(2), 308-318. DOI: 10.3183/npprj-2015-30-02-p308-318
Niskanen, K. (1998). *Papermaking Science and Technology Bookseries: Volume 16-Paper Physics*, Fapet Oy, Helsinki, Finland.
Paulapuro, H. (2000). *Papermaking Science and Technology Bookseries: Volume 18-Paper and Board Grades*, Fapet Oy, Helsinki, Finland.
Schulz, G., and Gracyalny, D. T. (1998). "Method and apparatus for pinch perforating multiply web material," U. S. Patent No. 5755654.
Wheeler, S. (1894). "Wrapping or toilet paper," U. S. Patent No. 511983.

Article submitted: December 20, 2020; Peer review completed: March 27, 2021; Revised version received and accepted: March 31, 2021; Published: May 13, 2021.
DOI: 10.15376/biores.16.3.4846-4861

Chapter 5 – Conclusions

1. Main Achievements

The research and development of the tissue industry are now focused on understanding how the converting machine affects tissue paper properties, in order to optimize operating conditions to obtain the best quality products at the lowest cost. Contrary to the tissue paper machine, there is less information available regarding the converting operations. Thus, the research presented here proves to be of extreme importance and relevance for a better understanding of the processes involved in the transformation of tissue paper and how they impact on its properties. The major findings of this thesis are divided into four levels as follows:

- ✓ Development of a laboratorial embossing system
- ✓ Impact of the embossing process on tissue paper products
- ✓ Development of a laboratorial perforation system
- ✓ Perforation efficiency evaluation

1.1 Development of a laboratorial embossing system

The laboratorial embossing system has proved to be a versatile system, as it allows the use of various types of rubbers with different hardness, testing all types of patterns intended to be engraved on the steel plates, controlling the process parameters both individually and combined, the use of different types of paper/cardboard, both industrial and laboratory, and from the prototypes produced, it allows the evaluation of their papermaking properties. As the results obtained with this laboratorial system do not depend on the equipment operator, high repeatability, and reproducibility with low dispersion of results were achieved.

1.2 Impact of the embossing process on tissue paper products

The first three works made it possible to optimize the operating conditions of the developed laboratorial embossing system. The first work allowed to conclude that there is an optimal pressure of 2.8 bar for the embossing process, in which the mechanical strength is maximized without losing much of the softness value. The effect of pressure when densifying the paper sheet gives it a gain in mechanical strength, but without showing great differences in terms of liquid absorption. The two embossing patterns presented different behaviors, the micro pattern being the one that most affected the structure of the paper sheet, both in terms of structural properties and in terms of mechanical strength. On the other hand, softness is more affected by the deco pattern. For both embossing patterns, there was a loss of mechanical properties and softness with the embossing process. This work also allowed to verify that the greater or lesser loss of mechanical properties or softness depends on the fibrous composition of each sample. The second work led to the conclusion that the best solution to obtain maximum softness is the

use of rubber rollers with an inner layer of low hardness and an outer layer of high hardness, which agrees with the results obtained for the 2-ply prototype. 60_48 Sh-A. The results obtained also point to an increase in softness with increasing rubber hardness, while the mechanical property losses and bulk gain are more pronounced for lower rubber hardness and for the micro embossing pattern. The third work, which focuses on the study of the impact of the finishing geometry of the line and dots (straight or round) of the 3D steel plates in the embossing process, allowed to conclude that although the plates individually present a higher HF value for straight finish, in the 2-ply prototype the greatest softness was obtained for the prototype with round finish geometry. Also, for individually engraved plates, it was found that the HF value decreases with increasing bulk, being more accentuated for the micro pattern. As the embossing process was carried out under ideal operating conditions for this laboratory system, in relation to the mechanical properties the losses were minimal, having been slightly higher for the micro pattern. It was also concluded that there are no marked differences in the dispersion kinetics of liquid droplets over time. For the four types of steel plate finishing's, the area occupied by the drops and their shapes were very similar. The only parameter that presents some differences is the "Ratio" of the shape assumed by the drops, which revealed a more pronounced ellipse for the tissue paper sample engraved with the patterns with a round finishing. Thus, it was found that the finishing geometry of the plates does not affect the absorption kinetics of this type of tissue products.

The flexibility of this laboratorial embossing system allowed further studies to be carried out. The first additional study was to compare embossing on industrial sheets and handsheets. This work showed that embossing has a negative impact on mechanical properties and a high increase in bulk, this effect being more pronounced with the micro embossing pattern. The effect of the presence of long fiber in the samples translates into a gain in tensile strength. It was also verified that the creping operation gives to the industrial paper a high elongation capacity, being practically non-existent in handsheets. Furthermore, due to this operation, industrial samples have a higher apparent porosity than handsheets samples. From the comparison between the two types of handsheets (100% hardwood and a mixture of hardwood and softwood), the handsheet with 100% eucalyptus composition presents greater softness, but lower mechanical strength than the other with a mixture of fibers. The industrial and handsheets samples with the same fibrous composition showed similar TSA softness results, except for the flexibility parameter D due to the creping process. Another additional study carried out is related to the impact of embossing on the absorption of this type of paper. The base tissue papers were produced on the same industrial tissue paper machine under the same conditions and similar fibrous compositions. It was concluded that the embossing operation substantially increased the thickness and consequently the bulk of the toilet papers. In addition, the embossing operation had no relevant implication on the water absorption time, because when comparing the base tissue papers with their respective toilet papers, they showed similar values with small variations within the standard deviations. However, the embossing operation had a great impact on the water absorption capacity, promoting water absorption, due to the

increase in bulk. Thus, with the embossing operation, the bulk increased by more than 150%, resulting in an increase in water absorption capacity above 60%. A last additional study was carried out related to the stacking sequence on an odd-numbered toilet paper. In this study, two configurations were used on a 5-ply paper, where the deco:micro ratio was 3:2 and 2:3 for configurations 1 and 2, respectively. For both configurations, the thickness and volume of the toilet papers increased due to the embossing process. As in the previous study, the water absorption times were similar without notable variation, so the embossing process had little impact on these values. While bulk increased by 46% and 40% for configurations 1 and 2, water absorption capacity increased by 2% and 17% for configurations 1 and 2, respectively. Therefore, the stacking sequence of the finished toilet paper sheets influenced the water absorption capacity. The tensile index, maximum strain and Young's modulus decreased considerably due to the embossing process, where configuration 1 had smaller losses in tensile index and maximum strain. However, configuration 1 had a greater Young's modulus loss than configuration 2. The negative impact on mechanical properties was greater for the deco pattern than for the micro in both configurations. This study found that the stacking sequence of sheets on finished toilet papers influenced their final characteristics. For commercial purposes and to meet end-user toilet paper preferences, configuration 1 was more suitable for mechanical strength and configuration 2 was more suitable for absorbency.

Finally, for all studies, simulations using the finite element method (FEM) allowed a better understanding of how the embossing process impacts the mechanical strength properties of the final tissue products with the variation of operating conditions (pressure, rubber hardness and finishing geometry of the engraved steel plates pattern). Through FEM, it was possible to corroborate the results obtained experimentally, obtaining the same trends and evolutions. Thus, the FEM proved to be a reliable tool to simulate the embossing process for the paper industry and predict the final mechanical characteristics of the paper. The computational results contribute to the understanding of how the shape pattern used in the embossing process affects the stress field of the paper and the final mechanical properties of the paper such as paper strength. Furthermore, this tool makes it possible to optimize process parameters in a virtual environment, thus avoiding an expensive trial-error approach. In the end, it is essential to make a compromise between the different properties in order to obtain a final product of excellent quality.

1.3 Development of a laboratorial perforation system

The laboratory perforation system proved to be a small, light, portable and low-cost system. In addition, it proved to be a versatile system, as it allows the use of various types of cutting blades (straight or patterned) that can be adapted to the type of perforation desired (desired cut distance). It also allows its use in various types of paper, namely tissue paper. As the results obtained with this laboratory system depend on the operator of the equipment (pressure applied to the perforation blade), in order to achieve high repeatability and reproducibility with low dispersion of results, the same operator must always carry out a particular study.

1.4 Perforation efficiency evaluation

Maximum perforation efficiency was obtained for a laboratory cut distance of 6 mm, which corresponds to an industrial cut distance of 5 mm. This study allowed us to determine what causes the greatest impact on perforation efficiency, reaching the conclusion that it is related to the dimensions of the perforation cuts and not to the fibrous composition and/or number of sheets that make up the toilet paper samples. This laboratory approach, in order to simulate industrial perforation and potentially explain the perforation behavior in the converting machine, requires the use of a perforation blade with a cut distance 15% greater than the industrial cut distance. From the analysis of 15 commercial toilet papers, it was found that samples of toilet paper with a stress concentration factor above 0.11 suffered tears outside the perforation line, what corresponds to a cut distance equal to or less than 2.0 mm. All other toilet paper samples with stress concentration factor below this limit of 0.11 tore at the perforation line. The results obtained through the simulation analysis using- finite element method (FEM) support the idea that the value of the perforation efficiency tends to an establishment from a specific cut distance of 6 mm. Through the FEM analysis, it was also possible to verify that the region of stress heterogeneity became wider due to a clearer geometry, as the cut distance increased. In addition, regions of higher stress were visible at higher cut distances, indicating a preferential cut in the perforated region.

2. Contribution of the Study

An in-depth understanding of the mechanisms of the embossing operation, allowed to optimize its operating conditions and consequently improve the properties of the final tissue products. Through extensive material characterization, an optimum pressure, rubber hardness and finishing geometry of the embossing patterns were achieved, indicating the trends that are in line with the maximization of the intended properties. Studies related to tissue paper embossing may directly impact the industry, enabling the improvement of final products. The industry will be able to achieve this by implementing small changes to the process, such as operating the converting machine at the optimum pressure in which the mechanical tensile strength is maximized, replacing the single hardness rubber counter-roll with one of variable hardness and preferably use a round embossing pattern finishing geometry. The embossing laboratory system developed will also help the industry, allowing studies to be carried out on new embossing patterns and how they affect paper properties, on a reduced scale and at a lower cost.

Regarding the performance of the perforation operation and the evaluation of perforation efficiency, based on the results achieved, it is possible to help the industry in avoiding this type of paper to tear outside the perforation line. For this, the industry should not use cut distances of less than or equal to 2 mm in this operation, with the optimized industrial cut distance being 5 mm. The 5 mm cut distance will be the best option for the producer as it is the point where the perforation efficiency is optimal. The laboratory perforation system could also assist the industry by testing new perforation patterns different from the straight ones currently used or

evaluate perforation in existing products that are object of complaints, in that way reducing costs.

For both studied operations, digital twining using finite element models, by being able to reproduce numerically the same mechanisms of deformation and geometries that occur industrially, proved to be an equally useful tool to find trends in process variables without having to run it experimentally.

3. Directions of Future Research

At the level of the laboratorial embossing system, it would be interesting to proceed to the next stage, developing a small pilot laboratory machine that operates in continuous mode and with embossing and rubber rollers instead of plates.

Regarding the operating conditions of the embossing, it would also be interesting to study the impact of temperature and humidity on the papermaking properties of this type of products, since they are environmental conditions that are not controlled in the manufacturing facilities and that may have decisive impacts. As a suggestion, these studies could be carried out by heating the plates (embossers and rubbers) at different temperatures, later evaluating their impact; and placing the paper sheets in an environmental chamber at different humidity percentages or in a desiccator with a saturated atmosphere at different times and measuring the amount of water absorbed, subsequently evaluating its impact.

Since no studies were found regarding the mechanical impact of the packaging and palletizing section on the final properties of the finished products, it would also be interesting to do some studies regarding this section.

Appendix

Appendix A – Additional Studies

A1. Article X – Experimental dataset supporting the physical and mechanical characterization of industrial base tissue papers

Vieira, J.C., Mendes, A.D.O., Carta, A.M., Fiadeiro, P.T., Costa, A.P.
Data in Brief, 2020, 33, 106434
https://doi.org/10.1016/j.dib.2020.106434

Article X is a date article. It presents a compilation of untreated results from characterizing the structural, physical and mechanical properties of 13 hygienic industrial base tissue papers. This article served as a basis for the studies previously presented, allowing to complement the other results obtained and making it possible to draw certain conclusions.

The overall contribution in Article X of Joana Costa Vieira was 75% to the concept development, analysis, drafting and revising the final submission; António de Oliveira Mendes contributed 10% with the TSA analysis, drafting and revising the final submission; Ana Margarida Carta, Paulo Torrão Fiadeiro and Ana Paula Costa contributed in reviewing, editing, and providing important technical inputs by 5%, respectively.

A2. Article XI – Characterization of absorbency properties on tissue paper materials with and without “deco” and “micro” embossing patterns

Morais, F.P., **Vieira, J.C.**, Mendes, A.O., Carta, A.M., Costa, A.P., Fiadeiro, P.T., Curto, J.M.R., Amaral, M.E.
Cellulose, 2022, 29(1), pp. 541–555
https://doi.org/10.1007/s10570-021-04328-1

The Article XI was created to understand better how the embossing operation acted on different types of tissue paper sheets (industrial and handsheets) on absorbency final property and a complementary study to the one presented in Article V. This study made it possible to verify that the creping effect has a greater influence on the structural properties and liquid absorption capacity in relation to the fiber mixture. The inverse was also verified for the Klemm capillary rise properties and scattering kinetics of the liquid, being dependent on the crepe wave alignment. The developed laboratory embossing system, proved to be a useful tool for this study. On the other hand, the optical system proved to be very useful auxiliary tools for a better understanding of the effects that occurred in this study.

The overall contribution in Article XI of Joana Costa Vieira was 20% to the analysis, drafting and revising the final submission; Flávia Morais contributed 50% concept development, analysis, drafting and revising the final submission; António de Oliveira Mendes contributed 15% with the optical system data, drafting and revising the final submission; Ana Margarida Carta, Joana Curto, Mª Emília Amaral, Paulo Torrão Fiadeiro and Ana Paula Costa contributed in reviewing, editing, and providing important technical inputs by 3%, respectively.

A3. Article XII – Influence of Tissue Paper Converting Conditions on Finished Product Softness

Mendes, A.O., **Vieira, J.C.**, Carta, A.M., Galli, E., Simões, R.S., Silva, M.J.S., Costa, A.P., Fiadeiro, P.T.
BioResources, 2020, 15(3), pp. 7178–7190
https://doi.org/10.15376/biores.15.3.7178-7190

Another important and complementary study to the one presented in Article VII is presented in Article XII and reports the impact on the softness final property of the stacking sequence in a tissue finished product with an odd number of plies. This study made it possible to verify that in a 5-ply toilet paper, having 2 or 3 sheets in the deco embossing and the rest in the micro embossing, had a different impact on the final softness of the tissue product, so corroborate that is another factor to consider when producing these types of products.

The overall contribution in Article XII of Joana Costa Vieira was 20% to the analysis, drafting and revising the final submission; António de Oliveira Mendes contributed 50% with the concept development, optical system data, drafting and revising the final submission; Ana Margarida Carta, Enrico Galli, Rogério Simões, Manuel Santos Silva, Paulo Torrão Fiadeiro and Ana Paula Costa contributed in reviewing, editing, and providing important technical inputs by 5%, respectively.

Data in Brief 33 (2020) 106434

Contents lists available at ScienceDirect

Data in Brief

journal homepage: www.elsevier.com/locate/dib

Data Article

Experimental dataset supporting the physical and mechanical characterization of industrial base tissue papers

Joana C. Vieira[a,*], António de O. Mendes[a], Ana M. Carta[b], Paulo T. Fiadeiro[a], Ana P. Costa[a]

[a] Fibre Materials and Environmental Technologies Research Unit (FibEnTech-UBI), Universidade da Beira Interior, Rua Marquês d'Ávila e Bolama, Covilhã 6201-001, Portugal
[b] Forest and Paper Research Institute (RAIZ), R. José Estevão, Eixo, Aveiro 3800-783, Portugal

ARTICLE INFO

Article history:
Received 26 August 2020
Revised 8 October 2020
Accepted 14 October 2020
Available online 20 October 2020

Keywords:
Industrial base tissue paper
Fiber morphology
Structural properties
Mechanical characterization
Absorption capacity
Tissue softness

ABSTRACT

Tissue paper is defined by its physical and mechanical properties, namely: high softness, low grammage, high bulk and high liquid absorption capacity. It is expected that the production of tissue paper will continue to grow, which increases the importance of better understanding the processes involved in its production as well as its optimization [1]. The experimental data presented in this article, are the physical-mechanical characterization of a group of 13 industrial base tissue papers, which were collected at the end of the tissue paper machine on Portuguese factories. These samples vary in grammage, composition and creping [2], enabling a later evaluation of the crepe type [3] and its relationship with the final properties of the tissue paper.

* Corresponding author.
E-mail address: joana.costa.vieira@ubi.pt (J.C. Vieira).

https://doi.org/10.1016/j.dib.2020.106434

Specifications Table

Subject	Materials Science (General)
Specific subject area	Industrial Base Tissue Paper
Type of data	Tables
How data were acquired	MorFi® analyzer (morphological analysis), ISO standards methods, AccuPyc® II 1340 helium pycnometer (porosity analysis), TSA - Tissue Softness Analyzer (softness analysis)
Data format	Raw and Analyzed data
Parameters for data collection	13 industrial base tissue papers with different grammages were obtained *in situ* on Portuguese factories
Description of data collection	Techpap MorFi® analysis was performed to determine the industrial base paper morphology. Papers grammage, thickness and bulk were measured using paper tissue standards ISO 12625-6 and ISO 12625-3 respectively. The porosity was determined using a Micromeritics AccuPyc® II 1340 helium pycnometer. The absorption capacity was measured according to ISO 12625-8 applying the immersion method. Tensile tests were done in machine and cross directions (MD and CD) according with ISO 12625-4. Handfeel, real softness, smoothness/roughness, and stiffness were measured using the Emtec TSA - Tissue Softness Analyzer. All these determinations were done at 23°C and 50% humidity (ISO 187).
Data source location	FibEnTech - Fiber Materials and Environmental Technologies Research Unit, Universidade da Beira Interior (UBI), Covilhã, Portugal RAIZ - Forest and Paper Research Institute, Eixo, Aveiro, Portugal
Data accessibility	With the article

Value of the Data

- The data are relevant in tissue paper materials research to obtain premium tissue paper materials.
- These data allow to evaluate the relationship between the final properties of the paper and the raw material.
- These data allow to evaluate the relationship between the raw material and the type of crepe obtained with a specific creping angle and blade.
- These data could make an important impact in the industrial production of tissue paper.

1. Data Description

In this article are presented the mean values and the standard deviations for all the measured data for the characterization of 13 industrial base tissue papers (identified from A to M) of different Portuguese factories. In Table 1 is showed the data of grammage, thickness and bulk for all the industrial base tissue papers. The morphological data for all the industrial base tissue papers, which is available in Tables 2 and 3, correspond to the number of fibers, length, width, coarseness, kink, curl, broken ends, and fines. Table 4 presents the results of the measured data in the porosity tests for all the industrial base tissue papers and the calculated apparent porosity [4]. The obtained data for water absorption time and water absorption capacity are shown in Table 5. In Tables 6 and 7 are listed the mechanical properties measured (tensile tests) in the machine direction (MD) and cross direction (CD) for all the industrial base tissue papers. The properties are the force, strength, tensile index, elongation at break, and Young modulus. Finally, the handfeel tests results (*HF*) and the corresponding TSA parameters, in particular, real softness/ fiber stiffness (*TS7*), paper surface roughness (*TS750*), frequency (*fTS750*), paper stiffness (*D*), plasticity (*P*), hysteresis (*H*), and elasticity (*E*) for all the industrial base tissue papers on top (Yankee side), bottom (Hood side), and globally are found in Tables 8,9,10,11 and 12. All

Table 1
Mean values and standard deviations of the grammage, thickness and bulk tests data for all the industrial base tissue papers.

	Grammage (g/m^2)		Thickness (μm)		Bulk (cm^3/g)	
Base paper	$\bar{x}$	$\pm\sigma$	$\bar{x}$	$\pm\sigma$	$\bar{x}$	$\pm\sigma$
A	19.1	0.1	121.0	2.1	6.33	0.10
B	18.8	0.2	137.8	4.4	7.32	0.26
C	16.2	0.2	122.9	1.5	7.58	0.10
D	17.2	0.1	113.0	1.2	6.55	0.07
E	15.8	0.1	113.3	0.9	7.16	0.06
F	16.3	0.2	126.2	1.9	7.74	0.10
G	15.7	0.3	116.2	2.7	7.41	0.25
H	15.8	0.2	116.3	2.7	7.37	0.24
I	15.7	0.3	110.0	2.4	7.03	0.22
J	16.0	0.3	112.5	0.7	7.09	0.14
K	16.0	0.4	110.7	1.9	6.89	0.26
L	17.5	0.2	126.7	1.3	7.25	0.09
M	17.3	0.2	131.4	2.3	7.62	0.11

Table 2
Mean values and standard deviations of the morphology test data for all the industrial base tissue papers.

	Fibers (million/g)		Length weighted in length (mm)		Width (μm)		Coarseness (mg/100 m)	
Base paper	$\bar{x}$	$\pm\sigma$	$\bar{x}$	$\pm\sigma$	$\bar{x}$	$\pm\sigma$	$\bar{x}$	$\pm\sigma$
A	18.0	1.1	0.850	0.007	19.5	0.1	8.04	0.00
B	14.7	0.2	0.930	0.004	20.8	0.2	9.47	0.00
C	16.7	0.2	0.860	0.006	20.1	0.1	8.80	0.00
D	14.7	0.2	0.930	0.004	20.8	0.2	9.47	0.00
E	16.8	0.4	0.862	0.010	20.0	0.1	8.73	0.26
F	17.4	0.2	0.859	0.002	20.3	0.3	8.48	0.12
G	18.1	0.5	0.814	0.006	19.4	0.1	8.32	0.25
H	18.3	0.5	0.812	0.005	19.4	0.1	8.22	0.21
I	21.2	0.3	0.733	0.005	19.6	0.1	7.87	0.09
J	20.4	0.3	0.742	0.002	19.6	0.1	8.11	0.11
K	20.8	0.1	0.732	0.001	19.8	0.1	8.04	0.06
L	22.4	0.1	0.740	0.001	19.3	0.0	7.14	0.03
M	17.3	0.2	0.784	0.003	20.7	0.1	9.25	0.06

Table 3
Mean values and standard deviations of the morphology test data for all the industrial base tissue papers.

	Kink fibers (%)		Curl (%)		Broken ends (%)		Fines (% area)	
Base paper	$\bar{x}$	$\pm\sigma$	$\bar{x}$	$\pm\sigma$	$\bar{x}$	$\pm\sigma$	$\bar{x}$	$\pm\sigma$
A	40.1	0.2	9.2	0.0	23.2	0.3	14.1	0.1
B	43.7	0.2	10.0	0.0	26.8	0.3	14.3	0.3
C	47.9	0.6	10.2	0.0	24.8	0.2	16.1	0.7
D	43.7	0.2	10.0	0.0	26.8	0.3	14.3	0.3
E	130.8	0.3	10.1	0.0	25.3	0.1	14.7	0.1
F	130.7	0.2	10.4	0.0	26.3	0.9	16.1	0.9
G	48.7	0.6	10.3	0.1	23.4	0.4	15.3	0.4
H	48.0	0.6	10.2	0.0	22.7	0.4	14.5	0.5
I	50.7	0.5	11.3	0.1	23.6	0.5	15.8	0.2
J	50.7	0.2	11.2	0.1	24.0	0.5	16.0	0.3
K	50.2	0.3	11.2	0.1	25.0	0.4	15.9	0.2
L	45.6	0.2	9.8	0.1	22.6	0.1	13.9	0.1
M	48.4	0.2	10.3	0.0	26.3	0.4	14.4	0.1

Table 4
Mean values and standard deviations of the porosity tests data for all the industrial base tissue papers and the results of the apparent porosity.

Base paper	Porosity (%)		Apparent Porosity (%)
	$\bar{x}$	$\pm\sigma$	
A	91.6	0.0	89.7
B	90.9	0.0	91.1
C	92.2	0.0	91.5
D	90.8	0.0	90.6
E	93.9	0.0	90.9
F	89.1	0.0	91.7
G	95.7	0.0	91.2
H	95.7	0.0	91.1
I	90.1	0.0	90.7
J	90.9	0.0	90.8
K	90.3	0.0	90.6
L	90.8	0.0	91.1
M	91.3	0.0	92.3

Table 5
Mean values and standard deviations of the water absorption time and water absorption capacity tests data for all the industrial base tissue papers.

Base paper	Water Absorption Time (s)		Water Absorption Capacity (g/g)	
	$\bar{x}$	$\pm\sigma$	$\bar{x}$	$\pm\sigma$
A	4.688	0.420	6.862	0.310
B	4.644	0.370	7.573	0.310
C	3.969	0.030	8.173	0.090
D	4.272	0.450	7.990	0.160
E	4.895	0.510	7.636	0.170
F	4.158	0.640	8.180	0.390
G	4.852	0.060	9.007	0.190
H	4.856	0.070	8.642	0.270
I	4.606	0.060	7.850	0.130
J	4.262	0.410	7.908	0.170
K	4.727	0.510	7.883	0.210
L	4.641	0.400	7.436	0.090
M	4.852	0.510	8.614	0.250

Table 6
Mean values and standard deviations of the tensile tests data (MD and CD) for all the industrial base tissue papers.

	Force (N)				Strength (N/m)				Tensile Index (Nm/g)			
	MD		CD		MD		CD		MD		CD	
Base paper	$\bar{x}$	$\pm\sigma$	$\bar{x}$	$\pm\sigma$	$\bar{x}$	$\pm\sigma$	$\bar{x}$	$\pm\sigma$	$\bar{x}$	$\pm\sigma$	$\bar{x}$	$\pm\sigma$
A	14.19	1.00	8.80	0.30	0.284	0.020	0.176	0.006	14.86	1.04	9.21	0.32
B	10.52	1.06	6.48	0.23	0.210	0.021	0.130	0.005	11.19	1.12	6.89	0.24
C	8.71	0.45	4.40	0.23	0.175	0.009	0.088	0.005	10.62	0.55	5.37	0.28
D	9.82	0.33	4.78	0.18	0.196	0.007	0.095	0.004	11.69	0.40	5.68	0.21
E	8.60	0.60	4.37	0.29	0.172	0.012	0.087	0.006	10.68	0.74	5.43	0.36
F	8.95	0.64	4.22	0.20	0.179	0.013	0.084	0.004	10.98	0.80	5.17	0.24
G	7.96	0.72	3.94	0.13	0.159	0.014	0.079	0.003	10.14	0.92	5.02	0.16
H	7.97	0.64	4.12	0.14	0.159	0.013	0.082	0.003	10.09	0.81	5.21	0.18
I	7.75	0.46	4.08	0.09	0.156	0.010	0.082	0.002	9.87	0.59	5.20	0.11
J	7.51	0.41	3.54	0.24	0.150	0.008	0.071	0.005	9.39	0.51	4.42	0.30
K	8.19	0.31	3.80	0.26	0.164	0.006	0.076	0.005	10.24	0.39	4.75	0.32
L	8.88	0.42	3.87	0.19	0.178	0.008	0.077	0.004	10.04	0.47	4.37	0.22
M	8.38	0.34	3.68	0.15	0.168	0.007	0.074	0.003	10.03	0.41	4.40	0.17

Table 7
Mean values and standard deviations of the tensile test data (MD and CD) for all the industrial base tissue papers.

	Elongation at Break (%)				Young Modulus (MPa)			
	MD		CD		MD		CD	
Base paper	$\bar{x}$	$\pm\sigma$	$\bar{x}$	$\pm\sigma$	$\bar{x}$	$\pm\sigma$	$\bar{x}$	$\pm\sigma$
A	28.97	1.49	2.90	0.13	13.21	1.67	74.29	6.30
B	24.16	1.53	3.02	0.15	8.36	0.97	42.22	2.42
C	25.04	1.00	3.44	0.38	8.70	0.36	28.68	1.42
D	22.53	1.78	4.00	0.47	15.04	2.36	31.53	2.19
E	24.56	1.28	3.23	0.32	9.43	0.80	33.59	1.13
F	26.27	1.29	3.89	0.44	7.80	0.28	24.58	1.37
G	23.48	1.89	4.36	0.30	10.54	1.92	22.11	1.38
H	23.22	2.13	4.15	0.27	10.17	0.79	23.79	1.62
I	24.80	1.59	3.30	0.21	8.51	0.73	35.56	0.92
J	25.76	1.16	3.50	0.52	7.81	0.44	27.73	1.10
K	24.64	1.10	3.32	0.39	9.51	0.69	30.49	3.61
L	27.04	1.04	2.88	0.43	6.84	0.25	29.02	2.32
M	22.96	0.975	3.25	0.25	10.13	0.45	22.34	1.16

Table 8
Mean values and standard deviations of the handfeel (*HF*) tests data for all the industrial base tissue papers.

	HF					
	Top		Bottom		Global	
Base paper	$\bar{x}$	$\pm\sigma$	$\bar{x}$	$\pm\sigma$	$\bar{x}$	$\pm\sigma$
A	59.1	3.4	49.5	2.3	54.3	5.7
B	54.2	3.6	52.7	3.2	53.5	3.3
C	71.3	1.5	67.7	1.9	69.5	2.5
D	67.4	2.8	61.1	1.7	64.3	4.0
E	74.7	1.7	67.6	2.6	71.2	4.3
F	73.2	1.8	64.3	2.3	68.7	5.1
G	73.1	0.9	71.0	0.6	72.1	1.3
H	71.5	1.9	68.6	1.7	70.0	2.3
I	71.4	1.6	71.0	4.0	71.2	2.9
J	72.3	4.3	64.9	2.9	68.6	5.2
K	63.0	4.7	63.0	2.6	63.0	3.6
L	72.3	2.7	69.4	1.7	70.9	2.6
M	74.2	1.9	65.2	1.6	69.7	5.0

Table 9
Mean values and standard deviations of the TSA parameters tests data for all the industrial base tissue papers.

	TS7 Parameter					
	Top		Bottom		Global	
Base paper	$\bar{x}$	$\pm\sigma$	$\bar{x}$	$\pm\sigma$	$\bar{x}$	$\pm\sigma$
A	25.6	1.8	30.7	1.2	28.2	3.0
B	27.9	1.9	28.7	1.7	28.3	1.8
C	19.6	0.8	21.4	1.0	20.5	1.3
D	21.7	1.4	24.9	0.9	23.3	2.1
E	18.0	0.9	21.7	1.3	19.9	2.2
F	18.5	0.9	23.2	1.2	20.8	2.6
G	18.8	0.4	20.0	0.3	19.4	0.7
H	19.7	1.0	21.2	0.8	20.4	1.1
I	19.8	0.8	20.1	2.0	20.0	1.5
J	19.4	2.2	23.2	1.5	21.3	2.7
K	24.2	2.4	24.2	1.4	24.2	1.8
L	18.9	1.4	20.5	0.9	19.7	1.4
M	17.8	1.0	22.5	0.8	20.1	2.6

Table 10
Mean values and standard deviations of the TSA parameters tests data for all the industrial base tissue papers.

	*TS*750 Parameter						*fTS*750 Parameter (Hz)					
	Top		Bottom		Global		Top		Bottom		Global	
Base paper	$\bar{x}$	$\pm\sigma$	$\bar{x}$	$\pm\sigma$	$\bar{x}$	$\pm\sigma$	$\bar{x}$	$\pm\sigma$	$\bar{x}$	$\pm\sigma$	$\bar{x}$	$\pm\sigma$
A	18.3	1.1	32.7	1.8	25.5	7.7	399.8	55.4	397.8	30.8	398.8	42.3
B	23.9	1.4	31.1	2.0	27.5	4.1	540.0	50.8	446.4	46.8	493.2	67.5
C	15.1	0.5	17.4	1.1	16.2	1.4	800.2	40.9	785.0	45.2	792.6	41.5
D	16.4	0.6	18.3	0.2	17.3	1.1	861.8	46.5	828.0	122.8	844.9	89.3
E	11.8	0.2	16.9	1.2	14.3	2.8	947.6	29.2	829.0	61.4	888.3	77.2
F	13.0	0.6	18.4	1.0	15.7	2.9	841.8	17.2	658.4	36.6	750.1	100.3
G	15.1	0.7	15.3	0.9	15.2	0.8	806.6	52.9	821.8	78.5	814.2	63.6
H	15.4	0.7	16.5	0.6	15.9	0.8	805.8	35.3	827.2	46.8	816.5	40.6
I	15.9	1.0	13.1	1.4	14.5	1.9	910.4	31.9	969.2	41.7	939.8	46.8
J	13.0	1.2	17.2	0.4	15.1	2.4	950.2	38.1	878.6	63.5	914.4	62.1
K	17.0	1.1	18.5	0.8	17.8	1.2	759.0	76.5	869.8	49.9	814.4	84.4
L	14.7	0.7	20.5	0.6	17.6	3.1	773.8	49.1	594.0	84.5	683.9	115.0
M	15.8	0.9	19.1	0.6	17.4	1.9	749.0	60.2	736.0	116.0	742.5	87.4

Table 11
Mean values and standard deviations of the TSA parameters tests data for all the industrial base tissue papers.

	D Parameter (mm/N)						*P* Parameter (μm)					
	Top		Bottom		Global		Top		Bottom		Global	
Base paper	$\bar{x}$	$\pm\sigma$	$\bar{x}$	$\pm\sigma$	$\bar{x}$	$\pm\sigma$	$\bar{x}$	$\pm\sigma$	$\bar{x}$	$\pm\sigma$	$\bar{x}$	$\pm\sigma$
A	2.0	0.0	2.1	0.0	2.0	0.0	-30.2	9.5	-50.1	5.1	-40.2	12.7
B	2.0	0.1	2.1	0.0	2.1	0.1	-17.8	5.3	-34.6	9.9	-26.2	11.6
C	2.4	0.0	2.5	0.0	2.4	0.0	-28.2	10.9	-47.3	12.4	-37.8	14.9
D	2.2	0.0	2.2	0.0	2.2	0.0	-20.9	6.4	-24.8	12.6	-22.9	9.7
E	2.4	0.0	2.4	0.0	2.4	0.0	-30.1	4.8	-54.2	19.1	-42.2	18.2
F	2.5	0.0	2.5	0.0	2.5	0.0	-48.4	6.3	-52.8	8.4	-50.6	7.4
G	2.4	0.1	2.5	0.0	2.5	0.1	-22.9	12.5	-38.7	3.8	-30.8	12.1
H	2.5	0.0	2.4	0.1	2.5	0.1	-38.8	12.7	-20.2	7.0	-29.5	13.8
I	2.4	0.0	2.5	0.1	2.5	0.1	-30.6	6.3	-48.9	11.8	-39.8	13.1
J	2.6	0.1	2.5	0.0	2.6	0.1	-53.5	13.8	-62.5	11.4	-58.0	12.8
K	2.5	0.1	2.4	0.0	2.4	0.0	-52.6	16.0	-49.8	6.9	-51.2	11.7
L	2.6	0.1	2.6	0.0	2.6	0.0	-105.2	14.8	-119.0	17.6	-112.1	17.0
M	2.5	0.0	2.5	0.0	2.5	0.0	-85.0	20.4	-91.3	11.5	-88.2	16.0

Table 12
Mean values and standard deviations of the TSA parameters tests data for all the industrial base tissue papers.

	H Parameter (J)						*E* Parameter (mm/N)					
	Top		Bottom		Global		Top		Bottom		Global	
Base paper	$\bar{x}$	$\pm\sigma$	$\bar{x}$	$\pm\sigma$	$\bar{x}$	$\pm\sigma$	$\bar{x}$	$\pm\sigma$	$\bar{x}$	$\pm\sigma$	$\bar{x}$	$\pm\sigma$
A	28.2	11.7	29.6	6.6	28.9	9.0	2.0	0.0	2.0	0.0	2.0	0.0
B	26.7	6.0	23.5	14.1	25.1	10.4	2.0	0.1	2.1	0.0	2.1	0.1
C	26.8	7.9	29.7	9.5	28.3	8.4	2.4	0.0	2.5	0.0	2.4	0.0
D	22.2	6.6	22.8	10.1	22.5	8.0	2.2	0.0	2.2	0.0	2.2	0.0
E	27.7	6.8	28.3	9.2	28.0	7.6	2.4	0.0	2.4	0.0	2.4	0.0
F	30.7	7.2	27.3	6.6	29.0	6.8	2.5	0.0	2.5	0.0	2.5	0.0
G	19.6	13.4	26.3	10.0	22.9	11.7	2.4	0.1	2.6	0.0	2.5	0.1
H	23.5	11.2	13.8	6.2	18.7	10.0	2.5	0.0	2.4	0.1	2.5	0.1
I	20.6	5.7	28.6	6.1	24.6	6.9	2.4	0.0	2.5	0.1	2.5	0.1
J	33.7	7.5	31.3	7.9	32.5	7.4	2.6	0.0	2.5	0.0	2.6	0.0
K	29.7	5.7	30.2	7.4	30.0	6.2	2.4	0.1	2.4	0.0	2.4	0.0
L	36.0	3.6	35.4	4.0	35.7	3.6	2.5	0.0	2.5	0.0	2.5	0.0
M	34.8	7.6	37.8	6.5	36.3	6.9	2.4	0.0	2.4	0.0	2.4	0.0

the raw data presented in this manuscript is available in the Excel file attached as an appendix supplementary material.

2. Experimental Design, Materials and Methods

An extensive characterization of the 13 different samples of the industrial base tissue papers was carried out, using different methods. We started by determining the grammage, thickness and bulk. The grammage, expressed in g/m^2 was determined in accordance with ISO 12625-6:2005 [5] and using a Mettler Toledo PB303 Delta Range analytical balance. The thickness was also determined using a FRANK-TPI® Micrometer according to ISO 12625-3:2014 [6]. Finally, the bulk, could be determined using the same standard as before, since it is the inverse of density. The morphology of all base papers was evaluated using the MORFI® Fiber and Shive Analyser from Techpap SAS, that provides us the quantity of fibers in the structure, fiber length and width, coarseness, kink fibers, curl, broken ends and fines percentage in area [7]. The Apparent porosity (theoretical) was determined, for all the industrial base tissue papers samples, using Eq. 1,

$$P\ (\%) = 100\ \times \left(1 - \frac{\rho_{sample}}{\rho_{cellulose}}\right) \tag{1}$$

where $\rho_{cellulose}$ is the density of the cellulose (which is assumed to be 1.6 g/cm^3) and ρ_{sample} is the density of the sample (g/cm^3), which is the inverse of the bulk (cm^3/g) [4]. The porosity was determined using a Micromeritics AccuPyc II 1340 helium pycnometer for all the samples too. The water absorption time and the water absorption capacity was measured according to ISO 12625-8:2010 [8]using a FRANK-TPI® tissue absorption tester to apply the immersion method. The industrial base tissue paper samples were cut, doing an adaptation to the above standard, with the dimensions, width 76±1 mm and length 100±1 mm, in the machine direction, since the toilet base paper does not have a defined service length. Tensile tests were done in machine and cross directions (MD and CD) for all the samples, according with ISO 12625-4:2005 [9], on a Thwing-Albert® VantageNX Universal Testing Machine. For the measurements of *HF, TS7, TS*750, *fTS*750, *D, P, H*, and *E*, the Tissue Softness Analyzer (TSA) from EMTEC was used [10]. The handfeel (*HF*) is one of the parameters calculated by the TSA combining several measurements of the samples to obtain a global quantification of softness of the papers. In this case the QA I algorithm was used for the calculation of the *HF*. All the toilet base paper samples were prepared accordingly with the machine specifications.

Declaration of Competing Interest

The authors declare that they have no known competing financial interests or personal relationships which have, or could be perceived to have, influenced the work reported in this article.

Acknowledgments

This work was carried out under the Project InPaCTus – Innovative Products and Technologies from Eucalyptus, Project N° 21874, funded by Portugal 2020 through European Regional Development Fund (ERDF in the frame of COMPETE 2020 N° 246/AXIS II/2017) .

Supplementary Materials

Supplementary material associated with this article can be found in the online version at doi:10.1016/j.dib.2020.106434.

References

[1] Raunio, Simulation of creping pattern in tissue paper, Nordic Pulp Paper Res. J. 27 (2012) 375–381, doi:10.3183/NPPRJ-2012-27-02-p375-381.
[2] P. Anukul, S. Khantayanuwong, P. Somboon, Development of laboratory wet creping method to evaluate and control pulp quality for tissue, TAPPI J. 14 (2015) 7.
[3] M.K. Ramasubramanian, D.L. Shmagin, An experimental investigation of the creping process in low-density paper manufacturing, J. Manuf. Sci. Eng. 122 (2000) 576, doi:10.1115/1.1285908.
[4] J.C. Vieira, A. de O. Mendes, A.M. Carta, E. Galli, P.T. Fiadeiro, A.P. Costa, Impact of Embossing on Liquid Absorption of Toilet Tissue Papers. 15 (2020) 3888–3898. doi:10.15376/biores.15.2.3888-3898.
[5] ISO 12625-6:2005 Tissue Paper and Tissue Products - Part 6: Determination of Grammage (2005).
[6] ISO 12625-3:2014 Tissue Paper and Tissue Products - Part 3: Determination of Thickness, Bulking Thickness and Apparent Bulk Density and Bulk, (2014).
[7] G. Tourtollet, F. Cottin, A. Cochaux, M. Petit-Conil, The use of MorFi analyser to characterise mechanical pulps, in: International Mechanical Pulping Conference, Quebec City, Canada, 2-5 June, 2003, pp. 225–232.
[8] ISO 12625-8:2010 Tissue Paper and Tissue Products - Part 8: Water-absorption Time and Water-absorption Capacity, Basket-immersion Test Method, (2010).
[9] ISO 12625-4:2005 Tissue Paper and Tissue Products - Part 4: Determination of tensile strength, stretch at break and tensile energy absorption, (2005).
[10] EMTEC Innovative Testing Solutions "TSA - Tissue softness analyzer," https://www.emtec-electronic.de/en/tsa-tissue-softness-analyzer.html, 2018 (accessed on June 7, 2018).

Cellulose
https://doi.org/10.1007/s10570-021-04328-1

ORIGINAL RESEARCH

Characterization of absorbency properties on tissue paper materials with and without "deco" and "micro" embossing patterns

Flávia P. Morais · Joana C. Vieira · António O. Mendes · Ana M. Carta · Ana P. Costa · Paulo T. Fiadeiro · Joana M. R. Curto · Maria E. Amaral

Received: 13 August 2021 / Accepted: 9 November 2021

Abstract Water absorption is a key property in several tissue paper materials and can be a differentiating factor in terms of consumer choice. The converting modifications applied in the tissue industry can improved absorbency properties. For this purpose, the main goal of the present work is to study the influence of "deco" and "micro" embossing on water absorption capacity, Klemm capillary rise, and liquid spreading kinetics in tissue papers. An industrial never-dried bleached eucalyptus kraft pulp, a creped industrial base tissue paper, and a disintegrated fibrous suspension obtained from the same industrial paper were used to produce structures with and without "deco" and "micro" embossing patterns. The results indicate that the "micro" embossing process promoted bulky and porous structures, enhancing water absorption capacity and Klemm capillary rise properties, while the "dec" embossing pattern decreased water absorption capacity properties. The creping process also increased the water absorption capacity but decreased Klemm capillary rise properties along with the fiber mixtures. Regarding the liquid spreading kinetics, both embossing patterns decreased this property in uncreped isotropic structures, contrary to creped anisotropic structures. The eucalyptus and softwood fibers mixture improved the spreading kinetics compared to the creping process. The performance of structures with and without embossing allowed to quantify the liquid retention properties, combining ISO experimental methods and an optical system that records the liquid interaction with fibrous structures. In conclusion, this laboratory embossing method can be used as an alternative method to optimize converting operations and the final tissue paper characterization, on a laboratory scale.

Keywords Absorbency materials characterization · Creping/embossing operations · Hardwood/softwood fibers · Liquid spreading kinetics · Optical liquid droplet system · Tissue papers

F. P. Morais (✉) · J. C. Vieira · A. O. Mendes · A. P. Costa · P. T. Fiadeiro · J. M. R. Curto · M. E. Amaral
Fiber Materials and Environmental Technologies Research Unit (FibEnTech-UBI), Universidade da Beira Interior, Rua Marquês d'Ávila e Bolama, 6201-001 Covilhã, Portugal
e-mail: flavia.morais@ubi.pt

A. M. Carta
Forest and Paper Research Institute (RAIZ), R. José Estevão, Eixo, 3800-783 Aveiro, Portugal

J. M. R. Curto
Chemical Process Engineering and Forest Products Research Centre (CIEPQPF), Universidade de Coimbra, R. Sílvio Lima, Polo II, 3004-531 Coimbra, Portugal

Published online: 21 November 2021

Introduction

In the last decades, the tissue paper industry has shown high growth and competitiveness due to the high hygiene products consumption worldwide. Tissue paper materials are creped fibrous structures with a low grammage between 5 and 40 g/m^2, presenting an elastic and porous structure, with good absorption capacity and softness (de Assis et al. 2018a). These materials are usually used to produce toilet papers, facial papers, towel papers, napkins, among others (de Assis et al. 2018a; Morais et al. 2019). High-quality tissue papers must present factors such as bulk, softness, strength, and absorption. Therefore, it is important to find strategies to produce premium materials to differentiate them in the market, understanding the relationship between their functional properties, and in which sense the modification of one property can affect others (de Assis et al. 2018a, b; Morais et al. 2019, 2020a; Vieira et al. 2020a). The development of optimized tissue paper properties is related to the fiber selection and their modification process steps, including enzymatic treatments, refining, and additives incorporation (Spiridon et al. 2003; Gigac and Fišerová 2008; Park et al. 2019; Guan et al. 2019; Zambrano et al. 2021; Morais et al. 2021a, b; Debnath et al. 2021). In the production of tissue paper materials, a mixture of eucalyptus fibers is used to enhance bulk, porosity, softness, and absorption properties, meanwhile, softwood fibers are also added to ensure strength properties, and the paper machine runnability. The proportion of this mixture depends on the manufacturer and the desired type of product (de Assis et al. 2018a, b; Morais et al. 2019, 2020a; Stankovská et al. 2020).

One of the fundamental operations in the tissue paper industry is the creping process, which consists of the formation of a uniformly rough structure (de Assis et al. 2020). In the paper machine, the Yankee cylinder is coated with chemical additives to promote both the wet paper sheet adhesion in the Nip, and the dry paper sheet detachment at the Yankee exit (Boudreau and Germgård 2014). In this phase, the doctor blade scrapes/removes the paper sheet from the Yankee cylinder surface, creating the paper rough folds. The creping process also includes a change in the fiber direction from the machine direction (MD) to the Z-direction, which results in the breaking of inter-fiber bonding, promoting higher softness and elongation capacity (Raunio and Ritala 2012; Pan et al. 2019). After the production of creped industrial base tissue papers, those are subjected to converting operations to produce the desired type of tissue paper materials. One of these operations is the embossing process in which surface deformations are carried out to the base tissue paper by applying localized pressures. Embossing occurs by placing multiple layers of base tissue paper on top of each other, penetrating a pattern into each layer, and holding them together in a final lamination. Embossing patterns are applied to tissue papers to improve porosity, hygroscopicity, thickness, flexibility, and liquid retention properties. Embossing can result in raised or lowered patterns on the paper, using heat, pressure, and stamping matrices (Spina and Covalcante 2018; Mendes et al. 2020; Vieira et al. 2020b, 2c). To the best of our knowledge, there is an absence of scientific data regarding the 3D tissue paper structure characterization and absorbency properties before and after the embossing operation.

As previously mentioned, the type of embossing pattern applied to tissue paper materials has an important impact on product perception. For example, the use of a "deco" pattern gives a decorative effect to the paper, while a "micro" circular pattern gives to the consumer a more absorbent paper perception. For this reason, water absorption properties are differentiating factors in terms of consumer choice. The two fundamental parameters in these properties are the water absorption speed and the global water absorption capacity. The first parameter consists of the time that a structure absorbs a quantity of water, while the second parameter includes the total water content that the paper can absorb in its 3D structure (Beuther et al. 2010; Gigac et al. 2019). The absorption properties depend on factors such as raw materials used, the type of 3D structure, fines content, bulk, porosity, sheet formation, additives, creping, and embossing (Ashari et al. 2010; Mullins and Braddock 2012; Stankovská et al. 2019). Therefore, different innovative approaches can be considered to optimize the tissue absorption properties, including the 3D simulation of these tissue structures, using 3D computational tools (Curto et al. 2015; Morais et al. 2020b, c). Additionally, an experimental optical prototype system, developed by our research members (Mendes et al. 2013), has been used to collect liquid deposition data over time, to characterize the liquid droplet spreading area and kinetics, through image analysis (Mendes et al.

2013; Fiadeiro et al. 2013; Sousa et al. 2014; Curto et al. 2015). Different studies of liquid droplet deposition and spreading kinetics have indicated that porous structure knowledge is one of the key parameters for optimizing absorption properties since the pore sizes influence the liquid droplet spreading and equilibrium state (Senden et al. 2000; Wågberg and Westerlind 2000; Clarke et al. 2002; Starov et al. 2003; Kannangara et al. 2006; Wang et al. 2007; Hilpert and Ben-David 2009; Rosenholm 2015; Chen et al. 2020).

In this context, the main goal of the present work was to compare the performance of structures with and without embossing made with eucalyptus fibers and a fiber mixture from a disintegrated creped industrial base tissue paper, investigating the effect of fibrous composition, creping, and embossing process on the water absorption properties. To address this objective, a laboratory embossing method was used with two embossing patterns, namely "deco" and "micro" patterns, and an evaluation of water absorption capacity, Klemm capillary rise, and liquid spreading kinetics was performed on uncreped and creped structures before and after embossing.

Materials and methods

Figure 1 presents the detailed diagram of the experimental plan design executed in this study.

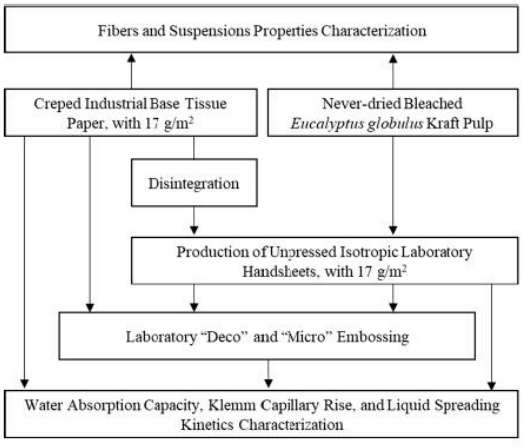

Fig. 1 Diagram of the experimental plan design

Table 1 Nomenclature of the tissue paper samples used in this study

Nomenclature	Composition	Embossing
H_h	Handsheet (hardwood)	None
H_hE_d		"Deco"
H_hE_m		"Micro"
HD_{Ihs}	Handsheet of the Disintegration of Industrial Sheet (hardwood + softwood)	None
$HD_{Ihs}E_d$		"Deco"
$HD_{Ihs}E_m$		"Micro"
I_{hs}	Industrial Sheet (hardwood + softwood)	None
$I_{hs}E_d$		"Deco"
$I_{hs}E_m$		"Micro"

Materials

A never-dried bleached *Eucalyptus globulus* kraft pulp (H_h) and creped industrial base tissue paper (I_{hs}) were selected for the present work. The I_{hs} sample was produced, approximately, with 49% of eucalyptus pulps, 27% of softwood pulps, and 24% of broke. The nomenclature of all samples is identified in Table 1. The HD_{Ihs} samples, described in this table, resulted from the disintegration of the I_{hs} sample.

Fibers and suspensions characterization

The fiber length/width ratio or slenderness ratio, coarseness, and fines elements properties were determined by image analysis of a diluted sample suspension of 20 mg/L, through a flow chamber, using the MorFi analyzer (TECHPAP, Grenoble, France). The Schöpper-Riegler degree, °SR method was used to measure the sample drainability, according to ISO 5267/1. The water retention value, WRV method was assessed using the method described by (Silvy et al. 1968).

Handsheets preparation and embossing operation

The samples were disintegrated according to the ISO 5263-1. The isotropic laboratory handsheets were prepared according to an adaptation of the ISO 5269-1. The H_h and HD_{Ihs} samples were produced with 17 g/m^2 and without pressing. This grammage is similar to

the I_{hs} sample. All the produced fibrous structures were conditioned at 23 ± 1 °C with a relative humidity of 50 ± 2%, according to ISO 187.

Meanwhile, samples of the produced fibrous structures were subject to the "deco" and "micro" embossing process using an innovative laboratory embossing prototype equipment. The nomenclature of all samples with these embossing patterns is also identified in Table 1.

Tissue structural and absorption characterization

The structural properties, water absorption capacity, Klemm capillary rise, and liquid droplet spreading kinetics of structures with and without embossing were characterized.

The grammage was determined according to ISO 12625-6, and the thickness and bulk were determined following the ISO 12625-3. For thickness measurements, the FRANK-TPI® Micrometer equipment (FRANK-PTI GMBH, Birkenau, Germany) was used. Apparent porosity was calculated using the following equation: $P\ [\%] = [1 - (\rho_{cellulose}/\rho_{structure})] \times 100$, where $\rho_{cellulose}$ is the cellulose density (1.6 g/cm^3) and $\rho_{structure}$ is the structure density (g/cm^3) (Costa et al. 2016).

The water absorption capacity method was determined by the immersion method, using a FRANK-TPI® Tissue Absorption Tester (FRANK-PTI GMBH, Birkenau, Germany), according to an adaptation to ISO 1265-8.

The water capillary rise was determined using the Klemm method, following an adaptation to ISO 8787.

An optical system (Prototype, Universidade da Beira Interior, Covilhã, Portugal), developed by our research members (Mendes et al. 2013) and applied in several materials studies (Fiadeiro et al. 2013; Sousa et al. 2014; Curto et al. 2015) was used to study the liquid droplet spreading kinetics. In this work, the optical system is a unique device to analyze the 3D structures on different tissue papers with and without embossing. This system works by ejecting microliter droplets toward the structure surface, whereas images of the droplets are being recorded for a given period. The liquid spreading kinetics and spreading dynamics data were collected from 35.7 ms to 3 s, and the snapshot images selected in this work were 35.7 ms (initial time), 250 ms and 1 s (intermediate times), and 3 s (final time).

Computational studies

A computational tissue simulator, the *SimTissue* (FibEnTech-UBI, Covilhã, Portugal) was developed specifically for tissue paper furnish materials and used to study different scenarios of the influence of the fiber mixtures, creping, and embossing processes on tissue end-use properties. This simulator works by integrating the key tissue fiber and structure properties, predicting the softness, strength, and absorption properties of different furnish and tissue paper process operations.

Results and discussion

Fibers and suspensions characterization

The eucalyptus sample, H_h, presented a slenderness ratio in the same range as the sample consisting of a mixture of eucalyptus and softwood fibers, HD_{Ihs}/I_{hs} (Fig. 2a), indicating that the H_h sample had fiber lengths and widths lower than the HD_{Ihs}/I_{hs} samples. These morphological properties of the HD_{Ihs}/I_{hs} samples directly contributed to the development of the mechanical properties, improving the tissue paper machine runnability. This ratio is also related to the paper structure density and pulp digestibility (Morais et al. 2020a; Dutt and Tyagi 2011). Compared to our previous study (Morais et al. 2019, 2020a), the H_h sample showed a low slenderness ratio compared to other eucalyptus pulps. This result indicates that this sample has shorter and thicker fibers, presenting a negative effect on the pulp mechanical properties, not ready for collapse, and providing less surface contact for bonding. Coarseness is influenced by the fiber thickness, width, and fiber pulp population (Morais et al. 2020b). Because this parameter depends on several factors, it should only be compared between fibers of similar species. The samples showed a difference of 48% for coarseness properties (Fig. 2a). This result is due to the presence of softwood fibers in the HD_{Ihs}/I_{hs} samples. Additionally, the HD_{Ihs}/I_{hs} sample presented a higher fine content than the H_h sample, with a difference of 22% (Fig. 2a). This result is due to the presence of refined softwood fibers and broken fibers in the HD_{Ihs}/I_{hs} samples. These broken fibers are obtained by the sheet breakage in the tissue paper machine, which is collected and recirculated to a

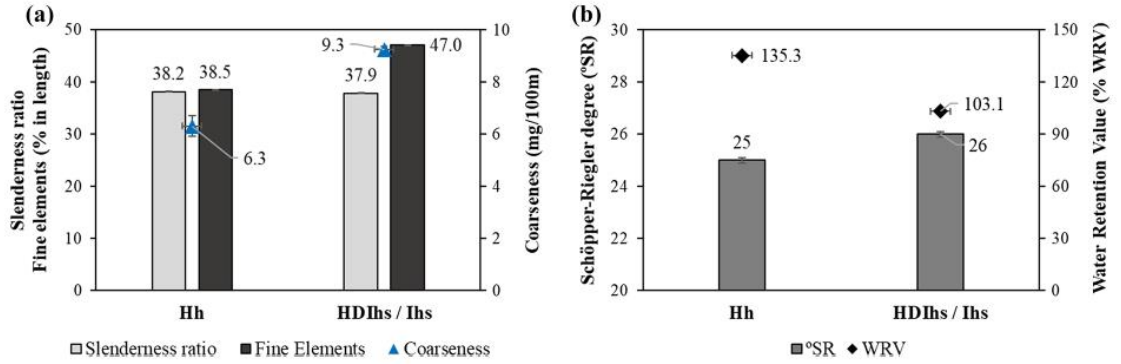

Fig. 2 Pulp fiber morphological properties, namely slenderness ratio, coarseness, and fine elements (**a**), and pulp suspension properties, such as °SR and WRV (**b**), of the H_h and HD_{Ihs}/I_{hs} samples

pulper and introduced again in the blend eucalyptus and softwood pulps process. Regarding the water drainage capacity (Fig. 2b), both samples showed °SR values in the recommended range to produce high-quality tissue papers (de Assis et al. 2018a), between 25 and 26 °SR. The small difference found in these measurements may be due to the presence of refined softwood fibers during the production process of the HD_{Ihs}/I_{hs} sample. Finally, the H_h sample showed a higher WRV (+ 28%) than the HD_{Ihs}/I_{hs} sample (Fig. 2b). This result can be explained by the absence of the hornification effect caused by the drying operation of the H_h pulp sample since this pulp is a never-dried eucalyptus sample (Weise et al. 1996; Giacomozzi and Joutsimo 2015).

Tissue structural and absorption characterization

The tissue paper's structural properties, such as bulk and porosity, influence the water absorption properties (Morais et al. 2019; Stankovská et al. 2019). The bulk and porosity properties of the structures with and without embossing are shown in Fig. 3a. The *SimTissue* was used to compare the influence of the furnish mixture composition, and different tissue process operations, such as the creping and embossing operations, and to predict the negative and positive trends for different furnish, properties, and process operations scenarios, as shown in Fig. 4. When comparing the samples without embossing, two effects must be considered: fiber mixing and creping process. The

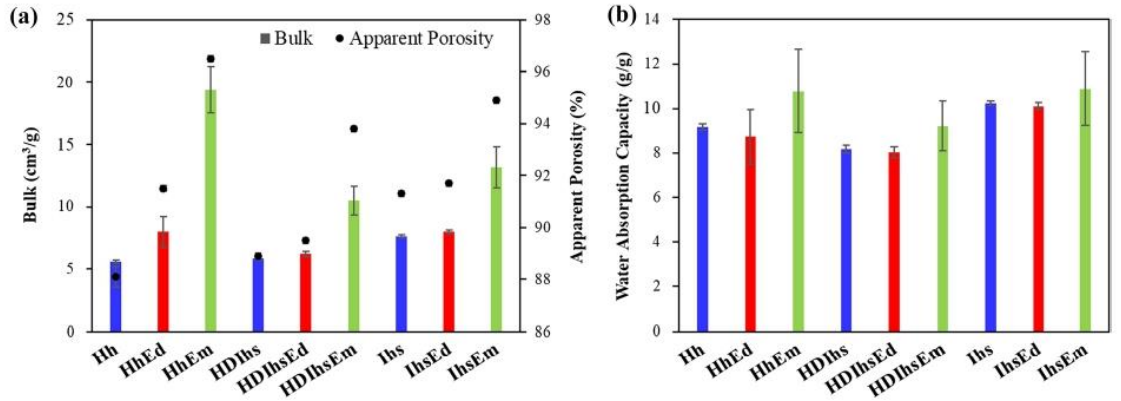

Fig. 3 Structural properties, namely bulk and apparent porosity (**a**), and water absorption capacity properties (**b**) of the samples without and with "deco" and "micro" embossing

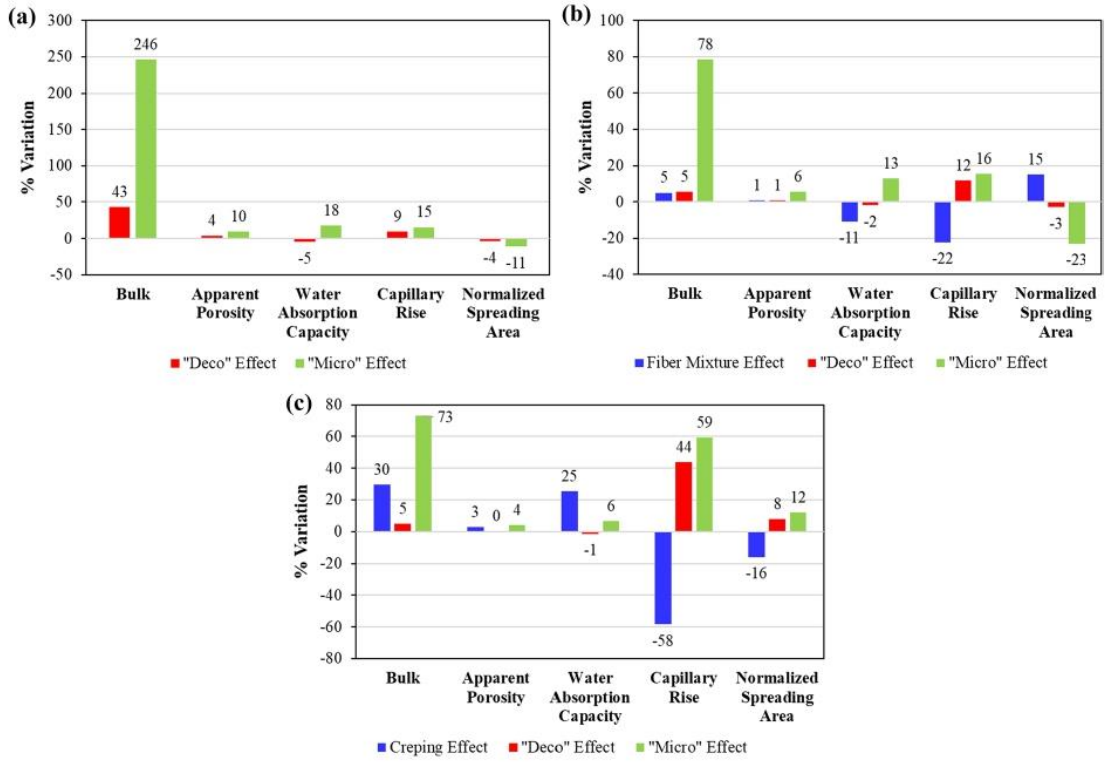

Fig. 4 Percentage of variation in the tissue structural and absorption properties for H_h sample (**a**), HD_{Ihs} sample (**b**), and I_{hs} sample (**c**), predicted using the *SimTissue*

effect of the blend of eucalyptus and softwood fibers is quantified by comparing the H_h and HD_{Ihs} samples, indicating that these softwood fibers increase the structure by 5% and the structure porosity by 1%. On the other hand, the creping effect is quantified by comparing the HD_{Ihs} and I_{hs} samples, indicating that this operation increases the structure bulk by 30% and the structure porosity by 3%. These results indicate that creping promotes the production of more bulky and porous structures compared to the fiber mixture. The effect of "deco" and "micro" embossing on H_h structures increases, respectively, the bulk by 43% and 246%, and the porosity by 4% and 10%. In HD_{Ihs} structures, the effect of "deco" and "micro" embossing increases the bulk by 5% and 78%, and the porosity by 1% and 5%, respectively. Finally, in the I_{hs} samples, the effect of "deco" and "micro" embossing increases the bulk by 5% and 73%, and the porosity by 0.4% and 4%, respectively. Overall, "micro" embossing has a higher influence on structural properties than "deco" embossing. In both patterns, the HD_{Ihs} embossed structures showed less bulk and porosity than the H_h and I_{hs} embossed samples. The "micro" pattern promoted bulkier and more porous H_h structures compared to the $I_{hs}E_m$ ("micro" embossed) structures, while the "deco" pattern obtained H_h and I_{hs} embossed structures with the same range of bulk and porosity. It was found that the structural properties of embossed structures are modified not only by the embossing pattern but also by the fiber mixture and creping operation. In this case, eucalyptus fibers were more suitable to produce more bulky and porous structures with embossing. The bulk and porosity of the embossed structures are decreased with the presence of softwood fibers in the mixture and increased with the creping process operation.

The water absorption capacity properties of the structures with and without embossing are shown in Fig. 3b, and its percentage of variation is shown in Fig. 4. The fiber mixture effect reduced this property

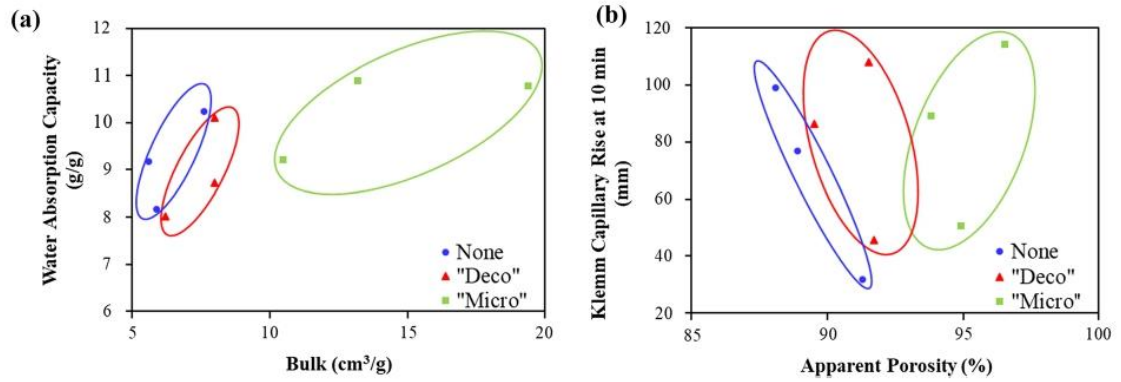

Fig. 5 Water absorption capacity as a function of bulk (**a**) and Klemm capillary rise at 10 min as a function of apparent porosity (**b**) of the structures without embossing, with "deco" embossing and with "micro" embossing

by 11%, comparing H_h and HD_{Ihs} samples. Although the structure bulk and porosity with a blend of eucalyptus and softwood fibers are slightly higher than those obtained with only eucalyptus fibers, the higher fines content of the HD_{Ihs} sample may have contributed to a water absorption capacity decrease, since inter-fiber bonds and low pore size and distribution prevailed in this property. Stankvska et al. (2020) also reported that by increasing the softwood fiber content in tissue formulations, the structure water absorption was decreased. The higher fiber water affinity (WRV, Fig. 2b) of the H_h sample also can explain this behavior. On the other hand, the creping effect improved this absorption property by 25%, comparing the HD_{Ihs} and I_{hs} samples, which is in accordance with the structural properties. The embossing process modified the absorption of tissue structures. In general, the "deco" pattern had a small negative influence on the water absorption capacity properties, while the "micro" pattern increased these properties. The "deco" embossing decreased the absorption capacity by 5%, 2%, and 1% of the H_h, HD_{Ihs}, and I_{hs} embossed structures. The "micro" embossing increased the absorption capacity by 18%, 13%, and 6% of the H_h, HD_{Ihs}, and I_{hs} embossed structures. As in the structural properties, the HD_{Ihs} embossed structures with both patterns showed less water absorption capacity than the H_h and I_{hs} embossed samples. In this case, the I_{hs} embossed structures with both embossing patterns showed better absorption properties than the H_h embossed structure. This result indicates that the creping process overcomes the water absorption compared to eucalyptus fibers, although the H_hE_m ("micro" embossed) structures were bulkier than the $I_{hs}E_m$ ("micro" embossed) structures. Figure 5a also presents the relationship between the bulk and the water absorption capacity, in which it is possible to observe two distinct zones in the graphic. From this analysis, it was found that, overall, the structures without embossing and with "deco" embossing are in a range with low bulk (5.6–8.0 cm^3/g) and water absorption (8.1–10.2 g/g), while structures with "micro" embossing are in a range with high bulk (10.5–19.4 cm^3/g) and water absorption (9.2–10.9 g/g).

The Klemm capillary rise depends on the adhesion and cohesion forces of the water molecules that rise through the fiber walls or between the pores. The Klemm capillary rise properties of the structures with and without embossing and their percentage of variation are shown in Figs. 4, 6, respectively. This assay was performed on the machine direction, MD (perpendicular to crepe folds), and cross direction, CD (parallel to crepe folds) of the I_{hs} sample. The results indicated that the CD direction enhanced a better Klemm capillary rise (+ 75% at 10 min) compared to the MD direction (Fig. 6a). The crepe lines improved this property. Klemm capillary rise studies for $I_{hs}E_d$ and $I_{hs}E_m$ samples were performed only in the MD direction. The fiber mixture effect decreased this property by 22% (Figs. 4b, 6b), comparing H_h and HD_{Ihs} samples, which is in accordance with the water absorption capacity properties. The creping effect also decreased the Klemm capillary rise by 58%,

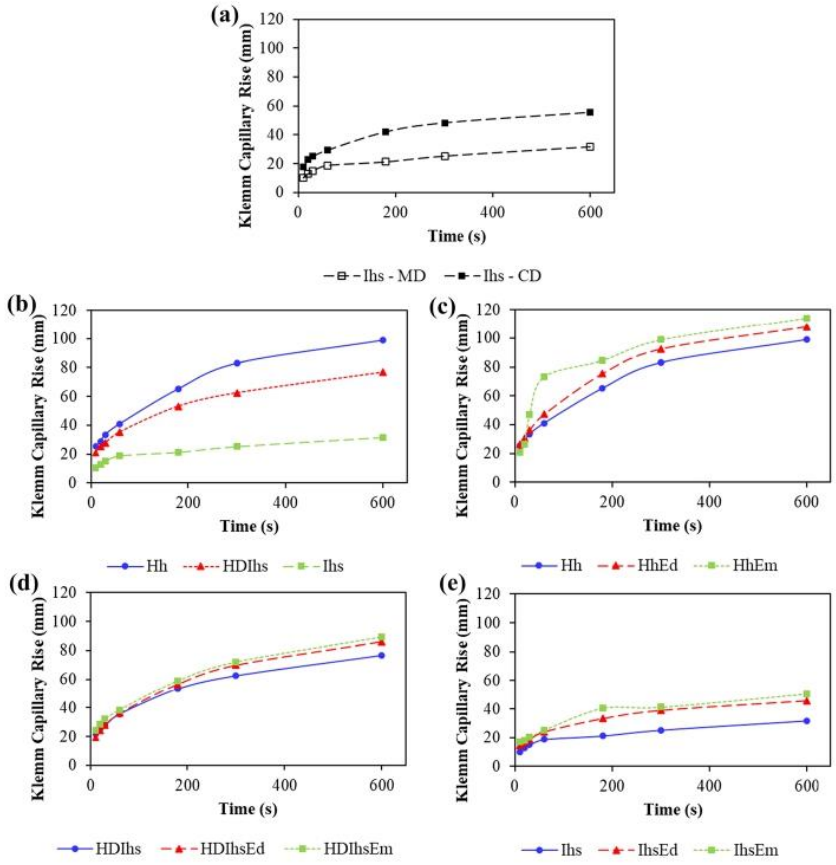

Fig. 6 Klemm capillary rise as a function of time of the I_{hs} structures in MD and CD direction without embossing (**a**), all handsheets without embossing (**b**), H_h structures with and without "deco" and "micro" embossing (**c**), HD_{Ihs} structures with and without "deco" and "micro" embossing (**d**), and I_{hs} structures with and without "deco" and "micro" embossing (**e**)

comparing the HD_{Ihs} and I_{hs} samples (Figs. 4c, 6b). The intermolecular bonding between fibers and water molecules in I_{hs} structures with higher pores may have decreased capillary rise. Additionally, in the case of very narrow channels due to creping process, the water progression may have been strangled by the limited space for capillary rise (Mullins and Braddock 2012). Regarding the embossing effect, capillarity absorption presented a different behavior to immersion absorption. In all samples, both "deco" and "micro" embossing increased capillary rise compared to samples without embossing. The "deco" embossing increased the capillary rise at 10 min by 9%, 12%, and 44% of the H_hE_d, $HD_{Ihs}E_d$, and $I_{hs}E_d$ embossed structures (Figs. 4, 6c–e). The "micro" embossing also increased the capillary rise at 10 min by 15%, 16%, and 59% of the H_hE_m, $HD_{Ihs}E_m$, and $I_{hs}E_m$ embossed structures (Figs. 4c, 6c–e). These results indicate that the "micro" pattern has a higher influence on the capillary rise properties than the "deco" pattern. In both patterns, capillarity absorption was more pronounced in the H_h embossed structures, followed by HD_{Ihs}, and I_{hs} embossed structures. It was found that eucalyptus fibers present a higher influence on the water capillary rise than the fiber mixture, followed by the creping process, both in structures with and without embossing. Additionally, Fig. 5b also presents the relationship between the apparent porosity and the capillary rise at 10 min, in which it is possible to observe three distinct zones in the graphic. From this analysis, it was found that, overall, the structures without embossing are in a range with low

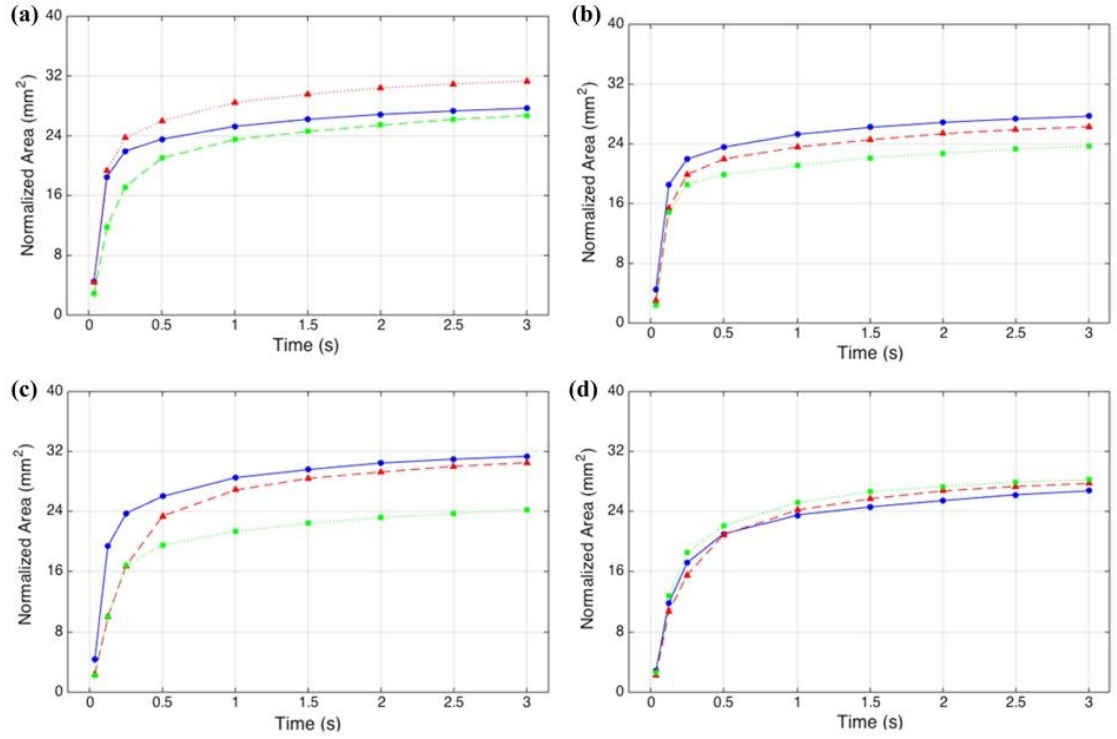

Fig. 7 The normalized liquid spreading area as a function of time for the structures without embossing (**a**), H_h structures with and without "deco" and "micro" embossing (**b**), HD_{Ihs} structures with and without "deco" and "micro" embossing (**c**), and I_{hs} structures with and without "deco" and "micro" embossing (**d**). In graphic (**a**), the colors blue, red, and green correspond to the structures H_h, HD_{Ihs}, and I_{hs}, respectively. In graphic (**b**–**d**), samples without embossing are represented in blue, with "deco" embossing in red, and with "micro" embossing in green

porosity (88.1–91.3%) and capillary rise (32–99 mm). The "deco" embossed structures are in a range with intermediate porosity (89.5–91.7%) and Klemm capillary rise (46–108 mm), while structures with "micro" embossing are in a range with high porosity (93.8–96.5%) and Klemm capillary rise (51–114 mm). Therefore, the pores of the structures should present uniform dimensions, since the contribution of the gravity force should not be higher than the force exerted by the water molecules that allows the molecules to ascend the channels. Hence, there must be a balance between the pore dimensions and distribution to promote the Klemm capillary rise efficiency (Beuther et al. 2010).

The kinetics of the liquid droplet spreading area over time in papers with and without embossing is presented in Fig. 7 and Table 2. This liquid spreading area of all samples is defined by initial fast kinetics for times below 0.5 s, followed by slower kinetics, towards a stabilization value for the liquid spreading area. The response of the liquid droplet deposition into the 3D fibrous structure made from fiber mixtures, HD_{Ihs}, indicates that the liquid spreading area is higher compared to 100% eucalyptus structure, H_h (Fig. 7a). These results indicated that the eucalyptus and softwood fiber mixture increased the liquid spreading kinetics properties by 15% (Fig. 4b), corresponding to a higher porous and bulky structure (Fig. 3a). However, this result is not in accordance with the immersion and capillary absorption properties (Figs. 3b, 6b). The liquid droplet spreading area of the creped structure, I_{hs}, was smaller (− 16%, Fig. 4c) than the laboratory-made structures produced by disintegration of this sample, HD_{Ihs} (Fig. 6a). This

Table 2 Kinetics of the liquid droplet spreading area overtime in structures with and without embossing

	t = 35.7 ms	t = 250 ms	t = 1.0 s	t = 3.0 s
H_h	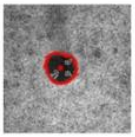	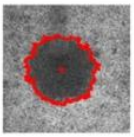	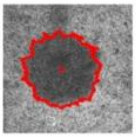	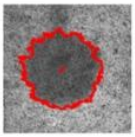
H_hE_d	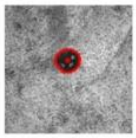	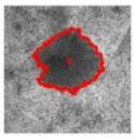	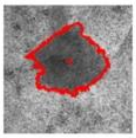	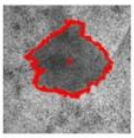
H_hE_m	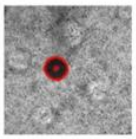	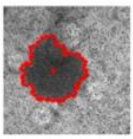	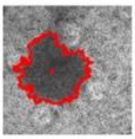	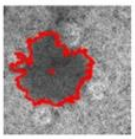
HD_{Ihs}	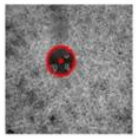	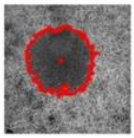	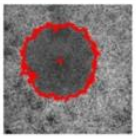	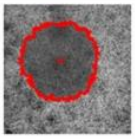
$HD_{Ihs}E_d$	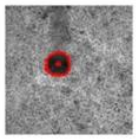	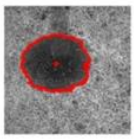	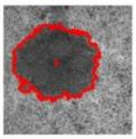	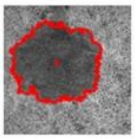
$HD_{Ihs}E_m$	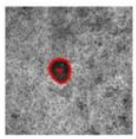	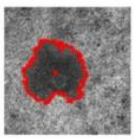	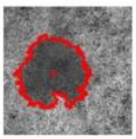	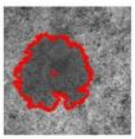
I_{hs}	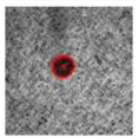	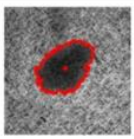	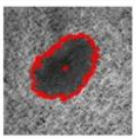	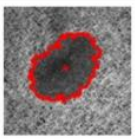
$I_{hs}E_d$	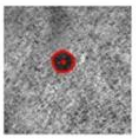	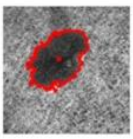	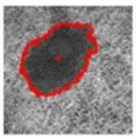	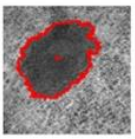
$I_{hs}E_m$	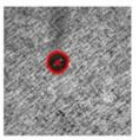	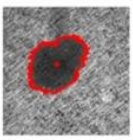	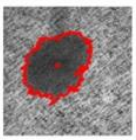	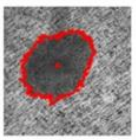

Table 3 Evolution of the liquid droplet spreading dynamics overtime in structures with and without embossing

	t = 35.7 ms	t = 250 ms	t = 1.0 s	t = 3.0 s
H_h	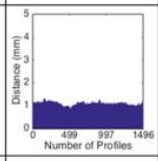	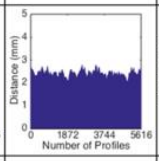	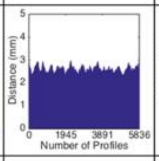	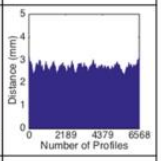
H_hE_d	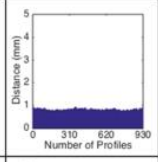	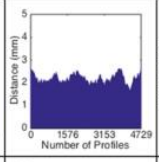	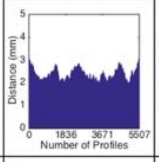	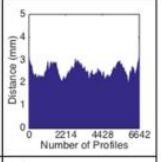
H_hE_m	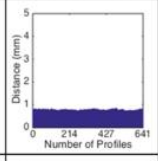	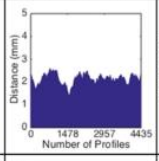	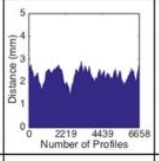	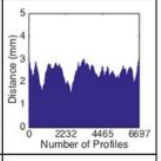
HD_{Ihs}	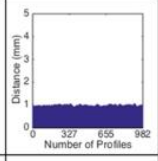	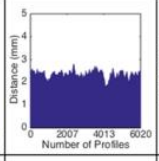	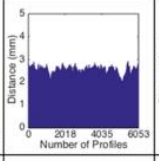	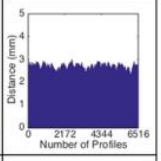
$HD_{Ihs}E_d$	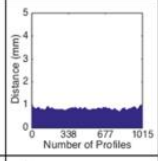	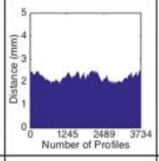	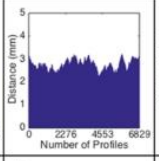	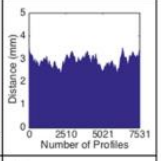
$HD_{Ihs}E_m$	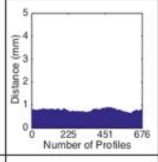	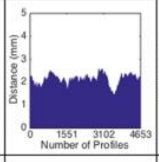	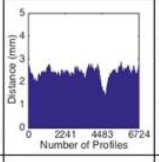	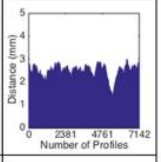
I_{hs}	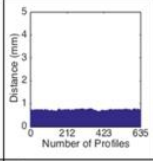	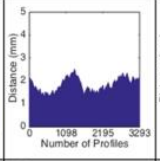	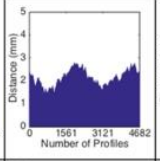	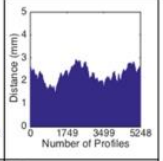
$I_{hs}E_d$	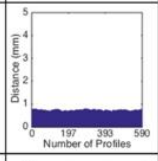	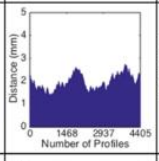	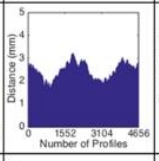	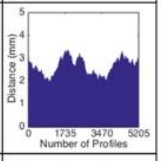
$I_{hs}E_m$	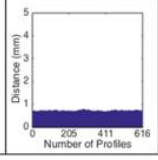	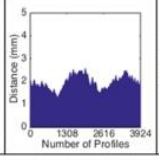	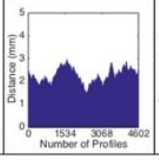	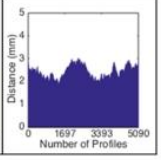

result is following the Klemm capillary rise properties. The creping lines enhance the tortuosity phenomenon since the liquid droplet presented higher difficulty to intrude into or pass through the cellulosic fibers, compared to the HD_{Ihs} structure. Additionally, the phenomenon of anisotropy was observed in I_{hs} structures, and isotropy in H_h and HD_{Ihs} structures (Table 2). The liquid droplet spreading area was direction-dependent of the creping lines in the creped industrial base tissue paper sample, presenting an elliptical shape. On the other hand, the liquid droplet spreading area tends to have a circular shape for isotropic laboratory samples without embossing. It was found that the fiber mixture in these structures improved the liquid droplet spreading kinetics over time, followed by eucalyptus fibers and the creping process. The "deco" embossing effect decreased the liquid spreading kinetics in both H_hE_d and $HD_{Ihs}E_d$ structures by 4% and 3%, respectively (Figs. 4, 7b, c), being in accordance with the water absorption capacity properties. However, this decrease is in the same range as structures without embossing. This result was also reported in Fig. 5a. Additionally, the same behavior was also observed for the "micro" embossing in these two samples (Fig. 7b, c). The "micro" embossing also decreased the liquid spreading kinetics by 11% and 23% of the H_hE_m, and $HD_{Ihs}E_m$, embossed structures (Fig. 4a, b). The "micro" embossing presented a negative influence on the liquid spreading kinetics compared to the "deco" embossing. This absorption property is modified by the creation of 3D effects of the embossing patterns on the structures, changing the water flow, initially around and then within the "deco" linear pattern and "micro" circular dots. Due to this 3D effect, the liquid has difficulty passing through the cellulose fibers, as seen in creped structures without embossing. This effect can be observed, for example, for $t = 3$ s in H_hE_d and H_hE_m structures (Table 2). Additionally, the liquid droplet spreading area can yield random and irregular shapes considering the embossing pattern present on the structure surface (Table 2). Regarding the I_{hs} sample, the structures with embossing showed a higher liquid spreading area than the structures without embossing (Fig. 7d). The "micro" pattern presented a higher influence (+ 12%, Fig. 4c) on the liquid droplet spreading kinetics compared to the "deco" embossing pattern (+ 8%, Fig. 4c), being in accordance with the Klemm capillary rise. In this case, the structure bulk and porosity enhanced this property. However, the differences found for both patterns in the creped structure are in the same range. With this study, it was found that the embossing pattern presents higher differences in liquid spreading kinetics of the isotropic laboratory samples than in anisotropy creped industrial samples.

In addition, Table 3 presents the liquid droplet spreading dynamics of the structures with and without embossing. The blue shaded area corresponds to the red line that circles the droplet outline in each structure, in Table 2. The number of profiles starts at the largest Euclidean distance between the centroid and the red line and extends in the clockwise direction. In isotropic structures, the blue shaded area is practically a rectangle with few irregularities, which is not the case for anisotropic structures. These differences are due to the circular and elliptical shape of the isotropic and anisotropic samples, respectively. For both "deco" and "micro" embossing patterns, an irregular area of the liquid droplet spreading dynamics for all samples is observed. This result is due to the random and irregular shapes presented in the embossed structures, in Table 2.

Conclusions

Our research highlights the importance of the absorbency properties characterization of different structures with and without embossing using standard methods, and an innovative optical liquid droplet system to quantify the liquid spreading kinetics. The characterization methodology developed and implemented on this study allowed the quantification of the influence of isotropic and anisotropic tissue papers formation, fiber mixtures, creping, and embossing operations, separately.

Overall, the creping effect has a higher influence on the structural and water absorption capacity properties compared to the fiber mixture; however, the reverse was verified for the Klemm capillary rise and liquid spreading kinetics properties. The "deco" embossing operation decreased the water absorption properties compared to the "micro" embossing. The water capillary rise overtime was higher in structures with "micro" embossing, followed by "deco" embossing. The same behavior was verified for the liquid spreading kinetics in the I_{hs} embossed structures, while an

inverse relationship was observed for the H_h and HD_{lhs} embossed structures. Considerable insight has been gain using the optical system to obtain the liquid spreading area kinetics and its spreading shape. With these findings it was proved that the type of 3D structure in which the liquid drop is deposited, the isotropic/anisotropic tissue structures, and the creping/embossing process operations are key parameters on the liquid/materials interaction.

The characterization methodology proposed in this work constitutes valuable information to optimize the embossing operation and the absorption properties, combining the water absorption capacity, Klemm capillary rise, and liquid spreading kinetics properties of tissue paper materials. In conclusion, the combination of the laboratory embossing method, 3D modeling, and optical liquid droplet system establishes an innovative approach to quantify and represent the 3D embossing effect of tissue structures, on a laboratory scale, to be used in the process optimization and furnish management, to enhance absorbency materials properties.

Acknowledgments This research was supported by Project InPaCTus—Innovative Products and Technologies from eucalyptus, Project N° 21 874 funded by Portugal 2020 through European Regional Development Fund (ERDF) in the frame of COMPETE 2020 n° 246/AXIS II/2017. The authors are also very grateful for the support given by Fiber Materials and Environmental Technologies Research Unit (FibEnTech-UBI) on the extent of the project reference UIDB/00195/2020.

Author contributions The manuscript was written through the contributions of all authors. All authors have given approval to the final version of the manuscript.

Data availability The raw/processed data required to reproduce the above findings cannot be shared at this time as the data also forms part of an ongoing study.

Declarations

Conflict of interest The authors declare that they have no conflict of interest.

References

Ashari A, Bucher TM, Tafreshi HV, Tahir MA, Rahman MSA (2010) Modeling fluid spread in thin fibrous sheets: effects of fiber orientation. Int J Heat Mass Transf 53:1750–1758. https://doi.org/10.1016/j.ijheatmasstransfer.2010.01.015

Beuther PD, Veith MW, Zwick KJ (2010) Characterization of absorbent flow rate in towel and tissue. J Eng Fiber Fabr 5:1–7. https://doi.org/10.1177/155892501000500201

Boudreau J, Germgård U (2014) Influence of various pulp properties on the Adhesion between tissue paper and Yankee cylinder surface. BioRes 9:2107–2114

Chen H, Nie Q, Fang H (2020) Dynamic behavior of droplets on confined porous substrates: a many-body dissipative particle dynamics study. Phys Fluids 32:102003. https://doi.org/10.1063/5.0020471

Clarke A, Blake TD, Carruthers K, Woodward A (2002) Spreading and imbibition of liquid droplets on porous surfaces. Langmuir 18:2980–2984. https://doi.org/10.1021/la0117810

Costa VLD, Costa AP, Amaral ME, Oliveira C, Gama M, Dourado F, Simões RM (2016) Effect of hot calendering on physical properties and water vapor transfer resistance of bacterial cellulose films. J Mater Sci 51:9562–9572. https://doi.org/10.1007/s10853-016-0112-4

Curto JMR, Mendes AO, Conceição ELT, Portugal ATG, Fiadeiro PT, Ramos AMM, Simões RMS, Santos Silva MJ (2015) Development of an innovative 3D simulator for structured polymeric fibrous materials and liquid droplets. In: Öchsner A, Altenbach H (eds) Mechanical and materials engineering of modern structure and component design advanced structured materials. Springer, Cham, pp 301–321

de Assis T, Reisinger L, Pal L, Pawlak J, Jameel H, Gonzalez R (2018) Understand the effect of machine technology and cellulosic fibers on tissue properties: a review. BioRes 13:4593–4629. https://doi.org/10.15376/biores.13.2.DeAssis

de Assis T, Reisinger LW, Dasmohapatra S, Pawlak J, Jameel H, Pal L, Kavalew D, Gonzalez RW (2018) Performance and sustainability vs. shelf price of tissue paper kitchen towels. BioRes 13:6868–6892. https://doi.org/10.15376/biores.13.3.6868-6892

de Assis T, Pawlak J, Pal L, Jameel H, Reisinger LW, Kavalew D, Campbell C, Pawlowska L, Gonzalez RW (2020) Comparison between uncreped and creped handsheets on tissue paper properties using a Creping simulator unit. Cellulose 27:5981–5999. https://doi.org/10.1007/s10570-020-03163-0

Debnath M, Salem KS, Naithani V, Musten E, Hubbe MA, Pal L (2021) Soft mechanical treatments of recycled fibers using a high-shear homogenizer for tissue and hygiene products. Cellulose 28:7981–7994. https://doi.org/10.1007/s10570-021-04024-0

Dutt D, Tyagi CH (2011) Comparison of various eucalyptus species for their morphological, chemical, pulp and paper making characteristics. Indian J Chem Technol 18:145151

Fiadeiro PT, Mendes AO, Ramos AMM, Sousa SCL (2013) Study of the ink-paper interaction by image analysis: surface and bulk inspection. In: Proceedings of SPIE - 8th Iberoamerican Optics Meeting and 11th Latin American Meeting on Optics, Lasers, and Applications, Porto, Portugal, pp. 8785BV-1/8785BV-8. https://doi.org/10.1117/12.2024991

Giacomozzi DE, Joutsimo O (2015) Drying temperature and hornification of industrial never-dried pinus radiata pulps. 1: strength, optical, and water holding properties. BioRes

10:5791–5808. https://doi.org/10.15376/biores.10.3.5791-5808
Gigac J, Fišerová M (2008) Influence of pulp refining on tissue paper properties. Tappi J 7:27–32
Gigac J, Fišerová M, Stankovská M, Maholányiová M (2019) Prediction of water-absorption capacity and surface softness of tissue paper products using photoclinometry. O Papel 80:91–97
Gil N, Gil C, Amaral ME, Costa AP, Duarte AP (2009) Use of enzymes to improve the refining of a bleached Eucalyptus globulus kraft pulp. Biochem Eng J 46:89–95. https://doi.org/10.1016/j.bej.2009.04.011
Guan M, An X, Liu H (2019) Cellulose nanofiber (CNF) as a versatile filler for the preparation of bamboo pulp-based tissue paper handsheets. Cellulose 26:2613–2624. https://doi.org/10.1007/s10570-018-2212-6
Hilpert M, Ben-David A (2009) Infiltration of liquid droplets into porous media: effects of dynamic contact angle and contact angle hysteresis. Int J Multiph Flow 35:205–218. https://doi.org/10.1016/j.ijmultiphaseflow.2008.11.007
Kannangara D, Zhang H, Shen W (2006) Liquid-paper interactions during liquid drop impact and recoil on paper surfaces. Colloids Surf A Physicochem Eng Aspects 280:203–215. https://doi.org/10.1016/j.colsurfa.2006.02.008
Mendes AO, Fiadeiro PT, Ramos AMM, Sousa SCL (2013) Development of an optical system for analysis of the ink-paper interaction. Mach vis Appl 24:1733–1750. https://doi.org/10.1007/s00138-013-0496-y
Mendes AO, Vieira JC, Carta AM, Gali E, Simões R, dos Santos Silva MJ, Costa AP, Fiadeiro PT (2020) Influence of tissue paper converting conditions on finished product softness. BioRes 15:7178–7190. https://doi.org/10.15376/biores.15.3.7178-7190
Morais FP, Bértolo RAC, Curto JMR, Amaral MECC, Carta AMMS, Evtyugind DV (2019) Comparative characterization of eucalyptus fibers and softwood fibers for tissue papers applications. Mater Lett X 4:100028. https://doi.org/10.1016/j.mlblux.2019.100028
Morais FP, Bértolo RAC, Curto JMR, Amaral MECC, Carta AMMS, Evtyugind DV (2020a) Characterization data of pulp fibres performance in tissue papers applications. Data Brief 29:105253. https://doi.org/10.1016/j.dib.2020.105253
Morais FP, Carta AMMS, Amaral ME, Curto JMR (2020) 3D fiber models to simulate and optimize tissue materials. BioRes 15:8833–8848. https://doi.org/10.15376/biores.15.4.8833-8848
Morais FP, Carta AMMS, Amaral ME, Curto JMR (2020c) Experimental 3D fibre for tissue papers applications. Data Brief 30:105479. https://doi.org/10.1016/j.dib.2020.105479
Morais FP, Carta AMMS, Amaral ME, Curto JMR (2021a) Micro/nano-fibrillated cellulose (MFC/NFC) fibers as an additive to maximize eucalyptus fibers on tissue paper production. Cellulose 28:6587–6605. https://doi.org/10.1007/s10570-021-03912-9
Morais FP, Carta AMMS, Amaral ME, Curto JMR (2021) Cellulose fiber enzymatic modification to improve the softness, strength, and absorption properties of tissue papers. BioRes 16:846–861. https://doi.org/10.15376/biores.16.1.846-861
Mullins BJ, Braddock RD (2012) Capillary rise in porous, fibrous media during liquid immersion. Int J Heat Mass Transf 55:6222–6230. https://doi.org/10.1016/j.ijheatmasstransfer.2012.06.046
Pan K, Das R, Phani AS, Green S (2019) An elastoplastic creping model for tissue manufacturing. Int J Solids Struct 165:23–33. https://doi.org/10.1016/j.ijsolstr.2019.01.022
Park JY, Melani L, Lee H, Kim JH (2019) Effect of chemical additives on softness components of hygiene paper. Nordic Pulp Paper Res J 34:173–181. https://doi.org/10.1515/npprj-2019-0002
Raunio J-P, Ritala R (2012) Simulation of creping pattern in tissue paper. Nordic Pulp Paper Res J 27:375–381. https://doi.org/10.3183/npprj-2012-27-02-p375-381
Rosenholm JB (2015) Liquid spreading on solid surfaces and penetration into porous matrices: coated and uncoated papers. Adv Colloid Interface Sci 220:8–53. https://doi.org/10.1016/j.cis.2015.01.009
Senden TJ, Knackstedt MA, Lyne MB (2000) Droplet penetration into porous networks: role of pore morphology. Nordic Pulp Paper Res J 15:554–563. https://doi.org/10.3183/npprj-2000-15-05-p554-563
Silvy J, Romatier G, Chiodi R (1968) Méthodes pratiques de controle du raffinage. ATIP 22:31–53
Sousa SCL, Mendes AO, Fiadeiro PT, Ramos AMM (2014) Dynamic interactions of pigment-based inks on chemically modified papers and their influence on inkjet print quality. Ind Eng Chem Res 53:4660–4668. https://doi.org/10.1021/ie403595f
Spina R, Covalcante B (2018) Characterizing materials and processes used on paper tissue converting lines. Mater Today Commun 17:427–437. https://doi.org/10.1016/j.mtcomm.2018.10.006
Spiridon I, Duarte AP, Curto JMR (2003) Influence of xylanase treatment on Pinus pinaster kraft pulp. Cell Chem Technol 37:497–504
Stankovská M, Gigac J, Fišerová M, Opálená E (2019) Relationship between structural parameters and water absorption of bleached softwood and hardwood kraft pulps. Wood Res 64:261–272
Stankovská M, Fišerová M, Gigac J, Opálená E (2020) Blending impact of hardwood pulps with softwood pulp on tissue paper properties. Wood Res 65:447–458. https://doi.org/10.37763/wr.1336-4561/65.3.447458
Starov VM, Zhdanov SA, Kosvintsev SR, Sobolev VD, Velarde MG (2003) Spreading of liquid drops over porous substrates. Adv Colloid Interface Sci 104:123–158. https://doi.org/10.1016/S0001-8686Ž03.00039-3
Vieira JC, Mendes AO, Carta AM, Fiadeiro PT, Costa AP (2020a) Experimental dataset supporting the physical and mechanical characterization of industrial base tissue papers. Data Brief 33:106434. https://doi.org/10.1016/j.dib.2020.106434
Vieira JC, Mendes AO, Carta AM, Galli E, Fiadeiro PT, Costa AP (2020) Impact of embossing on liquid absorption of toilet tissue papers. BioRes 15:3888–3898. https://doi.org/10.15376/biores.15.2.3888-3898
Vieira JC, Mendes AO, Carta AM, Fiadeiro PT, Costa AP (2020) Impact of 5-ply toilet paper configuration on its

mechanical and absorption properties. BioRes 15:7475–7486. https://doi.org/10.15376/biores.15.4.7475-7486

Wågberg L, Westerlind C (2000) Spreading of droplets of different liquids on specially structured papers. Nord Pulp Paper Res J 15:598–606. https://doi.org/10.3183/NPPRJ-2000-15-05-p598-606

Wang J, Gan M, Shi J (2007) Detection and characterization of penetrating pores in porous materials. Mater Charact 58:8–12. https://doi.org/10.1016/j.matchar.2006.02.016

Weise U, Maloney T, Paulapuro H (1996) Quantification of water in different states of interaction with wood pulp fibres. Cellulose 3:189–202. https://doi.org/10.1007/BF02228801

Zambrano F, Wang Y, Zwilling JD, Venditti R, Jameel H, Rojas O, Gonzalez R (2021) Micro- and nanofibrillated cellulose from virgin and recycled fibers: a comparative study of its effects on the properties of hygiene tissue paper. Carbohyd Polym 254:117430. https://doi.org/10.1016/j.carbpol.2020.117430

Influence of Tissue Paper Converting Conditions on Finished Product Softness

António de Oliveira Mendes,[a,*] Joana Costa Vieira,[a] Ana Margarida Carta,[b] Enrico Galli,[c] Rogério Simões,[a] Manuel José dos Santos Silva,[a] Ana Paula Costa,[a] and Paulo Torrão Fiadeiro [a]

Tissue paper conversion consists of the transformation of base tissue papers into finished tissue products to meet specific demands. When base tissue paper arrives at the converting line, it already holds different requirements that were met during its manufacture in the paper machine (*e.g.*, grammage, bulk, tensile index, *etc.*). However, what happens during converting can still influence the performance and quality of the finished products. The current work addresses this topic and aims to evaluate the influence of converting conditions on the final softness. For that, two 5-ply finished tissue products were analyzed using different methodologies for their proper characterization in terms of softness and surface analysis. The analyzed products are composed by the same base tissue papers, but some changes were applied on their settings in the converting line. In particular, the base tissue papers arrangement and the embossing pressure affected the finished products, resulting in one of them being softer and more pleasant to touch, with a global handfeel (HF) value of 75.3 units, and the other revealed to be rougher and less pleasant, with a global handfeel (HF) value of 68.0 units.

Keywords: Tissue paper; Converting conditions; Finished product; Softness; Handfeel; Image Analysis

Contact information: a: Fiber Materials and Environmental Technologies (FibEnTech-UBI), Universidade da Beira Interior, R. Marquês D'Ávila e Bolama, 6201-001 Covilhã, Portugal; b: Instituto de Investigação da Floresta e Papel (RAIZ), Quinta de S. Francisco, Rua José Estevão (EN 230-1), 3800-783 Eixo, Aveiro, Portugal; c: The Navigator Company, R. Bombeiros da Celulose, 3800-536 Cacia, Portugal;
** Corresponding author: ant.mendes@ubi.pt*

INTRODUCTION

Tissue is a special and unique type of paper, as its most important use is in hygiene daily routines. Examples of tissue products include bathroom tissue, kitchen towels, industrial wipes, table napkins, facial tissue, and many others (Kimari 2000). Commonly, tissue is very well distinguished from other paper grades, due to its low grammage, typically lower than 25 g/m^2 according to Hollmark (1983), and because of its creped structure, yielding a rather distinctive surface (Hollmark 1983; Abbott and Schnabel 2000; Kimari 2000; Ramasubramanian and Shmagin 2000; Ho *et al.* 2007; Gigac and Fišerová 2008; Ramasubramanian *et al.* 2011; Raunio and Ritala 2012; Boudreau and Germgård 2014; Anukul *et al.* 2015).

Depending on product end use, specific characteristics are targeted to achieve the desired requirements. In this sense, a wide variety of products exist with specific features for different applications. Examples include products designed to have extra-absorption, extra-resistance, or extra-softness (Kimari 2000; de Assis *et al.* 2018a).

Concerning bathroom tissue, a subcategory in which toilet papers are included,

softness is a key feature for consumers (Hollmark 1983; Abbott and Schnabel 2000; Kimari 2000; Furman *et al.* 2007; de Assis *et al.* 2018a). A paper that does not meet a certain level of softness, by being too rough or unpleasant to touch, may be rejected and replaced by others. Therefore, the proper assessment of softness is of the utmost importance in this category.

During production, many aspects influence tissue paper softness, such as the type of fibers, refining additives used, creping process, and converting process (Kimari 2000; Ramasubramanian and Shmagin 2000; Ho *et al.* 2007; Gigac and Fišerová 2008; Ramasubramanian *et al.* 2011; Raunio and Ritala 2012; Boudreau and Germgård 2014; Rosen *et al.* 2014; Anukul *et al.* 2015; de Assis *et al.* 2018a; de Assis *et al.* 2018b; Raunio *et al.* 2018; Spina and Cavalcante 2018). This last aspect consists of a series of operations, such as unwinding, embossing, printing, perforating, rewinding, cutting and packaging, as shown in Fig. 1, performed on base tissue paper sheets to form a multilayer finished product, ready to be placed into the market (Kimari 2000; Vieira *et al.* 2020).

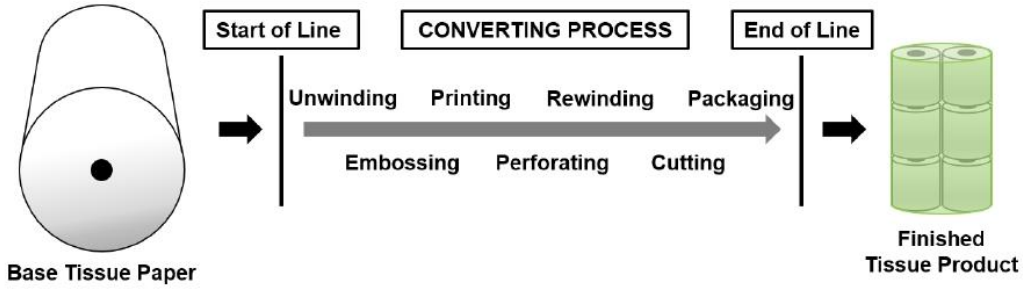

Fig. 1. Converting process operations performed on base tissue paper to obtain the finished tissue product

As already stated, before entering the converting process, the base tissue paper bears specific requirements, and the finished products will depend on these requirements. However, in the converting line, the performance and quality of the finished products may still be altered, depending on the applied converting conditions.

The current work is focused on this topic. Specifically, two commercial toilet tissue products composed of the same base tissue papers were made with changes on the settings in the converting line. All other aspects of base paper manufacture were the same. The main goal was to identify differences in both finished products in terms of softness, caused by their different converting conditions. The product characterization was carried out using two different methodologies.

EXPERIMENTAL

Materials

Two commercial toilet tissue products, identified as P2T and P3T, were collected in a factory line and used as the objects of this study. These products were formed using 2 different mother-reels, from which some samples were also collected. One of the mother-reels, identified as M2, was a 2-ply arrangement of a base tissue paper, whereas the other mother-reel, identified as M3 was a 3-ply arrangement of a different base tissue paper. These two base tissue papers were produced using mixtures of 85% hardwood eucalyptus

and 15% softwood pine and spruce European bleached kraft pulps. Although M2 and M3 were produced in different paper machines, both mother-reels have the same composition described above, with each tissue sheet having approximately the same grammage, 15 to 16 g/m^2 (ISO 12625-6 2005), and thickness, 110 to 116 µm (ISO 12625-3 2014).

Regarding the two finished products, the first P2T was converted having M2 on top and M3 on the bottom, whereas the second product P3T was converted having M3 on top and M2 on the bottom, as shown in Fig. 2. Overall, both commercial products P2T and P3T are 5-ply, with an inversion of the arrangement of the mother-reels defined at the start line of converting, in the unwinding step.

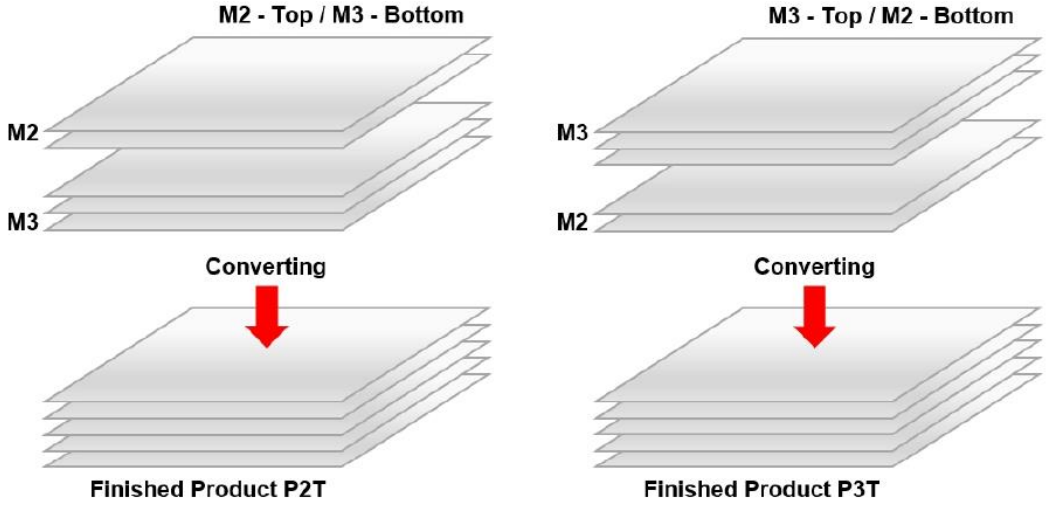

Fig. 2. Mother-reels arrangement in the converting of the 2 finished products P2T and P3T

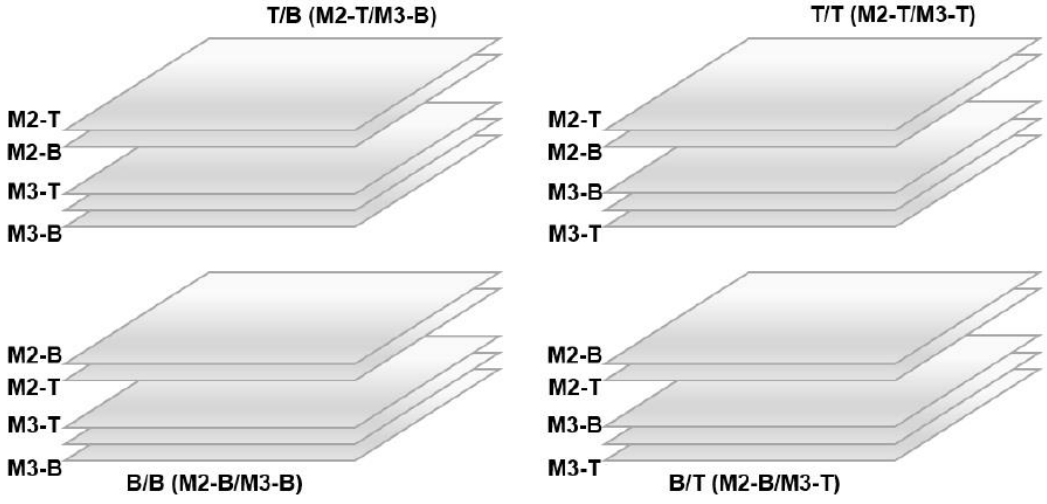

Fig. 3. The 4 tested assembled configurations T/B, T/T, B/B, and B/T using the mother-reels M2 and M3 without passing through the converting line

It is also noteworthy that products P2T and P3T consist of finished toilet tissue products, meaning that the samples of these commercial products were collected at the end of the factory converting line. However, the base tissue papers of the mother-reels M2 and M3 were completely free of any operation, as the corresponding samples of these 2 mother-reels were collected at the start of the factory converting line. Both mother-reels M2 and M3 were also assembled to create samples of all the 4 possible combinations used for production of P2T and P3T. In particular, they were simply stacked without adhesive nor any other operation conducted on them, respectively, top with bottom (configuration T/B), top with top (configuration T/T), bottom with bottom (configuration B/B), and finally bottom with top (configuration B/T), as shown in Fig. 3. These configurations were assembled to analyze if the top and bottom surfaces of the mother-reels M2 and M3, being oriented inwards or outwards in the final configurations, affect the softness results.

As a general experimental procedure rule, 10 samples of each product and of each of the 4 assembled configurations using the mother-reels were conveniently prepared according to the proper dimensions required for each equipment to be used for their characterization. Normally, from these samples, 5 were used to analyze the top surface, while the other 5 were used for analysis of the bottom surface. The results of the performed essays were expressed in terms of mean and standard deviation for the top and bottom surfaces, and in global.

Methods

Several experiments were conducted for analysis of the softness and surface properties of the samples collected and prepared for the products P2T and P3T and for the assembled configurations T/B, T/T, B/B, and B/T. There are many different approaches for the evaluation and assessment of these properties (Hollmark 1983; Rust *et al.* 1994; Hollmark and Ampulski 2004; Furman *et al.* 2007; Lima *et al.* 2009; Ruiz *et al.* 2010; Rosen *et al.* 2014; Rastogi *et al.* 2017; de Assis *et al.* 2018a; Ko *et al.* 2018; Perng *et al.* 2019; Wang *et al.* 2019). Based on those studies, two different methodologies were followed in the current work. The tissue softness analyzer (TSA) from Emtec Electronic GmbH (Leipzig, Germany), laboratory equipment, which is used in the tissue paper sector for quality control purposes, was used to perform the measurements of softness. The TSA works by simulating the sensation of the fingertips by touching the tissue samples with vertical lamella, fixed in a rotating disk, under a defined load and rotation speed. The vibrations generated during the rotation are detected by the equipment and are then processed to provide information about the samples. After this first measurement, a vertical displacement of the samples is also realized. Then, all the measured parameters, namely, the real softness (TS7), the felt smoothness/roughness (TS750), and the stiffness (D) are computed through specific algorithms to obtain a global quantification of handfeel (HF) of the analyzed samples (EMTEC Innovative Testing Solutions 2018).

A customized optical system previously used in research for other purposes was also considered for observation of the samples surfaces using specific magnifications and illumination conditions (Mendes *et al.* 2013, 2014, 2015). First, a tissue paper sample is fixed in a proper holder connected to a motorized XY motion stage, allowing the movement of the sample in both horizontal and vertical directions and for the scan of the sample across its entire area. The sample is observed from both sides (top and bottom surfaces) by two different image detectors. The registered images were set with a field of view of $\approx 10 \times 10$ mm^2, a resolution of 1024×1024 pixels, a bit depth of 10 bits (1024 gray levels), a gain of 1024 arbitrary units, and an exposure time of 6 milliseconds. The magnification used in

the system is controlled by two macro-objectives, making it possible to observe both surfaces of the sample with specific magnifications, depending on the application in use and of the required level of detail. Finally, the sample can be illuminated from only one side, from the other side, or from both sides through use of two LED light sources. These conditions were used to optimize the system for a convenient and correct observation of the samples in analysis. All the elements of the system are connected to several hardware control units and to a computer, being operated through a graphical user interface software application implemented using the MATLAB® programming language and the Toolboxes for Image Acquisition and Image Processing (Mendes *et al.* 2013, 2014, 2015).

Three experiments (A, B, and C) were performed in this work with the presented methods. Experiments A and B were focused on the TSA measurements, TS7, TS750, *D* and HF, this last calculated using the algorithm TPII of the equipment, to evaluate products P2T and P3T and the different assembled configurations T/B, T/T, B/B, and B/T. Experiment C was focused on the visualization of the samples surfaces with the customized optical system.

RESULTS AND DISCUSSION

Experiment A – TSA Measurements of the Products P2T and P3T

Table 1 contains the HF results for the products P2T and P3T, obtained using the TSA (EMTEC Innovative Testing Solutions 2018).

Table 1. HF for the 2 End-use Products P2T and P3T

Product	Top Surface HF	Bottom Surface HF	Global HF
P2T	75.5 ± 1.5	75.1 ± 2.0	75.3 ± 1.7
P3T	73.2 ± 1.4	62.9 ± 2.6	68.0 ± 5.8

Note: Values shown are the mean ± standard deviation

Considering the top surface of P2T and P3T, similar values of HF are shown for both cases. However, the case differed considerably for the bottom surface of each paper. For the product P3T, a value of 62.9 HF units was obtained, which is a large drop compared to its top surface (difference of 10.3 HF units) and compared to the bottom surface of P2T (difference of 12.2 HF units).

In terms of global results, the product P2T has a HF of 75.3 units, whereas the product P3T has a HF of 68.0 units. The global HF standard deviation of the product P3T is also very different and the highest, which is caused by the difference noted in the HF results between the top and bottom surfaces of the product.

These results raise a question. What happened in product P3T, more specifically on its bottom surface? Both products P2T and P3T are composed by the same mother-reels but with inverted arrangements. Was this the cause that led to a HF decrease in P3T comparatively to P2T, or something else? To further explore this question, let us consider the caliper (thickness), grammage and the remaining parameters measured by the TSA (Table 2).

Table 2. Caliper, Grammage, TS7, TS750 and *D* for the 2 End-use Products P2T and P3T

Product	Surface	Caliper (µm)	Grammage (g/m^2)	TS7	TS750	*D* (mm/N)
P2T	Top	-	-	14.1 ± 0.9	61.2 ± 7.2	1.7 ± 0.0
	Bottom	-	-	14.7 ± 0.9	50.4 ± 7.1	1.7 ± 0.0
	Global	695 ± 14	76.4 ± 0.5	14.4 ± 0.9	55.8 ± 8.8	1.7 ± 0.0
P3T	Top	-	-	15.2 ± 0.7	70.2 ± 5.4	1.8 ± 0.1
	Bottom	-	-	19.4 ± 1.1	123.4 ± 26.2	1.8 ± 0.1
	Global	725 ± 16	76.0 ± 0.2	17.3 ± 2.4	96.8 ± 33.2	1.8 ± 0.1

Note: Values shown are the mean ± standard deviation

From Table 2, it can be seen that P2T and P3T reveal similar values of caliper, grammage, and stiffness (*D*), although P3T was slightly thicker (30 µm more), and had a slightly lower grammage and stiffness (higher value of *D* indicates lower stiffness) than P2T. Regarding the other two parameters, TS7 and TS750, they are both higher for both surfaces of P3T comparatively to P2T, especially for its bottom surface. Higher values for these two parameters indicate lower surface softness and lower smoothness, respectively, being concordant with the HF values presented in Table 1.

At continuation, a second experiment was conducted considering now the 4 possible assembled configurations T/B, T/T, B/B, and B/T used for production of P2T and P3T.

Experiment B – TSA Measurements of the Arranged Configurations T/B, T/T, B/B and B/T

The HF for the assembled configurations T/B, T/T, B/B, and B/T are shown in Table 3.

Table 3. HF for the 4 Assembled Configurations T/B, T/T, B/B, and B/T

Configuration	Top Surface HF	Bottom Surface HF	Global HF
T/B	76.8 ± 0.6	78.0 ± 2.1	77.4 ± 1.6
T/T	77.6 ± 1.7	79.8 ± 0.7	78.7 ± 1.7
B/B	78.6 ± 0.9	80.1 ± 1.1	79.4 ± 1.2
B/T	79.1 ± 1.7	79.3 ± 2.6	79.2 ± 2.1

Note: Values shown are the mean ± standard deviation

From Table 3, only small variations of HF were noted for the four assembled configurations T/B, T/T, B/B, and B/T. After analyzing the results of each configuration, the maximum difference registered between the top and bottom surfaces was 2.2 HF units associated to the configuration T/T, which was very far from the 10.3 HF units registered for the product P3T in the previous experiment. The minimum difference registered from top to bottom was 0.2 HF units associated to the configuration B/T. The maximum difference registered between configurations was 2.3 HF units on the top surface and 2.1 HF units on the bottom surface. To further explore the four assembled configurations, their values of caliper (thickness), grammage, and of the remaining parameters measured by the TSA were also considered (Table 4).

Table 4. Caliper, Grammage, TS7, TS750, and *D* for the Four Assembled Configurations T/B, T/T, B/B, and B/T

Configuration	Surface	Caliper (µm)	Grammage (g/m^2)	TS7	TS750	*D* (mm/N)
T/B	Top	-	-	13.9 ± 0.4	35.5 ± 1.3	1.5 ± 0.0
	Bottom	-	-	13.5 ± 1.1	26.4 ± 2.5	1.5 ± 0.0
	Global	497 ± 4	79.0 ± 1.1	13.7 ± 0.8	31.0 ± 5.2	1.5 ± 0.0
T/T	Top	-	-	13.7 ± 1.0	31.3 ± 1.0	1.5 ± 0.0
	Bottom	-	-	12.6 ± 0.4	24.0 ± 3.0	1.5 ± 0.0
	Global	495 ± 3	79.0 ± 1.1	13.1 ± 0.9	27.7 ± 4.4	1.5 ± 0.0
B/B	Top	-	-	13.1 ± 0.5	28.1 ± 1.7	1.5 ± 0.0
	Bottom	-	-	12.3 ± 0.6	27.2 ± 1.4	1.5 ± 0.0
	Global	496 ± 5	79.0 ± 1.1	12.7 ± 0.7	27.7 ± 1.6	1.5 ± 0.0
B/T	Top	-	-	12.9 ± 1.0	26.3 ± 2.0	1.5 ± 0.0
	Bottom	-	-	12.9 ± 1.4	22.6 ± 1.1	1.5 ± 0.0
	Global	495 ± 6	79.0 ± 1.1	12.9 ± 1.1	24.5 ± 2.5	1.5 ± 0.0

Note: Values shown are the mean ± standard deviation

From Table 4, it can be seen that all four assembled configurations had the same grammage and stiffness (*D*) and had practically the same caliper. A special remark must be made to the lower caliper of the four assembled configurations comparatively to the finished products P2T and P3T, and also of their higher stiffness, both of them caused by the absence of embossing. The embossing operation usually increases the caliper and decreases the stiffness of the samples. Regarding the other two parameters, TS7 and TS750, they revealed fluctuations for the four assembled configurations. However, were shown to be concordant with the HF values, that is, higher HF values were globally associated with lower values of TS7 and TS750, whereas lower HF values were globally associated with higher values of TS7 and TS750.

Overall, this experiment showed two different things. First, the HF values presented in Table 3 only reveal small variations for the four assembled configurations. Therefore, whether the surfaces of the mother-reels are positioned inwards or outwards in the final configurations does not seem to be a crucial point that justifies the detected decrease in HF registered in the previous experiment. This can also be confirmed from the other parameters measured for the four assembled configurations presented in Table 4. There are cases in which relevant differences can be noted in softness on both surfaces of a mother-reel and therefore, how the mother-reel is positioned in the finished product can be a very relevant point. However, that is not what happened in this case since the tested surfaces were all very similar with analogous characteristics.

Second, the HF values obtained in the four assembled configurations are higher than those obtained in the two products P2T and P3T. This means that converting had a negative effect on the softness values, however, to different extents. Product P2T only showed a slight decrease in HF compared to the assembled configurations. Regarding product P3T, its top surface also suffered only a slight decrease in HF in comparison to the assembled configurations, although higher than P2T. The huge difference in HF, which deserved our attention, was clearly associated with the bottom surface of the product P3T. Once again, this can be confirmed from the other parameters measured for the four assembled configurations presented in Table 4. In particular, although some differences can be identified in the values of the parameters TS7 and *D* for the four assembled configurations comparatively to the finished products, it was the TS750 parameter that

revealed very large differences in the values obtained for the four assembled configurations in comparison to the finished products, this parameter being related with the surface geometry and with the embossing process.

In such way, this experiment strongly supports that the differences noted in softness, between products P2T and P3T, were generated in the converting process. Therefore, the next step will be to investigate what happens in the converting line. What exactly causes the considerable difference in HF between the top and bottom surfaces of product P3T? To further explore this question, a third experiment was conducted using the optical system for observation of the products surfaces of P2T and P3T and identify possible differences that might explain their distinct behaviors.

Experiment C – Image Analysis of the Products P2T and P3T

In this last experiment, both products P2T and P3T were analyzed using a customized optical system (Mendes *et al.* 2013, 2014, 2015). For the two products P2T and P3T, a set of 8 images was registered.

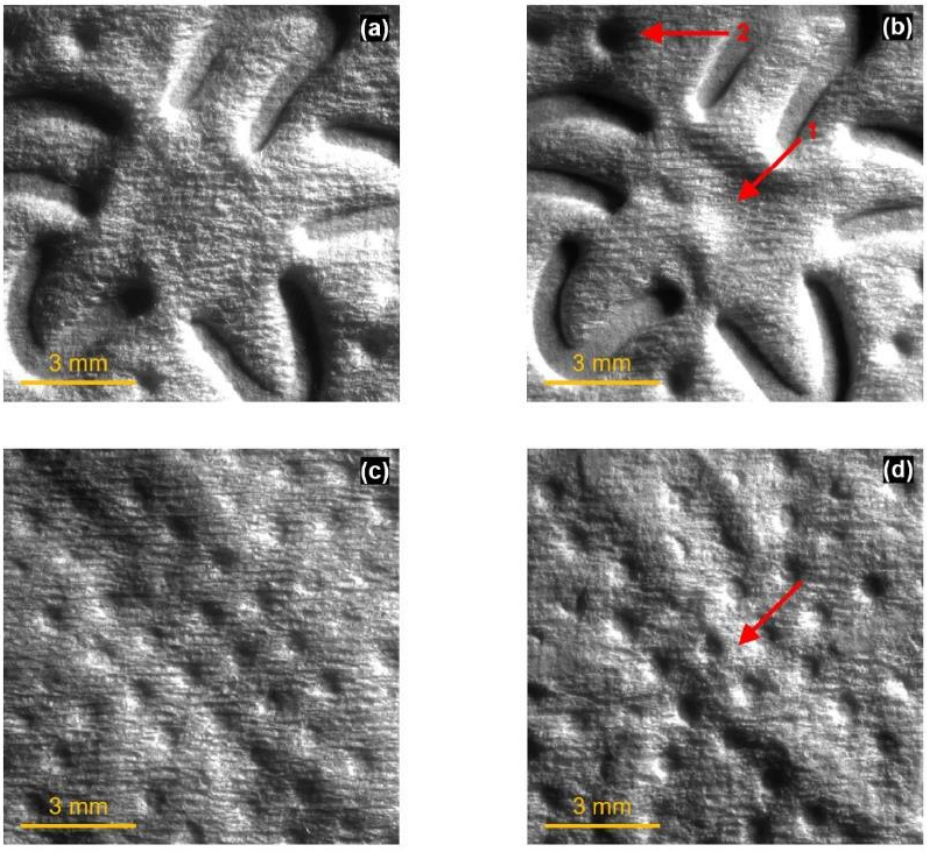

Fig. 4. Images of the embossed patterns engraved on the products a) *star* on top surface of P2T, b) *star* on top surface of P3T, c) *small holes* on bottom surface of P2T, and d) *small holes* on bottom surface of P3T. The images of c) and d), area ME_1were captured in the same exact location of the images of a) and b), area DE_1, but seen from the opposite side of the papers (size of images ≈ 10×10 mm^2).

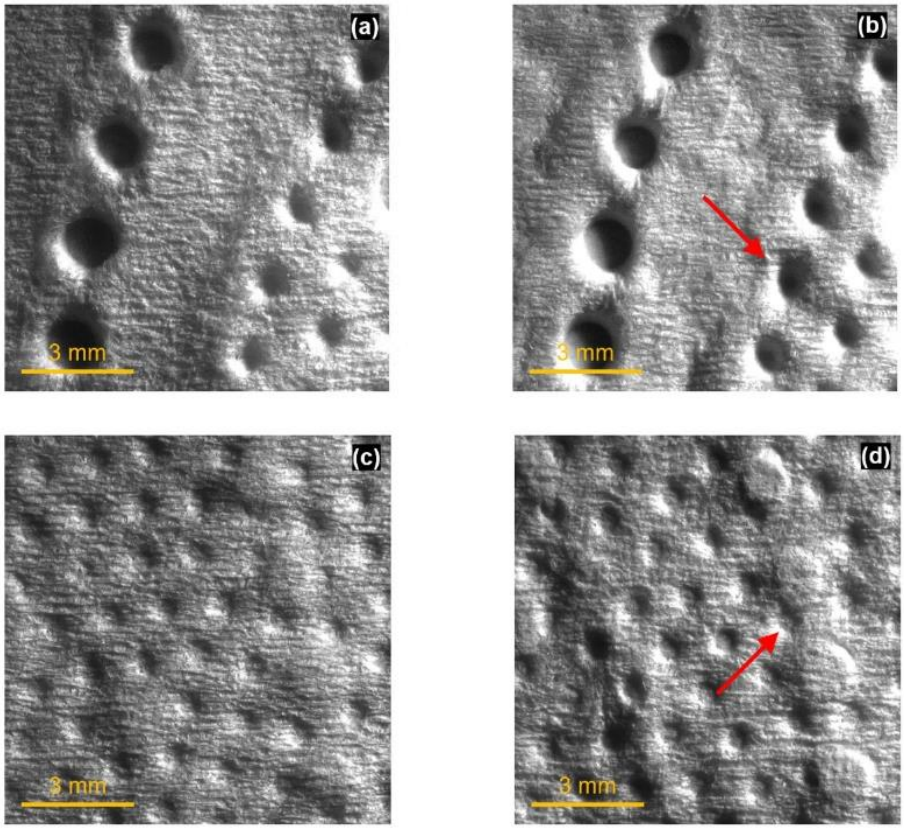

Fig. 5. Images of the embossed patterns engraved on the products a) *deep holes* on top surface of P2T, b) *deep holes* on top surface of P3T, c) *small holes* on bottom surface of P2T, and d) *small holes* on bottom surface of P3T. The images of c) and d), area ME_2, were captured in the same exact location of the images of a) and b), area DE_2, but seen from the opposite side of the papers (size of images ≈ 10×10 mm^2).

The images correspond to distinct areas of the "deco" (top surface) and "micro" (bottom surface) embossing drawings that were engraved on P2T and P3T at the converting line. The "deco" embossing shown in the images is composed of a *star* (area DE_1) and a pattern of *deep holes* (area DE_2). The "micro" embossing shown in the images is composed of a grid of *small holes* in the place where the *star* was engraved (area ME_1) and where the *deep holes* were engraved (area ME_2). The images in Fig. 4 and Fig. 5 correspond to these drawings' areas as seen from the corresponding top and bottom surfaces on both products.

Several interesting conclusions were made for both products. As shown in Fig. 4 a) and b), the top surface of P2T shows a flatter area for the embossed *star*, whereas P3T shows a curlier area for the same drawing (see red arrow 1 in Fig. 4 b). In addition, some details of the "deco" embossing appear to be a little deeper in PT3 than in PT2 (see red arrow 2 in Fig. 4 b). From Fig. 5 a) and b), the top surfaces of P2T and P3T show the pattern of *deep holes* embossed with practically the same aspect, but also some details of the "deco" embossing appeared to be deeper in PT3 than in PT2 (see red arrow in Fig. 5 b indicating the 5 holes located in the right inferior quadrant of the image). These observations are consistent with the similar values of HF on the top surfaces of P2T and P3T. Although, a slight decrease of HF was noted on P3T comparatively to P2T, the deeper

details do not affect seriously the top surfaces of the product.

Some differences were identified on the bottom surfaces of the products P2T and P3T. As shown in Fig. 4 and 5 c) and d), the grid of *small holes* embossed directly in the bottom surfaces of P2T and P3T is similar for both cases, yet slightly more pronounced in P3T than in P2T. However, the considerable difference between P2T and P3T lies in the "deco" engravings of P3T being seen more prominently from the bottom surface, comparatively to P2T. In Fig. 4 c) a slight curvature is noticed in P2T on the location on which the embossed *star* was engraved, whereas in Fig. 4 d) well defined marks coincident with the limits of the embossed *star* are easily noticed in P3T (see red arrow in Fig. 4 d). In Fig. 5 c) and d) the limits of the embossed pattern of *deep holes* are barely noticed in P2T, whereas in P3T they are a lot more pronounced and their limits are easily identified in the image (see red arrow in Fig. 5 d). In such way, the observations made for the bottom surfaces of the products P2T and P3T appear to be consistent with the results of HF which revealed a huge drop for the bottom surface of the product P3T comparatively to P2T.

Having in consideration these observations, the same question raised earlier can still be posed. Why do the products P2T and P3T have such different bottom surfaces? The answer is actually simple. In the converting line, the mother-reel placed on top is embossed with the "deco engravings" whereas the mother-reel placed on the bottom is embossed with the "micro engravings". The two mother-reels are then subjected to a last operation that joins together the entire set of tissue sheets (ply bonding). In the case of the two products addressed in this work, more pressure was applied in the "deco" embossing of P3T (≈ 38 to 40 kg/cm) than in P2T (≈ 20 to 30 kg/cm). This additional pressure resulted in the curlier *star*, the more pronounced pattern of *deep holes*, and in the deeper details engraved in the top surface of P3T relatively to P2T, as can be seen in Fig. 4 and 5 a) and b). This also resulted in the "deco engravings" of P3T being more prominent from the opposite side comparatively to P2T.

When the top surface of the products is under evaluation, either by an equipment or by touch, the "deco engravings" in its surface are perceived as depressions, and therefore, neither the equipment nor the consumer will notice them very negatively, since they do not affect considerably the global touch of the surface. The "micro engravings" in the bottom surface are not prominent, therefore not perceived on the top surface of the products, and also do not affect the top surface results. However, when the bottom surface of the products is being evaluated, the case differs. The "micro engravings" are not noticed overly by the equipment or by touch on the bottom surfaces, since the product P2T shows a softness comparable to that obtained in the top surfaces of P2T and P3T, suggesting that it has little effect on softness. In both products, similar values of pressure were applied in the "micro" embossing (≈ 20 to 30 kg/cm). However, a second effect happened in this case. The "deco" embossing drawings perceived as depressions in the top surfaces, were perceived as elevations from the other side. In such way, these embossed drawings were seen and felt from the bottom surface of the products. Notably, because the product P2T has the 3-ply mother-reel (M3) on bottom, it has an additional tissue sheet functioning as a protection minimizing the effect of the "deco" embossing on the bottom surface of P2T. On the other hand, the product P3T has the 2-ply mother-reel (M2) on the bottom, meaning that the additional sheet is not present in this case, leaving its bottom surface more exposed to the "deco" embossing. Therefore, this will result exactly in what was registered and seen through the performed experiments presented in this work, an overall softer and more pleasant to touch product P2T, and an overall rougher and less pleasant product P3T.

CONCLUSIONS

1. Two objective methodologies were used in this work to perform a complete analysis of two 5-ply finished tissue products for their softness and surface characterization. Both products were composed by the same base tissue papers, but with some changes made in their converting conditions.
2. The bottom surface of P3T exhibited the lowest softness. The remaining three surfaces, both tops of P2T and P3T and bottom of P2T, revealed similar values of softness.
3. The customized optical system enabled, through image analysis, the identification in both products of the causes behind the obtained differences in softness. In particular, it was found that the "deco" embossing was seen and felt differently in the bottom surface of both products. This occurrence depended on the embossing pressure and on the number of plies present in the bottom surface.
4. For this particular case, having the 2-ply mother-reel (M2) placed on top and the 3-ply mother-reel (M3) placed on bottom, instead of the other way around, and with lower pressure used to engrave the "deco" embossing drawings, resulted in a finished product with better overall performance in terms of softness. It is true that if only the top surface of the end-use products is assessed, the differences between products are not very relevant. However, if the products are analyzed as a whole, assessing both surfaces of the products, the differences between both products are relevant, and the product P2T is more pleasant to touch, having a better softness quality than the product P3T.

ACKNOWLEDGMENTS

The authors gratefully acknowledge the funding of this work that was carried out under the Project InPaCTus – Innovative Products and Technologies from Eucalyptus, Project Nº 21874 funded by Portugal 2020 through European Regional Development Fund (ERDF) in the frame of COMPETE 2020 nº 246/AXIS II/2017. The authors are also thankful for financial support from the Fiber Materials and Environmental Technologies (FibEnTech-UBI) research unit of the Universidade da Beira Interior on extent of the project UIDB/00195/2020. Finally, the authors acknowledge the materials, access to equipment and installations, and all the general support given by The Navigator Company, RAIZ, and the Optical Center, Department of Physics, Department of Textile Science and Technology, and Department of Chemistry of the Universidade da Beira Interior.

REFERENCES CITED

Abbott, J. C., and Schnabel, K. (2000). "Hygiene papers," in: *Papermaking Science and Technology, Book 17 – Pulp and Paper Testing*, J. E. Levlin, and L. Söderhjelm (eds.), Finnish Paper Engineers' Association and TAPPI, Helsinki, Chapter 11.

Anukul, P., Khantayanuwong, S., and Somboon, P. (2015). "Development of laboratory wet creping method to evaluate and control pulp quality for tissue," *TAPPI Journal* 14(5), 339-345. DOI: 10.32964/TJ14.5.339

Boudreau, J., and Germgård, U. (2014). "Influence of various pulp properties on the

adhesion between tissue paper and Yankee cylinder surface," *BioResources* 9(2), 2107-2114. DOI: 10.15376/biores.9.2.2107-2114

de Assis, T., Reisinger, L. W., Pal, L., Pawlak, J., Jameel, H., and Gonzalez, R. W. (2018a). "Understanding the effect of machine technology and cellulosic fibers on tissue properties – A review," *BioResources* 13(2), 4593-4629. DOI: 10.15376/biores.13.2.4593-4629

de Assis, T., Reisinger, L. W., Dasmohapatra, S., Pawlak, J., Jameel, H., Pal, L., Kavalew, D., and Gonzalez, R. W. (2018b). "Performance and sustainability *vs.* the shelf price of tissue paper kitchen towels," *BioResources* 13(3), 6868-6892. DOI: 10.15376/biores.13.3.6868-6892

EMTEC Innovative Testing Solutions (2018). "TSA - Tissue softness analyzer," (https://www.emtec-electronic.de/en/tsa-tissue-softness-analyzer.html), Accessed on June 7, 2018.

Furman, G., de Roever, E., Frette, G., and Gomez, S. (2007). "Analysis of the surface softness of tissue paper using confocal laser scanning microscopy," in: *Proceedings of Tissue World 2007 Conference*, Nice, France, pp. 1-10.

Gigac, J., and Fišerová, M. (2008). "Influence of pulp refining on tissue paper properties," *TAPPI Journal* 7(8), 27-32.

Ho, J., Hutton, B. F., Proctor, J., and Batchelor, W. (2007). "Development of a tissue creping test rig," in: *Proc. CHEMECA 2007*, Melbourne, Australia, pp. 1326-1332.

Hollmark, H. (1983). "Mechanical properties of tissue," in: *Handbook of Physical and Mechanical Testing of Paper and Paperboard*, Vol. 1., R. E. Mark (ed.), Dekker, New York.

Hollmark, H., and Ampulski, R.S. (2004). "Measurement of tissue paper softness: A literature review," *Nordic Pulp & Paper Research Journal* 19(3), 345-353. DOI: 10.3183/npprj-2004-19-03-p345-353

ISO 12625-3 (2014). "Tissue paper and tissue products – Part 3: Determination of thickness, bulking thickness and apparent bulk density and bulk," International Organization for Standardization, Geneva, Switzerland.

ISO 12625-6 (2005). "Tissue paper and tissue products – Part 6: Determination of grammage," International Organization for Standardization, Geneva, Switzerland.

Kimari, O. (2000). "Chapter 3 – Tissue" in: *Papermaking Science and Technology, Book 18 – Paper and board grades.* H. Paulapuro (ed.), Finnish Paper Engineers' Association and TAPPI, Helsinki.

Ko, Y. C., Park, J. Y., Melani, L., Park, N. Y., and Kim, H-J. (2018). "Principles of developing physical test methods for disposable consumer products," *Nordic Pulp & Paper Research Journal* 34(1), 75-87. DOI: 10.1515/npprj-2018-0029

Lima, M., Silva, L. F., Vasconcelos, R., and Carneiro, A. (2009). "FRICTORQ, Mechatonic design for the objective measurement of friction in 2D soft surfaces," in: *Proceedings of MECAHITECH'09*, Bucharest, Romania, pp. 144-153.

Mendes, A. O., Fiadeiro, P. T., Costa, A. P., Amaral, M. E., and Belgacem, M. N. (2013). "Retro-diffusion and transmission of laser radiation to characterize the paper fiber distribution and mass density," in: *Proceedings of SPIE 8785*, Porto, Portugal, 8785AY-1/8785AY-8. DOI: 10.1117/12.2022367

Mendes, A. O., Fiadeiro, P. T., Costa, A. P., Amaral, M. E., and Belgacem, M. N. (2014). "Study of repeatability of an optical laser system for characterization of the paper fiber distribution and mass density," in: *Proceedings of SPIE 9286*, Aveiro, Portugal, 92862Y-1/92862Y-8. DOI: 10.1117/12.2062697

Mendes, A. O., Fiadeiro, P. T., Costa, A. P., Amaral, M. E., and Belgacem, M. N. (2015). "Laser scanning for assessment of the fiber anisotropy and orientation in the surfaces and bulk of the paper," *Nordic Pulp & Paper Research Journal* 30(2), 308-318. DOI: 10.3183/npprj-2015-30-02-p308-318

Perng, Y. S., Teng, T. Y., and Chang, C. H. (2019). "A study of the softness of household tissues using a tissue softness analyzer and hand-felt panels," *TAPPI Journal* 18(3), 195-209. DOI: 10.32964/TJ18.3.195

Ramasubramanian, M. K., and Shmagin, D. L. (2000). "An experimental investigation of the creping process in low-density paper manufacturing," *Journal of Manufacturing Science and Engineering* 122(3), 576-581. DOI: 10.1115/1.1285908

Ramasubramanian, M. K., Sun, Z., and Gupta, S. (2011). "Modeling and simulation of the creping process," in: *PaperCon 2011 Vol 1*, Covington, USA, pp. 576-582.

Rastogi, V. K., Grossmann, H., Ray, A. K., and Greiffenberg, I. (2017). "Dependence of softness perception on tissue physical properties and development of neural model for predicting softness," *IPPTA – The official International Journal*, 29(2), 128-135.

Raunio, J. P., and Ritala, R. (2012). "Simulation of creping pattern in tissue paper," *Nordic Pulp & Paper Research Journal* 27(2), 375-381. DOI: 10.3183/npprj-2012-27-02-p375-381

Raunio, J. P., Löyttyniemi T., and Ritala, R. (2018). "Online quality evaluation of tissue paper structure on new generation tissue machines," *Nordic Pulp & Paper Research Journal* 33(1), 133-141. DOI: 10.1515/npprj-2018-3004

Rosen, B-G., Fall, A., Rosen, S., Farbrot, A., and Bergström, P. (2014). "Topographic modelling of haptic properties of tissue products," in: *Journal of Physics: Conference Series* 483(012010), Taipei, Taiwan, pp. 1-6. DOI: 10.1088/1742-6596/483/1/012010

Ruiz, J., Sacon, V. M., Pescatori Silva, F. H., Eichhorn, S., Bley, L., Sabel, H., Villette, M. J., Eymin Petot-Tourtollet, G., and Petit-Conil, M. (2010). "Tissue softness potential: An objective online industrial value," *ATIP* 64(3), 10-15.

Rust, J. P., Keadle, T. L., Allen, D. B., Shalev, I., and Barker, R. L. (1994). "Tissue softness evaluation by mechanical stylus scanning," *Textile Research Journal* 64(3), 163-168. DOI: 10.1177/004051759406400306

Spina, R., and Cavalcante, B. (2018). "Characterizing materials and processes used on paper tissue converting lines," *Materials Today Communications* 17, 427-437. DOI: 10.1016/j.mtcomm.2018.10.006

Vieira, J. C., Mendes, A. O., Carta, A. M., Galli, E., Fiadeiro, P. T., and Costa, A. P. (2020). "Impact of embossing on liquid absorption of toilet tissue papers," *BioResources* 15(2), 3888-3898. DOI: 10.15376/biores.15.2.3888-3898

Wang, Y., de Assis, T., Zambrano, F., Pal, L., Venditti, R., Dasmohapatra, S., Pawlak, J., and Gonzalez, R. (2019). "Relationship between human perception of softness and instrument measurements," *BioResources* 14(1), 780-795. DOI: 10.15376/biores.14.1.780-795

Article submitted: May 17, 2020; Peer review completed: July 3, 2020; Revised version received and accepted: July 28, 2020; Published: July 31, 2020.
DOI: 10.15376/biores.15.3.7178-7190
ERRATUM: August 11, 2020: The value in Table 4 was changed from 76.4 ± 0.5 to 79.0 ± 1.1. This edit does not change the conclusions of the paper.

Appendix B – Conference Presentations

B1. Abstract I – Embossing Pressure Effect on Mechanical and Softness Properties of Industrial Base Tissue Papers with Finite Element Method Validation

Vieira, J.C., Mendes, A.O., Ribeiro, M.L., Vieira, A.C., Carta, A.M., Fiadeiro, P.T., Costa, A.P.
Materiais 2022 – XX Congress of the Portuguese Society of Materials, XI International Materials Symposium, II Iberian Congress on Materials Science and Technology, 10 - 13 April 2022, Polytechnic of Leiria, Marinha Grande, Portugal.
Mater. Proc. 2022, 8, 52.
https://doi.org/10.3390/materproc2022008052

Abstract I correspond to the work developed, described, and later published in Article II. This work was presented at the above-mentioned congress as an oral communication.

B2. Abstract II – Embossing Influence on the 3D Structure and Key Properties of Tissue Paper

Curto, J.M.R., **Vieira, J.C.**, Morais, F.P., Mendes, A.O., Carta, A.M., Simões, R.S., Fiadeiro, P.T., Amaral, M.E., Costa, A.P.
XXV TECNICELPA – International Forest, Pulp and Paper Conference | XI CIADICYP 2021, 9 - 12 March 2021 – PORTUGAL

Abstract II corresponds to the work developed, described, and later published in Articles V and XI. This work was presented at the above-mentioned congress as an oral communication.

materials proceedings

MDPI

Abstract

Embossing Pressure Effect on Mechanical and Softness Properties of Industrial Base Tissue Papers with Finite Element Method Validation †

Joana Costa Vieira [1,*], António de O. Mendes [1], Marcelo Leite Ribeiro [1,2], André Costa Vieira [3], Ana Margarida Carta [4], Paulo Torrão Fiadeiro [1] and Ana Paula Costa [1]

[1] Fiber Materials and Environmental Technologies Research Unit (FibEnTech-UBI), Universidade da Beira Interior, Rua Marquês d'Ávila e Bolama, 6201-001 Covilhã, Portugal; ant.mendes@ubi.pt (A.d.O.M.); malribei@usp.br (M.L.R.); fiadeiro@ubi.pt (P.T.F.); anacosta@ubi.pt (A.P.C.)
[2] Aeronautical Engineering Department, São Carlos School of Engineering, University of São Paulo, São Carlos 05508-060, SP, Brazil
[3] Center for Mechanical and Aerospace Science and Technologies (C-MAST-UBI), Universidade da Beira Interior, Rua Marquês d'Ávila e Bolama, 6201-001 Covilhã, Portugal; andre.costa.vieira@ubi.pt
[4] Forest and Paper Research Institute (RAIZ), R. José Estevão, Eixo, 3800-783 Aveiro, Portugal; ana.carta@thenavigatorcompany.com
* Correspondence: joana.costa.vieira@ubi.pt
† Presented at the Materiais 2022, Marinha Grande, Portugal, 10–13 April 2022.

Keywords: embossing prototype; eucalyptus-based fibrous materials; FEM simulation; mechanical properties; pressure; softness; tissue paper

check for updates

Citation: Vieira, J.C.; Mendes, A.d.O.; Ribeiro, M.L.; Vieira, A.C.; Carta, A.M.; Fiadeiro, P.T.; Costa, A.P. Embossing Pressure Effect on Mechanical and Softness Properties of Industrial Base Tissue Papers with Finite Element Method Validation. *Mater. Proc.* **2022**, *8*, 52. https://doi.org/10.3390/materproc2022008052

Published: 31 May 2022

At this moment, the importance of tissue paper should be highlighted because of its high production increase in the last 10 years at a rate of 3.6% per year. Tissue paper is a product composed with virgin and/or recycled fibers, manufactured with low grammage, creped, and depending on the application, embossed. Embossing is a converting process in which the surface of a tissue paper sheet is changed under high pressure, allowing different functions such as toilet paper, kitchen towels, napkins, and facial paper. In this work, the authors intend to study how the embossing pressure affects the main properties of tissue paper, using a laboratory embossing system (see Figure 1) with two embossing patterns as shown in Figure 2. To perform this work, industrial base tissue paper (only creped) from two different Portuguese factories were used. Both papers are composed of a mixture of bleached hardwood (*Eucalyptus globulus*) and softwood (*Pinus*) kraft pulps, with hardwood being present in greater quantities. These two papers were selected because they have a very similar grammage and because the respective paper machines operate differently. The industrial base tissue paper designated by A was produced on a machine with a double headbox and steel creping blade, and the industrial base tissue paper designated by B was produced on a machine with a single headbox and ceramic creping blade.

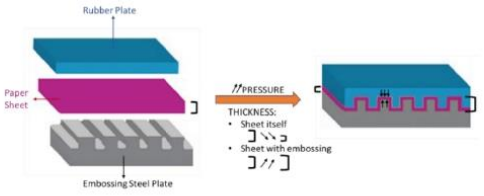

Figure 1. Schematic of the embossing process with pressure action effects.

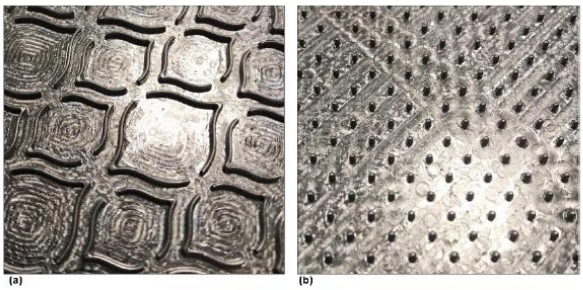

Figure 2. Photographs of steel embossing plates: (**a**) deco embossing and (**b**) micro embossing.

The behavior of the density and mechanical strength of the two samples for different pressures and without embossing patterns was studied. The effect of pressure when densifying the paper sheet provides a gain in mechanical strength as shown in Figure 3.

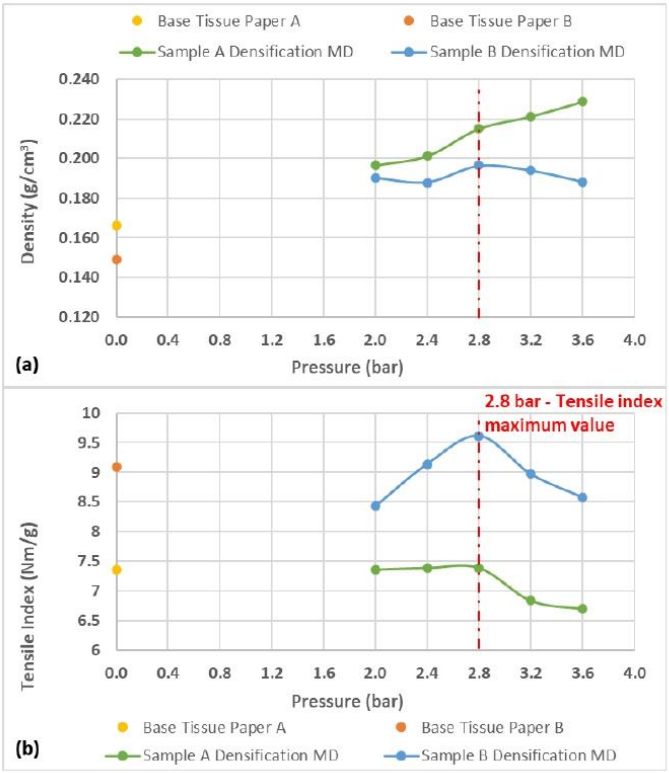

Figure 3. Results obtained for: (**a**) density and (**b**) tensile index with the pressure increase in the base tissue paper densification of the samples A and B.

Looking at the cross-section Scanning Electron Microscope (SEM) images in Figure 4, it is clear that in both cases, with increasing pressure, crepe waves decrease its height. In the case of sample B, the visible destruction of the crepe wave should be noted. These images corroborate the results discussed above in which sample B has a more fragile fibrous sheet structure.

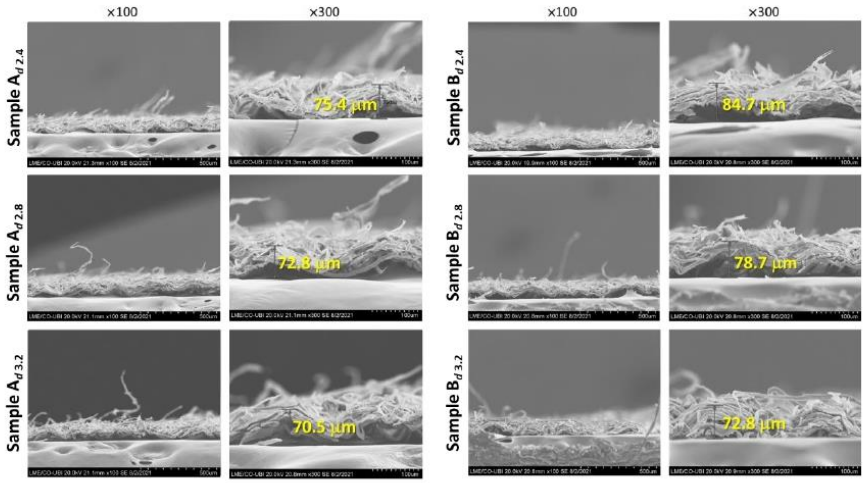

Figure 4. SEM images of cross-sections in samples A and B, at two magnifications (×100 and ×300), at pressures 2.4, 2.8, and 3.2 bar. In the images with x300 magnification, the distances from the base to the crepe of the crepe wave are shown.

As a result, there is an optimal pressure for the embossing process, where the effect of pressure when densifying the paper sheet can be advantageous, as the gain in mechanical strength can counterbalance the losses with the embossing operation. The liquid interaction with the different densified paper structures was also considered in this study to evaluate the spreading dynamic.

As expected, the structural properties of the paper sheet are more affected by the micro embossing pattern than by the deco. It should be noted that the structural property most affected is thickness, where, for the micro embossing pattern, an increase of 147% was obtained, while for the deco embossing pattern, it remained practically constant with increasing pressure. As the remaining structural properties are directly related to the thickness, they did not undergo major changes for the deco embossing pattern, but for the micro embossing pattern, the changes were in accordance with those obtained for the thickness. These findings were verified in both samples, A and B.

The mechanical strength behavior with the pressure for the two embossing patterns in samples A and B are represented in Figure 5.

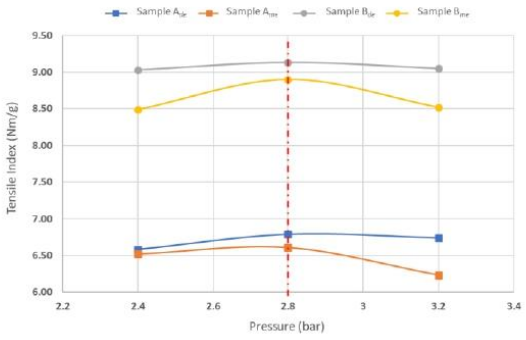

Figure 5. Results obtained for the tensile index, with the pressure increase in samples A and B with deco and micro embossing.

Comparing the industrial toilet base tissue paper with and without embossing, for the micro embossing pattern, we obtained a loss of about 10% and 2% for sample A and B, respectively. Regarding the embossing deco pattern, as expected, this loss is smaller, obtaining about 8% and 0% for samples A and B, respectively. These results are in line with what was previously discussed, proving that the densification of the sheet was advantageous so that the loss of mechanical properties by the embossing operation was minimized for the pressure of 2.8 bar.

This behavior was also studied using the Explicit Finite Element Method (FEM), considering densification as an associative isotropic hardening associate with an anisotropic elasto-plastic model. This model was implemented as a VUMAT (Vectored User MATerial), which is linked to Commercial Finite Element Software Abaqus™ version 6.14 (Waltham, MA, USA) to simulate the embossing process. The displacement fields can be observed in Figure 6 for both embossing patterns.

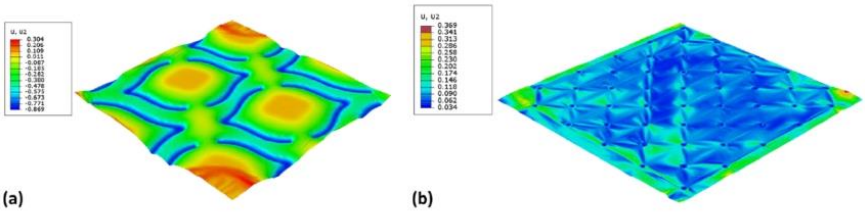

Figure 6. Displacement fields for both embossing patterns: (**a**) deco and (**b**) micro.

Finally, Figure 7 shows the behavior of the important softness property with embossing pressure for the two patterns alone and combined in a final 2-ply product.

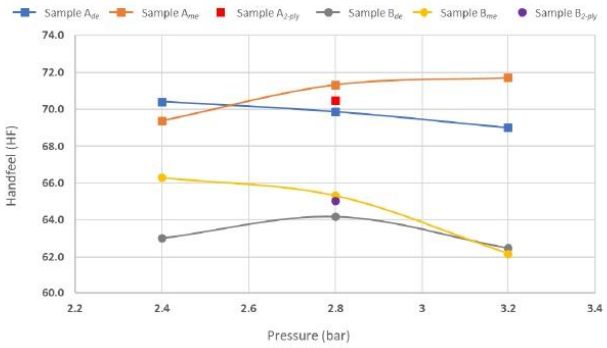

Figure 7. Results obtained for handfeel (HF), with the pressure increase in samples A and B with deco and micro embossing.

The handfeel (HF)value for a 2-ply final product with the two patterns can be located between the HF values obtained for each pattern separately. Furthermore, the embossing deco pattern, in both cases, has lower HF values than the micro pattern. Contrary to what happens with mechanical strength, it is not at 2.8 bar that the highest HF values are obtained. It is only for the case of the embossing deco pattern of sample B that the highest HF value is obtained for the pressure of 2.8 bar. Comparing the HF of industrial toilet base tissue paper with and without embossing, for the micro embossing pattern, a loss of about 9% and 12% was obtained for samples A and B, respectively. Regarding the embossing deco pattern, as expected, this loss was slightly higher, obtaining about 11% and 13% for samples A and B, respectively.

In conclusion, an optimum pressure was achieved at 2.8 bar to this embossing laboratory set-up for both embossing patterns. The two embossing patterns present different

behaviors, but both demonstrate losses in mechanical and softness properties. At the end, to achieve a final product with excellent quality, it is important to make a compromise between the various properties.

Author Contributions: FEM analysis, M.L.R. and A.C.V.; investigation, J.C.V.; simulation supervision, M.L.R. and A.C.V.; data curation, J.C.V., A.d.O.M.; writing—original draft preparation, J.C.V., A.d.O.M., M.L.R., A.C.V.; writing—review and editing, J.C.V., A.d.O.M., M.L.R., A.C.V., A.M.C., P.T.F. and A.P.C.; supervision, P.T.F. and A.P.C.; project pivot, A.M.C. All authors have read and agreed to the published version of the manuscript.

Funding: The authors gratefully acknowledge the funding of this work that was carried out under the Project InPaCTus—Innovative Products and Technologies from Eucalyptus, Project Nº 21874 funded by Portugal 2020 through European Regional Development Fund (ERDF) in the frame of COMPETE 2020 nº 246/AXIS II/2017. The authors are also very grateful for the support given by research unit Fiber Materials and Environmental Technologies (FibEnTech-UBI), on the extent of the project reference UIDB/00195/2020, and by the Center for Mechanical and Aerospace Science and Technologies (C-MAST-UBI), on the extent of the project reference UIDB/00151/2020, both funded by the Fundação para a Ciência e a Tecnologia, IP/MCTES through national funds (PIDDAC).

Institutional Review Board Statement: Not applicable.

Informed Consent Statement: Not applicable.

Data Availability Statement: Not applicable.

Conflicts of Interest: The authors declare no conflict of interest.

EFFEMBOSSING INFLUENCE ON THE 3D STRUCTURE AND KEY PROPERTIES OF TISSUE PAPER

Joana R. Curto[1], Joana C. Vieira[1], Flávia P. Morais[1], António O. Mendes[1], Ana M. Carta[2], Rogério S. Simões[1], Paulo T. Fiadeiro[1], Maria E. Amaral[1], Ana P. Costa[1]

[1] Fiber Materials and Environmental Technologies Research Unit (FibEnTech-UBI), Universidade da Beira Interior, Rua Marquês d'Ávila e Bolama, 6201-001 Covilhã, Portugal
[2] Forest and Paper Research Institute (RAIZ), Rua José Estevão, 3800-783 Eixo, Aveiro, Portugal

ABSTRACT

Premium tissue paper products are obtained with an optimized combination of softness, strength and liquid absorption properties, for each type of end-use product. The ability to predict the converting influence on the final paper properties, for different eucalyptus-based fibrous mixtures, constitutes valuable information to manage the furnish and to optimize end-use tissue paper properties. To the best of our knowledge, there is an absence of scientific data regarding the 3D paper structure before and after the tissue paper converting operations, such as embossing. The purpose of embossing is to change the physical properties of the materials and in some cases, it is used to bond two or more plies of material. Embossing tissue paper improves absorbency and flexibility, it increases the bulk, but it also changes their mechanical properties.

This work aims to study the embossing influence on the 3D structure and key properties of tissue paper. Distinct sources of materials, namely, eucalyptus bleached kraft pulp, never dried, and a deconstructed industrial machine tissue base paper, were used to produce tissue paper handsheets, and were compared to the industrial anisotropic creped base paper. The fibrous materials were characterized in terms of its morphological properties, as well as, drainage resistance, water retention value and chemistry-related properties. Isotropic laboratory handsheets were produced with a grammage of 17 g/m^2 using an adaptation of the ISO 5269, non-pressed, to mimic industrial tissue paper.

To study the embossing influence on eucalyptus-based tissue paper, a laboratory embossing prototype was designed allowing to modify the pressure applied between rolls and the influence of the deco and micro pattern designs. A complete experimental plan was executed using ISO standards and innovative complementary characterization methods. Laboratory handsheets and industrial tissue base papers were characterized and compared in terms of their physical properties before and after embossing. Besides these essays, the fiber structure interaction with water was evaluated using a 3D liquid drop prototype. This system enables liquid drop deposition, and the quantification of its kinetics, such as absorption spreading area on the paper porous structure over time.

The embossed patterns and the process operation conditions have a major influence on the 3D structure, resulting in a paper bulk increase, which impacts differently on final end-use tissue properties. The embossing process had also an impact on the absorption spreading area, reflecting the influence of the two used patterns and process conditions.

Therefore, the development of an original embossing laboratory prototype constitutes an important achievement of this study. The experimental data obtained with controlled embossing process parameters constitutes valuable information, not only for the study and quantification of the embossing effect on eucalyptus-based papers, but also for the 3D representation of these structures and consequently 3D modeling with predictive capability to be used in process optimization and management.

Keywords: 3D Paper Structure; Eucalyptus; Embossing Prototype; 3D Liquid Drop Prototype; Tissue Paper Properties